

# Investigation of the control mechanisms regulating fatty acid availability during infection.

By

Katherine Jane Hampton, MSc

A thesis submitted for the degree:

**Doctor of Philosophy**

Centre for Metabolic Health,

Faculty of Medicine and Health

University of East Anglia, Norwich, UK

Date of Submission: August 2025

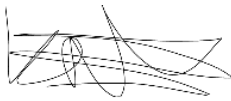


This copy of my thesis has been supplied on condition that anyone who consults it is understood to recognise that its copyright rests with the author and that use of any information derived there from must be in accordance with current UK Copyright Law. In addition, any quotation must include full attribution.

## **Declaration**

I declare that the contents of this thesis entitled 'Investigation of the control mechanisms regulating fatty acid availability during infection' was undertaken and completed by myself, unless otherwise acknowledged and has not been submitted in an application for another degree or qualification in this or any other university or institution.

This thesis is approximately 67,000 in length.

A handwritten signature in black ink, appearing to read 'Katherine Jane Hampton', written over a set of horizontal lines.

Katherine Jane Hampton

## Acknowledgements

This thesis is dedicated to everyone involved in 'Team Thesis' over the past four years. This PhD hasn't been without its difficulties, and it truly takes a village to complete a PhD, especially when the project got stuck and nothing seemed to work, or when I had to take time off for surgery (twice!).

To Stuart and James, who were there whenever I had questions or wanted to talk through data, even if I did knock on your door sometimes multiple times in one day. Your support and guidance has helped shape who I am as a scientist and for that I am truly grateful. With your help and supervision, I now feel ready to continue my scientific journey and am able to start my post-doc with confidence.

To every member of the Rushworth Lab that I have worked with, both past and present, I am grateful for all of the help you have given me, not only in the lab but also in support and friendship (including baked goods). You have set incredibly high expectations for any future lab that I work in. I have made friends for life in not only in the lab group, but also in BCRE itself. To Naiara, Edyta and Kris, who were also an important part of my support network, and were always available to bounce ideas off of when I got stuck. I am grateful for all of the help, guidance and support you have provided me throughout my scientific training in Norwich.

To my swim school family, and in particular to my boss Michelle, thank you for all of your help and support over the years, and for being so understanding when experiments ran long and I ended up being late to poolside. Thank you for reminding me that there is a world outside of the lab, and that even when things feel like they are falling apart, it is never as bad as it seems. I will miss you all.

And finally, a thesis support network would not be complete without help from your family. To my mum, who despite not having any scientific background, gave up many of her evenings to proofread my entire thesis and would never let me give up. To my sister, Jennifer, who found time to help me talk through my research when I was stuck and give me feedback on my work and presentations even when revising for her own exams as part of her emergency medicine speciality training. Last but not least, to Jack, who is everything I could have wished for in a partner. Despite being in a completely different scientific field and being busy with your own PhD, you were always there for me and picked me up when I was down or frustrated. Your unwavering support, patience and ability to cope with me when I get stressed is truly amazing and I couldn't have done this PhD without you.

## Abstract

During infection, hematopoietic stem and progenitor cells (HSPCs) rapidly expand to coordinate an effective immune response. Fatty acid uptake and metabolism are central to providing sufficient energy for HSPC expansion. However, the mechanisms that drive these changes are unknown. This study investigates the regulation of fatty acid availability to support this HSPC expansion.

Within 6 hours of lipopolysaccharide (LPS) administration, liver fatty acid uptake and metabolism was significantly downregulated. This downregulation was associated with a significant increase in circulating long-chain fatty acids (LCFAs). *In vitro* assays using hepatocytes demonstrated that circulating cytokines released in response to LPS caused this downregulation. Of these cytokines, only Plasminogen activator inhibitor-1 (PAI-1) significantly decreased LCFA uptake and metabolism in hepatocytes. Pharmacological inhibition of PAI-1 using TM5441 prevented the downregulation of hepatic fatty acid metabolism both *in vitro* and *in vivo*, resulting in a reduction in the availability of circulating LCFAs in response to LPS. Subsequently, pre-treating mice with TM5441 prior to LPS injection resulted in a significant reduction in HSC expansion normally seen in response to LPS.

Up to 90% of PAI-1 is stored in platelets. This thesis provides evidence that platelets can rapidly release PAI-1 in response to LPS. Depleting platelets from mice prior to LPS treatment significantly reduced the downregulation of liver fatty acid metabolism, reducing circulating LCFAs. Taken together, findings demonstrate that circulating LCFAs increase in response to infection to support immune cell expansion. Increased circulating LCFAs is at least partly driven by PAI-1 released from platelets, downregulating liver LCFA uptake and metabolism, allowing LCFAs to remain in circulation necessary to fuel HSC expansion during emergency haematopoiesis.

## **Access Condition and Agreement**

Each deposit in UEA Digital Repository is protected by copyright and other intellectual property rights, and duplication or sale of all or part of any of the Data Collections is not permitted, except that material may be duplicated by you for your research use or for educational purposes in electronic or print form. You must obtain permission from the copyright holder, usually the author, for any other use. Exceptions only apply where a deposit may be explicitly provided under a stated licence, such as a Creative Commons licence or Open Government licence.

Electronic or print copies may not be offered, whether for sale or otherwise to anyone, unless explicitly stated under a Creative Commons or Open Government license. Unauthorised reproduction, editing or reformatting for resale purposes is explicitly prohibited (except where approved by the copyright holder themselves) and UEA reserves the right to take immediate 'take down' action on behalf of the copyright and/or rights holder if this Access condition of the UEA Digital Repository is breached. Any material in this database has been supplied on the understanding that it is copyright material and that no quotation from the material may be published without proper acknowledgement.

# Table of Contents

<b>Declaration</b> .....	1
<b>Acknowledgements</b> .....	2
<b>Abstract</b> .....	3
<b>List of relevant publications and conference papers</b> .....	10
<b>List of figures</b> .....	11
<b>List of tables</b> .....	16
<b>List of abbreviations</b> .....	17
<b>1. Introduction</b> .....	22
<b>1.1 The bone marrow</b> .....	22
<b>1.2 Haematopoiesis in health</b> .....	25
<b>1.2.1 Haematopoietic stem cells</b> .....	27
<b>1.2.2 The HSC niche</b> .....	28
<b>1.2.3 Supporting cells within the HSC niche</b> .....	31
<b>1.2.3.1 Megakaryocytes</b> .....	31
<b>1.2.3.2 Macrophages</b> .....	31
<b>1.2.3.3 Bone marrow mesenchymal stromal cells</b> .....	32
<b>1.2.3.3.1 Osteoblasts</b> .....	32
<b>1.2.3.3.2 CXCL12-abundant reticular (CAR) cells</b> .....	32
<b>1.2.3.3.3 Adipocytes</b> .....	33
<b>1.2.3.3.4 Endothelial cells</b> .....	33
<b>1.2.3.4 Importance of hypoxia</b> .....	34
<b>1.3 Energy production in steady-state haematopoiesis</b> .....	35
<b>1.3.1 Metabolism</b> .....	36
<b>1.3.2 Glycolysis</b> .....	37
<b>1.3.3 Mitochondria</b> .....	39
<b>1.3.4 The TCA cycle</b> .....	40
<b>1.3.5 Oxidative phosphorylation</b> .....	41
<b>1.3.6 Fatty acid metabolism</b> .....	43
<b>1.3.6.1 Fatty acid length and structure</b> .....	44
<b>1.3.6.2 Cholesterol</b> .....	45
<b>1.3.6.3 Fatty acid transport</b> .....	46

1.3.6.3.1	Lipoproteins.....	46
1.3.6.3.2	Fatty acid transport proteins .....	46
1.3.6.4	Fatty acid oxidation .....	48
1.3.6.5	Ketogenesis .....	50
1.3.6.6	Master regulators of fatty acid metabolism .....	50
1.3.6.6.1	The PPAR family .....	51
1.3.6.6.2	SREBP family .....	52
1.3.6.6.3	Other central metabolic regulators .....	53
1.4	Haematopoiesis in response to stress .....	54
1.4.1	Haematological malignancies.....	54
1.4.2	Chemotherapy and Radiation.....	55
1.4.3	Ageing.....	56
1.4.4	Infection .....	56
1.4.4.1	Use of LPS as a model of infection.....	58
1.4.4.2	Salmonella typhimurium.....	59
1.4.4.3	Treatments for infection.....	60
1.4.4.4	The role of inflammation in the immune response.....	60
1.4.4.5	The SREBP family and the immune response.....	61
1.5	Energy requirements in stressed haematopoiesis .....	62
1.5.1	Increased mitochondrial mass via mitochondrial transfer .....	62
1.5.2	HSC fatty acid uptake and utilisation .....	64
1.5.3	Dysregulation of HSC expansion e.g. ageing/ obesity .....	65
1.6	The regulation of fatty acid availability .....	67
1.6.1	Adipose tissue .....	67
1.6.1.1	Uptake and storage .....	68
1.6.1.2	Export .....	68
1.6.2	The liver .....	69
1.6.2.1	Liver cellularity and structure .....	70
1.6.2.2	Hepatocytes .....	71
1.6.2.3	Kupffer cells .....	71
1.6.2.4	Biliary epithelial cells.....	72
1.6.2.5	Sinusoidal endothelial cells .....	73
1.6.2.6	Hepatic stellate cells .....	73

1.6.3	Liver fatty acid regulation .....	74
1.6.3.1	Fatty acid uptake and synthesis .....	74
1.6.3.2	Cholesterol synthesis and degradation .....	75
1.6.3.3	Fatty acid storage and export .....	75
1.6.4	Liver fatty acid regulation .....	76
1.6.5	The liver and the immune response .....	77
1.6.6	The role of inflammation in fatty acid availability .....	78
1.7	Rationale .....	79
1.8	Hypothesis .....	80
1.9	Aims and objectives .....	80
2	Materials and methods .....	81
2.1	Materials .....	81
2.2	Animal Models .....	85
2.2.1	Animal maintenance .....	85
2.2.2	Animal procedures .....	85
2.2.3	Intraperitoneal injections .....	86
2.2.4	Oral gavage .....	86
2.2.5	Intravenous injections .....	86
2.2.6	Schedule 1 sacrifice .....	87
2.3	Murine tissue collection and processing .....	88
2.3.1	Bone marrow isolation .....	88
2.3.2	Liver isolation .....	88
2.3.3	Fat pad isolation .....	88
2.3.4	Blood analysis .....	89
2.3.5	Platelet isolation .....	89
2.3.6	Serum .....	89
2.3.7	Bone marrow cell count .....	89
2.4	Flow Cytometry .....	90
2.4.1	HSC LCFA uptake .....	91
2.4.2	Mature and peripheral blood cell panel .....	91
2.4.3	Platelet quantification .....	91
2.4.4	Liver immune cell isolation .....	92
2.5	Cell culture .....	93

2.5.1	Cell counting with trypan blue .....	93
2.5.2	Primary mouse hepatocytes .....	93
2.5.3	AML12 cells.....	94
2.5.4	Cell cryopreservation .....	95
2.5.5	Hepatocyte serum and cytokine experiments .....	95
2.5.6	Seahorse metabolic flux analysis.....	96
2.5.7	Platelet activation assay .....	98
2.6	Serum analysis .....	99
2.6.1	Liquid chromatography-mass spectrometry .....	99
2.6.2	Proteome profiler array .....	100
2.6.3	PAI-1 ELISA.....	101
2.7	Histological analysis.....	102
2.7.1	Embedding and sectioning.....	102
2.7.2	Haematoxylin and Eosin .....	102
2.8	Molecular biology .....	103
2.8.1	RNA extraction.....	103
2.8.2	RNA quantification.....	104
2.8.3	Bulk-RNA sequencing .....	104
2.8.4	cDNA synthesis.....	105
2.8.5	Real-time quantitative PCR.....	105
2.9	Quantification and statistical analysis .....	107
3	<b>Characterising the kinetics of circulating fatty acids in response to LPS</b>	<b>108</b>
3.1	Introduction.....	108
3.2	Defining HSPC expansion and circulating LCFA availability in response to LPS <i>in vivo</i> .....	109
3.3	Characterising the changes in circulating LCFAs in response to LPS treatment over time .....	114
3.4	Characterising the role of the liver in circulating LCFA availability in response to LPS .....	123
3.5	Summary .....	135
4	<b>Determining the cause of the downregulation of liver fatty acid metabolism in response to LPS</b> .....	<b>136</b>
4.1	Introduction.....	136

4.2	Short-term LPS treatment does not downregulate hepatocyte fatty acid metabolism .....	137
4.3	Serum from LPS-treated mice downregulated hepatic fatty acid metabolism <i>in vitro</i> .....	143
4.4	PAI-1 downregulates hepatocyte fatty acid metabolism .....	150
4.5	Mice treated with recombinant PAI-1 display a similar phenotype to LPS treated mice .....	163
4.6	Summary .....	166
5	Pharmacological inhibition of PAI-1 prevents LPS-induced downregulation of hepatic liver fatty acid metabolism .....	167
5.1	Introduction.....	167
5.2	Tiplaxtinin did not reduce circulating PAI-1 in LPS-treated mice .....	169
5.3	Tiplaxtinin partially reverses the downregulation of hepatic fatty acid metabolism <i>in vitro</i> .....	176
5.4	TM5441 reverses PAI-1 induced downregulation of hepatic fatty acid metabolism and LCFA uptake <i>in vitro</i> . .....	184
5.5	TM5441 attenuates LPS-induced downregulation of liver fatty acid metabolism associated gene expression <i>in vivo</i> .....	195
5.6	Pre-treating mice with TM5441 impacted HSC expansion in response to LPS in the bone marrow .....	207
5.7	Summary .....	220
6	Platelets play an important role in the LPS-induced PAI-1 response .....	221
6.1	Introduction.....	221
6.2	Platelets release PAI-1 when stimulated with LPS .....	222
6.3	Depleting platelets partially reverses LPS-induced downregulation of liver fatty acid metabolism .....	224
6.4	Summary .....	239
7	Discussion.....	240
7.1	General Discussion.....	240
7.2	Key findings .....	241
7.2.1	Circulating LCFAs increase in response to LPS.....	241
7.2.2	LPS induces a downregulation of genes associated with liver fatty acid metabolism.....	241
7.2.3	PAI-1 regulates liver fatty acid metabolism and increases the availability of LCFAs .....	243

7.2.4	PAI-1 may work specifically to downregulate hepatocyte fatty acid metabolism without affecting glucose metabolism. ....	245
7.2.5	PAI-1 inhibition using TM5441 but not Tiplaxtinin prevented LPS-induced increase in circulating LCFAs .....	246
7.2.6	PAI-1 inhibition impaired HSC expansion in response to LPS ....	249
7.2.7	Platelets release PAI-1 when stimulated with LPS .....	251
7.2.8	Platelet depletion partially ameliorates the LPS-induced increase in circulating LCFAs .....	252
7.2.9	PAI-1 and immune cells .....	254
7.3	Limitations .....	256
7.4	Future work.....	258
7.5	Conclusion .....	259
8	References .....	260
9	Appendix .....	299

## **List of relevant publications and conference papers**

**Hampton, K.,** Polski-Delve, A., Hellmich, C., Rushworth S. A., 2025. Linking mitochondria, fatty acids and HSC expansion during infection: implications for aging and metabolic diseases. *Cell Stem Cell*.

In response to infection plasminogen activator inhibitor 1 induces long-chain fatty acid availability to allow metabolic reprogramming and expansion of immune cells.

**Oral Presentation. International Society for the Study of Fatty Acids and Lipids (ISSFAL) 16<sup>th</sup> international congress 2025. New investigator award winner.**

## List of figures

Figure 1.1, Bone structure.....	23
<b>Figure 1.2, The process of haematopoiesis.</b> .....	26
Figure 1.3, The haematopoietic stem cell niche. ....	30
Figure 1.4, Glycolysis pathway.....	38
<b>Figure 1.5, The Tricarboxylic acid cycle.</b> .....	41
Figure 1.6, The electron transport chain. ....	43
Figure 1.7, Fatty acid oxidation. ....	49
Figure 1.8, Mechanism for haematopoietic stem cell expansion in response to infection. ....	65
Figure 1.9, Lipolysis pathway.....	69
Figure 2.1, Cell counting using trypan blue exclusion. ....	93
Figure 2.2, Seahorse MitoStress test profile. ....	97
Figure 2.3, RT-qPCR SYBR-Green programme settings.....	106
Figure 3.1, LPS induced an increase in the proportion of HSPCs in the bone marrow. ....	110
Figure 3.2, LPS increased HSC palmitic acid uptake in the bone marrow. ....	111
Figure 3.3, LPS increased the level of LCFAs in the serum by 16 hours. ....	113
Figure 3.4, Time-course of total serum LCFA in response to LPS. ....	115
Figure 3.5, Time-course of different serum LCFA in response to LPS.....	116
Figure 3.6, Time-course of blood glucose and ketone levels in response to LPS treatment. ....	118
Figure 3.7, Time-course of monitoring changes in mouse weight in response to LPS treatment. ....	119
Figure 3.8, Time-course of monitoring changes in mouse fat pad weight in response to LPS treatment. ....	120
Figure 3.9, Time-course of lipolysis associated gene expression in inguinal and gonadal fat pads in response to LPS treatment. ....	122
Figure 3.10, Histological staining of liver tissue to assess histological changes in cellularity in response to LPS. ....	124
Figure 3.11, Bulk RNA sequencing revealed distinct differences in liver gene expression between control and LPS treated mice. ....	125
Figure 3.12, Kegg enrichment analysis of bulk RNA sequencing for the most significantly upregulated pathways in liver gene expression between control and LPS treated mice. ....	126
Figure 3.13, Kegg enrichment analysis of bulk RNA sequencing for the most significantly downregulated pathways in liver gene expression between control and LPS treated mice. ....	127
Figure 3.14, Bulk RNA sequencing revealed distinct differences in liver gene expression of LCFA transporters between control and LPS treated mice. ....	128
Figure 3.15, Gating strategy to identify liver immune cells populations. ....	129

Figure 3.16, Liver immune cell numbers in response to LPS treatment. ....	130
Figure 3.17, Liver monocyte numbers in response to LPS treatment. ....	131
Figure 3.18, Liver macrophage numbers in response to LPS treatment. ....	131
Figure 3.19, Determining the expression of key fatty acid metabolism genes in the liver in response to LPS over time. ....	133
Figure 3.20, Determining the expression of key fatty acid transport genes in the liver in response to LPS over time. ....	134
Figure 4.1, Short-term LPS treatment did not significantly alter hepatic fatty acid metabolism gene expression <i>in vitro</i> . ....	138
Figure 4.2, Short-term LPS treatment did not significantly alter hepatic LCFA uptake <i>in vitro</i> . ....	140
Figure 4.3, Short-term LPS treatment did not downregulate hepatic fatty acid associated mitochondrial respiration <i>in vitro</i> . ....	142
Figure 4.4, Serum from LPS-treated mice but not control mice downregulated hepatic fatty acid metabolism gene expression <i>in vitro</i> . ....	144
Figure 4.5, Serum from LPS-treated mice but not control mice downregulated hepatic LCFA uptake <i>in vitro</i> . ....	146
Figure 4.6, Serum from LPS-treated mice but not control mice downregulated hepatic fatty acid associated mitochondrial respiration <i>in vitro</i> in AML12 cells....	148
Figure 4.7, Serum from LPS-treated mice but not control mice downregulated hepatic fatty acid associated mitochondrial respiration <i>in vitro</i> in primary hepatocytes.....	149
Figure 4.8, Schematic of cytokine array experimental design. ....	151
Figure 4.9, Cytokine release into the serum in response to LPS. ....	152
Figure 4.10, The most increased cytokines were tested on AML12 cells <i>in vitro</i> to assess their effect on hepatic fatty acid metabolism.....	153
Figure 4.11, The most increased cytokines were tested on primary hepatocytes <i>in vitro</i> to assess their effect on hepatic fatty acid metabolism.....	154
Figure 4.12, PAI-1 worked in a dose dependent manner to downregulate hepatic fatty acid metabolism. ....	155
Figure 4.13, PAI-1 downregulated hepatic LCFA uptake <i>in vitro</i> . ....	157
Figure 4.14, PAI-1 downregulated hepatic fatty acid associated mitochondrial respiration <i>in vitro</i> in AML12 cells. ....	159
Figure 4.15, PAI-1 downregulated hepatic fatty acid associated mitochondrial respiration <i>in vitro</i> in primary hepatocytes. ....	160
Figure 4.16, PAI-1 did not downregulate hepatic glucose associated mitochondrial respiration <i>in vitro</i> in AML12 cells. ....	161
Figure 4.17, PAI-1 did not downregulate hepatic glucose associated mitochondrial respiration <i>in vitro</i> in primary hepatocytes. ....	162
Figure 4.18, Time-course of total PAI-1 in response to LPS in the serum.....	163
Figure 4.19, PAI-1 treatment decreased the expression of key liver fatty acid metabolism genes by 4 hours <i>in vivo</i> . ....	164

Figure 4.20, PAI-1 treatment increased serum levels of LCFA by 4 hours <i>in vivo</i> . ..	165
Figure 5.1, Schematic of Tiplaxtinin with LPS experimental design. ....	169
Figure 5.2, Serum PAI-1 levels in response to LPS both with and without Tiplaxtinin pre-treatment. ....	170
Figure 5.3, Tiplaxtinin did not affect the LPS-induced downregulation of key liver fatty acid metabolism genes. ....	171
Figure 5.4, Tiplaxtinin did not affect the LPS-induced downregulation of key liver LCFA transporter genes. ....	172
Figure 5.5, Tiplaxtinin did not alter the LPS-induced increase in serum LCFAs.....	173
Figure 5.6, Tiplaxtinin did not affect the LPS-induced downregulation of blood glucose levels. ....	174
Figure 5.7, Fat pad weight did not significantly change in Tiplaxtinin or LPS treated mice after 6 hours. ....	175
Figure 5.8, Tiplaxtinin treatment partially reverses PAI-1-induced downregulation of key hepatic fatty acid metabolism gene expression <i>in vitro</i> in a dose dependent manner.....	177
Figure 5.9, Tiplaxtinin treatment reverses PAI-1-induced downregulation of key hepatic fatty acid metabolism gene expression <i>in vitro</i> .....	178
Figure 5.10, PAI-1-induced reduction in LCFA uptake is not prevented by Tiplaxtinin pre-treatment <i>in vitro</i> .....	179
Figure 5.11, Tiplaxtinin treatment partially reversed the downregulation of key of hepatic fatty acid metabolism genes in response to serum from LPS-treated mice <i>in vitro</i> .....	181
Figure 5.12, The reduction in LCFA uptake in response to serum from LPS-treated mice was not prevented by Tiplaxtinin pre-treatment <i>in vitro</i> .....	182
Figure 5.13, Chemical structure of PAI-1 inhibitors.....	185
Figure 5.14, TM5441 treatment reversed PAI-1-induced downregulation of key hepatic fatty acid metabolism gene expression <i>in vitro</i> in a dose dependent manner. ....	186
Figure 5.15, TM5441 treatment reversed PAI-1-induced downregulation of key hepatic fatty acid metabolism gene expression <i>in vitro</i> .....	187
Figure 5.16, TM5441 prevented PAI-1-induced reduction of LCFA uptake in AML12 cells <i>in vitro</i> . ....	188
Figure 5.17, PAI-1 downregulated hepatic fatty acid associated mitochondrial respiration <i>in vitro</i> in AML12 cells was reversed by TM5441 treatment. ....	190
Figure 5.18, TM5441 treatment prevented the downregulation of key of hepatic fatty acid metabolism genes in response to serum from LPS-treated mice <i>in vitro</i> . ....	191
Figure 5.19, the reduction in LCFA uptake in response to serum from LPS-treated mice was prevented by TM5441 pre-treatment <i>in vitro</i> .....	193
Figure 5.20, Schematic of TM5441 with LPS experimental design. ....	195
Figure 5.21, Serum PAI-1 levels decreased in mice pre-treated with TM5441 before LPS administration. ....	196

Figure 5.22, TM5441 prevented the LPS-induced downregulation of key liver fatty acid metabolism genes. ....	197
Figure 5.23, TM5441 reversed the LPS-induced downregulation of key liver LCFA transporter genes. ....	198
Figure 5.24, TM5441 prevented the LPS-induced increase in serum LCFAs. ....	199
Figure 5.25, TM5441 did not affect the LPS-induced downregulation of blood glucose levels. ....	200
Figure 5.26, 6-hours of TM5441 did not affect mouse weight. ....	201
Figure 5.27, Fat pad weight did not significantly change in TM5441 or LPS treated mice after 6 hours. ....	202
Figure 5.28, Liver immune cell numbers in response to TM5441 and LPS treatment. ....	203
Figure 5.29, Liver monocyte numbers in response to TM5441 and LPS treatment. ....	204
Figure 5.30, Liver macrophage numbers in response to TM5441 and LPS treatment. ....	205
Figure 5.31, Serum PAI-1 levels decreased in mice pre-treated with TM5441 before LPS administration at 16 hours. ....	207
Figure 5.32, TM5441 partially prevented the LPS-induced downregulation of key liver fatty acid metabolism genes at 16 hours. ....	208
Figure 5.33, TM5441 partially reversed the LPS-induced downregulation of key liver LCFA transporter genes at 16 hours. ....	209
Figure 5.34, TM5441 prevented the LPS-induced increase in serum LCFAs at 16 hours. ....	211
Figure 5.35, There were no significant differences in blood glucose levels in TM5441 treated mice compared to LPS alone at 16 hours. ....	212
Figure 5.36, Weight loss was similar in LPS treated mice and mice treated with both TM5441 and LPS at 16 hours. ....	213
Figure 5.37, TM5441 partially prevents the LPS induced increase in the proportion of HSPCs in the bone marrow. ....	214
Figure 5.38, LPS increases HSC palmitic acid uptake in HSCs with and without TM5441. ....	215
Figure 5.39, Gating strategy for mature immune cell populations in the peripheral blood and bone marrow. ....	216
Figure 5.40, Bone marrow mature immune cells in response to TM5441 and LPS treatment at 16 hours. ....	217
Figure 5.41, Peripheral blood mature immune cells in response to TM5441 and LPS treatment at 16 hours. ....	219
Figure 6.1, Schematic of pilot experiment assessing speed of PAI-1 release in response to LPS. ....	222
Figure 6.2, Serum PAI-1 levels in response to LPS over a short time course. ....	222
Figure 6.3, Platelets isolated from WT mice release PAI-1 when stimulated with LPS. ....	223

Figure 6.4, Schematic of experimental design for platelet depletion prior to LPS infection. ....	224
Figure 6.5, Gating strategy used to quantify the number of platelets within the peripheral blood.....	225
Figure 6.6, R300 treatment successfully depleted platelets from the peripheral blood of mice.....	226
Figure 6.7, Depleting platelets prior to LPS treatment partially prevented the downregulation of key liver fatty acid metabolism genes. ....	227
Figure 6.8, Depleting platelets prior to LPS treatment partially prevented the downregulation of key liver LCFA transporter genes. ....	228
Figure 6.9, Depleting platelets prior to LPS injection partially prevented the increase of serum LCFAs.....	229
Figure 6.10, Serum PAI-1 levels were reduced in platelet depleted mice treated with LPS. ....	230
Figure 6.11, Depleting platelets prior to LPS treatment increased the expression of the gene encoding PAI-1 in the liver. ....	231
Figure 6.12, Depleting platelets from mice prior to LPS treatment did not affect the LPS-induced downregulation of blood glucose levels.....	232
Figure 6.13, Short-term platelet depletion did not affect mouse weight. ....	232
Figure 6.14, Short-term platelet depletion did not significantly affect fat pad weight. ....	233
Figure 6.15, Liver immune cell numbers in response to platelet depletion and LPS treatment. ....	234
Figure 6.16, Liver monocyte numbers in response to platelet depletion and LPS treatment. ....	236
Figure 6.17, Liver macrophage numbers in response to platelet depletion and LPS treatment. ....	237
Figure 6.18, TM5441 did not affect platelet number in the peripheral blood of mice. ....	238
Figure 7.1, Predicted binding site for Tiplaxtinin and TM5441. ....	248
Figure 9.1, FMOs for HSC panel.....	299
Figure 9.2, FMOs for liver immune cell panel. ....	300
Figure 9.3, FMOs for peripheral blood and mature bone marrow cell panels. ....	301

## List of tables

Table 2.1, Reagents used with manufacturer and catalogue number. ....	81
Table 2.2, Antibody panels used for flow cytometry assays. ....	90
Table 2.3, Concentrations of LCFAs added to the LC-MS calibration solution. ....	99
Table 2.4, Details of primers used for RT-qPCR analysis. ....	105
Table 3.1, Results of the BestKeeper algorithm to determine housekeeping gene stability for inguinal and gonadal fat pad samples. ....	121
Table 3.2, Results of the BestKeeper algorithm to determine housekeeping gene stability in the liver. ....	132
Table 4.1, Results of the BestKeeper algorithm to determine housekeeping gene stability for AML12 cells. ....	137
Table 4.2, Results of the BestKeeper algorithm to determine housekeeping gene stability for primary hepatocytes. ....	137

## List of abbreviations

<b>Abbreviation</b>	<b>Full name</b>
<b>ABC</b>	ATP-binding cassette
<b>ACADM</b>	Acyl-CoA dehydrogenase
<b>ACAT</b>	Acetyl-CoA acetyltransferase
<b>ACC</b>	Acetyl-CoA carboxylase
<b>ACSL1</b>	Acyl-CoA synthetase long-chain family member 1
<b>ADP</b>	Adenosine diphosphate
<b>AML</b>	Acute myeloid leukaemia
<b>AML12</b>	Alpha mouse liver 12
<b>apoB</b>	Apolipoprotein B
<b>APR</b>	Acute phase response
<b>ATGL</b>	Adipose triglyceride lipase
<b>ATP</b>	Adenosine triphosphate
<b>BAT</b>	Brown adipose tissue
<b>BMSC</b>	Bone marrow mesenchymal stromal cells
<b>BSA</b>	Bovine serum albumin
<b>BSO</b>	L-buthionine-sulfoximine
<b>CAR</b>	CXCL12-abundant reticular
<b>CCL</b>	C-C motif ligand
<b>CDKI</b>	Cyclin-dependent kinase inhibitors
<b>CLEC4G</b>	C-type lectin domain family 4 member G protein
<b>CLEC4M</b>	C-type lectin domain family 4 member
<b>CLP</b>	Common lymphoid progenitors
<b>CMP</b>	Common myeloid progenitors
<b>CPT</b>	Carnitine palmitoyltransferase
<b>CPT1A</b>	Carnitine palmitoyl transferase 1A
<b>CPT2</b>	Carnitine palmitoyl transferase II
<b>Ct</b>	Cycle threshold
<b>CX43</b>	Connexin 43
<b>CXCL12</b>	CXC chemokine ligand 12
<b>CXCR4</b>	CXC chemokine receptor 4

<b>CYP7A1</b>	Cholesterol 7 $\alpha$ -hydroxylase
<b>DAMPs</b>	Damage-associated molecular patterns
<b>DEG</b>	Differentially expressed gene
<b>DMEM F12</b>	Dulbecco's Modified Eagle Medium F12
<b>DMSO</b>	Dimethyl sulfoxide
<b>DO</b>	Disease Ontology
<b><i>E. coli</i></b>	<i>Escherichia coli</i>
<b>EDTA</b>	Ethylenediaminetetraacetic acid
<b>ESI</b>	Electrospray ionisation
<b>FABP</b>	Fatty acid binding protein
<b>FAD</b>	Flavin adenine dinucleotide
<b>FADH</b>	Flavin adenine dinucleotide (partially reduced)
<b>FADH2</b>	Flavin adenine dinucleotide (fully reduced)
<b>FAO</b>	Fatty acid oxidation
<b>FAO</b>	Fatty acid oxidation
<b>FAS</b>	Fatty acid synthase
<b>FATP</b>	Fatty acid transport protein
<b>FBS</b>	Foetal bovine serum
<b>FCCP</b>	Carbonyl cyanide-4-(trifluoromethoxy) phenylhydrazone
<b>FGF21</b>	Fibroblast growth factor 21
<b>FMO</b>	Fluorescence minus one
<b>FPKM</b>	Fragments Per Kilobase of exon per Million mapped fragments
<b>GAPDH</b>	Glyceraldehyde-3-phosphate dehydrogenase
<b>G-CSF</b>	Granulocyte-colony stimulating factor
<b>GLUT1</b>	Glucose transporter 1
<b>GMP</b>	Granulocyte-monocyte progenitors
<b>GO</b>	Gene Ontology
<b>GPAT</b>	Glycerol-3-phosphotase acyltransferase
<b>GSEA</b>	Gene Set Enrichment Analysis
<b>GTP</b>	Guanosine triphosphate
<b>H-</b>	Hydride ion
<b>H&amp;E</b>	Haematoxylin and eosin
<b>HDL</b>	High-density lipoprotein

<b>HIF</b>	Hypoxia-inducible factor
<b>HMGCR</b>	3-hydroxy-3-methylglutaryl-CoA reductase
<b>HMGCS2</b>	3-hydroxy-3-methylglutaryl-CoA synthase 2
<b>HNF4<math>\alpha</math></b>	Hepatocyte nuclear factor 4 $\alpha$
<b>HPRT</b>	Hypoxanthine phosphoribosyltransferase
<b>HSC</b>	Haematopoietic stem cell
<b>HSL</b>	Hormone-sensitive lipase
<b>HSPCs</b>	Hematopoietic stem and progenitor cells
<b>I.P.</b>	Intraperitoneal
<b>IL</b>	Interleukin
<b>IL-1<math>\beta</math></b>	Interleukin-1 $\beta$
<b>IL-6</b>	Interleukin-6
<b>IRF3</b>	Interferon regulator factor 3
<b>ITP</b>	Immune thrombocytopenia
<b>ITS</b>	Insulin-transferrin-sodium selenite
<b>KEGG</b>	Kyoto Encyclopaedia of Genes and Genomes
<b>LBP</b>	LPS binding protein
<b>LBP</b>	LPS binding protein
<b>LCAD</b>	Long-chain acyl-CoA dehydrogenase
<b>LCFA</b>	Long-chain fatty acids
<b>LC-MS</b>	Liquid chromatography-mass spectrometry
<b>LDH</b>	Lactate dehydrogenase
<b>LDHA</b>	Lactate dehydrogenase A
<b>LDL</b>	Low-density lipoprotein
<b>LDLR</b>	LDL receptor
<b>Lin-</b>	Lineage negative
<b>LIPE</b>	Lipase E
<b>LMPP</b>	Lymphoid multipotent progenitors
<b>LPL</b>	Lipoprotein lipase
<b>LPS</b>	Lipopolysaccharide
<b>LRP1</b>	Low-density lipoprotein receptor-related protein 1
<b>LSECs</b>	Liver sinusoidal endothelial cells
<b>LSK</b>	Lineage negative, Sca-1 positive, c-Kit positive

<b>LXR</b>	Liver X receptor
<b>MACS</b>	Magnetic-activated cell sorting
<b>MASLD</b>	Metabolic dysfunction-associated steatosis liver disease
<b>MCAD</b>	Medium-chain acyl-CoA dehydrogenase
<b>MCFA</b>	Medium-chain fatty acids
<b>MEM</b>	Minimum Essential Media
<b>MEP</b>	Megakaryocyte-erythrocyte progenitors
<b>MFI</b>	Median fluorescent intensity
<b>MGL</b>	Monoacylglycerol
<b>MPC</b>	Mitochondrial pyruvate carriers
<b>mRNA</b>	Messenger RNA
<b>mtDNA</b>	Mitochondrial DNA
<b>MyD88</b>	Myeloid differentiation primary response 88
<b>NAC</b>	N-acetyl-cysteine
<b>NAD+</b>	Nicotinamide adenine dinucleotide
<b>NADH</b>	Nicotinamide adenine dinucleotide (reduced)
<b>NAFLD</b>	Non-alcoholic fatty liver disease
<b>NEFA</b>	Non-esterified fatty acid
<b>NF-κB</b>	Nuclear factor κB
<b>NOD</b>	Nucleotide-binding and oligomerisation domain
<b>OCR</b>	Oxygen consumption rate
<b>PAI-1</b>	Plasminogen activator inhibitor-1
<b>PAMPs</b>	Pathogen-associated molecular patterns
<b>PBS</b>	Phosphate buffered saline
<b>PCA</b>	Principal component analysis
<b>PDK</b>	Pyruvate dehydrogenase kinase
<b>PGC1</b>	PPARgamma coactivator 1
<b>Pi</b>	Phosphate group
<b>PI3K</b>	Phosphatidylinositol 3 kinase
<b>PNPLA2</b>	Patatin like domain 2, triacylglycerol lipase
<b>PPAR</b>	Peroxisome proliferator-activator receptor
<b>PPM</b>	Parts per million
<b>PPRE</b>	Peroxisome proliferator response element

<b>PRRs</b>	Pattern recognition receptors
<b>RARs</b>	Retinoic acid receptors
<b>ROS</b>	Reactive oxygen species
<b>ROS</b>	Reactive oxygen species
<b>RotA</b>	Rotenone/Antimycin A
<b>RPM</b>	Rotations per minute
<b>RPS18</b>	Ribosomal protein S18
<b>RT-qPCR</b>	Real-time qualitative polymerase chain reaction
<b>RXR</b>	Retinoid X receptor
<b>Sca-1</b>	Stem-cell antigen 1
<b>SCAD</b>	Short-chain acyl-CoA dehydrogenase
<b>SCD1</b>	Stearoyl-CoA desaturase-1
<b>SCF</b>	Stem cell factor
<b>SCFA</b>	Short-chain fatty acids
<b>SREBP</b>	Sterol regulatory element-binding protein
<b>STAT3</b>	Signal transducer and activator of transcription 3
<b>TCA</b>	Tricarboxylic acid
<b>TGF</b>	Transforming growth factor
<b>TLR2</b>	Toll-like receptor 2
<b>TLR4</b>	Toll-like receptor 4
<b>TLRs</b>	Toll-like receptors
<b>TNF-<math>\alpha</math></b>	Tumour necrosis factor- $\alpha$
<b>tPA</b>	Tissue-type plasminogen activator
<b>TPO</b>	Thrombopoietin
<b>TRIF</b>	TIR-domain-containing adapter-inducing interferon- $\beta$
<b>VDAC</b>	Voltage-dependent anion channel
<b>vLCFA</b>	Very-long-chain fatty acids
<b>vLDL</b>	Very-low-density lipoprotein
<b>vLDLR</b>	vLDL receptor
<b>WAT</b>	White adipose tissue

# 1. Introduction

## 1.1 The bone marrow

The human skeleton is formed of two main types of bone ultra-structure. Compact, or cortical bone, accounts for around 80%, whilst trabecular, or spongy, makes up the remaining 20% (1). Some bones, such as the femur, are a composite, with spongy trabecular in the centre surrounded by compact bone along the edges (2). These different ultra-structures are specially adapted for particular functions. Compact bone is hard but light, containing densely packed concentric rings which are able to withstand compression and thus forms the weight bearing component of bone (3). On the other hand, trabecular bone is much more porous and contains bone marrow, the main site of haematopoiesis, where nearly all of the haematopoietic system is formed (2, 4). Haematopoiesis refers to the process of mature blood cell production (5). Bone marrow is highly dynamic, with multiple endogenous and exogenous factors influencing bone homeostasis (6).

Red marrow is found within the spongy end regions of these composite bones, whereas yellow marrow is located primarily towards the centre of the bone (4). Yellow marrow has a high fat content due to its large volume of adipocytes, with minimal vasculature and acts as a reservoir of stored fat which can be utilised for energy production in times of need, Figure 1.1 (7, 8). Alternatively, red marrow is where the majority of blood cells are produced, including erythrocytes, platelets and leukocytes, and contrastingly is highly vascularised, Figure 1.1 (7, 9, 10). In fact, nearly one-third of the total area of bone marrow is taken up by microvasculature (2), giving the red marrow its characteristic colour due to high haem content (11).

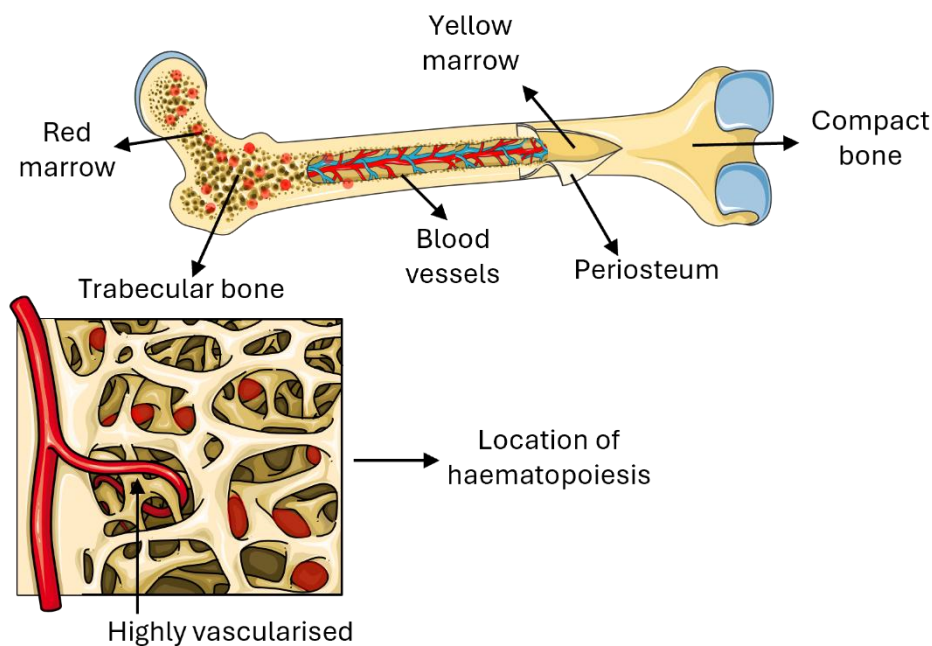


**Figure 1.1, Bone structure.**

The structure of bone marrow within a composite bone containing both compact and trabecular bone. Yellow marrow is found centrally whereas red marrow is located nearer to the ends within the trabecular bone. Red marrow is highly vascularised and is the site of haematopoiesis.

The ratio of red to yellow marrow changes as we age, with red marrow slowly replaced by yellow marrow (12). At birth, all bone marrow is red, however throughout childhood and into early adulthood, red marrow is converted into yellow marrow in a constant, predictable manner, starting in the limbs (13). By age 25, the balance of red and yellow marrow stabilises, with most of the red marrow now restricted to the axial skeleton (for example the ribs and skull) and proximal metaphysis of long bones such as the femur and humerus (2, 9-11). This is because the accumulation of densely packed adipocytes within the marrow dislodges the red marrow, and thus nearly all haematopoietic activity to the proximal ends of long bones (8, 10, 14). Multiple factors including age and disease can affect marrow composition and rheology (9, 11). Due to the finite space within bones, the ratio of red to yellow marrow changes in response to alterations in the microenvironment (10, 15). For example, when increased haematopoietic activity is required, the adipocytes within the yellow marrow are reabsorbed to provide more space as well as energy (11).

The surrounding bone marrow microenvironment is crucial to provide signals to help maintain and regulate haematopoiesis, helping to ensure fluctuating demands under

both homeostatic and stress conditions are met (15). Haematopoiesis is tightly regulated, with the surrounding bone marrow microenvironment containing a highly organised heterogenous population of non-haematopoietic cells including stromal cells, endothelial cells and adipocytes playing an essential regulatory role (16-18). For example, central to haematopoiesis are haematopoietic stem cells (HSCs), which reside in one of the most studied bone marrow microenvironments, the HSC niche. This niche plays a pivotal role for HSC survival, highlighting the important role of the bone marrow microenvironment.

## 1.2 Haematopoiesis in health

Haematopoiesis refers to the generation of all mature blood cell lineages, which play a pivotal role in tissue oxygenation and immunity (19). During both human and mouse development, haematopoiesis first takes place in the yolk sack, before transitioning into the aorta-gonad-mesonephros region of the embryonic mesoderm and foetal liver (15, 20, 21). Eventually, it will permanently move to the bone marrow, where it remains, however remnant haematopoietic activity can occur in the liver and spleen into adulthood (22-24). At the centre of haematopoiesis is a small population of approximately 10,000 HSCs, which are responsible for producing billions of blood cells every day, following a tree-like hierarchy of sequential multilineage differentiation to produce a complete blood system, Figure 1.2 (15, 25-27). These lineage-restricted blood oligo-, bi-, and unipotent progenitors are generated in a stepwise manner following this hierarchy (28).

Within their niche, long-term HSCs differentiate into short-term HSCs, which then give rise to either lymphoid or myeloid multipotent progenitors (29, 30). Common myeloid progenitors (CMPs) then give rise to granulocyte-monocyte progenitors (GMPs) and megakaryocyte-erythrocyte progenitors (MEP). GMPs ultimately form the granulocytes, eosinophils, basophils, neutrophils and monocytes, whereas MEPs differentiate and mature into megakaryocytes and erythrocytes. Some megakaryocytes will fragment into thrombocytes, more commonly known as platelets (31, 32). Meanwhile lymphoid multipotent progenitors (LMPPs) give rise to common lymphoid progenitors (CLPs), which then go on to form the T-lymphocytes, B-lymphocytes and natural killer cells (28, 30, 33). This hierarchy is depicted in Figure 1.2.

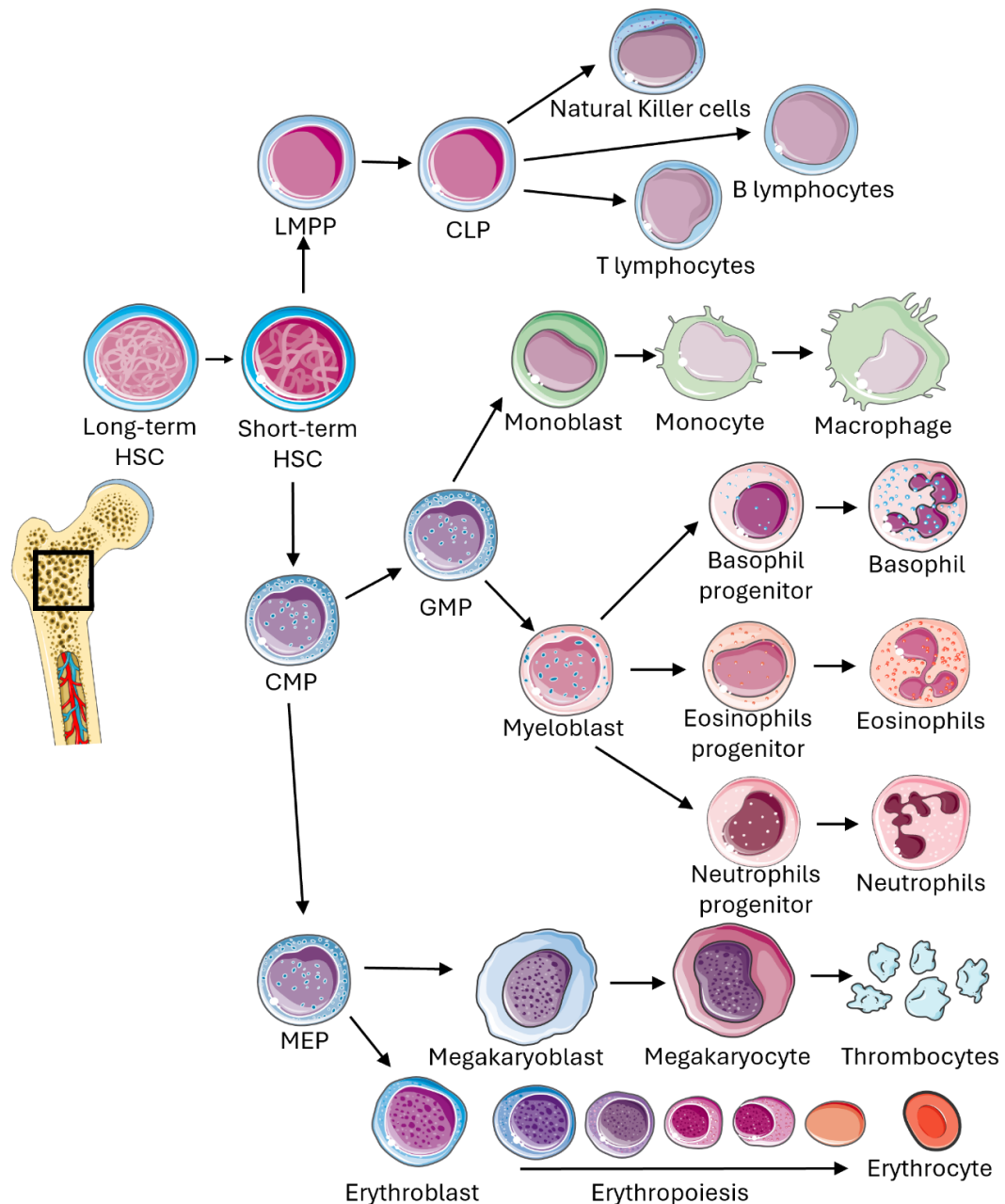


**Figure 1.2, The process of haematopoiesis.**

Haematopoiesis refers to the continuous self-renewal and production of mature blood cells from immature haematopoietic stem cells (HSC). Within their niche, there are long-term and short-term HSCs, which give rise to either common myeloid progenitors (CMP) or common lymphoid progenitors (CLP). CMPs differentiate into granulocyte monocyte progenitors (GMPs) and megakaryocyte-erythrocyte progenitors (MEP). GMPs ultimately form the granulocytes, eosinophils, basophils, neutrophils and monocytes, whereas MEPs differentiate and mature into megakaryocytes and erythrocytes. CLPs go on to form the T lymphocytes, B-lymphocytes and natural killer cells.

Cells derived from GMPs and CLPs are all part of the adaptive and innate immune response. However, in more recent years, the true complexity of haematopoiesis has started to be recognised, with this tree-like hierarchy now thought not to be entirely accurate. Some researchers argue that science should move away from this static

model (32, 33). For example, studies have shown that megakaryopoiesis (the process of HSC differentiation into megakaryocytes) does not always strictly follow this hierarchy. A distinct subset of HSCs, termed 'platelet-primed HSCs' can unilaterally differentiate into megakaryocytes. This direct differentiation is thought to be influenced by the presence of thrombopoietin (34, 35).

### **1.2.1 Haematopoietic stem cells**

HSCs make up around 0.01% of the total cells found in the bone marrow but are responsible for indirectly producing over 500 billion blood cells every day (17, 36, 37). In humans, this represents 90% of total cell turnover (38). Studies which transplanted even just one single HSC into lethally irradiated mice proved that HSCs are able to reconstitute and maintain all haematopoietic lineages long-term (39, 40), demonstrating that they are the central component responsible for haematopoiesis.

Within their niche, HSCs can be identified by their unique set of cell surface markers. HSCs are lineage negative (Lin-), meaning that they do not express any of the cell surface markers which are normally found on other more mature haematopoietic cells. However, HSCs do express high levels of stem-cell antigen 1 (Sca-1) and CD117, also known as c-Kit (36). Experimentally cells identified as being Lin-Sca-1+CD117+ are referred to as LSKs and represent immature cells including HSCs and downstream progenitor cells (41). HSCs can be further identified from LSK cells as they express CD150 but not CD48 (42).

Clinically, due to their immense self-renewal and multipotency potential, HSCs have been used as a treatment for multiple diseases including haematological malignancies such as leukaemia and lymphoma since the 1960's (37). For this, HSCs for transplant are traditionally collected from umbilical cord blood, bone marrow or even collected in peripheral blood samples (43). However, due to only being able to collect very low numbers from patients and the difficulty in finding adequately matched donors, the use of HSC transplants clinically remains challenging (44).

Under normal, low stress conditions, kinetic studies have shown that the majority of HSCs are kept in G0 phase, remaining dormant and rarely dividing (45). This is partly due to the hypoxic environment they reside in, which is discussed further in section

1.2.3.4. These dormant HSCs are often referred to as long-term HSCs and have the greatest 'stemness' compared to more active HSCs (46). The predicted rate at which HSCs divide varies between studies and species. For mice, studies suggest long-term HSCs divide in mice as much as once every 56 days (ranging between 56-145 days) (47-49), whereas humans studies using segmented regression predict that adult HSCs divide less than once every two years (50). These differences are likely explainable due to the vastly different lifespan as well as methods and markers used to label and trace HSC division. In mice, this replication rate would mean that quiescent HSCs undergo around 5 divisions throughout a mouse's whole lifetime (47, 51). Each division has been associated with a decreased likelihood that the HSC re-exits the cell cycle and returns to its quiescent state (45, 52, 53). Thus, HSC quiescence and repression cell division is an important mechanism to prevent premature exhaustion due to excessive replication (54, 55).

When required, HSCs can become activated, becoming short-term HSCs and entering the cell cycle (37, 56). CD34 expression is a common characteristic used to differentiate the two HSC populations, as long-term HSCs are thought to be CD34<sup>low</sup> and short-term HSCs CD34<sup>+</sup> (57, 58). Whilst long-term HSCs can sustain haematopoiesis for an entire organism's lifespan, studies have shown that short-term HSCs are only able to maintain haematopoiesis for around 6-8 weeks (29, 59). However, it is this smaller population of more active HSCs that are responsible for producing the necessary immune and blood cells each day during haematopoiesis. Short-term HSCs are also able to rapidly proliferate and differentiate in response to stress stimuli to increase haematopoietic cell production (60). Conversely, long-term HSCs are unsuitable for rapid immune cell production. Whilst the exact reason for this is not yet fully understood, it is thought that their quiescence and location within the niche plays a major role in their slower response (40, 61). Overall, this demonstrates the complexities and heterogeneity of HSCs and their regulation.

## **1.2.2 The HSC niche**

Stem cell niches offer a dynamic microenvironment to support a population of stem cells throughout their lifecycle (62) and were first hypothesised by Schofield in 1978 (63). The surrounding microenvironment, or HSC niche, is crucial to HSC homing,

self-renewal and differentiation, including both intrinsic and extrinsic signals such as oxygen availability, growth factors, cell cycle regulators and transcription factors (64-68). Stem cell niches also rely on cell-cell adhesion. For example, the close proximity and spatiotemporal organisation of multiple cell types including bone marrow mesenchymal stromal cells (BMSCs), osteoblasts and endothelial cells play a particularly important role in retaining HSCs within their niche (69, 70). Cell-cell adhesion is essential for HSC homing within its bone marrow niche (71). In addition, stem cell niches also utilise biomechanical cues such as extracellular matrix stiffness and cell-intrinsic forces to support HSCs (72).

However, due to the complexities of haematopoiesis, one singular niche is unable to fully support HSCs. Instead, more recent research has established that there are at least two distinct HSC niches. The endosteal osteoblastic niche, which helps maintain quiescence and self-renewal, and the vascular niche which aids HSC mobilisation for proliferation and differentiation (18, 73). Therefore, it is now thought that long-term HSCs reside in the endosteal niche, supported by surrounding cells including osteoblast and endothelial cells (74). Whereas the vascular niche sits adjacent to blood vessels, allowing easy access to the necessary nutrients and signalling molecules needed for differentiation and proliferation (74, 75). Important supporting cells in this vascular niche include endothelial, perivascular and mesenchymal cells (76). Despite the complexities, development of single cell technologies and complex image-based transcriptomics have revolutionised our understanding of the bone marrow microenvironment and the complexity of the HSC niche. Furthermore, computational frameworks such as scNiche allow a deeper, more robust analysis of single-cell omics data to identify cell niches (77). With this and future technological advancements, our understanding of stem cell niches is likely to continue to improve.

Growth factors, cytokines and chemokines secreted within the HSC niche are also crucial for HSC regulation, determining HSC fate and functionality (18). Examples of these important factors include CXC chemokine ligand 12 (CXCL12), angiopoietin-1, thrombopoietin (TPO) and stem cell factor (SCF) (78). HSCs express CXC chemokine receptor 4 (CXCR4), the major receptor for CXCL12 (79, 80). Signalling through CXCR4/CXCL12 directly influences HSC migration, proliferation, quiescence and

their ability to stay within the niche (81-83). Loss of bone marrow CXCR4 detrimentally impacts the long-term reconstitution capacity of HSC and progenitor cells, in part by increasing their sensitivity to oxidative stress and causing DNA damage and apoptosis (84). SCF is the ligand for the c-Kit receptor and has been shown to be important for HSC self-renewal (85, 86). SCF has also been shown to increase HSC adhesion to extracellular matrix proteins as well as to BMSCs themselves (87, 88), highlighting its importance in HSC homing. Furthermore, HSCs are unable to remain in their niche if either SCF or CXCL12 is lost (89, 90), and thus both are critically important factors for HSC maintenance.

Some of the cells produced during haematopoiesis can also help to support and maintain HSCs, contributing to the HSC niche. Additionally, multiple cell types within the bone marrow help support haematopoiesis without being directly involved in the process, and instead form part of the supporting bone marrow microenvironment such as stromal cells. The most important cell types and the factors they secrete within the HSC niche are depicted in Figure 1.3 described below.

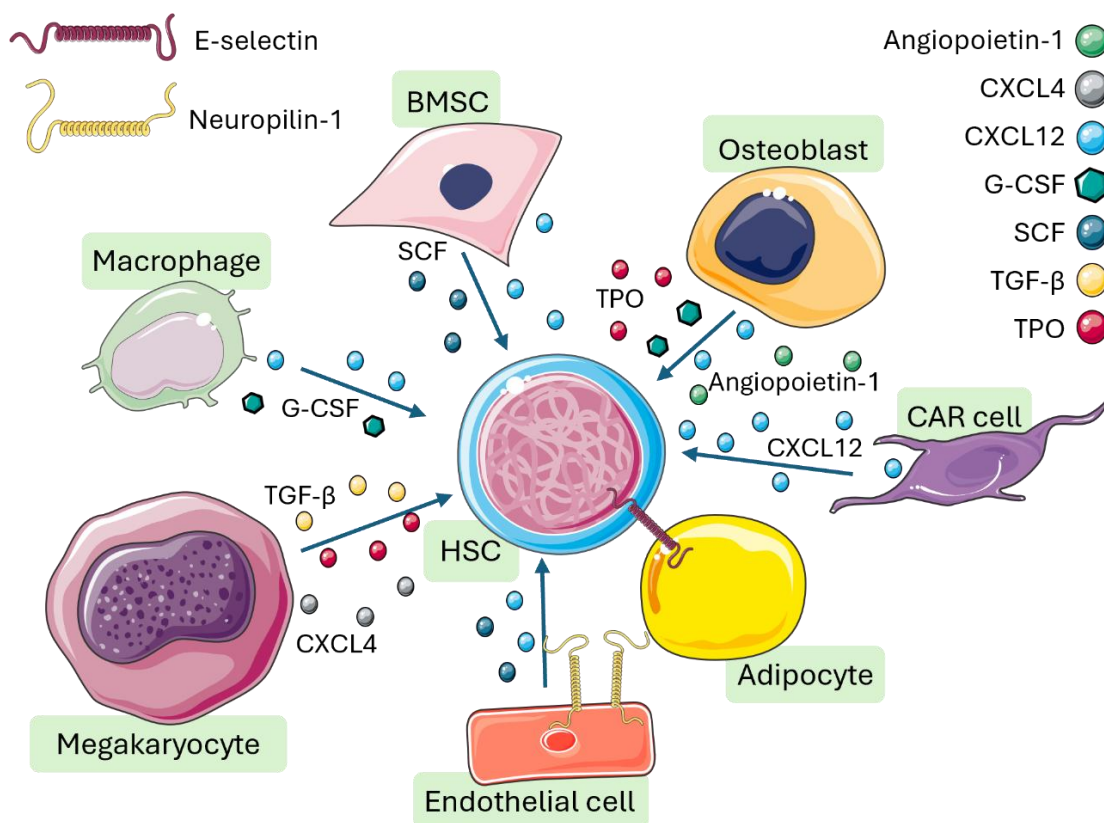


**Figure 1.3, The haematopoietic stem cell niche.**

Important cells supporting the HSC niche include macrophages, megakaryocytes, CXCL12-abundant reticular (CAR) cells and BMSCs. These cells secrete multiple factors such as SCF, TPO and CXCL12 to support HSC maintenance.

### **1.2.3 Supporting cells within the HSC niche**

#### **1.2.3.1 Megakaryocytes**

Within the bone marrow, megakaryocytes are easily recognisable due to their large size and multi-nucleation (91). As a part of haematopoiesis, megakaryocytes become multi-nucleated through the process of endomitosis (DNA replication without cell division), and then mature into several proplatelets, before releasing platelets into the circulations (92). Besides their role in platelet production, megakaryocytes play a role in HSC maintenance as they produce CXCL4, transforming growth factor (TGF)- $\beta$  and TPO, all important factors in maintaining HSC quiescence (93-96). Mouse models have demonstrated that around 20% of HSCs are located directly adjacent to megakaryocytes (97, 98). Loss of megakaryocytes caused the HSC population to grow, with a greater proportion actively cycling (97), demonstrating the importance of megakaryocytes in HSC maintenance.

#### **1.2.3.2 Macrophages**

Macrophages are critically important in both innate and adaptive immunity as well as tissue homeostasis. Derived from monocytes, macrophages are an important population of phagocytes able to clear cellular debris and apoptotic cells independent of immune cell signalling and stimulation (99, 100). Macrophages are scattered throughout the bone marrow, including in the lining of the bone, where they help support osteoblasts (101). Additionally, macrophages have been implicated in HSC maintenance, promoting HSC retention within the HSC niche (73). Although the macrophage's role within HSC regulation is still not fully understood, macrophages are able to dynamically respond to different signals to help maintain optimal HSC function. For example, in low stress macrophages can secrete CXCL12 to support HSC homing. Macrophage depletion using drugs such as clodronate increases the number of circulating HSCs (101, 102). However, during increased demands for immune cells, macrophages instead secrete granulocyte-colony stimulating factor (G-CSF) which suppresses CXCL12, driving HSC mobilisation (103, 104). Thus, macrophages also play an important role in the HSC niche and controlling HSC mobilisation.

### **1.2.3.3 Bone marrow mesenchymal stromal cells**

BMSCs, also known as mesenchymal stem cells, are important in adipose, bone, muscle and cartilage regeneration (11). BMSCs encompass a diverse population of multipotent stem cells and mature cells including osteolineage cells, endothelial cells, adipocytes and CXCL12-abundant reticular (CAR) cells which are separate from haematopoiesis (105, 106). BMSCs play a pivotal role in maintaining the HSC niche by secreting multiple cytokines and growth factors including interleukins, CXCL12 and SCF (107, 108).

#### **1.2.3.3.1 Osteoblasts**

Outside of their role in bone formation, osteoblasts, which are derived from BMSCs, were one of the first cell types shown to be involved in the regulation of HSC and progenitor cells (109). Osteoblasts produce multiple important cytokines involved in HSC regulation including G-CSF, TPO, angiopoietin-1 and CXCL12 (110-113). Depletion of osteoblasts is associated with a reduction in bone marrow HSCs and a switch to extramedullary haematopoiesis (114), evidencing the importance of osteoblasts in HSC maintenance. However, their exact role in HSC maintenance has been called into question. Multiple studies have demonstrated that *in vivo* osteoblasts have very little contact with HSCs (82, 115-117). Instead, it has been suggested that more immature, not mature, osteoblasts are involved in HSC regulation rather than the mature osteoblasts as initially thought (118). However, there are many different populations of osteoblasts and thus it remains unclear which of these are truly important in HSC maintenance.

#### **1.2.3.3.2 CXCL12-abundant reticular (CAR) cells**

Spatial analysis has shown that many HSCs keep close contact with CAR stromal cells in both endosteal and vascular niches (82). CAR cells are the highest expressors of CXCL12 within the HSC niche and thus are particularly important for HSC maintenance. Ablation of CAR cells *in vivo* caused a notable reduction in bone marrow CXCL12 levels (90). This resulted in reduced numbers of long-term HSCs (119, 120). Additionally, CAR cells secrete high levels of SCF. When SCF was conditionally deleted from leptin receptor expressing cells, a marker for CAR cells

(121), this also resulted in severely reduced HSC numbers (89, 122). Taken together, this provides evidence for the importance of CAR cells in HSC regulation and maintenance.

#### **1.2.3.3.3 Adipocytes**

Additionally, BMSCs can differentiate and specialise into adipocytes. Adipocytes form an important part of the bone marrow microenvironment, accounting for up to 70% of total bone marrow volume (14, 123). Bone marrow adiposity increases with age, from around 15% of the bone marrow in young adults to significantly over half in older individuals (124, 125). Adipocytes are lipid storage cells and thus can provide energy to the bone marrow. Aside from their role as an energy store, adipocytes have been shown to negatively regulate haematopoiesis, particularly within conditions of stress and ageing (8, 126, 127). Adipocytes can block HSC differentiation via neuropilin-1 interactions mediated by cell-to-cell contact (128). This can result in total arrest of the HSC population and subsequent apoptosis (129), highlighting the important role adipocytes play in HSC regulation.

#### **1.2.3.3.4 Endothelial cells**

Endothelial cells help to form the bone marrow blood vessel network (130). This endothelial cell barrier lining the blood vessels maintains a clear separation between circulating blood cells and the cells within the bone marrow, aiding HSC development and haematopoiesis (131, 132). They do this by controlling blood vessel permeability. When permeability is low, HSCs are exposed to low levels of reactive oxygen species (ROS), helping maintain HSC quiescence. However endothelial cells can increase blood vessel permeability, subsequently increasing ROS levels within the bone marrow microenvironment, which in turn increases HSC activation (133, 134). Too much ROS can result in HSC exhaustion and damage (135, 136).

Furthermore, bone marrow endothelial cells express SCF, CXCL12, pleiotrophin and E-selectin (137). Loss of SCF, CXCL12 or pleiotrophin in endothelial cells results in reduction of the HSC pool (138-140), further demonstrating their essential role in HSC maintenance. However, interestingly, loss of E-selectin actually enhanced HSC

quiescence and self-renewal (141), demonstrating that E-selectin may play more of a role in aiding HSC proliferation instead of maintenance in the vascular niche.

#### **1.2.3.4 Importance of hypoxia**

In mammals, the HSC niche is hypoxic, helping to maintain HSC quiescence, holding them in G0 of the cell cycle, and are supported by the surrounding cortical and trabecular regions (54, 142-144). HSCs express high levels of hypoxia-inducible factor (HIF)-1 $\alpha$  messenger RNA (mRNA) due to the low oxygen concentration within their niche (145). Culturing HSC and progenitor cells (or LSKs) isolated from mouse bone marrow in hypoxic (1% O<sub>2</sub>) compared to normoxic conditions (20% O<sub>2</sub>) increased the proportion of HSCs held in G0 phase, and reduced cell proliferation (146-148). Mechanistically, this cell cycle arrest relies on hypoxia-induced HIF-1 $\alpha$  stabilisation, upregulating cyclin-dependent kinase inhibitors (CDKIs), including p27 and p57 (146). Loss of this hypoxic environment results in increased proliferation and HSC exhaustion, detrimentally affecting engraftment efficiency (149-151). p27, p57 and HIF-1 $\alpha$  knockout models also show similar results, including reduced engraftment potential during transplantation (152, 153). This demonstrates the importance of a hypoxic environment for HSC maintenance. Furthermore, multiple cytokines including TPO and SCF also stabilise HIFs, including HIF-1 $\alpha$  (144, 154, 155), further linking the hypoxic microenvironment to the cells supporting the HSC niche.

### 1.3 Energy production in steady-state haematopoiesis

There is evidence for the role of HSC metabolism in regulating haematopoietic cell fate (156). In steady state, quiescent HSCs reside in their hypoxic niche with minimal mitochondrial activity, maintaining characteristically low levels of ROS (47, 56, 67). These metabolically inactive HSCs favour anaerobic glycolysis to meet their low energy requirements (52, 157, 158). The glycolytic activity of HSCs is maintained by the translocation of glucose transporters on the cell surface of HSCs to ensure the sufficient uptake of glucose to fuel them. This is partly due to hypoxia induced HIF-stabilisation, including HIF-1 $\alpha$ , within HSCs which drives increased expression of several glycolytic enzymes and controls glucose transporter expression, including lactate dehydrogenase A (LDHA) and glucose transporter 1 (GLUT1) (145, 159).

The restriction of mitochondrial metabolism helps HSCs to maintain low ROS levels, preventing HSC differentiation and lineage commitment, and essentially maintaining their 'stemness' (160, 161). This means that HSCs have a different metabolic profile compared to that of more committed haematopoietic cells (162). Thus, during HSC differentiation and maturation into mature haematopoietic cells, metabolic reprogramming must also occur to meet the different energy requirements of erythroid, myeloid and lymphoid cells (163). HIF-1 $\alpha$  also induces pyruvate dehydrogenase kinase (PDK) expression in HSCs (164). PDKs block pyruvate dehydrogenase activity, preventing the conversion of pyruvate (the product of glycolysis) into acetyl-CoA, which then feeds into the tricarboxylic acid (TCA) cycle (165-167). This essentially blocks mitochondrial oxidative metabolism of pyruvate (168). Loss of HIF-1 $\alpha$  reduced glycolysis and increased mitochondrial metabolism (164). This resulted in loss of HSC quiescence, and a progressive loss in ability to maintain their population long-term following stress (78, 169, 170). Taken together, these studies demonstrate the key link between the hypoxic microenvironment HSCs reside in, HIF-1 $\alpha$  expression and their glycolytic activity. Furthermore, loss of lactate dehydrogenase (LDH) in HSCs, the enzyme responsible for the conversion between pyruvate and lactate, has been shown to increase the amount of pyruvate entering the TCA cycle (171, 172). This subsequently increases oxidative phosphorylation, increasing ROS levels and resulting in reduced long-term reconstitution potential of HSCs (172). Increased levels of ROS has been shown to induce HSC-specific p38

phosphorylation and MAPK activation, associated with a reduction in HSC self-renewal (173). Taken together, this demonstrates the importance of HSCs maintaining low oxidative phosphorylation to preserve HSC stemness.

However, fatty acid oxidation (FAO) has still been shown to be important in the maintenance of quiescent HSCs. Inhibiting FAO using drugs such as etomoxir detrimentally affected maintenance of the HSC pool and eventually resulted in HSC exhaustion and haematopoietic failure (174). Thus, this demonstrates the importance of understanding the role of metabolism in HSC maintenance and differentiation during haematopoiesis.

### **1.3.1 Metabolism**

Metabolism refers to the biochemical reactions that occur within cells to produce or consume energy. To fuel these reactions, all living organisms must take up and use nutrients from their environment. In general, metabolism comprises of more than 8000 different reactions which use over 16000 metabolites (175). In mammals, the most abundant nutrients can be categorised into carbohydrates, amino acids and fatty acids, which cells utilise to produce energy using high energy compounds. These high energy compounds transfer either inorganic phosphate groups (Pi) or hydride (H-) ions, which are a vital part of energy storage and release (176). The most common example of this is adenosine triphosphate (ATP), also referred to as the universal currency of energy, which is comprised of adenine, a ribose sugar and three sequentially bonded phosphate groups. It provides a link between catabolic reactions that produce energy in the form of ATP, and anabolic reactions which utilise energy via the hydrolysis of ATP (177). When hydrolysed, these high energy phosphoric anhydride bonds with Pi yield large amounts of energy to drive metabolism (178). Hydrolysis of the terminal phosphate group in ATP generates 7.3 kcal/mol of energy, producing adenosine diphosphate (ADP) + Pi (179). Each molecule of ATP is recycled back into ADP more than a thousand times each day to generate sufficient energy, a process which primarily occurs during oxidative phosphorylation (180). Whilst ATP provides energy for around 73% of small molecule synthesis, a notable minority (27%) comes from guanosine triphosphate (GTP) (181).

Hydride ions are hydrogen atoms which have an extra electron, making them negatively charged. High energy intermediates can be reduced (gain a hydride ion) or oxidised (lose a hydride ion). Common examples include the reduction of nicotinamide adenine dinucleotide (NAD)<sup>+</sup> to NADH, and flavin adenine dinucleotide (FAD) to either FADH or FADH<sub>2</sub> (182, 183). These high energy molecules can then donate their electrons during the electron transport chain to produce ATP. Multiple different metabolic pathways are used to generate ATP, both with and without oxygen. In aerobic conditions, cellular respiration, beta-oxidation, ketosis, lipid and protein catabolism produce ATP. Cellular respiration can be broken into three main steps: glycolysis, the TCA cycle and oxidative phosphorylation. Lower volumes of ATP can also be produced anaerobically when oxygen is scarce (184).

### **1.3.2 Glycolysis**

Glycolysis refers to the metabolic pathway occurring in the cytoplasm of cells that converts one six carbon glucose molecule into two three carbon pyruvate molecules, producing two molecules of ATP, and is the first step of cellular respiration. There are several steps to this process, depicted in Figure 1.4.

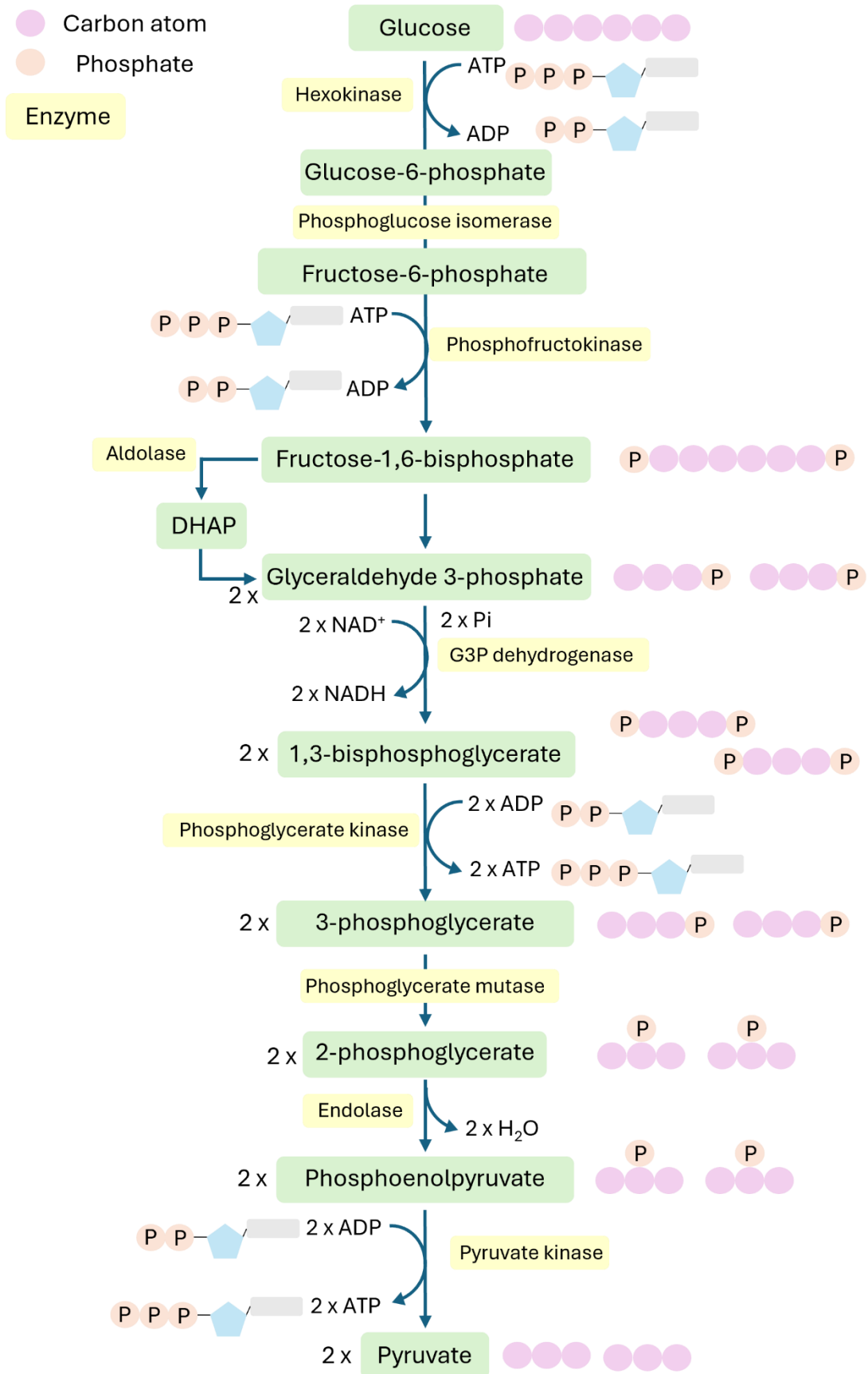


**Figure 1.4, Glycolysis pathway.**

The glycolysis pathway converts one glucose molecule into two pyruvate molecules through several enzymatically controlled steps, producing two ATP molecules in the process.

Glycolysis occurs independently of oxygen, however the fate of pyruvate produced during glycolysis depends on the availability of oxygen and functional mitochondria. In anaerobic conditions, or in cells without mitochondria such as erythrocytes, pyruvate is reduced to oxidise NAD<sup>+</sup> into NADH for ATP production, releasing lactate as a byproduct. This reaction is catalysed by LDH and is fully reversible (185). However, in aerobic conditions pyruvate moves into the mitochondria, entering the TCA cycle. To do this, pyruvate first crosses the outer mitochondrial membrane via passive diffusion through voltage-dependent anion channels (VDACs) (186, 187). It is then actively transported by mitochondrial pyruvate carriers (MPCs) across the inner mitochondrial membrane, using a proton gradient (188).

### **1.3.3 Mitochondria**

The majority of ATP is produced within the mitochondria, mainly through oxidative phosphorylation and thus mitochondria play a central role in metabolism. Mitochondria have a highly specialised structure, containing two membranes which separate the internal matrix from the intermembrane space (189). The inner mitochondrial membrane is folded to form cristae, increasing its surface area to maximise ATP generation via the electron transport chain. Uniquely, mitochondria contain their own mitochondrial DNA (mtDNA), which differs from a cell's genomic DNA.

Mitochondria alter their numbers and morphology to match energy demands whilst also maintaining mitochondrial health by cycling between fission and fusion continuously (190). They do this by dynamically responding to both intrinsic and extrinsic factors (191). A cell's mitochondrial mass is determined by carefully balancing mitochondrial biogenesis to increase mitochondrial number, and mitophagy to remove unwanted or damaged mitochondria (192). This is an important factor in determining a cell's metabolic activity. Cells with a greater mitochondrial mass will produce higher levels of ATP due to their increased capacity for oxidative phosphorylation (193). Mitochondria produce up to 90% of cellular ROS (194). As a consequence of increased ATP production, more ROS will be produced as a byproduct of oxidative phosphorylation (195). If ROS levels become too high, they can become toxic and induce apoptosis (196). Therefore, a cell maintains the

minimum number of mitochondria needed to meet current energy demands whilst limiting ROS production, dynamically adjusting when demands change.

HSCs' preference for glycolysis and restriction of mitochondrial metabolism ensures low levels of ROS are maintained. Low ROS maintains HSC quiescence and 'stemness' by preventing HSC differentiation and lineage commitment (160). Therefore, in low stress, healthy conditions only a very small proportion of oxygen consumed by mitochondria are metabolised into ROS (197).

#### **1.3.4 The TCA cycle**

Within the mitochondria, the TCA cycle, also known as Krebs cycle, is an important part of ATP production, as it produces high-energy electrons (in the form of hydride ions) which can then be used to drive ATP production during oxidative phosphorylation (198). The TCA cycle is an aerobic process which uses acetyl-CoA and therefore pyruvate must first be converted into acetyl-CoA via the enzyme pyruvate dehydrogenase, producing carbon dioxide as a byproduct (199). It is this pyruvate dehydrogenase complex which links glycolysis to the TCA cycle. Whilst in low stress conditions the majority of acetyl-CoA comes from pyruvate produced during glycolysis, acetyl-CoA can also be produced from the oxidation of fatty acids and amino acids (198). The TCA cycle refers to a cyclical series of reactions in which acetyl-CoA combines with oxaloacetate to form citrate. Citrate is then slowly converted back to oxaloacetate through eight step-wise reactions, producing three NADH, one FADH<sub>2</sub> and one GTP per acetyl-CoA molecule, the full steps of which are shown in Figure 1.5 (200). Each glucose molecule produces two pyruvate molecules, thus the products of the TCA cycle can be doubled.

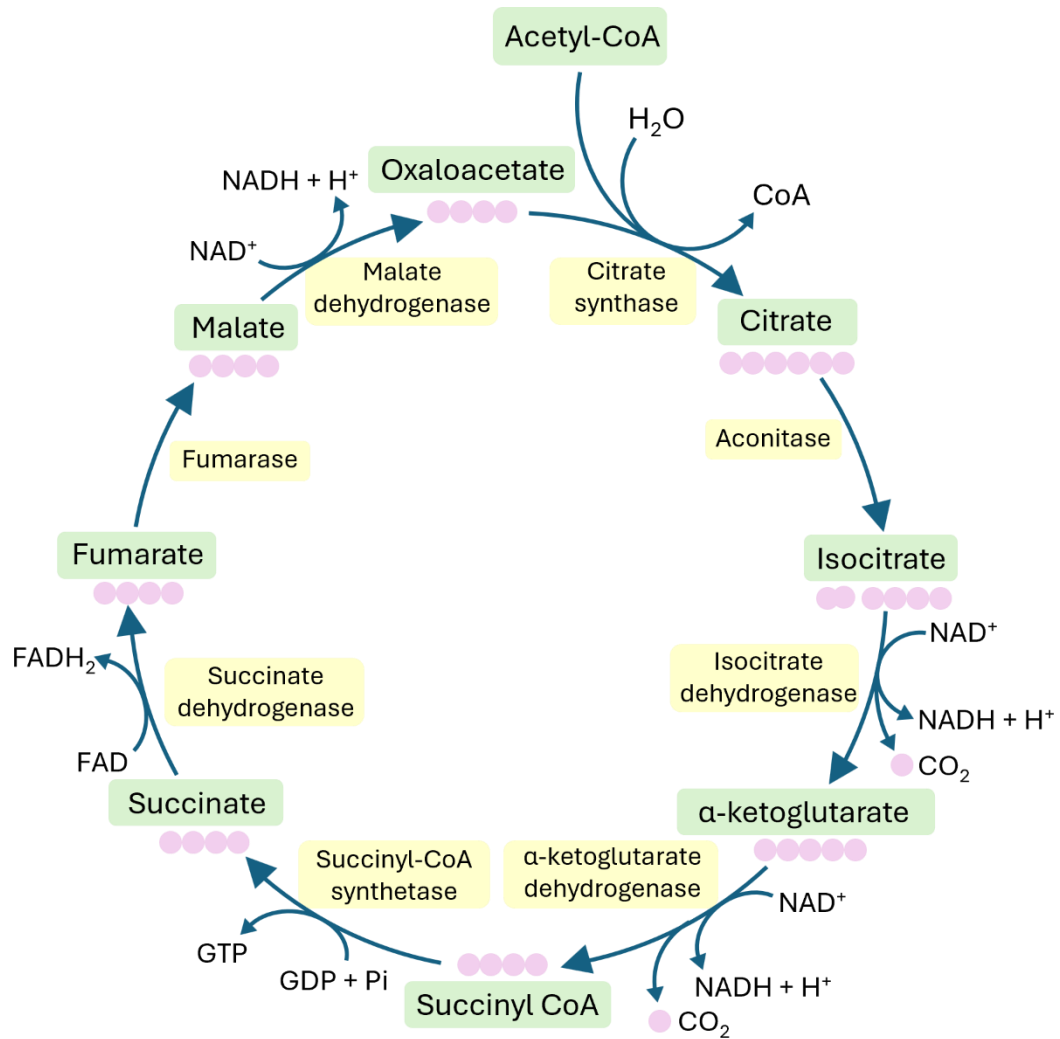


**Figure 1.5, The Tricarboxylic acid cycle.**

Acetyl-CoA feeds into the TCA cycle, which involves eight sequential steps. Acetyl-CoA combines with oxaloacetate to form citrate, which is then slowly converted back to oxaloacetate through eight stepwise reactions, producing two CO<sub>2</sub> molecules, three NADH, one FADH<sub>2</sub> and one GTP per acetyl-CoA molecule.

### 1.3.5 Oxidative phosphorylation

The electron transport chain and proton-motive force was first suggested by Peter Mitchell in the 1960s (201) and is depicted in Figure 1.6. Electrons in the hydride ions of high energy molecules produced during the TCA cycle are used to fuel the electron transport chain (202). Hydrogen atoms from NADH and FADH<sub>2</sub> are split into protons (H<sup>+</sup> ions) and electrons (183). These high energy electrons then enter the electron transport chain. Mitochondrial complex I transfers the electrons from NADH, and complex II from FADH<sub>2</sub> to ubiquinone. Within complexes I and II, ubiquinone is reduced into ubiquinol, transferring electrons to cytochrome C in the process using

complex III. Complex IV then transfers these electrons from cytochrome C to oxygen molecules, generating water in the process (203). During these electron transfers, the energy released fuels the proton transport from the mitochondrial matrix across the inner mitochondrial membrane and into the intermembrane space, creating a proton or electrical potential gradient, referred to as the proton-motive force (204, 205). Due to this proton-motive force, these protons then re-cross the inner mitochondrial membrane to return to the matrix via facilitated diffusion through the channel protein ATP synthase, sometimes referred to as complex V (206). ATP synthase is a large enzyme consisting of multiple subunits including an intrinsic membrane domain ( $F_0$ ) linked to a globular catalytic domain ( $F_1$ ) through a central stalk (207). ATP synthase uses a rotary motor mechanism to catalyse the formation of ATP from ADP and  $P_i$ , utilising the proton-motive force, which drives the rotation of  $F_0$ , subsequently rotating  $F_1$  and ATP synthesis.  $F_0$  is made up of one  $\alpha$ -, two  $\beta$ - and 8-15  $c$ -subunits (208). Each proton enters into a  $c$ -subunit from the intermembrane space, neutralising the negatively charged aspartate residue within the  $c$ -subunit. This charge neutralisation allows the ring of  $c$ -subunits to rotate by one. This process repeats. In most vertebrates, the  $c$ -ring is formed of eight subunits, and therefore eight protons are needed for one full rotation (207). The rotation of the  $F_0$  subunit drives the rotation of the  $F_1$  subunit, promoting ATP synthesis via the binding change mechanism. Three molecules of ATP are produced during one full rotation of the  $F_1$  subunit. NADH and  $FADH_2$  release ten and six protons respectively (209). Therefore, the net ATP synthesis from one glucose molecule from oxidative phosphorylation alone is 28.

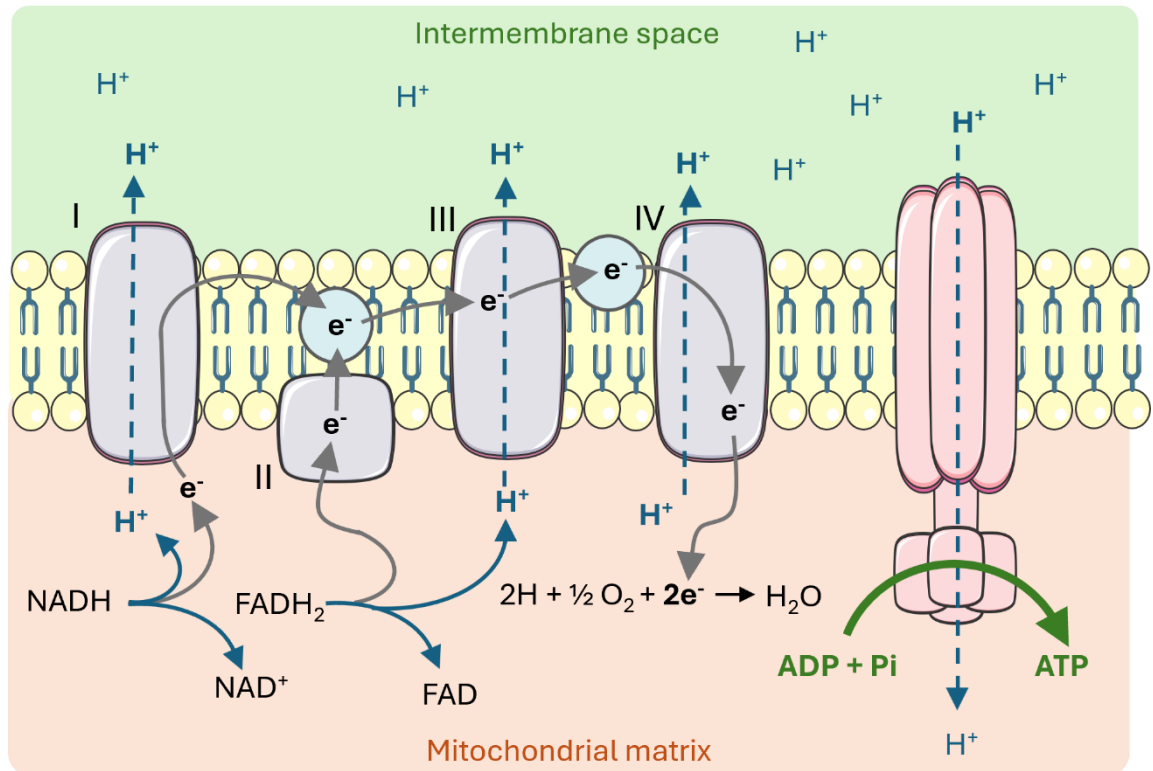


**Figure 1.6, The electron transport chain.**

The electron transport chain is comprised of a series of 5 protein complexes embedded into the inner mitochondrial membrane. Electrons and positively charged hydrogen ions are separated from  $NADH$  and  $FADH_2$  molecules through a series of redox reactions. These travel through protein complexes I-IV, creating a proton motive force.  $ATP$  synthase then utilises this to generate  $ATP$  for energy.

### 1.3.6 Fatty acid metabolism

Lipids including cholesterol and fatty acids are important molecules, forming essential components of cell membranes, metabolic intermediates and can also act as signalling molecules (210). Fatty acid metabolism refers to the synthesis, processing and degradation of fatty acids. Once fatty acids have been taken up into a cell, their fate can be split into two distinctive pathways: oxidation or esterification, controlled by carnitine palmitoyltransferase (CPT) or glycerol-3-phosphotatase acyltransferase (GPAT) respectively (211). Whilst FAO is primarily used for energy generation, esterification is used as part of the storage process (212). Location, cell substrate preference and enzyme availability all influence the metabolism and fate of these fatty acids (213). Multiple varieties of long-chain acyl-CoA synthetases catalyse each fatty acid into their respective acyl-CoAs, which are then channelled into either oxidation or glycerolipid synthesis (211).

When the availability of glucose is low or energy demand is high, the acetyl-CoA needed to fuel the TCA cycle is generated by the  $\beta$ -oxidation of fatty acids (214). Fatty acids are stored primarily as triacylglycerols (uncharged fatty acid esters with a glycerol group attached) within adipose tissue. Once esterified into glycerol-3-phosphate, fatty acids enter the cytidine 5'-diphosphocholine pathway, also known as the Kennedy pathway, first discovered by Kennedy and Weiss in 1956 (215, 216). The end product of this pathway yields the production of either triacylglycerols or phospholipids (217). When needed for energy production, these fatty acids can then be re-mobilised into circulation for cells to take up and metabolise (218). There are three main stages involved in processing fatty acids for energy production: 1) mobilisation, degradation and transport of triacylglycerol releasing fatty acids and glycerol from adipose tissue for other cells to use; 2) activation and subsequent transport of fatty acids into the mitochondria; before 3) these fatty acids are broken down into useable fatty acyl-CoA molecules which can directly feed into the TCA cycle (219).

#### **1.3.6.1 Fatty acid length and structure**

Fatty acids comprise of a long-chain hydrocarbon with a terminal carboxylate group attached and a methyl group at the other end. The vast majority of fatty acids are between 2-24 carbons in length. Short-chain fatty acids (SCFAs) have less than 6 carbons, whilst medium-chain fatty acids (MCFAs) are between 6-12 carbons long. Long-chain fatty acids (LCFAs) are between 13-21 carbons in length and very-long-chain fatty acids (vLCFAs) are anything above 21 carbons (220). Chain length is important, as it affects characteristics such as melting point.

LCFAs come from triglycerides within the food we eat and are absorbed primarily in the jejunum and ileum of the small intestine. They can only enter the lymphatic system once re-esterified and packaged into chylomicrons as triglycerides which then travel through the lymphatic system and into the blood stream through the thoracic duct (221). Whilst some LCFAs are used by cells immediately, the vast majority are processed by the liver and then stored in adipose tissue (222).

SCFAs and MCFAs can be absorbed much faster than LCFAs as they can directly travel from the intestine to the liver via the portal vein and do not require fatty acid

transporter proteins to cross cell membranes (223). SCFAs are primarily produced by bacteria in our gut microbiota within our intestine through anaerobic fermentation of dietary fibre (224, 225). They are important in maintaining intestinal and microbiome health, and are thought to play an anti-inflammatory role, acting as signalling molecules (223). The vast majority of SCFAs are metabolised by enterocytes (intestinal cells) and the liver (223). The majority of MCFAs from our diet are rapidly metabolised into energy and not stored due to their shorter chain length (226).

Fatty acids can be saturated (meaning they contain only single carbon bonds), or unsaturated (contain at least one carbon-carbon double bond). If it contains only one double bond, it is considered monounsaturated, the majority of which are LCFAs between 16-22 carbons in length (220). Polyunsaturated fatty acids contain more than one double bond and can only be synthesised by plants and phytoplankton, and thus are considered an essential part of our diet. Double bonds create bends within the fatty acid hydrocarbon chain, making them more difficult to stack, lowering their melting point and reducing their stability making them much more susceptible to oxidation (227). By comparison, saturated fatty acids are much more stable.

As well as their role as fuel molecules, fatty acids are also important for the synthesis of phospholipids and glycolipids, essential for cell membrane structure and function (228). Additionally, many important proteins have fatty acids covalently attached, allowing them to anchor within cellular membranes. This is especially important for many transport proteins to allow the movement of molecules into and out of and within cells. Furthermore, fatty acids are required during the production of many important hormones and intracellular messengers and thus form an important part of many signalling and regulatory pathways (227).

#### **1.3.6.2 Cholesterol**

Cholesterol is either absorbed from our diet or synthesised within cells, the majority of which occurs in the liver (229). It is not only an important component of the phospholipid bilayer but also plays a key role in many metabolic processes. For example, cholesterol is a precursor molecule in the synthesis of vitamin D and steroid hormones such as cortisol, testosterone and oestrogen (230). Within the cell membrane, cholesterol helps regulate membrane fluidity and permeability.

Additionally, it can interact with adjacent lipids and bind to multiple transmembrane proteins to aid conformational changes (231). Cholesterol is an important component of bile acid synthesis, which is needed to aid dietary lipid absorption within the intestine (232).

### **1.3.6.3 Fatty acid transport**

An important characteristic of fatty acids is their hydrophobicity. LCFAs are particularly water insoluble. Therefore, in order to be transported in circulating plasma, they must either become esterified, remain non-esterified but loosely bound to albumin, or combine with a glycerol molecule to form triacylglycerol which can then be packaged into lipoproteins (233).

#### **1.3.6.3.1 Lipoproteins**

Lipoproteins are molecules specially synthesised to transport hydrophobic lipids through hydrophilic liquids such as blood plasma (234). Lipoproteins consist of phospholipid and apolipoprotein outer shell with a triglyceride or cholesterol centre, the most common being high-density lipoprotein (HDL), low-density lipoprotein (LDL) and very-low-density lipoprotein (vLDL) as well as chylomicrons (235). Cholesterol (via HDL and LDL) and triglycerides (via vLDL) are transported through blood within these lipoproteins. Apolipoproteins provide lipoproteins with structural stability, for example apolipoprotein B (apoB) forms an essential structural component of nearly all lipoproteins including vLDL (236).

#### **1.3.6.3.2 Fatty acid transport proteins**

The cell membrane phospholipid bilayer comprises of a hydrophilic head of glycerol attached to a phosphate group which is connected to a hydrophobic tail made of two fatty acid chains. The tails of two monolayers of these phospholipids face together to form the cell or organelle membrane. The composition of the phospholipid bilayer including its cholesterol content directly affects its fluidity and thus function (237). A large number of important proteins undergo post-translational modification, including lipidation (attachment of a lipid to the protein), which is important for protein trafficking, localisation and stability (238). Lipidation includes palmitoylation and myristylation, where palmitic and/or myristic acid is covalently bound to the

protein and is often used to anchor it to the cell membrane (239, 240). Other types of lipidation include prenylation, glycosylphosphatidylinositol anchors and cholesterylation (238). These are often referred to as lipid-anchored proteins. Whilst research into how many fatty acid transporter proteins are anchored to the membrane is very limited, it is likely that they do so by lipidation. Research in this area is limited partly due to the difficulty in purifying membrane bound proteins in their native environment. Many have to be purified in non-authentic environments, making it difficult to study the true anchoring (241). Additionally, membrane bound proteins are inherently difficult to express, purify and then crystallise to solve the structure (242).

Lipidation, or more specifically palmitoylation has so far only been identified in CD36, an important LCFA transporter protein (238, 243). Palmitoylation is essential for localisation of CD36 to the plasma membrane and its ability to uptake fatty acids (244-247). The extracellular binding domain of CD36 binds LCFAs, and through conformational changes not fully understood, allows the fatty acids to cross the phospholipid bilayer and into the cell (248-250). However, more recent studies have demonstrated the importance of dynamic switching between palmitoylated and depalmitoylated states in CD36-mediated LCFA transport. Depalmitoylation allows for CD36 to detach from the membrane and re-localise within the cytoplasm. Holding CD36 in either its palmitoylated or depalmitoylated state completely prevented CD36 fatty acid uptake (245, 251), implicating the importance of CD36 being able to switch between being membrane bound to the cell surface and its internalisation to inside the cytoplasm for fatty acid transport.

Other membrane proteins have been identified as fatty acid transporters including fatty acid binding proteins (FABPs) and fatty acid transport proteins (FATPs) (252, 253). FABPs are a family of intracellular lipid chaperones important for lipid trafficking. There are at least nine distinctive members of the FABP family which bind both saturated and unsaturated fatty acids along with other lipids, allowing their uptake into cells (250, 254). The six member FATP family not only facilitate fatty acid uptake but also play an important role in regulating it (255).

#### 1.3.6.4 Fatty acid oxidation

FAO can be broken into three main stages: 1) the activation of fatty acids, 2) transport of these activated fatty acids into the mitochondrial matrix and 3) FAO. Once inside the cytosol, fatty acids are then shuttled through the cell to the mitochondria by FABPs. For the LCFAs to enter the mitochondria, they have to be enzymatically activated into fatty acyl-CoA via fatty acyl-CoA synthetase on the mitochondrial membrane (256). Next, carnitine palmitoyl transferase 1A (CPT1A) catalyses the transfer of the fatty acyl from the Coenzyme A to carnitine to form fatty acyl-carnitine which can then be transported into the mitochondrial matrix via a translocase for FAO (257, 258). Without CPT1A, fatty acids would be unable to enter the mitochondria, and thus it is often considered the rate limiting enzyme of FAO (213, 257).

Once inside the mitochondrial matrix, the fatty acyl group is transferred back to Coenzyme A to reform fatty acyl-CoA, a reaction catalysed by carnitine palmitoyl transferase II (CPT2) (259). The fatty acyl-CoA then goes through a sequence of four reactions together termed  $\beta$ -oxidation. The  $\beta$ -carbon of the fatty acid chain is successively oxidised to remove two carbon atoms from the carboxyl terminal end of the fatty acyl-CoA to produce one acetyl-CoA molecule, and a fatty acyl-CoA that is now two carbons shorter than it was at the start. The now shortened fatty acyl-CoA will repeat the four steps shown in Figure 1.7 until two acetyl-CoA molecules are produced in the final step (260, 261). Each of the enzymes involved in  $\beta$ -oxidation represent families of enzymes which contain members that are specific to different chain lengths. For example, acyl-CoA dehydrogenase includes long-chain, medium-chain and short-chain acyl-CoA dehydrogenase or LCAD, MCAD and SCAD respectively (262). The acetyl-CoAs produced during  $\beta$ -oxidation are then used to fuel the TCA cycle and subsequently the electron transport chain as described above. LCFA metabolism produces around double the amount of ATP than glucose when compared per mole, however when also taking into account the time taken to process fatty acids, the efficiency of fatty acid metabolism is comparable to that of glucose metabolism (263).

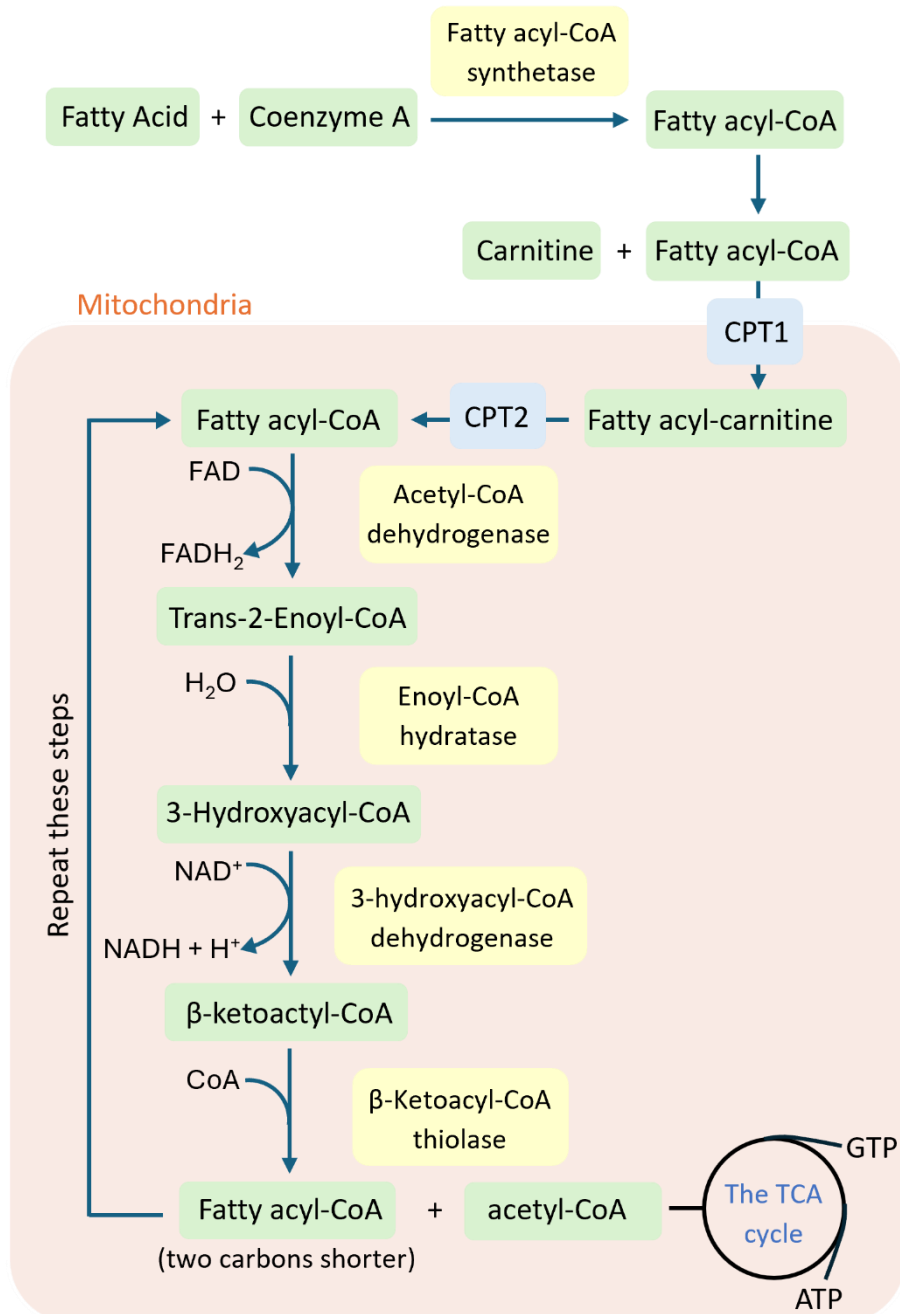


**Figure 1.7, Fatty acid oxidation.**

Activated fatty acids are transported into the mitochondria where they then undergo fatty acid oxidation (FAO), which comprises of four steps. Each cycle of FAO shortens the fatty acid chain by two carbons, producing acetyl-CoA in the process. This continues until two acetyl-CoA molecules are produced and the fatty acid has been fully oxidised.

Whilst mitochondria are the primary site for medium and long-chain FAO, a distinct subset of fatty acids including vLCFAs, branched-chain fatty acids and bile acid intermediates are oxidised within peroxisomes (264). vLCFAs do not rely on carnitine to be transported into peroxisomes and instead use ATP-binding cassette transporter (ABC) transporters fuelled by ATP (265). However, peroxisomes are not equipped for

the TCA cycle and subsequent metabolic pathways (266), and thus the acetyl-CoA produced during FAO is shuttled out of peroxisomes and into neighbouring mitochondria (267).

#### **1.3.6.5 Ketogenesis**

Whilst the majority of acetyl-CoA produced during FAO is used by the TCA cycle, during periods of increased energy demands the amount of acetyl-CoA being produced can exceed the amount which can be processed by the TCA cycle due to limited amounts of intermediates. When this occurs, to prevent an excessive and potentially toxic build-up of acetyl-CoA and to increase ATP production, the cell can use ketogenesis (268). When fatty acids are metabolised during ketogenesis, acetone, acetoacetate and beta-hydroxybutyrate molecules are produced (269). These ketones are water-soluble lipids, meaning that they do not need to be transported by lipoproteins.

The primary site of ketogenesis is within the mitochondria of liver cells (270). Acetoacetyl-CoA is produced via acetyl coenzyme A acetyltransferase (ACAT) from two acetyl-CoA molecules (271). Next, acetoacetyl-CoA is converted into HMG-CoA, catalysed by HMG-CoA synthase, which is then subsequently converted into acetoacetate (272). Acetoacetate can then either be decarboxylated into acetone, an enzyme free reaction, or catalysed into beta-hydroxybutyrate using beta-hydroxybutyrate dehydrogenase (273). These ketones are then transported to target cells, where they are converted back into acetyl-CoA where they then enter the TCA cycle and oxidative phosphorylation to produce ATP (274).

#### **1.3.6.6 Master regulators of fatty acid metabolism**

Whilst the majority of cells are able to utilise fatty acids for synthesis of cellular components, energy production and for the formation of lipid droplets, the availability of circulating fatty acids is tightly controlled. Metabolism can be regulated over both longer and shorter time scales. Long-term regulation of metabolism, especially between tissues, relies on slower acting molecules including hormones (275). Whereas shorter-term regulation at a cellular level utilises changes in genes

expression of enzymes and regulatory factors to coordinate a tissue specific response.

Prolonged elevation of circulating lipid levels is a prominent risk factor for cardiovascular disease and associated metabolic diseases, which collectively account for the leading cause of global mortality (276). Fatty acid metabolic regulation encompasses not only fatty acid uptake and synthesis, but also the storage, oxidation and secretion of these fatty acids (277). There are two main groups of transcriptional regulators of enzymes involved in fatty acid metabolism: the sterol regulatory element-binding protein (SREBP) family and the peroxisome proliferator-activator receptor (PPAR) family (278). These two families work alongside other transcription factors such as retinoid X receptor (RXR) and liver X receptor (LXR) (279).

#### **1.3.6.6.1 The PPAR family**

The biggest and arguably most important family of metabolic regulatory genes is the PPAR family. This family of nuclear receptors play an important regulatory role in transcription of genes linked to lipid metabolism as well as in inflammation and cell growth (280, 281). PPARs are able to bind and be activated both by cellular fatty acids as well as their metabolites, and thus act as a cardinal transcriptional sensor for fatty acids (282). In general, when activated PPARs form a heterodimer with RXR, which can then bind to promoter regions on specific DNA sequences called peroxisome proliferator response element (PPRE), recruiting coactivator complexes that activate transcription of target genes (283-285).

PPARs can be divided into three main isoforms: PPAR $\alpha$ , PPAR $\delta$  and PPAR $\gamma$  (278). *In vivo*, each isoform is differentially distributed within different tissues, allowing for a unique function despite many structural and functional similarities (284, 286). PPAR $\alpha$  was the first to be identified, and plays a role in fatty acid uptake, esterification and trafficking. It is also important in the regulation of lipoprotein metabolism genes (287). Its primary role is thought to be mobilisation and catabolism of fatty acids (279). For example, PPAR $\alpha$  regulates the expression of fatty acid synthase (FAS), the enzyme which helps catalyse lipogenesis (the synthesis of fatty acids from other metabolites such as glucose and amino acids), in particular palmitate (C16) (288). It

has also been shown to affect CD36 and FATP expression, CPT1 and thus FAO (289). PPAR $\alpha$  is highly expressed in skeletal muscle, heart and liver tissue (284). Fatty acids can bind and act as ligands to PPAR $\alpha$  (290), creating a negative feedback loop.

PPAR $\delta$  regulates mitochondrial function and fatty acid desaturation to increase lipid and glucose usage (280). In particular, it has been shown to play a role in regulating SREBP-1c and lipogenesis (291). Due to this, PPAR $\delta$  is ubiquitously expressed but still plays an essential role in skeletal muscle, liver and adipose tissue metabolic function (282, 292). The primary natural ligand for PPAR $\delta$  is also fatty acids (293). Finally, PPAR $\gamma$  has been shown to regulate fatty acid uptake and the formation and storage of triglycerides, thereby increasing glucose metabolism (280, 294). It has been shown to regulate fatty acid uptake by regulating the expression of CD36 and FATP receptors. PPAR $\gamma$  has also been shown to regulate SCD-1, an important part of fatty acid metabolism (295). The highest expression of PPAR $\gamma$  is found in adipose tissue, although certain isoforms are expressed in multiple tissues (296).

PPARs are expressed in HSCs (295). For example, PPAR $\delta$  activation has been shown to enhance the regenerative capacity and maintenance of HSCs, and this is reversed in models using bone marrow specific deletion of PPAR $\delta$  (174). Blocking FAO using etomoxir also prevented the benefits of PPAR $\delta$  activation in a similar way to PPAR $\delta$  deletion. This provides evidence that PPAR $\delta$  is an activator of FAO and highlights the importance of FAO in HSC maintenance.

#### **1.3.6.6.2 SREBP family**

Cellular lipid metabolism and homeostasis are controlled via a regulatory feedback system, which is at least in part modulated by the SREBP family of transcription factors (210, 297). Whilst SREBPs are initially assembled and bound to endoplasmic reticulum membranes in their inactive form, when intracellular levels of cholesterol and fatty acids drop below a certain threshold, SREBPs are proteolytically cleaved from the membrane. These now free SREBPs travel to the nucleus and trigger the transcription of genes related to lipid uptake synthesis (298). Inversely, excess intracellular levels of lipids inhibits SREBP activation and cleavage, thus reducing cellular lipid uptake until levels stabilise (297).

Within the SREBP family, different members have been shown to have distinctive roles within lipid metabolism (299). For example, SREBP-1c takes more of a role within fatty acid synthesis (lipogenesis) and energy storage, whilst SREBP2 regulates cholesterol. SREBP-1c regulates the expression of important lipid synthesis associated enzymes such as FAS and stearoyl-CoA desaturase, to help regulate lipid metabolism within the liver (300). Polyunsaturated fatty acids can suppress the expression of SREBP-1c and inhibit the maturation of the SREBP-1c protein. This in turn causes the suppression of SREBP-1c target genes including FAS and ultimately the downregulation of fatty acid and triglyceride synthesis (301).

#### **1.3.6.6.3 Other central metabolic regulators**

Other well-known lipid transcription factors include LXR, which is a master regulator for cholesterol homeostasis (302, 303). LXR forms a heterodimeric complex with RXR, binding to DNA to regulate the transcription of target genes (304). LXR has also been shown to be involved in lipogenesis, and *in vivo* activation of LXR induced expression of SREBP-1c, and increased circulating triglyceride levels (305). Disruptions in the LXR gene resulted in the deficiency of multiple lipogenic genes including FAS (306). RXR has also been shown to play an important role in lipid metabolism. As well as LXR, RXR can form heterodimers with retinoic acid receptors (RARs) (307). The RAR/RXR complex has been shown to regulate lipid metabolism including lipid synthesis and bile acid production (308). RAR/RXR regulates fibroblast growth factor 21 (FGF21) expression, an important growth factor also implicated in lipid homeostasis (309). *In vitro*, cells overexpressing RAR had increased FGF21 production and enhanced FAO (308). Thus, LXR and RXR are both important regulators of lipid metabolism, and in particular are highly expressed in the liver (279), one of the major organs involved in systemic fatty acid regulation and metabolism.

## **1.4 Haematopoiesis in response to stress**

Whilst haematopoiesis in general remains relatively homeostatic, this is not the case during stress. Stress-mediated changes to the bone marrow microenvironment subsequently impact resident HSCs and overall bone marrow function (279). This is in part caused by increased proinflammatory cytokine production often accompanying other pathophysiological changes found within the bone marrow during disease, both acute and chronic (310). For example, during stress, such as acute infection or severe blood loss, a state of emergency haematopoiesis can be triggered, during which HSCs undergo rapid expansion to produce up to 10-fold more downstream differentiated immune cells (311). Many pathologies including leukaemia and ageing trigger significant morphological and functional alterations in HSCs and their downstream immature progenitors, and this is normally accompanied with dysregulated metabolic reprogramming (163). Despite the initial immune response being critical in response to infection and damage, prolonged, chronic inflammation can create a cycle of increased damage and prevent healing (312, 313). This emphasises the need for an appropriate and fast immune response during stress.

### **1.4.1 Haematological malignancies**

Like all cancers, haematological malignancies alter their surrounding microenvironment to support tumour cell proliferation, angiogenesis, and metastasis, referred to as the tumour microenvironment (314). Haematological malignancies can be broadly separated into lymphomas, myelomas and leukaemias (315). Cancer cells often have far greater energy demands than their healthy counterparts and therefore rewire multiple metabolic pathways to sustain their high levels of proliferation and enhanced survival (316). Haematological malignancies are no exception to this, and it has been well established that leukaemia stem cells have increased mitochondrial mass, oxidative phosphorylation and catabolism of TCA cycle metabolites (317-319). Whilst leukaemia stem cells have been shown to rely on oxidative phosphorylation, leukaemia blast cells rely heavily on glycolysis for ATP production (316). In fact, highly glycolytic acute myeloid leukaemia (AML) blasts collected from patients were much more resistant to chemotherapy compared to

moderately glycolytic AML blasts (320, 321). This demonstrates the importance of metabolism in haematological malignancy progression and treatment. The loss of either pyruvate kinase or lactate dehydrogenase in bone marrow cells significantly extended the latency period of AML (172), further highlighting the importance of metabolism in leukaemia progression.

#### **1.4.2 Chemotherapy and Radiation**

Both solid and haematological malignancies are still commonly treated with radiation or chemotherapy, both of which create a stressful environment for haematopoiesis (322). Both chemotherapy and ionising radiation are considered carcinogens and thus can cause long-term damage to the bone marrow microenvironment, including apoptosis and senescence in proliferating haematopoietic progenitor cells, as well as damage to the HSCs themselves (323-325). If severe enough, this can result in bone marrow failure (326). In the short-term, unlike more mature, proliferative haematopoietic cells, HSC's quiescence enhances their ability to resist radiation induced apoptosis, in part due to their enhanced ability to repair DNA damage through p53 and Ku70 expression (327, 328). Many chemotherapies can be very damaging to the bone marrow. Chemotherapy can cause myeloablation, loss of osteoblasts and increased adiposity (329, 330). It has also been associated with major damage to blood vessels and sympathetic nerves. This impairs signalling within the bone marrow microenvironment, resulting in loss of HSC mobilisation and compromises haematopoietic recovery (331, 332).

Due to significant improvements in early detection and available treatment options, the number of cancer patients reaching remission and surviving at least five years is also increasing (333). Whilst this is initially good, unfortunately these survivors have significantly increased risk of developing serious treatment-related side effects including secondary cancer, and long-term bone marrow injury which can cause hypoplastic anaemia and myelodysplastic syndrome (323, 331). This demonstrates the need to understand chemotherapy and radiation induced alterations to the bone marrow and HSCs. This will aid the development of new strategies to protect against long-term bone marrow failure and irreversible HSC damage. One such example demonstrating the benefits of this comes from studies demonstrating that inducing

HSC cell cycle arrest before administering chemotherapy can help protect against HSC exhaustion (334). Additionally, mice given SCF and TPO within two hours of total body irradiation had increased survival rates (335). These examples demonstrate the possibility of reducing chemotherapy and radiation damage. However, more work is required to find safe and effective options that do not affect the desired anti-cancer effects of the treatment itself.

### **1.4.3 Ageing**

Frailty describes the progressive decline of a person's physical and cognitive health and is commonly associated with ageing. Frailty significantly impacts immune function, exponentially increasing the risk of an elderly individual being hospitalised for an infection by up to 78% (336, 337). Over one million patients were hospitalised for infection in England in just one year, two-thirds of those admitted were aged over 65 (338). Ageing populations in many westernised countries highlight the importance of understanding how the immune system responds to infection to aid the development of better therapeutic strategies and reduce the burden it places on healthcare systems.

HSCs age with us, accumulating damage at the genetic level. Organelle function including mitochondrial health also declines with ageing (339). Reduced regenerative potential and a shift towards a pro-inflammatory microenvironment are both hallmarks of HSC ageing. Increased oxidative phosphorylation increases ROS levels in aged HSCs, which contributes to the loss of HSC quiescence, with many HSCs becoming permanently active (160, 340, 341). This coupled with diminished mitochondrial health and function could be contributing to HSC exhaustion often seen in frail individuals (342). Furthermore, aged HSCs display a bias towards myeloid cell production, significantly increasing the risk of myeloproliferative diseases and certain myeloid malignancies, including both chronic and acute myeloid leukaemia (343, 344).

### **1.4.4 Infection**

The first line of defence against an infection is the innate immune response, which quickly but non-specifically reacts to pathogens (345). Pattern recognition

molecules, either expressed as receptors on innate immune cells, bound to the extracellular matrix or circulating within the blood are responsible for the initiation and regulation of the innate immune response (346). They recognise pathogen-associated molecular patterns (PAMPs) as well as damage-associated molecular patterns (DAMPs). There are several classes of pattern recognition receptors (PRRs), including toll-like receptors (TLRs), C-type lectin receptors and nucleotide-binding and oligomerisation domain (NOD)-like receptors (347). PRRs on the surface of phagocytes including macrophages, neutrophils and dendritic cells aid the phagocytosis of pathogens and unwanted cells. Phagocytosis refers to the engulfment of pathogens, debris and unwanted cells into phagosomes, which then fuse to nearby lysosomes to allow the necessary enzymes access to degrade and digest the captured matter (348-351). Macrophages and other phagocytes can also present antigens from the phagocytosed pathogens to nearby lymphocytes to facilitate the activation of the adaptive immune response (352). In response to pathogens, PRRs, including those on phagocytes, activate nuclear factor  $\kappa$ B (NF- $\kappa$ B), type I interferon and other inflammasome signalling pathways. This results in the production of a myriad of proinflammatory cytokines and chemokines, some of which are responsible for initiating the adaptive immune response (353). This acute inflammatory response is also accompanied by vasodilation and vascular leakage, regulated by endothelial cells (354, 355). This allows for easier immune cell infiltration to the site of infection, allowing for efficient phagocytosis of pathogens and damaged cells (356) and helping to efficiently clear the infection.

During an infection, the massive increase in proinflammatory signals triggers a state of emergency haemopoiesis, significantly increasing the volume of blood cells being produced (15, 331). Central to this response, HSCs themselves can sense and appropriately respond to pathogen-derived molecules, adjusting their migration patterns and replication cycles (357-359). The bone marrow microenvironment also plays a key role in HSCs response to infection. For example, the endothelial cells lining blood vessels within the bone marrow can also sense pathogens (331).

Lipopolysaccharide (LPS) is a PAMP produced by *Escherichia coli* (*E. coli*). It increases endothelial cell expression of Toll-like receptor 4 (TLR4) and myeloid differentiation primary response 88 (MyD88), both important factors in neutrophil

recruitment (360). This then subsequently increases G-CSF secretion and activation of emergency granulopoiesis (361, 362). Granulocytes are a critical part of the innate immune response to infection, however due to their phagocytic function and degranulation, they have a short lifespan of only a few days (363). Therefore, there is an immense demand for granulopoiesis to produce vast numbers of basophils, neutrophils and mast cells (364). Increased levels of G-CSF also decreases the number of macrophages within the bone marrow, which is then thought to mobilise HSC and progenitor cells as part of the immune response (101, 365, 366). However, G-CSF has also been shown to negatively affect HSC repopulating abilities, reducing self-renewal capacity (367). This happens independently of, and thus does not affect, HSC homing. Mechanistically, G-CSF increases Toll-like receptor 2 (TLR2) expression on HSCs and induces HSC expansion (367). This demonstrates the importance of the bone marrow microenvironment and stem cell niche in helping to coordinate the haematopoietic response to infection.

#### **1.4.4.1 Use of LPS as a model of infection**

LPS is the primary component of the outer membrane of nearly all gram-negative bacteria including *E. coli* (368, 369), and thus is commonly used to model infection. LPS, normally administered intraperitoneally, causes a powerful immune response. LPS is indirectly sensed by TLR4, a transmembrane receptor which is widely expressed on immune cells, including myeloid cells such as monocytes, macrophages and dendritic cells. TLR4 is unable to directly bind LPS, and instead the lipid A component of LPS on gram-negative bacteria is recognised and bound by LPS binding protein (LBP), a glycoprotein synthesised by the liver (370). This complex combined with CD14 triggers the TLR4 signalling cascade and subsequent immune response (371). Activated TLR4 subsequently leads to NF- $\kappa$ B activation, a powerful pro-inflammatory transcription factor, which then triggers the production of several pro-inflammatory cytokines and chemokines and helps to orchestrate the wider immune response (372).

Furthermore, LPS also induces the sharp increase in ROS seen in many infections. As part of the pro-inflammatory response to infection, ROS levels sharply rise (373). This is because ROS are key signalling molecules helping to drive the inflammatory

response. ROS levels measured in mice treated with LPS were comparable to mice treated with l-buthionine-sulfoximine (BSO), a known inducer of intracellular ROS (374). This LPS-induced increase in ROS could be reversed by pre-treating these mice with the ROS scavenger N-acetyl-cysteine (NAC) (375). Thus, demonstrating LPS specific induction of ROS in the innate immune response.

However, whilst LPS activates the TLR4 signalling pathway and increased ROS production found in response to most bacterial infections, this model is missing the virulence factors often secreted from the bacterial cell itself (376). Other TLRs and PRRs are then activated by these virulence factors, further supporting the immune response (377). Therefore, using LPS to model bacterial infections may not accurately represent the full immune response. That being said, it has been shown to closely mimic many, and thus is still widely used as an infection model both *in vivo* and *in vitro*.

#### **1.4.4.2 *Salmonella typhimurium***

The most common cause of nontyphoidal *Salmonella* infection is the *Salmonella typhimurium* (*S. typhimurium*), a rod-shaped gram-negative bacterium (378). It can spread through foodborne transmission and thus remains a threat in both developed and developing countries (379). *S. typhimurium* induces a pro-inflammatory response in the intestine, essential for its successful colonisation (380, 381). This is because inflammation causes intestinal dysbiosis, allowing *S. typhimurium* to colonise (382). *S. typhimurium* uses a type III secretion system to replicate (383). Once these bacteria have crossed the intestinal epithelial barrier, they are recognised by TLRs located on the outer membrane of the cell or within intracellular vesicles (384). Activated TLRs then initiate a downstream signalling cascade through MyD88 and TIR-domain-containing adapter-inducing interferon- $\beta$  (TRIF), which results in NF- $\kappa$ B and interferon regulator factor 3 (IRF3) transcription factor activation and the production of multiple proinflammatory cytokines including IL-8, IL-1 $\beta$  and type I interferon (385).

Mouse models are often used to study *S. typhimurium* infection, however disease presentation differs between species, and thus mouse models do not fully represent human infection (386). Despite this, it is thought that the proinflammatory immune

response is very similar between host species as well as between other intestinal bacterial infections(387). Thus, the use of *S. typhimurium* in mouse models is a helpful tool to study the immune response to bacterial infections.

#### **1.4.4.3 Treatments for infection**

The body's immune system response is not always sufficient to clear infections effectively, which lead to the use of antibiotics to improve treatments and outcomes. Most bacterial infections are treated with antibiotics, whilst fungal infections are more commonly treated with antifungal medicines. Antibiotics can be split into two main categories: bactericidal and bacteriostatic antibiotics, both of which can target the metabolism of the bacterial cell to elicit these effects (388). Bacteriostatic antibiotics prevent cell growth and proliferation, downregulating key cellular pathways including glycolysis and the TCA cycle (389). Alternatively, bactericidal antibiotics target essential functions within the cell, damaging the cell beyond repair and inducing cell death (390). Many do this through the upregulation of the electron transport chain and dysregulation of the TCA cycle (388). This highlights the importance of understanding metabolism in infection.

#### **1.4.4.4 The role of inflammation in the immune response**

Inflammation is often referred to as the central host response to infection, and is caused by the activation of the innate immune response by a diverse array of harmful stimuli including pathogens, damaged cells, irradiation and toxic compounds, many of which trigger PRRs (386, 391). Inflammation is an important defence mechanism, aiding the removal of the damaged or harmful cells, initiating healing processes (392). Several of these inflammatory signals have also been linked to activation of the extrinsic coagulation cascade, which is thought to help limit the spread of the pathogen (393). Innate immune cells such as neutrophils and macrophages are recruited to the site of inflammation, driven by these signals (394). As well as phagocytosis, these recruited cells also secrete multiple cytokines including the pro-inflammatory factors tumour necrosis factor- $\alpha$  (TNF- $\alpha$ ), interleukin (IL)-1 $\beta$  and IL-6 (395), making them an essential part of the pro-inflammatory immune response.

Inflammation promotes HSC expansion and subsequent differentiation into immune cells (396). The inflammatory cytokines produced in response to infection can directly influence HSC function or act on cells within the surrounding HSC niche, triggering BMSCs, endothelial cells and other mature haematopoietic cells to secrete secondary inflammatory signals (397). For example, TNF- $\alpha$  is a key player in the inflammatory response. TNF- $\alpha$  has been shown to induce myeloid progenitor cell apoptosis, but can promote HSC survival through an NF- $\kappa$ B dependant mechanism (398). Other key proinflammatory signals produced as part of the innate immune response include type 1 interferon, IL-1 $\beta$ , IL-6 and G-CSF (399-402). Many of these cytokines have been studied using single-cytokine stimulation mouse models. Prolonged and unresolved chronic inflammation can cause HSC myeloid bias and subsequent reduction in the ability to produce lymphoid cells (403), but may not necessarily prevent HSCs from returning to dormancy (404).

#### **1.4.4.5 The SREBP family and the immune response**

Studies have started to link lipid metabolism to the wider immune response to infection. For example, the regulation of the SREBP family has been shown to be important in preventing the toxic overproduction of proinflammatory cytokines in macrophages treated with LPS (299, 405). LPS stimulated mTOR activation causes the proteolytic cleavage and thus activation of SREBPs, which results in increased cholesterol uptake within macrophages. At the same time, to prevent a toxic build-up of cholesterol, a negative feedback loop overrides SREBP2 activation and thus suppresses cholesterol synthesis within LPS-activated macrophages (405). Without these suppressive mechanisms, the toxic overaccumulation of cholesterol within the mitochondria of macrophages would cause mitochondrial DNA to leak into the cytosol and trigger IL-1 $\beta$  secretion and thus further proinflammatory responses (406). This demonstrates the importance of SREBP regulation within the immune response.

## **1.5 Energy requirements in stressed haematopoiesis**

Infection can influence HSC biology, either directly by the pathogen itself or indirectly through the proinflammatory cytokine response and changes within the bone marrow microenvironment (397, 407). Stress such as acute infection, triggers a state of emergency haematopoiesis, during which HSCs expand more rapidly to produce up to ten-fold more downstream differentiated immune cells (408). Without HSC expansion and subsequent emergency granulopoiesis, the effectiveness of the innate immune response would be compromised. Any delay in the immune response exponentially increases the risk of significant morbidity and mortality from infection. In particular, older patients, immunocompromised patients, and those with other comorbidities such as obesity are at greatest risk of impaired immunity.

HSCs are able to transition from quiescence to active cell cycling, partly due to factors secreted within their niche, but also due to dynamic alterations in HSC metabolism (163, 409). Major transcriptional and metabolic changes associated with HSC division are well documented (162, 410-413). To cope with the rapid expansion of HSCs during emergency haematopoiesis, HSCs increase their energy production by switching from low ATP-yielding glycolysis to high ATP-yielding mitochondrial oxidative phosphorylation. It is this metabolic switch which provides enough energy to enable rapid HSC expansion and differentiation into downstream progeny to increase the immune cell pool and effectively clear the infection. For this metabolic switch to occur, there needs to be enough healthy mitochondria for ATP production and adequate fuel to drive the necessary production of cellular components.

### **1.5.1 Increased mitochondrial mass via mitochondrial transfer**

Increasing mitochondrial mass has been shown to benefit HSCs during stress (339). Whilst there are multiple ways for a cell to increase its mitochondrial mass, the most obvious is to increase the number of mitochondria within the cell via mitochondrial biogenesis. However, studies have demonstrated that an initial increase in HSC mitochondrial mass occurs within 2 hours of LPS administration, preceding any upregulation of mitochondrial biogenesis genes (375). Therefore, other alternative but faster methods to allow HSCs to increase their mitochondrial content have been studied. One such example is the process of transferring mitochondria between two

neighbouring cells, termed functional mitochondrial transfer, which was first described by Spees et al. It allows cells to quickly alter their mitochondrial mass, either by releasing unwanted mitochondria to reduce their mitochondrial mass or internalizing mitochondria released from other cells to increase it (414). Mitochondrial transfer therefore allows cells to quickly alter their mitochondrial mass whilst bypassing the need for mitochondrial biogenesis or mitophagy (the selective degradation of mitochondria via autophagy) (415).

Whilst there are several different methods by which mitochondrial transfer can occur, studies have demonstrated that HSCs utilise the transfer of mitochondria through direct cell-cell contact via gap junctions (416). *In vivo* transplant models support the role for mitochondrial transfer, demonstrating that BMSCs in the surrounding HSC niche transfer their mitochondria to HSCs in response to LPS. This led to a reduction in BMSC mitochondrial mass (375).

Mechanistically, the increase in ROS as part of the pro-inflammatory response to infection has been shown to drive this mitochondrial transfer from BMSCs to HSCs. Pre-treating mice with NAC and thus reducing ROS levels prevented this LPS-driven mitochondrial transfer from BMSCs to HSCs (375). The importance of ROS in this process has also been demonstrated in other cell types. For example, human fibroblast cell lines treated with BSO to induce ROS had increased mitochondrial mass and mtDNA content (417, 418). Increased ROS activates phosphatidylinositol 3 kinase (PI3K) and drives the subsequent mitochondrial transfer from BMSCs to HSCs via connexin 43 (CX43) gap junctions (375). PI3K has been shown to regulate the activation of HSCs following LPS stimulation through an IL-1 $\beta$  dependent mechanism (399). Infection-induced increases in ROS levels have also been shown to activate PI3Ks and drive emergency granulopoiesis (373). Pharmacological inhibition of either PI3K or CX43 gap junctions blocked mitochondrial transfer in response to LPS (375). The reliance of PI3K activation for CX43 connections has been further demonstrated by other studies (419) and although the literature is limited, taken together these studies demonstrate the role of ROS induced PI3K activation to drive CX43 gap junction-mediated mitochondrial transfer from BMSCs to HSCs in response to infection. The ability to rapidly transfer mitochondria into HSCs provides

the necessary machinery to increase ATP production and allow emergency haematopoiesis to occur efficiently.

### **1.5.2 HSC fatty acid uptake and utilisation**

Whilst increased mitochondrial mass is important, without the necessary fuel to drive ATP production, the extra mitochondria transferred to HSCs are unable to effectively support rapid HSC activation and proliferation. The LCFA transporter CD36 is expressed on many haematopoietic cells including HSCs (420). The expression of CD36 on HSCs significantly increases in response to infection (421). This allows HSCs to increase their fatty acid uptake. Loss of CD36 prevented fatty acid uptake into HSCs, impairing HSC cycling and expansion (420, 421). Furthermore, loss of CD36 has also been shown to directly affect the rate of FAO (422), highlighting the importance of CD36 on HSC fatty acid uptake and FAO, and thus subsequent ATP production.

Although it is not yet fully understood how CD36 is regulated, it is thought that it is at least partly regulated by transcription factors linked to FAO such as the PPARs including PPAR $\alpha$  (423). PPAR $\alpha$  is an important component of the infection response (424). Studies have demonstrated that activation of PPARs can affect the expression of CD36 (425, 426). Therefore, it is possible that mechanistically CD36-mediated fatty acid uptake into HSCs in response to infection is centred around the availability of circulating fatty acids themselves via master regulators of lipid metabolism such as the PPAR family. Increased levels of intracellular lipids in HSCs correlated with increased FAO and subsequent oxidative phosphorylation in mice treated with both *S. typhimurium* and LPS (421). Once inside the cell, the fatty acids transported into HSCs by CD36 must enter the mitochondria via CPT1A ready for FAO. Loss of CPT1A resulted in loss of quiescent HSCs, with increased HSC differentiation without self-renewal (427). Thus, loss of CPT1A in hematopoietic cells resulted in defective HSCs, demonstrating the importance of fatty acid in HSC metabolism. Additionally, a HSC and progenitor cell specific knockdown of CPT1A demonstrated that loss of CPT1A, and thus fatty acid transport into the mitochondria, prevented HSC expansion in response to LPS (421). This highlights HSC's reliance on FAO to produce enough ATP for HSC expansion during emergency haematopoiesis.

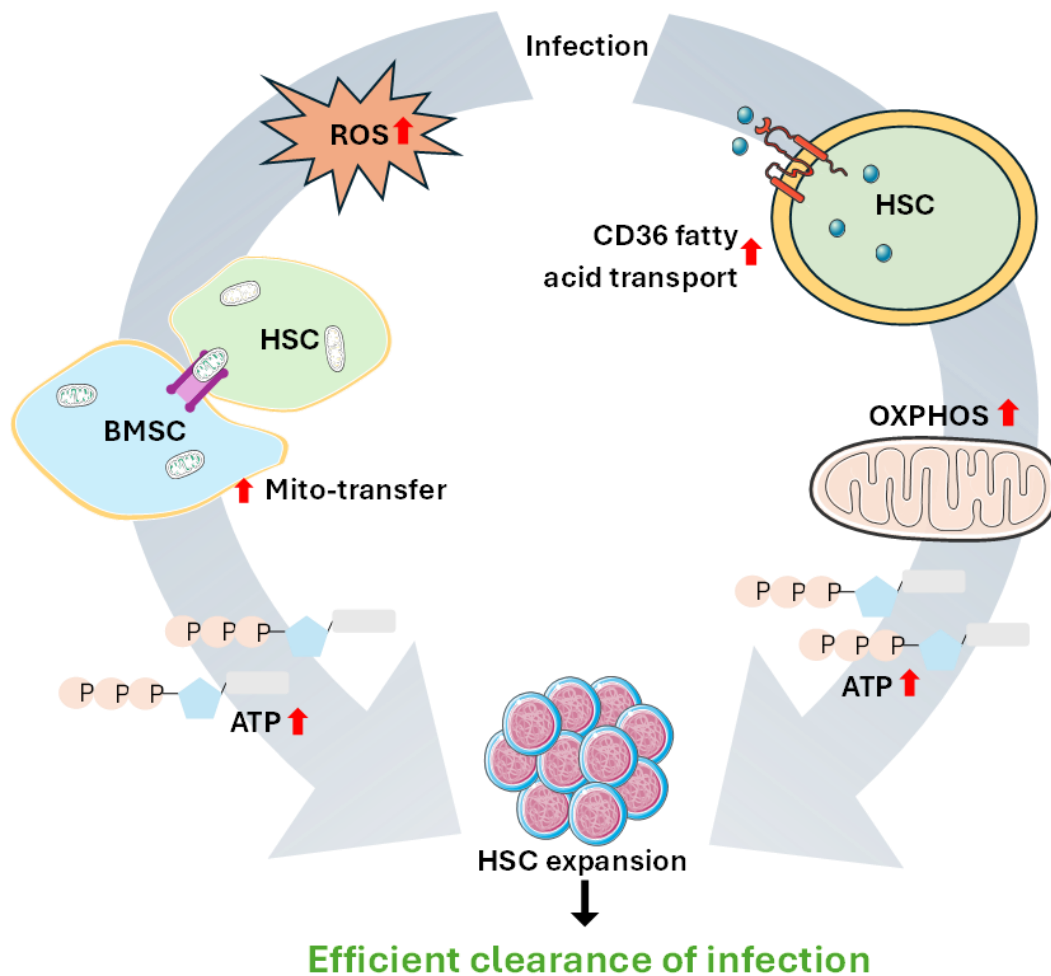


**Figure 1.8, Mechanism for haematopoietic stem cell expansion in response to infection.**

In response to infection, BMSCs transfer mitochondria to HSCs. HSCs increase CD36 expression to allow for increased LCFA uptake. Together this then allows HSCs to produce enough energy to rapidly expand and produce enough downstream immune cells to coordinate an effective immune response.

### 1.5.3 Dysregulation of HSC expansion e.g. ageing/ obesity

Delays due to dysregulation of HSC expansion and thus the innate immune response to infection significantly increases the risk of mortality and infection-related morbidities. Examples of this come from models of ageing and obesity. Studies using aged mice have shown that in response to LPS, aged mice are unable to increase their HSC and progenitor cell numbers in a manner normally seen in young mice (428). However, this loss of HSC expansion occurs independently of defects in mitochondrial transfer, as aged mice are still able to efficiently transfer their mitochondria between cells (428). Instead, it is associated with the age-related decline in mitochondrial health, meaning that the transferred mitochondria are more

damaged and thus less functional in aged mice (429). Therefore, it is likely that the transfer of non-functional mitochondria from aged BMSCs to aged HSCs is part of the cause of loss of HSC expansion seen in ageing. This can be partially restored by targeting age-related changes in BMSCs to improve mitochondrial health (428). Chronic infection can result in a decline in HSC function, a reduction in repopulating capacity and a bias towards the myeloid lineage (397). Myeloid bias is commonly described in ageing and thus, chronic infections are thought to accelerate the ageing phenotype.

Metabolic disorders such as obesity have also been associated with a premature ageing phenotype, including mitochondrial dysfunction and increased CD36 expression (430). For example, CD36 knockout mice are more resistant to diet induced obesity (431). This highlights a role for CD36 in obesity. Furthermore, obesity causes a chronic pro-inflammatory state with increased ROS and cytokine production associated with HSC and immune dysfunction and increases the risk of HSC exhaustion (432). Whilst the effect of obesity on HSC expansion during infection is still widely undefined, obesity has been shown to affect mitochondrial transfer in other immune cells. For example, within white adipose tissue, obesity impairs adipocyte mitochondrial transfer to macrophages, which forms part of the normal immune response (433).

## **1.6 The regulation of fatty acid availability**

Lipids either come from diet or can be synthesised during *de novo* fatty acid biosynthesis. This occurs primarily in the liver and adipose tissue (434) and thus are the main two tissues involved in fatty acid metabolism and regulation. In health, nearly all cells take up exogenous fatty acids to meet their lipid requirements, and thus lipogenesis is primarily restricted to hepatocytes within the liver and adipocytes (435). Briefly, the liver synthesises fatty acids before then exporting them within lipoproteins to provide other cells within the body with energy and structural components for building membranes (436). Whereas in adipose tissue, the fatty acids are used for long-term energy storage (437). However, many other factors are involved in the regulation of fatty acid availability including inflammation and metabolic disorders.

### **1.6.1 Adipose tissue**

Adipose tissue can be divided into two main types: white adipose tissue (WAT) and brown adipose tissue (BAT). Up to 70% of cells in adipose tissue are adipocytes, fat cells derived from mesenchymal stem cells (438, 439). Other cell types found in adipose tissue include macrophages, pericytes and endothelial cells (440). Structurally, white adipocytes contain one large lipid droplet, whereas brown adipocytes contain multiple smaller lipid droplets and a much higher mitochondrial content (440). This makes them specialised for different functions. Brown adipocytes primarily burn fatty acids to generate heat, a process called thermogenesis, whilst white adipocytes' main role is for fatty acid storage (438, 441). Storage (lipogenesis) and release (lipolysis) of fatty acids by adipocytes is carefully controlled, primarily by insulin and leptin (442). Patients with lipodystrophy have dysfunctional adipose tissue, causing fatty acids to be taken up and stored in hepatocytes instead, resulting in metabolic dysfunction-associated steatosis liver disease (MASLD), formerly known as non-alcoholic fatty liver disease (NAFLD) (443). This highlights the importance of adipose tissue in the regulation of fatty acids.

### **1.6.1.1 Uptake and storage**

In a well-fed state, the majority of dietary fatty acids released from lipoproteins by the enzyme lipoprotein lipase (LPL) are taken up and stored in WAT (444). LPL is synthesised within adipocytes before being transported to the luminal surface of capillaries within adipose tissue. The vLDL receptor (vLDLR) is highly expressed in multiple tissues including adipose tissue and skeletal muscle, but not in the liver. vLDLR allows adipose tissue to take up triglyceride rich vLDL particles. Once taken up, LPL hydrolyses and releases the triglycerides within the vLDL particle as fatty acids which can then be taken up into adipocytes for use by the cell or for storage. For storage, these fatty acids are esterified into triglycerides and stored within lipid droplets (445).

The main fatty acid transporter in both BAT and WAT is CD36, which is localised in caveolae within the plasma membrane, facilitating fatty acid uptake via caveolae-dependent endocytosis (251). Additionally, loss of or defects within caveolae proteins such as caveolin-1 results in lipodystrophy and dysfunctional WAT (446, 447). Unlike in other cells, in adipocytes CD36 is usually already palmitoylated and localised on the cell surface, ensuring that it is ready to capture and transport any extracellular fatty acids (244), however fatty acid endocytosis is still tightly controlled by the dynamic palmitoylation of CD36 (448).

### **1.6.1.2 Export**

Adipose tissue releases fatty acids from lipid droplets through the process of lipolysis, which involves several steps including multiple acylglycerol lipases such as adipose triglyceride lipase (ATGL), hormone-sensitive lipase (HSL) and monoacylglycerol (MGL), depicted in Figure 1.9. The fatty acids released from WAT are non-esterified fatty acids (NEFAs), also known as free fatty acids, meaning they can circulate in the plasma when bound to albumin (449).

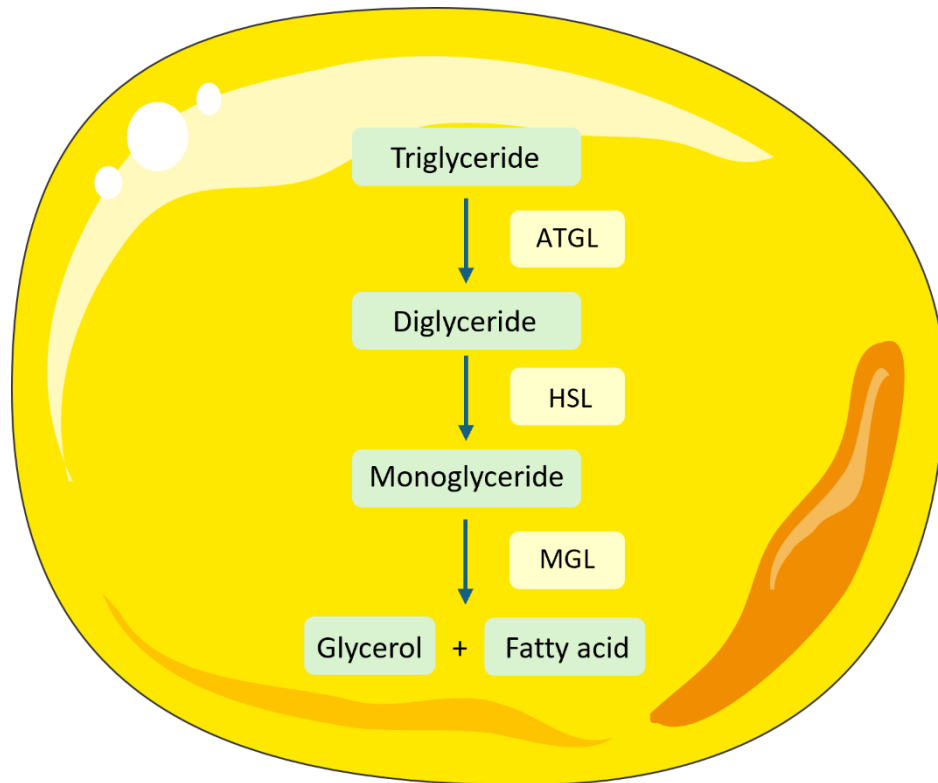


**Figure 1.9, Lipolysis pathway.**

Adipocytes release fatty acids via lipolysis. Stored triglycerides are hydrolysed into diglycerides and glycerol, catalysed by ATGL. Diglycerides are hydrolysed into monoglycerides and glycerol, catalysed by HSL and monoglycerides are hydrolysed into fatty acids and glycerol, catalysed by MGL. These fatty acids can then be exported out of the adipocyte.

In a fasted state, WAT releases the stored fatty acids via lipolysis as NEFAs for the liver to then take up and metabolise to produce ketones to fuel the brain, heart and skeletal muscle (448). Release of fatty acids from WAT is also triggered when the body temperature drops in cold conditions, or in response to liver or skeletal muscle damage. When cold, WAT releases fatty acids for the BAT to take up and utilise to generate heat and maintain optimal internal temperature (450). In response to damage, fatty acids released from WAT are taken up into the damaged tissue to fuel regeneration (451).

### 1.6.2 The liver

The liver is a diverse and complex organ central to many critical bodily functions including control of blood volume, supporting the immune system, detoxification of drugs including xenobiotics and metabolism (452). The liver is central for lipogenesis,

gluconeogenesis and cholesterol metabolism and thus acts as a major site for the synthesis, storage and redistribution of lipids, proteins and carbohydrates (453). In health, the liver is the primary organ responsible for regulating fatty acid metabolism to meet systemic energy requirements by coordinating the uptake, storage and release of lipids (277). This works in both fasted and fed states. Whilst the liver does oxidise lipids when needed, it is also responsible for processing, packaging and secreting excess lipids as triglyceride-rich vLDLs for storage in other tissues including adipose tissue (454). In health, the liver stores only small amounts of fatty acids in the form of triglycerides and is equipped to deal with short-term fluxes in free fatty acids levels. However, excessive or chronic elevations in fatty acid levels can lead to pathologically increased lipid accumulation within the liver (455). This can cause chronic inflammation and fibrosis, resulting in the development and progression of liver diseases including MASLD. The liver is also responsible for producing cholesterol and also plays an important role in glucose metabolism, as it is not only able to store glucose as glycogen but also increase glucose availability when required through gluconeogenesis (452).

#### **1.6.2.1 Liver cellularity and structure**

The liver is the largest internal organ, accounting for nearly 2% of an adult's total body weight (456). It is located just below the diaphragm in the upper supracolic part of the abdomen. Structurally, the liver is formed of 4 lobes. The right lobe is the largest, with a smaller left lobe. The posteromedial caudate and quadrate lobes are functionally considered part of the right lobe. The liver is a highly vascularised organ, requiring nearly a quarter of all blood that is pumped from the heart, but uniquely receives supply from both arterial and venous supplies (457). Around 25% of the blood supply to the liver comes from the hepatic artery, providing oxygenated blood, whilst the remaining 75% comes from the portal vein, which carries nutrient-rich blood from the stomach, small and large intestine (458). Branches of the hepatic artery and portal vein along with the bile duct form the portal triad, found at the peripheries of hepatic lobules. Hepatic lobules are the functional hexagonal structures of the liver, with each containing a central vein. The portal triad connects to each corner of the hexagonal lobule (459). In order to carry out its complex role, the liver contains many different specialised cell types, the most important of which are detailed below.

### **1.6.2.2 Hepatocytes**

The most common cell type in the liver are hepatocytes, a type of specialised epithelial cell accounting for around 80% of all liver cells. They play a central role in metabolism and blood detoxification (460). Hepatocytes are also important for the synthesis and secretion of key immune regulatory proteins including LPS binding protein (LBP), C-reactive protein and other complement proteins (460, 461). Many of these proteins are considered acute-phase proteins and are produced rapidly after stimulation and thus are often elevated in response to bacterial infections (462, 463). These proteins can either then directly target the pathogen themselves or orchestrate and help coordinate a larger immune response. Hepatocytes respond to multiple pro-inflammatory cytokines including IL-6, IL-1 $\beta$  and TNF- $\alpha$ , producing vast quantities of these acute phase proteins via signal transducer and activator of transcription factor 3 (STAT3) and NF- $\kappa$ B signalling pathways (464). Many of these pro-inflammatory cytokines are produced by immune cells, and thus hepatocytes can be considered to form part of the downstream immune response.

### **1.6.2.3 Kupffer cells**

Kupffer cells account for nearly 90% of all tissue resident macrophages, making them by far the largest population found outside of the bone marrow itself. They are a key component of not only the hepatic but also the systemic response to pathogens (465). Kupffer cells are also important in monitoring blood circulating through the liver, endocytosing debris, damaged cells and other harmful materials (466). This includes the recycling of damaged and unwanted erythrocytes, and thus they play a role in haematopoiesis. In response to stress, such as infection, Kupffer cells can rapidly differentiate into mature macrophages to form an important part of the inflammatory immune response (467). For example, activated Kupffer cells can secrete large volumes of pro-inflammatory cytokines including TNF- $\alpha$ , IL-1 $\beta$  and IL-6 (468).

Kupffer cells can act as a sensor for free fatty acids. Free fatty acids have been shown to bind to TLR4 receptors on the surface of Kupffer cells (469). In response to elevated levels of free fatty acids, Kupffer cells release pro-inflammatory cytokines including TNF- $\alpha$ . This secreted TNF- $\alpha$  then binds to TNF-receptor 1 on hepatocytes, increasing

free fatty acid uptake, *de novo* lipogenesis, and triacylglycerol synthesis. However, this can result in increased triacylglycerol storage and eventual steatosis (an accumulation of fat within the liver) (469). Therefore, chronic elevation of fatty acids, such as in obesity can drive liver steatosis and associated liver diseases. Interestingly, this Kupffer cell TLR4-mediated pathway also acts in response to increased LPS (360).

#### **1.6.2.4 Biliary epithelial cells**

Biliary epithelial cells, also called cholangiocytes, line the intra- and extrahepatic biliary tree (470, 471). Cholangiocytes account for between 3-5% of total liver cells, with varying size and functions depending on their location within the biliary tree (472-474). They play a crucial role in lipid metabolism, and in particular cholesterol metabolism but also fatty acid metabolism, partly due to their important role in bile acid synthesis and transport. Bile acids form an important part of lipid metabolism and are formed from catabolism of insoluble cholesterol. Bile acids help facilitate the digestion and absorption of dietary lipids and fat-soluble vitamins including vitamins A, D and E (475). The biliary tree encompasses a network of ducts and vessels responsible for transporting newly synthesised bile acids to the gallbladder and duodenum. The cholangiocytes lining this network contain mechanoreceptors to monitor the flow of bile as well as multiple bile acid transporters, modifying bile acids via both secretion and absorption aiding bile acid modification (476, 477). These modified bile acids are then transported to the duodenum to aid with lipid absorption. Furthermore, bile acids themselves have also been shown to be potent modulators of lipid metabolism (478), further supporting the important role of cholangiocytes in bile acid and thus lipid metabolism.

Beyond their role in bile acid modification and transport, studies have also shown that cholangiocytes primarily express LXR $\beta$  and PPAR $\delta$ . Cholangiocytes treated with either LXR $\beta$  or PPAR $\delta$  agonists had increased expression of the cholesterol pump ABCA1, which in turn increased cholangiocyte cholesterol export (479). Cholesterol secreted into the biliary tree is transported to the duodenum, where a proportion is then excreted within faeces (480).

### **1.6.2.5 Sinusoidal endothelial cells**

Liver sinusoidal endothelial cells (LSECs) help to regulate substance exchange and hepatic blood flow by acting as a selective barrier between the nutrient-rich blood and the space of Disse where hepatocytes and hepatic stellate cells are located (481). LSECs cells can be identified from other endothelial cell populations by their C-type lectin domain family 4-member (CLEC4M) and CLEC4G expression on their cell surface (482). They make up around 15% of all liver cells but only 3% of total liver volume and thus are small in size (483). LSECs play an intermediary role in the exchange of lipids including fatty acids between the blood and hepatocytes through two main mechanisms. Small lipoproteins are able to freely pass through the fenestrae (transcellular pores within LSECs) to be taken directly up into hepatocytes, and larger or more complex lipids can be actively transported by LSECs via endocytosis into the space of Disse (484). The differentiation and lipid homeostasis via LSECs is maintained by BMP9, VEGF and WNT signalling pathways (482). Multiple liver diseases which affect metabolism such as MASLD and fibrosis causes the de-differentiation of LSECs, causing them to become dysfunctional and impair fenestrae. This causes the release of pro-inflammatory cytokines and impaired lipid transport, causing an accumulation of lipids within hepatocytes (485). Therefore, LSECs play an important role in lipid metabolism and homeostasis in the liver.

### **1.6.2.6 Hepatic stellate cells**

Hepatic stellate cells account for around 5% of total liver cells and are located alongside hepatocytes in the space of Disse. Hepatic stellate cells are the main site of vitamin A (or retinol) storage, accounting for around 80% of total vitamin A reserves, which is primarily stored as retinyl palmitate (486). Because vitamin A is an essential fat-soluble vitamin, retinyl palmitate and other retinyl esters are stored in lipid droplets within hepatic stellate cells (486, 487). When activated, hepatic stellate cells transform into myofibroblasts and subsequently lose their lipid droplets (488). This means that the body's main store of vitamin A is depleted which can affect immune system function and vision.

### 1.6.3 Liver fatty acid regulation

#### 1.6.3.1 Fatty acid uptake and synthesis

The liver obtains fatty acids either by taking up circulating fatty acids both directly and indirectly from lipoproteins and residual chylomicrons or by *de novo* lipogenesis (489). The liver proportionally takes up free fatty acids or NEFA circulating in the blood depending on their current concentration via transporter proteins. Unlike in adipose tissue, CD36, FATP2 and FATP5 have all been shown to be important in hepatic fatty acid uptake. Loss of any of them using knockout mouse models has been shown to significantly decrease hepatic triglyceride levels (490-494). Whereas enhanced palmitoylation and thus increased plasma membrane localisation of CD36 has been shown to be involved in the development of liver diseases and is associated with dysregulated lipid metabolism (495).

FABP1 is also highly expressed in the liver and has also been shown to be important in liver fatty acid uptake, transport and metabolism, particularly for LCFAs but also for other lipid ligands (496). Within hepatocytes, fatty acids with more than 14 carbons covalently bind to and activate FABPs or acetyl-CoA synthetases located primarily on the outer mitochondrial matrix, transporting them into the mitochondria for FAO (497). Some FABPs and acetyl-CoA synthetases are found within microsomes and these can transport NEFAs into the nucleus to interact with transcription factors, regulating fatty acid metabolism genes (498). *In vitro*, the overexpression of FABP1 in human hepatocytes significantly increased fatty acid uptake (499). CD36 has been shown to participate in fatty acid uptake and storage as well as secretion of triglycerides (500). CD36 has also been shown to negatively regulate lipophagy, the process of releasing fat from lipid droplets, within liver cells (501). Thus, LCFA transport proteins are important for fatty acid uptake into the liver.

The liver is also able to synthesise fatty acids via *de novo* lipogenesis using the three critical enzymes acetyl-CoA carboxylase (ACC), FAS and stearoyl-CoA desaturase-1 (SCD1) (502). ACC enzymatically converts acetyl-CoA into malonyl-CoA, which in turn is then converted into palmitate by FAS (503). SCD1 converts stearoyl-CoA and palmitoyl-CoA into oleate and palmitoleate (504). These newly synthesised fatty

acids can then undergo modifications such as elongation and desaturation before being stored or exported (503).

### **1.6.3.2 Cholesterol synthesis and degradation**

The liver is the only known organ capable of degrading and eliminating large quantities of cholesterol via hepatocytes. Cholesterol synthesis is regulated via end-product feedback inhibition of 3-hydroxy-3-methylglutaryl CoA reductase (HMGCR), the rate limiting step in cholesterol biosynthesis from fatty acids (210). Cholesterol uptake is mediated by the LDL receptor (LDLR) (505). A portion of the lipoprotein cholesterol taken up is then enzymatically converted to bile acids, which are then conjugated to amino acids to form bile salts (506). Cholesterol 7 $\alpha$ -hydroxylase (CYP7A1) is the rate-limiting cytochrome P450 enzyme involved in this conversion and is only known to be highly expressed within hepatocytes (475), highlighting the unique role of the liver in processing cholesterol.

### **1.6.3.3 Fatty acid storage and export**

Hepatic fat acts as an important source of fatty acids which can be mobilised to supply energy (507, 508). For efficient regulation of fatty acid availability, the liver, in particular hepatocytes, needs to be able to store and release fatty acids as needed (277). Fats stored within hepatocytes comes from three main sources: directly from diet, *de novo* lipogenesis and uptake of circulating NEFAs primarily derived from adipose tissue lipolysis (509).

Unlike in adipocytes, where the storage of fat has been studied extensively, control of lipid storage in the liver is still poorly understood (211). This is partly because even though hepatocytes store fat in lipid droplets similarly to adipocytes, they only express HSL at very low levels (211, 510). Recent studies have instead demonstrated that hepatocyte nuclear factor 4 $\alpha$  (HNF4 $\alpha$ ) may instead be responsible for hepatic fat mobilisation. Fatty acids binding directly to the ligand binding pocket of HNF4 $\alpha$  regulate its activity which in turn influences the rate of lipophagy (508). Only a small amount of the triglycerides produced within the liver are stored locally within hepatocyte lipid droplets (511). The majority of the hepatic triglycerides are packaged into vLDL particles, which are then secreted out of the liver and into circulation to fuel

the rest of the body (512). In hepatocytes, vLDLs are synthesised within the endoplasmic reticulum. In the presence of triglycerides, ApoB is partially lipidated into a primordial vLDL particles. This can then fuse with triglyceride-rich particles to become nascent vLDL, which is then transported to the Golgi via protein transport vesicles (236). Once in the Golgi, they are glycosylated further (513). Mature vLDL particles are then transported to the plasma membrane and secreted into the circulation (236, 512).

#### **1.6.4 Liver fatty acid regulation**

Hepatocyte triacylglycerol content is regulated through a careful balance of fatty acid uptake coupled with hepatic FAO and triacylglycerol export (277). Regulation of hepatic fatty acid metabolism is complex, involving the harmonious interaction of hormones, nuclear receptors, transcription factors and intracellular signalling pathways (453). Furthermore, fatty acids themselves are also able to regulate lipid metabolism in general by binding to nuclear factors controlling gene transcription, adding to this complexity (278). FAO and fatty acid synthesis are mainly regulated by two pathways: PPAR $\alpha$  and the LXR/SREBP, both of which can cross regulate each other too (514), highlighting the complexity of fatty acid metabolism regulation. For example, LXR is a key regulator of hepatic lipogenesis. LXR upregulates SREBP-1c, a known regulator of hepatic lipogenesis, FAS, SCD1 and ACC (515). Hepatocyte-specific SREBP-1c overexpression upregulated these FABP key *de novo* lipogenesis enzymes and subsequently hepatic lipid accumulation (516), highlighting the importance of careful regulation of hepatic lipid metabolism. LXR also forms heterodimers with RXR, known to be important in liver lipid metabolism. Liver specific RXR knockout mice had increased accumulation of triglycerides and cholesterol within their liver. Furthermore, within hepatocytes, the nuclear receptor PPAR $\alpha$  has been shown to positively regulate FAO, the expression of FATPs, ketogenesis and gluconeogenesis, but negatively regulate amino acid catabolism and inflammation (283, 287). Glucose and fatty acid metabolism are also interlinked, as insulin signalling plays an important role in fatty acid metabolism (517). Changes to liver fatty acid uptake, synthesis and export not only influences hepatic energy metabolism, but also whole-body energy metabolism and thus often contributes towards multiple metabolic associated diseases (518).

### 1.6.5 The liver and the immune response

Whilst its main role is metabolism and detoxification, more recently the liver has been shown to play an important role within the immune response. As part of the gut-liver axis, the liver regularly receives both dietary and commensal bacterial products which can trigger an inflammatory response (519). PRRs expressed on hepatocytes and Kupffer cells quickly recognise, bind to and phagocytose DAMPs and PAMPs delivered via the portal vein (520, 521). Normally, these hepatocytes and Kupffer cells degrade these microbial patterns including LPS before inflammatory mediator production can occur, preventing a full immune response being triggered (519). This is partly due to Kupffer cells producing anti-inflammatory cytokines including IL-10 and prostaglandins, which downregulates antigen presentation and thus prevents T cell activation and the adaptive immune response (522, 523). This, combined with the continuous, dynamic regulation of hepatic metabolism, results in regular but controlled inflammatory responses (524).

Inflammation, generated by liver-resident immune cells and non-haematopoietic cells, plays an essential role in liver homeostasis (519). Inflammatory cytokines released into the circulation from sites away from the liver can be detected by hepatocytes within the liver, triggering the systemic acute phase response (APR) and IL-6 production (525, 526). The APR aids haematopoietic white blood cell production and subsequent immune cell infiltration at the site of inflammation, but also attempts to prevent an excessive inflammatory response. It does this by several approaches, including limiting Kupffer cell TNF- $\alpha$  production (527). Additionally, any cell death or damage in the liver occurring due to injury or infection triggers hepatocytes themselves to release DAMPs, which activates surrounding hepatocytes, hepatic stellate cells and liver-resident immune cells. Activated cells then release inflammatory cytokines including IL-1, IL-6, TGF- $\beta$  and TNF- $\alpha$ , aiding leukocyte infiltration and initiation of fibrosis (528). Fibrosis is an essential part of the liver repair mechanism. Hepatic stellate cells become activated and proliferate, increasing production of extracellular matrix proteins such as collagen (529). This enables tissue regeneration and allows the liver to return to homeostatic conditions, resolving the inflammatory response (519). Multiple inflammatory cytokines have been shown to be important in liver regeneration, including IL-6 (530). IL-6 helps drive

hepatocyte proliferation and mice with targeted disruption of IL-6 have reduced hepatocyte proliferation and impaired liver regeneration (531). Furthermore, as well as its role in metabolism, PPAR $\alpha$  has also been shown to be important in inflammatory cytokine regulation. It is thought that in the liver IL-1 and IL-6 production are at least partly controlled by PPAR $\alpha$ . Using fenofibrate, a PPAR $\alpha$  agonist, attenuated both IL-1 and IL-6 production and prevented the APR response both *in vitro* and *in vivo* (532). This demonstrates the importance of inflammation in the immune response and liver regeneration as well as its close links to metabolic regulation.

### **1.6.6 The role of inflammation in fatty acid availability**

Levels of circulating fatty acids exponentially increase in response to infection. This has been observed in both animal models as well as humans (421, 533, 534). The pro-inflammatory response is thought to play an important part of this increase. For example, in both pre-clinical models and human studies, IL-6 has been shown to stimulate lipolysis, regulating downstream FAO genes such as PPARgamma coactivator 1 (PGC1)- $\alpha$  (535, 536). This provides a direct link between the inflammation, IL-6 and FAO. IL-6 levels are consistently high in a variety of different infections including COVID-19 and bacterial infections, and this correlates with increased circulating fatty acids (537). The importance of IL-6 is further supported by the fact that pharmacologically inhibiting IL-6 in healthy human volunteers caused a reduction in levels of circulating fatty acids, but did not affect glucose levels, lipolysis or FAO (538). Contrastingly, healthy human volunteers given recombinant IL-6 had a significant increase in systemic circulating fatty acids and FAO, however glucose was still unaffected (539). Mouse models of stress including infection and fasting also show similar findings, demonstrating increased IL-6 levels, which correlated with increased serum fatty acids (400, 421, 540). Using either an IL-6 neutraliser or an IL-6 knockout model to reduce IL-6 levels partially reversed the increase in circulating free fatty acids seen in response to infection (421, 540). Taken together, this data supports the argument that the availability of circulating fatty acids increases in response to infection, however how this occurs is currently still unclear but a role for IL-6 is strongly possible. Despite this, the aforementioned studies only measured free fatty acid levels in general and did not measure individual lipid species.

## 1.7 Rationale

In the UK alone, over 1 million patients are admitted to hospital with serious infections each year with a median length of stay of 3 days (338). On average it is estimated that the daily cost of patient care on a general admissions ward is nearly £600 per patient. Thus, serious infections cost the NHS over a billion pounds each year, demonstrating a real need to improve therapeutic strategies to manage infections and reduce the burden they present on healthcare systems. Infection is a major area of research, with many research groups investigating the role of HSCs in the infection response. Therefore, it is well established that HSCs rely on free fatty acids to fuel their rapid expansion during infection triggered emergency haematopoiesis. This expansion is a critical part of the acute immune response. However, the source of these fatty acids fuelling HSC expansion is currently unclear. This study aims to understand the mechanisms regulating the availability of free fatty acids during infection. It is important to understand how the immune system functions in a healthy state, as findings can then be used to help identify new therapeutic targets, with the aim to improve patient outcomes. Additionally metabolic associated diseases, such as obesity, may affect how these fatty acids are regulated and thus lead to an impaired immune response. Understanding the immune response in healthy individuals can be used as a baseline for identifying how it becomes dysregulated during disease.

## **1.8 Hypothesis**

This project hypothesises that acute infection driven changes in the availability of circulating free fatty acids is mediated by the inflammatory response. Furthermore, it hypothesises that targeting certain inflammatory cytokines can prevent the accumulation of free fatty acids in response to infection and that this will impact HSC expansion.

## **1.9 Aims and objectives**

1. To characterise the kinetics of circulating fatty acids in response to LPS.
2. To determine the role of the liver in regulating the availability of fatty acids in response to LPS.
3. To identify the factor(s) involved in regulating liver fatty acid metabolism in response to LPS.
4. To investigate the impact of preventing the increase of circulating free fatty acids in response to LPS on HSC expansion.

## 2 Materials and methods

### 2.1 Materials

In this study, all reagents and materials used are described below. Reagents were obtained from the indicated manufacturers.

**Table 2.1, Reagents used with manufacturer and catalogue number.**

Agilent (Santa Clara, CA, USA), Amazon (Seattle, WA, USA), ATCC (Manassas, VA, USA), BD Biosciences (Franklin Lakes, NJ, USA), Biolegend (San Diego, CA, USA), Cambridge Bioscience (Cambridge, UK), Elkay Laboratory Products (Rotherham, UK), Fisher Scientific (Hampton, New Hampshire, USA), Linton Instruments (Diss, UK), Merck (Darmstadt, Germany), Nexcelom Bioscience (Lawrence, MA, USA), PCR Biosystems (London, UK), Peptidech (Rocky Hill, NJ, USA), Promega (Madison, WI, USA), R&D Systems (Minneapolis, MN, USA), Sarstedt (Nümbrecht, Germany), Scientific Laboratory Supplies (Nottingham, UK), Sigma-Aldrich (St Louis, MO, USA), Stem Cell Technologies (Cambridge, UK), TebuBio (Le Perray-en-Yvelines, France), ThermoFisher (Waltham, MA, USA), VWR (Lutterworth, UK).

Product Name	Company	Catalogue ID
1 mL syringe	Fisher Scientific	15489199
10% neutral buffered formalin	Sigma-Aldrich	1004960700
20-gauge/33 mm polypropylene animal feeding tubes	Linton Instrumentation	FTP-20-33
26-gauge needle	Fisher Scientific	12349169
27-gauge needle	Fisher Scientific	10204444
384-well RT PCR plates PCR plates, Roche style	VWR	211-0305
40 µm sterile cell strainer	ThermoFisher Scientific	22363547
Agilent 250 µL insert -polypropylene	Scientific Laboratory Supplies	5182-0549
AML12 cell line	ATCC	CRL-2254
APC anti-mouse CD41 Antibody (Clone: MWReg30)	Biolegend	133913
APC anti-mouse Ly-6A/E (Sca-1) Antibody (Clone: W18174A)	Biolegend	160903
APC anti-mouse/human CD11b Antibody (Clone: M1/70)	Biolegend	101211
APC/Cyanine7 anti-mouse CD4 Antibody (Clone: GK1.5)	Biolegend	100413
APC/Cyanine7 anti-mouse CD45 Antibody (Clone: 30-F11)	Biolegend	103115
APC/Cyanine7 anti-mouse CD48 Antibody (Clone: HM48-1)	Biolegend	103431

APC/Cyanine7 anti-mouse CD8b Antibody (Clone: YTS156.7.7)	Biologend	126619
APC/Cyanine7 anti-mouse TER-119/Erythroid Cells Antibody (Clone: TER-119)	Biologend	116223
BD FACSToow™ Sheath Fluid	BD Biosciences	12756528
Blood Ketone Test Strips for The on Call Dual Ketone	Amazon	B0CGB23K9H
Bovine serum albumin (BSA)	Fisher Scientific	BP1600-100
Calcium chloride - CaCl <sub>2</sub>	Sigma-Aldrich	C1016
Cellometer SD100 counting chamber	Nexcelom Bioscience	CHT4-SD100-002
Corning® Costar® TC-Treated Multiple Well Plates - 24 well	Merck	CLS3524-100EA
Cytiva Percoll™ Centrifugation Media	Fisher Scientific	11530734
DAPI	ThermoFisher Scientific	10566016
Dexamethasone	Sigma-Aldrich	D4902
Dimethyl sulfoxide (DMSO)	Fisher Scientific	BP231-100
EDTA coated tubes	Sarstedt	6.265 374
ELISA Plates x 5 (96 well plates)	R&D Systems	DY008B
Eosin Y-solution 0.5% alcoholic	Merck	1024390500
Epredia Polysine Adhesion Slides	Fisher Scientific	10219280
Ethylenediaminetetraacetic (EDTA)	Sigma-Aldrich	E9886
FACS 12x75 mm Polystyrene Test Tube, non-sterile	Elkay	2052-004
Fisherbrand PCR tube 0.2 mL flat cap, PP, natural - FB-0620	Fisher Scientific	12134102
Fisherbrand™ Adhesive Plate Seals	Fisher Scientific	15963620
Fisherbrand™ Bulk Beads 1.4 mm	Fisher Scientific	15515809
Fisherbrand™ Sterile Cell Strainers - 70 µm	Fisher Scientific	11597522
Fisherbrand™ Sterile Syringes for Single Use - 5 mL	Fisher Scientific	15869152
FITC anti-mouse F4/80 Antibody	Biologend	123108
Foetal bovine serum (FBS)	ThermoFisher Scientific	105000056
Gibco Trypan Blue solution, 0.4%	Fisher Scientific	11538886
Gibco™ Dulbecco's Modified Eagle Medium F12 (DMEM F12)	ThermoFisher Scientific	10565018
Gibco™ Penicillin-Streptomycin (10,000 U/mL)	Fisher Scientific	15276355
Gibco™ Trypsin-EDTA (0.25%), phenol red	Fisher Scientific	11560626
Histoclear II	Scientific Laboratory Supplies	NAT1334

Insulin-Transferrin-Selenium (ITS -G) (100X)	ThermoFisher Scientific	41400045
Invitrogen™ BODIPY™ FL C16 (4,4-Difluoro-5,7-Dimethyl-4-Bora-3a,4a-Diaza-s-Indacene-3-Hexadecanoic Acid)	Fisher Scientific	10654623
Invitrogen™ OneComp eBeads™ Compensation Beads	Fisher Scientific	15242448
Lineage Cocktail, anti-mouse Pacific Blue Antibody (Clone: 17A2; RB6-8C5; RA3-6B2; Ter-119; M1/70)	Biolegend	133310
Lipopolysaccharide (LPS)	Sigma-Aldrich	L2630
Millex™-GP Filter Unit (Sterile), 0.22 µm, diam. 33 mm	Merck	SLGP033RS
Minimum essential medium (MEM)	ThermoFisher Scientific	11095080
Mito Stress test kit	Agilent	103595-100
Mouse IL-6 Recombinant Protein, PeproTech®	ThermoFisher Scientific	216-16
Mouse TNF-alpha Recombinant Protein, PeproTech®	ThermoFisher Scientific	315-01A
Neo-Mount	Merck	1090160100
Nunc EasYFlask 75 cm <sup>2</sup>	ThermoFisher Scientific	156499
On Call Dual Ketone Monitor	Amazon	B0196U6MVA
PAI-1 ELISA reagents (5 x plates)	R&D Systems	DY3828-05
Palmitic acid	Sigma-Aldrich	P5585
Paraformaldehyde Solution, 4% in PBS	Fisher Scientific	J19943.K2
Paraplast® paraffin	Merck	P3558-1KG
PE anti-mouse Ly-6C Antibody (Clone: HK1.4)	Biolegend	128008
PE/Cyanine5 anti-mouse CD150 (SLAM) Antibody (Clone: TC15-12F12.2)	Biolegend	115911
PE/Cyanine7 anti-mouse CD117 (c-kit) Antibody (Clone: ACK2)	Biolegend	135111
PE/Cyanine7 anti-mouse Ly-6G Antibody (Clone: 1A8)	Biolegend	127617
Phosphate buffered saline (PBS) (Dulbecco A)	Oxoid	BR0014G
Polyethylene glycol 400 (PEG400)	Merck	P3265
Potassium chloride - KCl	Sigma-Aldrich	P9541
Potassium phosphate monobasic - KHPO <sub>4</sub>	Sigma-Aldrich	P9791
Primers for qPCR	See Table 2.4	

Proteome Profiler Mouse XL Cytokine Array	R&D Systems	ARY028
qPCRBIO SyGreen Mix Lo-Rox	PCR Biosystems	PB20.11-01
Recombinant Mouse Serpin E1 Protein	TebuBio	230-00730-100
Recombinant Murine JE/MCP-1 (CCL2)	PeproTech	250-10
Recombinant Murine KC (CXCL1)	PeproTech	250-11
Recombinant Murine MIP-2 (CXCL2)	PeproTech	250-15
Recombinant Murine MIP-3 $\alpha$ (CCL20)	PeproTech	250-27
Recombinant Murine RANTES (CCL5)	PeproTech	250-07
Red Blood Cell (RBC) Lysis Buffer (10X)	Biologend	420301
ReliaPrep™ RNA Miniprep Systems - cells	Promega	J8022
Seahorse XF 1.0 M glucose solution	Agilent	103577-100
Seahorse XF 100 mM pyruvate solution	Agilent	103578-100
Seahorse XF 200 mM glutamine solution	Agilent	103579-100
Seahorse XF Calibrant Solution	Agilent	100840-000
Seahorse XF DMEM medium	Agilent	103575-100
Seahorse XFe96 Flux pack mini (6 x cartridges and culture plates)	Agilent	103793-100
Sinocare (Safe Aq Smart) Blood Sugar Test monitor	Amazon	B08ZY7FFWG
Sinocare (Safe Aq Smart) Blood Sugar Test Strips	Amazon	B097T25B7X
Sodium bicarbonate - NaHCO <sub>3</sub>	Sigma-Aldrich	S5761
Sodium chloride - NaCl	Sigma-Aldrich	S3014
Sphero™ Blank Calibration Particles, 6.0 - 6.4 $\mu$ m	BD Biosciences	556296
Tiplaxtinin (PAI-039)	TebuBio	T2030
Tissue embedding cassettes with lid	Merck	Z672122-500EA
TM5441	Cambridge Bioscience	332-11765-4
Tween80	Merck	P1754-500ML
Ultrascript® cDNA synthesis kit	PCR Biosystems	PB30.11-02

## **2.2 Animal Models**

All animal research was carried out in accordance with regulations set by the UK Home Office and the Animal Scientific Procedures Act 1986 under project license PP0023671 (Dr. Stuart Rushworth) and housed in the Disease Modelling Unit (DMU) at the University of East Anglia, a pathogen free, containment level 3 laboratory. All *in vivo* experiments were preplanned, with drugs and reagents tested *in vitro* first, taking into consideration the 3R's (replacement, reduction and refinement), whilst ensuring they were properly powered for statistical analysis.

### **2.2.1 Animal maintenance**

This study used wild-type C57BL/6J mice which were purchased from Charles Rivers (Kent, UK). This is the most commonly used inbred mouse strain which are long-lived and breed well. Mice between 6-8 weeks old were used to set up breeding pairs, which were used for no more than 6 months before they were subsequently separated. Pup litters were weaned at 3 weeks old and were only allocated to experiments once they reached an appropriate age and weight, and were checked for good health. The mice used for this study were young adult mice between 8-20 weeks old, with an average age of 12 weeks. Due to availability, *in vivo* experiments were performed using female mice, whilst primary mouse hepatocytes were isolated from male mice. Their response to infection was tested using LPS treatment to mimic infection.

### **2.2.2 Animal procedures**

All animal procedures were performed by myself, under UK Home Office personal licence I211627388, with help from Dr Stuart Rushworth (ICD3874DB), Dr Charlotte Hellmich (IE10ADD51), Dr Rebecca Maynard (I32269130) and Miss Alyssa Polski-Delve (108750454). Full training for animal procedures was provided by Mr Richard Croft (IGEBEF87) and Mrs Anya Croft (L8A2ACED). Mice were weighed at the beginning and end of experiments as part of monitoring for any adverse effects.

### **2.2.3 Intraperitoneal injections**

LPS and recombinant mouse Plasminogen activator inhibitor-1 (PAI-1) were administered by intraperitoneal (I.P.) injections. For all I.P. injections, a volume of 200  $\mu$ L was injected into the peritoneum of mice restrained using a scruff technique, using a sterile 26-gauge needle. For the infection model, mice were administered with 0.5 mg/kg LPS and sacrificed after 2, 6, or 16 hours, or when a humane endpoint was reached prior to experimental endpoint. Due to its limited half-life, recombinant mouse PAI-1 was administered at 0.05 mg/kg at 0 and 2 hours in before sacrifice 4 hours after the first injection was administered. Any mice given multiple I.P. injections were injected in alternate flanks. All reagents were made up to the correct dose and volume listed above by dilution in sterile phosphate buffered saline (PBS) just before I.P. injection. Mice were monitored following the procedure until fully recovered.

### **2.2.4 Oral gavage**

Tiplaxtinin and TM5441 were administered by oral gavage at a dose of 10 mg/kg 1 hour prior to LPS I.P. injections. The drug was weighed out and resuspended sequentially in 5% Dimethyl sulfoxide (DMSO), 40% polyethylene glycol 300, 5% Tween80 and 50% deionised filtered water. Mice were administered 200  $\mu$ L of the freshly prepared solution via oral gavage using a 33 mm polypropylene animal feeding tube and a scruff technique. Mice were monitored following the procedure until fully recovered.

### **2.2.5 Intravenous injections**

For platelet depletion models, a mixture of purified rat monoclonal antibodies directed against mouse CD42b was intravenously administered 16 hours prior to LPS treatment. Mice were placed into a 37 °C heat chamber for 10 minutes to promote vasodilation. Using a benchtop holding cone, mice were injected into the tail vein with 100  $\mu$ L 2 mg/kg R300 anti-CD42b antibodies by Dr Charlotte Hellmich using a 27-gauge needle. Mice were returned to their home cage and monitored until fully recovered.

### **2.2.6 Schedule 1 sacrifice**

Mice were monitored daily and humanely sacrificed at first sign of illness or distress (weight loss, reduced mobility, severe over grooming, hind limb paralysis, hunched posture, and piloerection), or at the end point of the experiment using schedule 1 methods. Mice were sacrificed via gradual CO<sub>2</sub> asphyxiation followed by neck dislocation or when blood was required by exsanguination via a jugular slit. A portion of the blood was collected into ethylenediaminetetraacetic acid (EDTA) tubes to prevent clotting and used for the ketone, glucose and platelet analysis. Remaining blood was collected into non-coated Eppendorf tubes. Samples of adipose and liver tissue were then collected and bone marrow harvested for analysis.

## **2.3 Murine tissue collection and processing**

### **2.3.1 Bone marrow isolation**

The femur and tibia from each mouse were removed after schedule 1, cut in half and placed into a 0.5 mL Eppendorf with a hole at the bottom inside a 1.5 mL Eppendorf. This was then centrifuged for 5 seconds to spin out the bone marrow cells into the 1.5 mL Eppendorf. All cells from the same mouse were resuspended and pooled together in 1 mL of magnetic-activated cell sorting (MACS) buffer. MACS buffer consists of PBS, pH 7.4, containing 0.5% bovine serum albumin (BSA) and 1 mM EDTA. The buffer was then filter sterilised using a 0.22 µm filter before use. Once resuspended in MACS, the bone marrow was filtered through 40 µm filters, ready for counting and flow cytometry analysis.

### **2.3.2 Liver isolation**

A small incision just below the sternum was made large enough for liver lobes to be gently pushed through and removed. The gall bladder was carefully separated and lobes sectioned. The largest lobe was immediately snap frozen in cryopreservation tubes placed into dry ice ready for RNA extraction. Two smaller lobes were placed into histology cassettes and submerged into 10% neutral buffered formalin, which contains approximately 4% formaldehyde, for 24 hours before being transferred into 50% ethanol for at least 48 hours. Finally, when required, one smaller lobe was placed into an Eppendorf containing 1 mL PBS supplemented with 2% foetal bovine serum (FBS) on wet ice ready for liver immune cell isolation.

### **2.3.3 Fat pad isolation**

Inguinal and gonadal fat pads were isolated and weighed from mice post schedule 1. An incision was made from sternum to tail and the skin was carefully peeled back from the hind legs, and the inguinal fat pad from each side scraped out. The gonadal fat pad was then isolated from around the sex organs. Once weighed, fat pads were then snap frozen for further analysis.

### **2.3.4 Blood analysis**

To measure blood glucose and ketone levels at experiment endpoint, 3  $\mu$ L of blood from the EDTA collection tube was used to fill the tip of each test strip. Strips were then placed into either the glucose (Sinocare, Changsha, China) or ketone meters (Swiss Point of Care, Ijssel stein Netherlands) and results recorded.

### **2.3.5 Platelet isolation**

Remaining blood in the EDTA collection tube was then centrifuged at 100 x g for 5 minutes. Next, 50  $\mu$ L of the straw-coloured platelet rich plasma layer on top was collected into 1.5 mL Eppendorf tubes. This was then centrifuged for 6 minutes at 800 x g to pellet the platelets. The supernatant was removed, and the pellet of platelets was either snap frozen or used for further experiments.

### **2.3.6 Serum**

Blood collected from the mouse during schedule 1 into 1.5 mL Eppendorf tubes was allowed to clot. The clotted blood was then centrifuged at 3000 x g for 10 minutes. The top layer of serum was then collected and kept at -20 °C until used for further analysis or in cell culture experiments.

### **2.3.7 Bone marrow cell count**

For mouse experiments, an automatic Cellometer T4 Bright Field Viability Cell Counter (Nexcelom Bioscience LLC, Lawrence, MA, USA) was used to quantify total, dead and viable cells. To do this, isolated and filtered bone marrow cells were diluted 1 in 10 in MACS buffer and then further diluted using a 1:1 ratio with trypan blue. Then, 20  $\mu$ L of this 1 in 20 dilution was loaded into the cell counting chamber, and focus was adjusted. The automatic counter then calculated the total number of viable cells using this dilution.

## 2.4 Flow Cytometry

All flow cytometry was performed using a BD FACSymphony A1 flow cytometer, which has a violet, blue, yellow-green, and red laser allowing up to 16 colours to be used at one time. Flow cytometry was used to analyse different bone marrow, blood and liver immune cell populations. For each panel, compensations were run using either live bone marrow cells or OneComp eBeads™ Compensation Beads. Gating for positive and negative populations was determined using FMOs (fluorescence minus one), to account for cell autofluorescence and fluorophore spillover, example plots of which can be found in the appendix. The antibodies and fluorophores used are detailed below in Table 2.2. Data was analysed using FloJo software version 10.10.0 software (FlowJo LLC, Ashland, OR, USA).

**Table 2.2, Antibody panels used for flow cytometry assays.**

Panel	Antibody	Fluorophore
HSC LCFA uptake	Lin-	Pacific blue
	Sca-1	APC
	CD117	PE-Cy7
	CD48	APC-Cy7
	CD150	PE-Cy5
	C16 BODIPY	FITC
Peripheral blood and mature cell panel	CD4	APC-Cy7
	CD8	APC-Cy7
	CD11b	APC
	CD19	PE-Cy5
	Ly6G	PE-Cy7
	Nuclei	DAPI
Platelet quantification	CD41	APC
	Ter119	APC-Cy7
Liver immune cells	CD45	APC-Cy7
	CD11b	APC
	Ly6C	PE
	Ly6G	PE-Cy7
	F4/80	FITC

### **2.4.1 HSC LCFA uptake**

To quantify LCFA uptake in HSCs, 2 million of the isolated and filtered bone marrow cells were aliquoted into a clean Eppendorf tube. Cells were stained with 1  $\mu$ M C16 BODIPY for 30 minutes at room temperature in the dark. After, 1 mL MACS buffer was added to dilute the dye, and cells were centrifuged at 300 x g for 5 minutes. The supernatant was discarded, and cells were resuspended in 50  $\mu$ L of HSC antibody mix (which contained 0.5  $\mu$ L of each antibody per sample diluted in MACS buffer). Samples were left to stain at 4  $^{\circ}$ C in the dark for 20 minutes before adding 250  $\mu$ L sheath fluid. Cells were transferred into flow tubes and run through the flow cytometer, collecting 100,000 events.

### **2.4.2 Mature and peripheral blood cell panel**

For peripheral blood sample preparation, 10  $\mu$ L of the blood collected in EDTA tubes during schedule 1 was resuspended in 100  $\mu$ L red blood cell lysis and incubated at room temperature for 5 minutes. After, 1 mL MACS buffer was added to each Eppendorf to dilute the red cell lysis and centrifuged at 400 x g for 5 minutes. The supernatant was discarded, and cells were resuspended in 50  $\mu$ L of the antibody mix containing 0.5  $\mu$ L of each antibody per sample diluted in MACS buffer. For bone marrow cells, 2 million cells from each sample were aliquoted into Eppendorf tubes and 50  $\mu$ L of the same antibody mix was added. Samples were incubated at 4  $^{\circ}$ C in the dark for 20 minutes to allow time to stain. Next, 300  $\mu$ L of sheath fluid containing 80 ng/mL of DAPI was added to each sample to identify any dead cells. Samples were then transferred into flow tubes before being run and recorded on a medium flow rate (35  $\mu$ L/min) for 30 seconds for the peripheral blood or until 100,000 events were collected for bone marrow samples. Time was used for the peripheral blood samples to account for any un-lysed red blood cells or debris.

### **2.4.3 Platelet quantification**

To quantify the number of platelets, or to assess platelet levels in the platelet depleted mice, blood collected into EDTA tubes during schedule 1 was used. A 1 in 100 dilution was made by adding 1  $\mu$ L of blood to 99  $\mu$ L MACS buffer. Then, 3  $\mu$ L of this mix was added to 25  $\mu$ L antibody mix, containing 0.5  $\mu$ L of CD41 and 1  $\mu$ L of Ter119 per sample. For platelet depletion experiments, 0.5  $\mu$ L of Sphero™ beads were

also added as a positive control. Samples were incubated for 20 minutes at room temperature in the dark. After incubation, 275  $\mu\text{L}$  sheath fluid was added and samples transferred into flow tubes. Samples were run for 1 minute on medium flow rate (35  $\mu\text{L}/\text{min}$ ) and platelet count was quantified. The number of platelets recorded was multiplied by the dilution factor and then adjusted to calculate the number of platelets per  $\mu\text{L}$  of peripheral blood based on the flow rate.

#### **2.4.4 Liver immune cell isolation**

The liver lobe collected after schedule 1 into PBS supplemented with 2% FBS (referred to as PBS/FBS from this point) was transferred into 1 mL of pre-warmed 6.25  $\mu\text{g}/\text{mL}$  collagenase IV in PBS/FBS. The lobe was then cut into smaller pieces and placed into 37  $^{\circ}\text{C}$  chamber for up to 30 minutes, or until the tissue was digested. To aid digestion, livers were passed up and down through a 3 mL syringe and then filtered through a 70  $\mu\text{m}$  filter into a 15 mL centrifuge tubes. Cells were then centrifuged for 10 minutes at 1300 rotations per minute (RPM), 4  $^{\circ}\text{C}$ . The supernatant was discarded, and the pellet was resuspended in 5 mL of 35% Percoll<sup>®</sup> in PBS/FBS and centrifuged at 1700 RPM for 40 minutes at room temperature. The top layer and supernatant were removed, and the bottom pellet resuspended in 1 mL red blood cell lysis. Samples were incubated in red blood cell lysis for 3 minutes before 5 mL of PBS/FBS was added to dilute it. Cells were then centrifuged for 10 minutes at 1300 RPM for 10 minutes, 4  $^{\circ}\text{C}$ . The supernatant was discarded, and cells resuspended in 50  $\mu\text{L}$  of the antibody mix listed in Table 2.2, containing 0.5  $\mu\text{L}$  of each antibody per sample diluted in PBS/FBS. Samples were then incubated at 4  $^{\circ}\text{C}$  in the dark for 30 minutes to allow to stain before being topped up with 200  $\mu\text{L}$  sheath fluid. Samples were then transferred into flow tubes and 50,000 events collected per sample.

## 2.5 Cell culture

### 2.5.1 Cell counting with trypan blue

Excluding animal experiments, to determine the number of viable cells and seed cells at the correct density, cells were stained with trypan blue. Cells which have intact cell membranes will remain unstained, making them appear bright relative to the trypan background colour. Damaged non-viable cells take up the trypan dye, blending into the background. Cells were diluted using MACS buffer to a 1 in 10 or 1 in 20 dilution depending on total expected cells. Trypan blue was then added to make a 1:1 ratio and a final dilution of 1 in 20 or 1 in 40. Then 10  $\mu\text{L}$  of this mix was loaded into the haemocytometer and viable cells were counted in each of the 4 outer quadrants. The sum of the counts in all 4 quadrants was then calculated. Total number of viable cells was calculated per mL of cell suspension, shown in Figure 2.1.

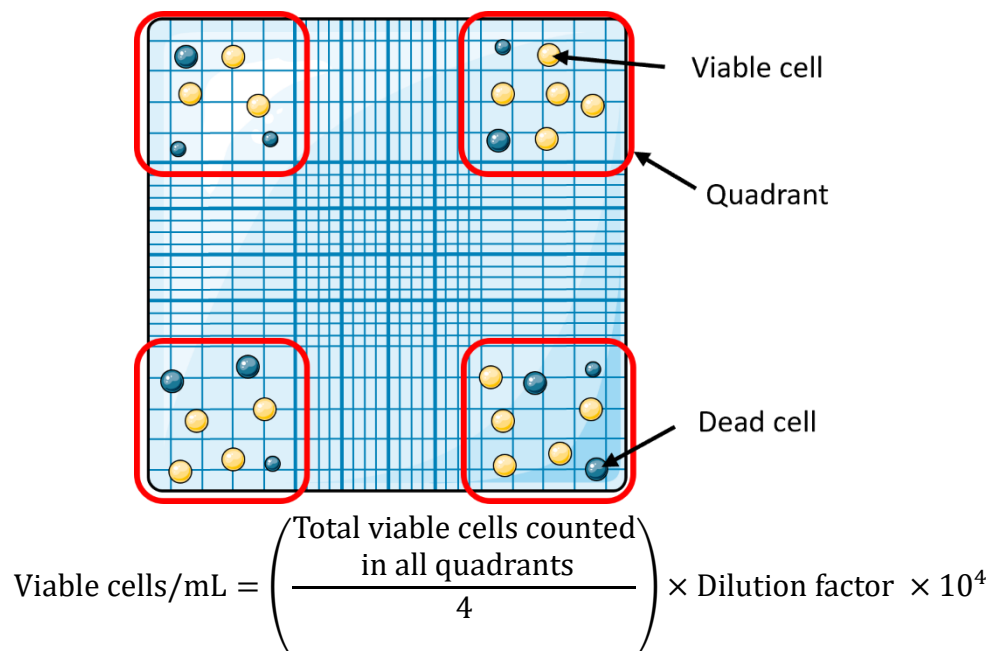


**Figure 2.1, Cell counting using trypan blue exclusion.**

Layout of the haemocytometer with cells showing the outer 4 quadrants that were counted. Dead cells are shown in blue as these take up trypan blue staining. Viable cells are shown in yellow. The formula to calculate the total cell number per mL is shown on the diagram.

### 2.5.2 Primary mouse hepatocytes

Primary mouse hepatocytes were isolated by collagenase perfusion from wild-type C57Bl/6J mice by Dr Naiara Beraza and Dr Paula Ruiz. Livers were perfused with pre-

warmed perfusion buffer, containing 0.02 M glucose, 0.12 M NaCl, 4 mM KCl, 0.024 M NaHCO<sub>3</sub>, 0.2 M KHPO<sub>4</sub>, 0.15 M MgSO<sub>4</sub> and 0.2 mM EDTA in deionised water pH 7.4, until the solution ran clear and then further digested with collagenase Type 1 and 1.3 mM CaCl<sub>2</sub>. The isolated hepatocytes were then thoroughly washed and pelleted by centrifugation at 1000 RPM for 5 minutes. The supernatant was discarded, and cells were resuspended in Minimum Essential Media (MEM), supplemented with 10% FBS, 1% penicillin/streptomycin and 2 mM glutamine. Hepatocytes were then counted and seeded into Type 1 collagen-coated plates at a concentration of 2 x 10<sup>5</sup> cells/mL and placed into an incubator at 37 °C, 5% CO<sub>2</sub>. After 2 hours, the media was removed and replaced with serum free MEM and returned to the incubator overnight for use in experiments the next day.

### **2.5.3 AML12 cells**

The alpha mouse liver 12 (AML12) cell line was purchased from ATCC (Manassas, VA, USA). This cell line was generated from hepatocytes isolated from a healthy 12-week-old adult male mouse. ATCC state that AML12 cells exhibit typical hepatocyte features and thus can be used as a healthy control hepatocyte. AML12 cells were cultured in Dulbecco's Modified Eagle Medium F12 (DMEM F12) supplemented with 10% FBS, 1% Penicillin-Streptomycin, 10 µg/mL insulin, 5.5 µg/mL transferrin, 5 ng/mL selenium and 40 ng/mL dexamethasone. The insulin, transferrin and selenium were purchased as a combined Insulin-transferrin-sodium selenite (ITS) media supplement. The prepared media was then filter sterilised using a 0.22 µm filter and pre-warmed at 37 °C for at least 15 minutes to ensure correct pH. Cells were maintained in a T75 flask kept in an incubator at 37 °C, 5% CO<sub>2</sub> and fed with fresh media every 2-3 days. Once confluent or required for experiments, these adherent cells were split. Media was removed from the flask and cells washed with sterile PBS. Then 2 mL 0.25% Trypsin-EDTA was added, and the flask was placed back into the incubator for 10-15 minutes until the majority of cells were floating and no longer stuck down. The Trypsin-EDTA was then diluted by adding 10 mL PBS and the cell suspension was transferred into a 50 mL. If splitting cells only, 1/2 - 3/4 of this solution (depending on cell confluency) was then discarded before centrifugation. If seeding cells into plates for experiments, 3/4 of the cell suspension was placed into separate centrifuge tubes for counting and seeding, and the remaining 1/4 was used to maintain

the flask of cells and topped up with PBS to balance the centrifuge. Cells were then centrifuged for 5 minutes at 130 x g at room temperature. Supernatant was discarded and cells resuspended in 8 mL pre-warmed media for reseeding into the flask. The flask was then returned to the incubator. For experimental set up, pellets were resuspended in 10 mL media and 100  $\mu$ L was removed and used to count viable cells described in section 2.5.1. The correct volume of media was then added to create a cell suspension containing  $1 \times 10^5$  cells/mL and 1 mL was added to each well of a 24 well plate. Plates were then returned to the incubator and allowed to re-adhere overnight before further use in experiments.

#### **2.5.4 Cell cryopreservation**

AML12 cells were cryopreserved for long-term storage. Cells were collected using the Trypsin-EDTA method described above in section 2.5.3, and centrifuged at 130 x g for 5 minutes at room temperature. Supernatant was discarded and cells resuspended at a concentration of  $2 \times 10^6$  cells/mL in 1 mL ice-cold normal AML12 maintenance media supplemented with 10% DMSO in cryotubes. Tubes were then placed into a Mr Frostey™ Freezing Container at -80 °C overnight. This container slowly freezes cells, lowering in temperature by 1 °C per minute. Once fully frozen, cells were transferred to liquid nitrogen for long-term storage.

#### **2.5.5 Hepatocyte serum and cytokine experiments**

To assess hepatocyte response to mouse serum and cytokines, both primary hepatocytes and AML12 cells seeded in 24 well plates were used. LPS and cytokines were used at a 100 ng/mL concentration unless otherwise stated and serum pooled from 9 control mice or LPS-treated mice was added in a 1 in 8 dilution in the media. For RNA expression analysis, hepatocytes were treated for 2 hours before media was removed and 500  $\mu$ L RNA lysis buffer was added, and the plate was placed into the freezer ready for RNA extraction.

For LCFA uptake assays, 1  $\mu$ M C16 BODIPY was added 1 hour after cytokines or serum was added and incubated for an additional hour (for a total of a 2 hour timepoint). Media was then removed and 250  $\mu$ L 4% paraformaldehyde was added to each well to fix the cells. Cells were incubated in the paraformaldehyde for 20

minutes at room temperature in the dark. Cells were then washed 3 times using 1 mL PBS to remove any remaining fixative. Then 1 mL PBS containing 80 ng/mL DAPI was added to each well to stain the nuclei and incubated at 4 °C for 30 minutes in the dark. The DAPI PBS solution was then removed, and cells were washed with 1 mL PBS twice. Plates were then imaged using the FITC channel for to measure the C16 BODIPY uptake and DAPI channel to quantify nuclei on the BioTek Cytation7 (Agilent, Santa Clara, CA, USA) at 20x magnification. ImageJ Fiji (541) was used to analyse images. First, the image was split so to separate the FITC channel. Using only the FITC channel, individual hepatocytes were drawn around using the freeform tool, and fluorescence intensity was measured. For each condition 100 hepatocytes were measured (20 hepatocytes per image, across 5 images per condition).

### **2.5.6 Seahorse metabolic flux analysis**

Hepatocyte mitochondrial metabolism was measured using the Agilent Seahorse XFe96 Analyser (Agilent, Santa Clara, CA, USA), according to manufacturer's instructions. Briefly, either  $1 \times 10^4$  primary hepatocytes or AML12 cells were seeded per well into the 96-well cell culture plate in 200  $\mu$ L of their cell specific media and allowed to adhere. The XFe96 flux cartridge was hydrated overnight at 37 °C in XF Calibrant and protected from light. Hepatocytes were then pre-treated with recombinant PAI-1 or LPS at a concentration of 100 ng/mL, or with serum from a control or LPS-treated mouse at a dilution of 1 in 8 for 2 hours. After 2 hours, media was removed and replaced with 200  $\mu$ L Seahorse DMEM Medium, pH 7.4, supplemented with 1 mM sodium pyruvate and 2 mM glutamine with either 10 mM glucose (termed glucose media) or 100  $\mu$ M palmitic acid (termed palmitic acid media). To prevent the palmitic acid from precipitating out of the media, palmitic acid was added to a carrier of 0.3 g/ml of BSA in water in a ratio of 9 carrier: 1 fatty acid stock. This palmitic acid/BSA carrier mix was then added directly into the media. The flux cartridge was loaded with 2  $\mu$ M Oligomycin, 1  $\mu$ M carbonyl cyanide-4-(trifluoromethoxy) phenylhydrazone (FCCP) and 0.5  $\mu$ M Rotenone/Antimycin A (RotA) and placed into the machine. Once the flux cartridge was successfully calibrated, the cell culture plate containing hepatocytes was loaded and the assay run.

The Seahorse MitoStress Test assesses mitochondrial function by directly measuring cell oxygen consumption rate (OCR). The 3 drugs loaded into the flux cartridge are sequentially injected at set timepoints, illustrated in Figure 2.2. First the baseline OCR, termed basal respiration is measured. After 20 minutes, oligomycin is injected, which inhibits ATP synthase in the electron transport chain. The decrease in OCR after the addition of oligomycin is termed ATP-linked respiration. Next, FCCP is injected, which is an uncoupling agent which deliberately disrupts mitochondrial membrane potential and collapses the proton motive force. This results in uninterrupted electron flow through the electron transport chain and thus measures the maximum OCR and is termed maximal respiration. Spare capacity can then be calculated by subtracting basal respiration from maximal respiration. Finally, RotA is injected which is a mixture of rotenone, which inhibits complex I of the electron transport chain, and antimycin A, which inhibits complex III. This results in the complete shutdown of mitochondrial respiration and any remaining OCR can be determined as non-mitochondrial oxygen consumption.

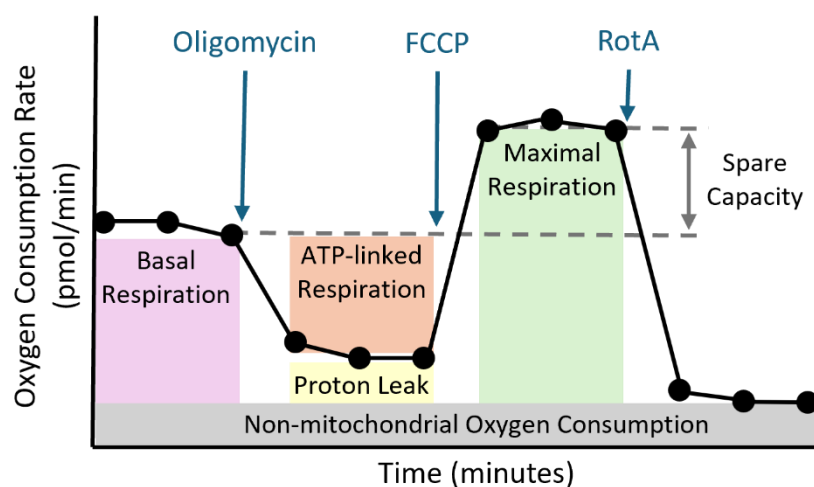


**Figure 2.2, Seahorse MitoStress test profile.**

Schematic showing the Agilent Seahorse XF Cell Mito Stress Test profile, which measures key parameters of mitochondrial function. Oligomycin, FCCP and Rotenone are added to cells at pre-determined time points. The OCR was measured at set intervals, which can then be used to calculation basal, ATP-linked and maximal respiration in each sample.

Once the assay was completed, cells were fixed and quantified to normalise results according to cell number and to calculate viability of treatments. Media was removed and 50  $\mu$ L 4% paraformaldehyde was added to each well and incubated for 20 minutes at room temperature in the dark. The paraformaldehyde was then removed,

and cells were washed 3 times using 200  $\mu$ L PBS to remove any remaining fixative. Then, 200  $\mu$ L PBS containing 80 ng/mL DAPI was added to each well to stain the nuclei and incubated at 4 °C for 30 minutes in the dark. The DAPI PBS solution was then removed, and cells were washed with 200  $\mu$ L PBS twice. Plates were then imaged using the DAPI channel to quantify nuclei on the BioTek Cytation7 (Agilent, Santa Clara, CA, USA) at 20x magnification. To do this, 4 images were taken per well at 10x magnification, and a mask was set up on the Cytation7 to identify and quantify the number of nuclei per image. After checking image quality, an average cell count per image was calculated for each well and then multiplied by 23.27 to calculate the total nuclei present per well. This is because, at the magnification used, the imaged area was 0.49 mm<sup>2</sup> and the total area of each well within the Seahorse plate was 11.4 mm<sup>2</sup>, and thus these were used to calculate the factor needed to multiply by. Next, the data generated during the MitoStress Test was normalised accounting for cell number. For this the average cell count per well across the whole plate was calculated, and cell count per well divided by this mean to give a relative factor (the proportion of cells within each well compared to the mean count). For each well, OCR values were then normalised using the calculated factor.

### **2.5.7 Platelet activation assay**

To assess if LPS could activate platelets, platelet rich plasma was isolated from whole blood using the method described in section 2.4.3. Platelets were counted using a haemocytometer as described in section 2.5.1, and 500,000 cells were seeded per well, remaining in their platelet rich plasma. Wells were evenly split between conditions (Control, 30 minutes and 60 minutes). Then, 100 ng/mL LPS was added to each 60 minute well. After 30 minutes, 100 ng/mL LPS was added to each 30 minute well. After a further 30 minutes, all samples were collected. This was done to ensure that the control platelets were treated in the exact same way as the LPS conditions. Samples were centrifuged at 800 x g at room temperature for 6 minutes. The supernatant was collected separately to the platelet pellet and was stored at 20 °C until they were analysed for PAI-1 content using a PAI-1 ELISA.

## 2.6 Serum analysis

### 2.6.1 Liquid chromatography-mass spectrometry

Liquid chromatography-mass spectrometry (LC-MS) was performed on serum collected during *in vivo* experiments to quantify LCFA abundance using a Waters Acquity UPLC system and Xevo TQ-S Cronos mass spectrometer controlled by MassLynx 4.1 software (Waters Corporation, MA, USA). A calibration standard was prepared containing 4 (low abundance) or 16 (high abundance) parts per million (ppm) in methanol, detailed below in Table 2.3. A serial dilution of this calibration standard was then performed 6 times to create 8 standards, including one containing only pure methanol only, with concentrations ranging between 0 – 10,000 ng/mL for highly abundance fatty acids and 0 – 2,000 ng/mL for low abundance fatty acids.

**Table 2.3, Concentrations of LCFAs added to the LC-MS calibration solution.**

Fatty acid calibration solution			
Concentration at 4 ppm		Concentration at 16 ppm	
C14	Myristic acid	C16	Palmitic acid
C15	Pentadecanoic acid	C18	Stearic acid
C16.1	Palmitoleic acid	C18.1	Oleic acid
C18.3	Linolenic acid	C18.2	Linoleic acid
C20.5	Eicosapentaenoic acid	C20.4	Arachidonic acid
C22.6	Docosahexaenoic acid		

Samples were prepared by adding 10  $\mu$ L serum to 490  $\mu$ L of ice-cold methanol and then incubated at -20  $^{\circ}$ C for 15 minutes. Samples were then vortexed and centrifuged at max speed 16,000 x g for 5 minutes. After centrifugation, 50  $\mu$ L of the samples or calibration serial dilution was added into glass vials containing plastic inserts. Then 20  $\mu$ L of the internal standard C19 at 50 ppm was added to each sample, which were then capped and vortexed. LCFAs were detected using negative mode electrospray ionisation (ESI). A CORTECS T3 2.7  $\mu$ m (2.1 x 30 mm) analytical column (Waters Corporation, Milford, MA, USA) was used to chromatographically separate samples. Eluent A, containing 0.2 mM ammonium acetate, 0.01% formic acid in deionised water, and eluent B, containing 0.2 mM ammonium acetate, 0.01% formic acid in 1:1 ratio of isopropanol and acetonitrile were run at a constant rate of 1.3 mL/min. The

gradient began at 50% eluent B before linearly increasing to 85% after 1.2 minutes. This was held for 0.5 minutes before it was linearly decreased in gradient back to 50%. The gradient was held at 50% for another 5 mins. Using a flow rate of 1.3 mL/min, 5 µL of each sample was individually injected into the column starting with the calibration solutions and the column temperature was maintained at 60 °C. An Agilent high performance autosampler with an injection program was used to minimise carry-over effects between samples. Chromatogram peak analysis was done using MassLynx TargetLynx software (Waters Corporation, Milford, MA, USA). For the analysis, the ratio of the C19 internal standard to metabolite was used to create calibration curves and quantify each metabolite. Excellent linear response range was ensured for each calibration curve with correlation coefficients ( $r^2$ ) 0.99 or higher for all calibration curves generated. A principal component analysis (PCA) plot was used to visualise mass spectrometry data, using R Studio (version 2025.05.1+513), with the ggplot2 package. Statistical ellipse was calculated using a 95% confidence interval.

### **2.6.2 Proteome profiler array**

To analyse the cytokines and chemokines present in the serum of mice, a Proteome Mouse XL Cytokine Array was used according to manufacturer's instructions. This kit is able to detect 111 different cytokines, chemokines and growth factors. The nitrocellulose membrane contains 111 different capture antibodies printed in duplicate. Briefly, after hydrating and preparing the membrane, 100 µL serum from control or LPS treated mice was prepared as directed and the membranes were incubated overnight at 4 °C on a rocking platform shaker. After washing and detection steps were performed, the membranes were developed using the prepared Chemi Reagent Mix and imaged using a Syngene™ G:BOX Chemi XRQ (Syngene, Cambridge, UK) using multiple exposure times between 1-10 minutes. The best exposure image was then selected for analysis and was analysed by measuring the fluorescence intensity of each dot using an Fiji ImageJ (National Institutes of Health, Bethesda, MD, USA).

### **2.6.3 PAI-1 ELISA**

Serum PAI-1 protein content was measured using a mouse PAI-1 ELISA kit according to manufacturer's instructions. ELISA plates were coated overnight at room temperature before use. Serum isolated from mice and platelet supernatant was diluted using the supplied reagent diluent. Plate absorbance was measured using the BioTek Cytation7 (Agilent, CA, USA), and analysis was performed using GraphPad Prism (GraphPad by Dotmatics, Boston, MA, USA), software version 10.3.1.

## **2.7 Histological analysis**

### **2.7.1 Embedding and sectioning**

Fixed histological samples were dehydrated using the Leica tissue processor (Leica Biosystems, Sheffield, UK) according to manufacturer's instructions. Dehydrated samples were then embedded in paraffin and sectioned at 3  $\mu\text{M}$  thick using a Leica microtome (Leica Biosystems, Sheffield, UK). Slides were allowed to dry for at least 12 hours before staining.

### **2.7.2 Haematoxylin and Eosin**

For haematoxylin and Eosin (H&E) staining, pre-sectioned livers at 3  $\mu\text{M}$  thick were stained using the following protocol: 5 minutes in Histoclear twice, 2 minutes in 100% ethanol, 2 minutes in 80 % ethanol, 2 minutes in 70% ethanol, 5 minutes in H<sub>2</sub>O, 5 minutes in Haematoxylin, 5 minutes tap water, 15 seconds in 1% acid, rinsed in tap water, 1 minute 0.1% sodium bicarbonate, 5 minute tap water, 30 seconds Eosin, 2 minute 70% ethanol, 2 minute 80% ethanol, 2 minutes in 100% ethanol, 5 minutes in Histoclear twice. Samples were then mounted using NeoMount, and imaged using a Leica light microscope (Leica Biosystems, Sheffield, UK).

## 2.8 Molecular biology

### 2.8.1 RNA extraction

To assess the gene expression of hepatocytes used in *in vitro* and livers from *in vivo* experiments real-time qualitative polymerase chain reactions (RT-qPCRs) were performed. To do this, first RNA needed to be extracted, using the ReliaPrep RNA cell miniprep RNA extraction kit according to manufacturer's instructions. For *in vivo* experiments, a small grain of rice-sized piece of snap frozen liver was sectioned and placed into homogeniser tubes containing 3 homogeniser beads. For fat pads, the whole inguinal or gonadal fat pad up to 0.3 g in weight was added into a homogeniser tube containing 5 homogeniser beads and cut using sterile scissors into smaller pieces. For both liver and fat pads, 500  $\mu$ L RNA lysis buffer was added to the tubes and were then homogenised using a Precellys 24 tissue homogeniser (Bertin Technologies SAS, France), settings 2 x 30 seconds, 6000 RPM. For *in vitro* experiments, plates of cells frozen in RNA lysis buffer were defrosted and collected into Eppendorf tubes ready for extraction. Briefly, 170  $\mu$ L isopropanol was added to each sample in RNA lysis and vortexed for 30 seconds. The lysates were then loaded into the provided ReliaPrep mini-columns and centrifuged at 13,000 x g for 30 seconds. All centrifugations for this protocol were at room temperature. Flow-through was discarded and 500  $\mu$ L of RNA wash solution was added to the column. Columns were then centrifuged for 30 seconds at 13,000 x g. Columns were then washed with 200  $\mu$ L of column wash solution and centrifuged at 13,000 x g for 15 seconds. Flow-through was discarded and 500  $\mu$ L RNA wash solution was added into each column. Samples were centrifuged at 13,000 x g for 30 seconds and waste was discarded. Next, 300  $\mu$ L of RNA wash solution was added into each column, and they were then centrifuged at 13,000 x g for 2 minutes. Columns were then allowed to dry for 2 minutes, before being placed into the 1.5 mL elution tubes provided in the kit. For *in vitro* experiments, 20  $\mu$ L of nuclease free water was added to each column and for *in vivo* experiments using whole-liver lysates 50  $\mu$ L of nuclease free water was used. A final centrifugation at max speed for 1 minute was done to collect the RNA in the elution tubes. RNA was then placed onto ice ready for immediate quantification and cDNA synthesis or stored at -20 °C until use.

### **2.8.2 RNA quantification**

The purity and concentration of the extracted RNA was measured using the NanoDrop Spectrophotometer (ThermoFisher Scientific, MA, USA). The NanoDrop was blanked using 1  $\mu$ L of nuclease free water. Then, 1  $\mu$ L of each sample was loaded onto the NanoDrop and RNA concentration was measured in ng/mL. RNA purity was also measured using the 260/280 score. Acceptable values for 260/280 ratio for samples subsequently used were between 1.8-2.

### **2.8.3 Bulk-RNA sequencing**

RNA extracted from whole-liver lysates of control mice and mice treated with 0.5 mg/kg LPS treated were sent for bulk-RNA sequencing to NOVOGene sequencing (Cambridge, UK). Briefly, mRNA was purified from total RNA using poly-T oligo-attached magnetic beads. Following fragmentation, both the first and second strands of cDNA were synthesised. The library was checked with Qubit and real-time PCR for quantification, and bioanalyzer for size distribution detection. Quantified libraries were pooled and sequenced using a NovaSeq 6000 Illumina sequencing system. Raw reads were checked for quality control before being aligned to the reference genome using Hisat2. The Fragments Per Kilobase of exon per Million mapped fragments (FPKM) was used to calculate the relative expression of each gene. Differential expression analysis was performed comparing the two groups using the DESeq2Rpackage (1.20.0) and the calculated p-values were then adjusted to control for false discovery rate using the Benjamini and Hochberg's approach. The threshold for significantly differentially expressed genes was defined as having an adjusted p-value  $< 0.05$  and an absolute foldchange of at least 2. Gene Ontology (GO) enrichment analysis of differentially expressed genes was done using the clusterProfiler R package to test the statistical enrichment of differential expression genes in Kyoto Encyclopaedia of Genes and Genomes (KEGG) and Disease Ontology (DO) pathways as well as the Reactome and DisGeNET databases. Gene Set Enrichment Analysis (GSEA) was done by ranking the genes according to the degree of differential expression in the two samples and then the predefined Gene Set was tested to see if they were enriched at the top or bottom of the list.

#### 2.8.4 cDNA synthesis

Extracted RNA was then used to synthesise cDNA via reverse transcription using the PCRBIOSystems cDNA ultrascript kit according to manufacturer's instructions. For each reaction, 2 µL of 5X cDNA Synthesis Mix, 0.5 µL of 20XRTase, 5.5 µL nuclease free water and 2 µL of the RNA sample was added to PCR tubes. Samples were then placed into a Thermocycler (Bio-Rad, Watford, UK) and run on a pre-defined program consisting of 30 minutes at 42 °C, 10 minutes at 85 °C and an indefinite hold step at 4 °C until samples were removed. cDNA was then diluted in 140 µL nuclease free water and stored at -20 °C until used.

#### 2.8.5 Real-time quantitative PCR

RT-qPCR was performed on a QuantStudio 7 Flex Real-Time PCR System (ThermoFisher Scientific, MA, USA), using SYBR-green technology to analyse gene expression. QuantiTect primers were obtained from Qiagen, and KiCqStart® primers from Sigma-Aldrich, with details of primers used in Table 2.4 below. A 1 in 20 dilution containing forward and reverse primers was made for each KiCqStart® primer pair using nuclease free water.

**Table 2.4, Details of primers used for RT-qPCR analysis.**

<b>KiCqStart® SYBR® Green Primers (Qiagen)</b>		
<b>Gene</b>	<b>Forward Primer 5'-3'</b>	<b>Reverse Primer 5'-3'</b>
<i>Acs11</i>	CAGGTCAAAGGCATTGCTGTG	AGGGGAAATGTAAACCTCGA
<i>Cd36</i>	CATTTGCAGGTCTATCTACG	CAATGTCTAGCACACCATAAG
<i>Cpt1a</i>	GGGAGGAATACATCTACCTG	GAAGACGAATAGGTTTGAGTTC
<i>Hmgcr</i>	AGGAGCCTGGAATTGAACTC	ATGACATCTCTCCTGCCGAG
<i>Hprt</i>	ATGTCATGAAGGAGATGGGA	CTTAAAATCTTAAATAAAA
<i>Ldlr</i>	CATCTTCTCCCTATTGCAC	ATGCTGTTGATGTTCTTCAG
<i>Lipe</i>	AACTCCTTCCTGGAACTAAG	CTTCTTCAAGGTATCTGTGC
<i>Pnpla2</i>	CAACCTTCGCAATCTCTAC	TTCAGTAGGCCATTCTCCTC
<i>Serpine1</i>	CTGAACTCATCAGACAATGG	CAGTCTCCAGAGAGAACTTAG
<i>Slc27a2</i>	AAGAAGTGAATGTGTATGG	GTTTTCTTTGATCTTGAGGGAG
<b>QuantiTect SYBR-Green Primers (Qiagen)</b>		
<b>Gene</b>	<b>Primer Assay Name</b>	<b>GeneGlobe ID</b>
<i>Acadm</i>	Mm_Acadm_1_SG	QT00111244
<i>Gapdh</i>	Mm_Gapdh_3_SG	QT01658692
<i>Hmgcs2</i>	Mm_Hmgcs2_1_SG	QT00169029
<i>Rps18</i>	Mm_Rps18_1_SG	QT00324940

A 384-well plate was used for all RT-qPCRs and each well was loaded with 0.5  $\mu$ L of the primer mix, 2.5  $\mu$ L qPCRBIO SyGreen Mix Lo-Rox and 2  $\mu$ L cDNA. Once loaded, the plate was sealed and centrifuged at 300 x g for 15 seconds. The plate was then transferred into the RT-qPCR machine and run on a pre-programmed cycle described in Figure 2.3.

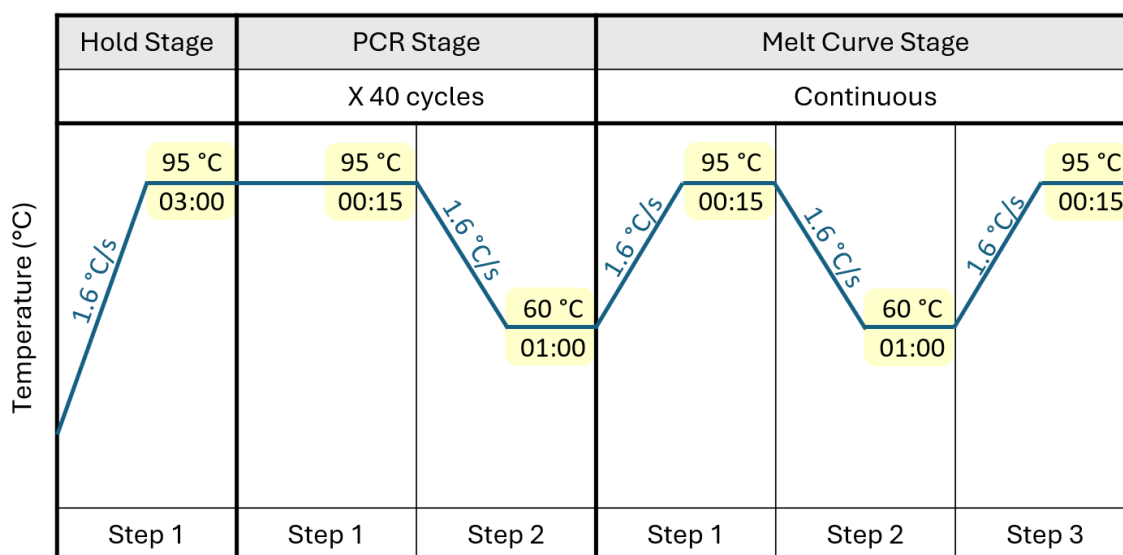


**Figure 2.3, RT-qPCR SYBR-Green programme settings.**

Details of the RT-qPCR SYBR-Green programme settings used for the QuantStudio 7 Flex Real-Time PCR System.

The cycle threshold (Ct) value for each gene was normalised against ribosomal protein S18 (*Rps18*) or Hypoxanthine Phosphoribosyltransferase (*Hprt*), depending on cell type. The Livak method was used to calculate relative gene expression. The Ct value of the target gene was subtracted from the housekeeping gene to calculate the  $\Delta$ Ct, then the  $\Delta\Delta$ Ct was calculated by subtracting the control sample from the different treatments. Finally, the expression ratio, or fold-change was calculated by  $2^{-\Delta\Delta Ct}$ . Each sample was run in duplicates as a minimum and standard deviation between duplicates was checked as part of the quality control.

Housekeeping gene stability for each tissue and cell type was assessed using the ‘BestKeeper’ method, which calculates the Pearson correlation between genes (542). The gene with the highest correlation coefficient and with a standard deviation of Ct values below 1 was then selected as the most appropriate housekeeping gene.

## 2.9 Quantification and statistical analysis

All analysis in this study was carried out using FlowJo software version 10.8.1 (FlowJo, LLC, Ashland, OR, USA), GraphPad Prism software version 10.3.1 (GraphPad Software, Santa Clara, CA, USA), R studio version 025.05.1+513.pro3 (Boston, MA, USA), Fiji ImageJ version 2.7.0 (541) and Microsoft Excel (Redmond, WA, USA). Results were statistically analysed using GraphPad Prism 10. Parametric test assumptions were checked; a Levene's test for equal variance and Kolmogorov-Smirnov test for normal distribution. Most data did not meet these assumptions, and therefore the non-parametric equivalent was chosen. For results directly comparing two groups, a Mann-Whitney test was performed and for results comparing more than two groups, a Kruskal-Wallis test was chosen, using a post hoc Dunn's test for multiple comparisons. For results comparing three or more groups that are categorised by at least two independent variables, a two-way ANOVA was done with a Dunnett's correction for multiple comparisons. Any significant differences are marked using an Asterix (\* =  $p < 0.05$ , \*\* =  $P < 0.01$ , \*\*\* =  $p < 0.001$  and \*\*\*\* =  $p < 0.0001$ ).

### **3 Characterising the kinetics of circulating fatty acids in response to LPS**

#### **3.1 Introduction**

During infection, hematopoietic stem and progenitor cells (HSPCs) rapidly expand in order to produce enough downstream immune cells to coordinate an effective immune response. Fatty acid uptake and metabolism are central to providing sufficient energy for this HSPC expansion. For example, it has been well documented that the HSC pool expands as part of the infection response (543). Previous research published by the Rushworth lab has demonstrated that in response to infection, using models of both LPS and *S. Typharium*, HSCs have increased CD36 expression and LCFA uptake 16 hours after LPS or 72 hours after *S. Typharium* infection (421). Additionally, it has been shown that circulating fatty acids increase during the infection response (534, 544). For example, during bacterial infections, the endotoxin LPS has been shown to alter metabolism, such as increased energy expenditure and elevated levels of serum circulating fatty acids in both humans and animal models (533). Whilst this has been known and published for over 30 years, the vast majority only measure the overall increase in circulating free fatty acids within the serum. Therefore, literature regarding which specific fatty acids are elevated and by how much in response to infection or LPS models is incredibly limited and not well defined. Furthermore, the mechanisms that drives these changes in serum fatty acid availability remains unclear.

This chapter aims to define the infection-induced changes in circulating fatty acid availability to support HSPC expansion, using mice treated with LPS to mimic the infection response. Additionally, the kinetics of specific, individual circulating LCFAs was explored. It is known that the liver and adipose tissue are the two main organs involved in fatty acid metabolism, storage and regulation (545), and thus their roles here were also explored.

### **3.2 Defining HSPC expansion and circulating LCFA availability in response to LPS *in vivo***

To analyse HSC expansion in response to acute infection, female WT C57/Bl6 mice between 8-16 weeks old were injected via I.P. with 0.5 mg/kg LPS. After 16 hours, these mice, along with 8 WT control mice, were then sacrificed. Bone marrow was extracted from femurs and tibias by centrifugation and stained with antibodies for HSPC markers (Figure 3.1A). The gating strategy used to identify LSKs, MPPs and HSCs is shown in Figure 3.1B. Positive and negative populations were identified using FMO controls, see appendix for FMO plots. The population of LSKs, MPPs and HSC per 100,000 bone marrow cells all significantly increased in response to LPS stimulation (Figure 3.1C). This is consistent with previously published data, that HSCs and their downstream progenitors expand in response to infection.

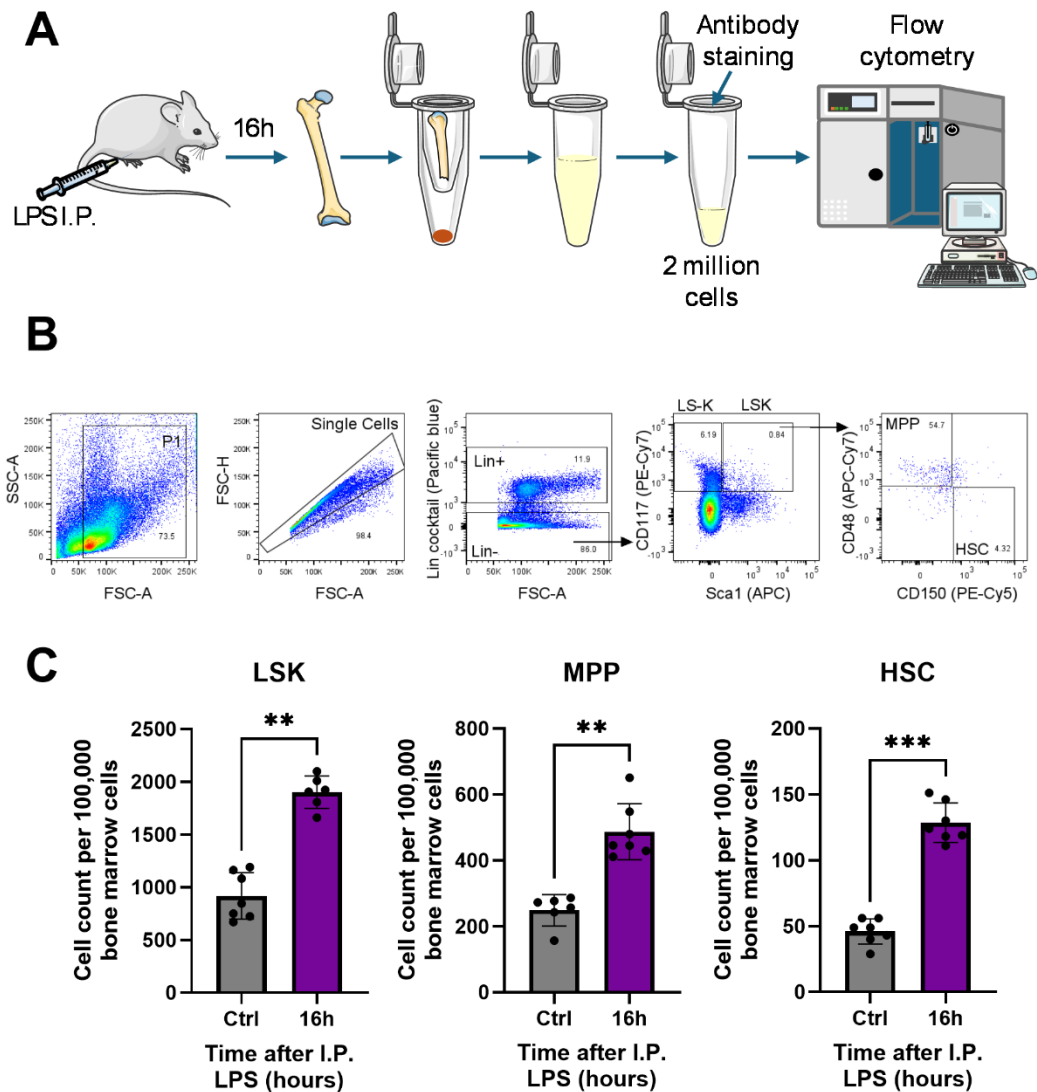


**Figure 3.1, LPS induced an increase in the proportion of HSPCs in the bone marrow.**

WT mice were injected with 0.5 mg/kg LPS via I.P. for 16 hours before being sacrificed. **A)** Schematic of experimental design and method of bone marrow extraction. Isolated bone marrow cells were stained with an antibody panel using markers for LSK, MPP and HSC populations. **B)** Flow cytometry gating strategy to identify HSPC populations. **C)** Number of LSKs, MPPs and HSCs per 100,000 BM cells recorded in control and LPS treated mice ( $n = 7$ ). Means and standard deviations were calculated and shown on each graph. A Mann-Whitney test was performed, and significant differences are marked using asterisks (\* =  $p < 0.05$ , \*\* =  $P < 0.01$ , \*\*\* =  $p < 0.001$  and \*\*\*\* =  $p < 0.0001$ ).

Whilst HSC expansion is a hallmark of the immune response to acute infection, it is important to demonstrate that HSCs utilise LCFAs to fuel this expansion. Thus, the bone marrow isolated from control and LPS-treated mice was incubated with C16-tagged BODIPY (palmitic acid) before being washed and stained with the same HSC antibody panel shown in Figure 3.1. The same gating strategy as Figure 3.2B was used

to identify the HSC population and a histogram of BODIPY fluorescent intensity revealed a distinct difference C16 uptake between control and LPS treated mice, indicating that LPS treated HSCs had increased LCFA uptake (Figure 3.2B). Due to washing off any excess BODIPY stain, any remaining fluorescence indicates C16 taken up directly into the cell. The median fluorescent intensity (MFI) of BODIPY of the HSC population was measured for each sample (Figure 3.2B). Results demonstrate a significant increase in palmitic acid uptake by HSCs in response to LPS, suggesting that HSCs have an increased reliance and need for LCFAs during expansion in response to LPS. This is in line with previous literature that HSCs rely on fatty acids for expansion in response to infection (546).

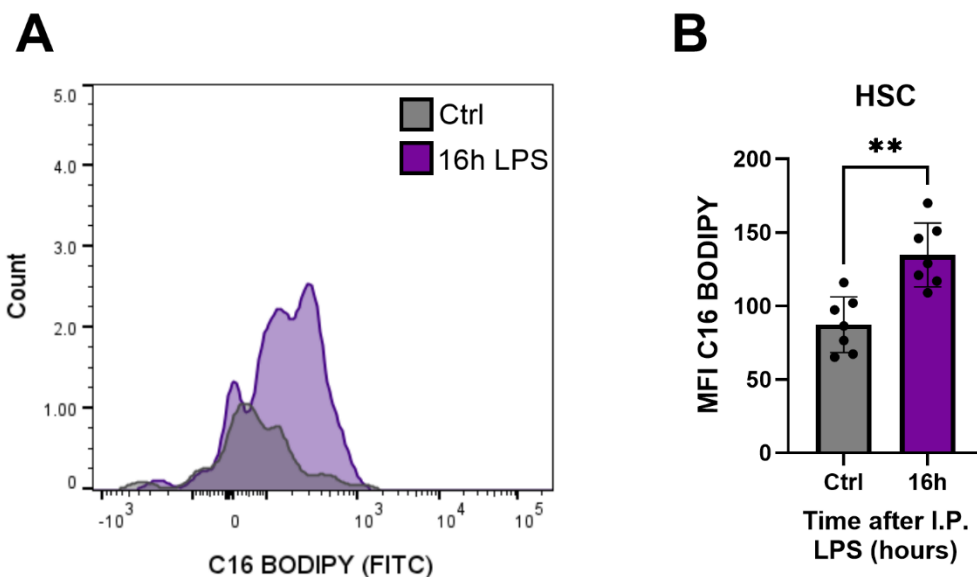


**Figure 3.2, LPS increased HSC palmitic acid uptake in the bone marrow.**

WT mice were injected with 0.5 mg/kg LPS via I.P. for 16 hours before being sacrificed. **A)** Representative flow cytometry histogram of HSC C16 BODIPY uptake in control and LPS treated mice. **B)** Median fluorescent intensity of BODIPY in HSCs in control and LPS treated mice (n = 7). Mean and standard deviation was calculated and shown on the graph. A Mann-Whitney test was performed, and significant differences are marked using asterisks (\* = p < 0.05, \*\* = P < 0.01, \*\*\* = p < 0.001 and \*\*\*\* = p < 0.0001).

Due to this increased uptake of LCFAs into HSCs, the abundance of circulating LCFAs within the serum from control or LPS treated mice was analysed using LC-MS (Figure 3.3A). Similarities between the two groups was assessed using a PCA plot (Figure 3.3B), which revealed distinct differences in LCFA abundance between control and LPS treated mice. Total serum LCFA concentration was calculated by adding the

concentration of each individual LCFA that was measured. Results confirmed that the abundance of LCFAs significantly increased in mice treated with LPS (Figure 3.3C). Each individual LCFA was then normalised to a control mouse to calculate the relative abundance of each LCFA within the serum (Figure 3.3D). Results show that there was a universal increase in LCFAs in LPS treated mice, with the exception of C15 (pentadecanoic acid). At 16 hours, the most significant increase was in C14, myristic acid.

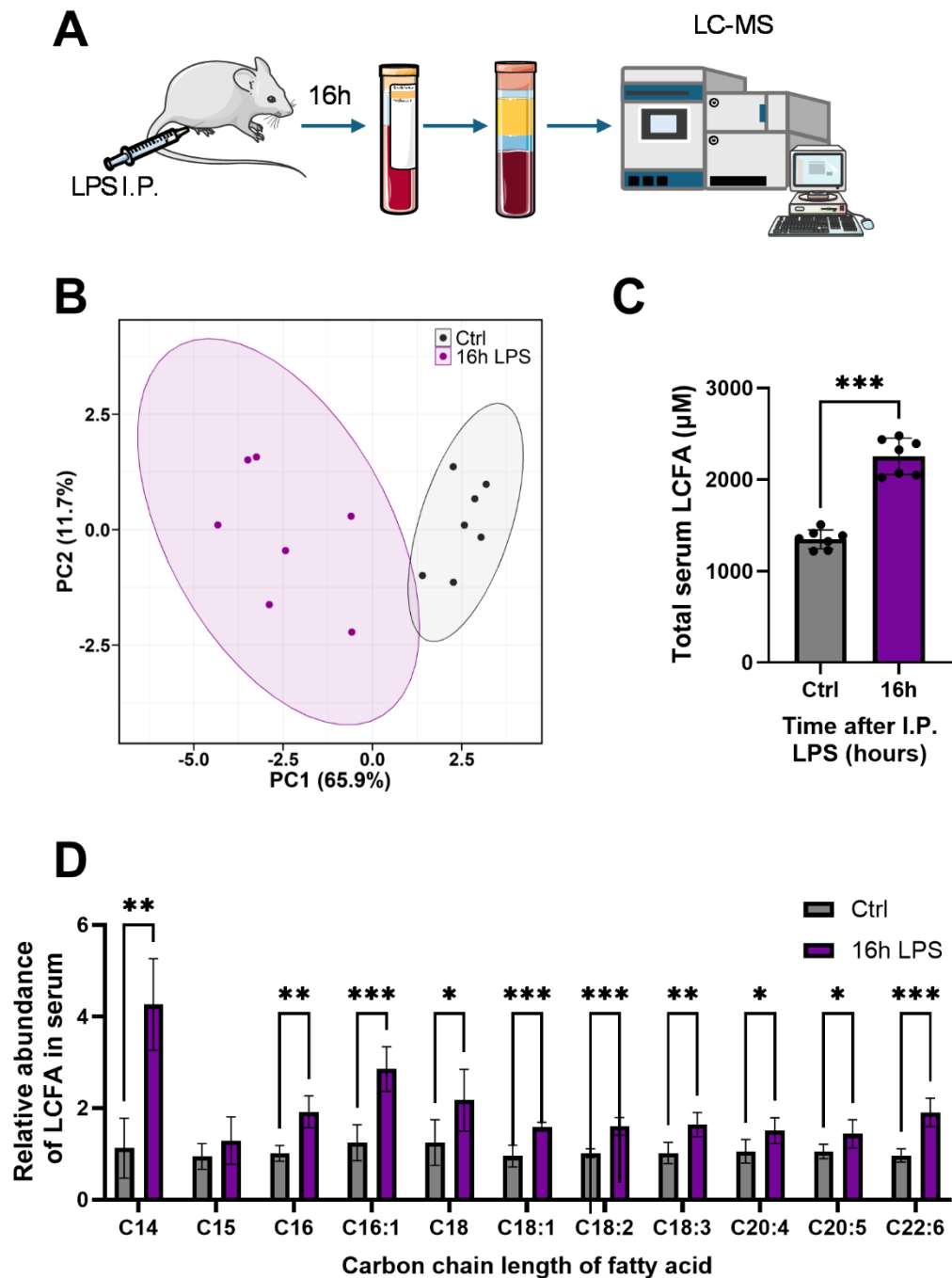


**Figure 3.3, LPS increased the level of LCFAs in the serum by 16 hours.**

WT mice were injected with 0.5 mg/kg LPS via I.P. for 16 hours before being sacrificed. **A)** Serum was separated from whole blood and LCFA content was analysed using LC-MS. **B)** PCA plot of serum LCFA abundance from control and LPS treated mice. **C)** Total serum LCFA was calculated by adding the concentration of each individual LCFA measured. **D)** Relative abundance of each LCFA measured in the serum normalised to a control mouse. Mean and standard deviation was calculated and shown on the graph (n = 7). A Mann-Whitney test was performed comparing control and LPS treated groups for each individual LCFA and significant differences are marked using asterisks (\* = p < 0.05, \*\* = P < 0.01, \*\*\* = p < 0.001 and \*\*\*\* = p < 0.0001).

### **3.3 Characterising the changes in circulating LCFAs in response to LPS treatment over time**

Whilst it is known that the availability of circulating fatty acids is increased in response to infection (421), the dynamics of this response remains unclear. Therefore, a time-course was set up to study the kinetics of circulating LCFAs in response to LPS. WT mice were injected with 0.5 mg/kg LPS via I.P. and sacrificed after 2, 6 or 16 hours. Serum was isolated from whole blood taken at time of sacrifice and analysed using LC-MS to determine the concentration of different circulating LCFAs present in the serum. Results within and between groups were compared using a PCA plot to assess the similarities and differences (Figure 3.4A). Control and mice treated with LPS for 2 hours clustered closely together, meaning they had a similar composition of LCFAs. The 6-hour group clustered furthest away from the control group, indicating the biggest difference in LCFA composition and abundance between these groups. Total serum LCFA concentration was calculated by adding the concentration of each individual LCFA that was measured (Figure 3.4B). In line with the PCA plot in Figure 3.4A, total serum LCFA concentration was highest 6 hours after LPS I.P. (Figure 3.4B).

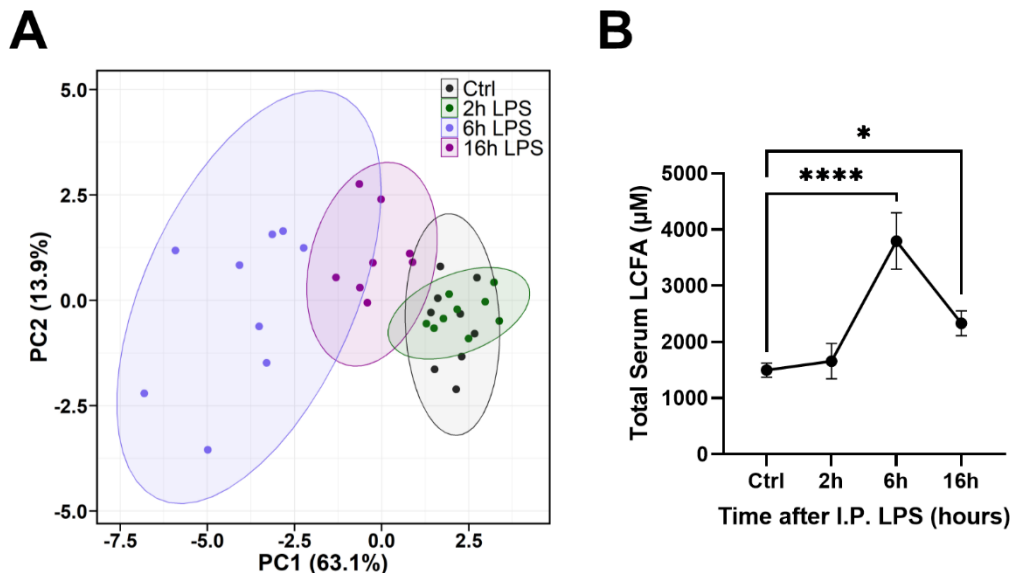


**Figure 3.4, Time-course of total serum LCFA in response to LPS.**

WT mice were injected with 0.5 mg/kg LPS via I.P. for 2, 6 and 16 hours before being sacrificed. Serum was separated from whole blood and LCFA content was analysed using LC-MS. **A)** PCA plot of serum LCFA abundance from control and LPS treated mice. **B)** Total serum LCFA was calculated by adding the concentration of each individual LCFA measured. Mean and standard deviation was calculated and shown on the graph (n = 9). A Kruskal-Wallis test with a Dunn's correction for multiple comparisons was performed, comparing each timepoint against the control group, and significant differences are marked using asterisks (\* =  $p < 0.05$ , \*\* =  $P < 0.01$ , \*\*\* =  $p < 0.001$  and \*\*\*\* =  $p < 0.0001$ ).

Each individual LCFA measured by LC-MS was then plotted for the time-course to identify which LCFAs increased the most and when, in response to LPS, from least abundant to most abundant (Figure 3.5). Interestingly, stearic acid (C18) was the only LCFA to significantly increase 2 hours after LPS treatment. Some LCFAs decreased 2 hours after LPS treatment including myristic acid (C14) and arachidonic acid (C20:4). At 6 hours, the largest increase was seen in myristic acid (C14), which increased 4-fold compared to controls. Palmitic acid (C16), palmitoleic acid (C16:1), and docosahexaenoic acid (C22:6) were the next largest increase, with their abundance increasing 3.5-fold 6 hours after LPS treatment. Pentadecanoic acid (C15) and eicosapentaenoic acid (C20:5) were the only two LCFAs to not significantly increase throughout the time-course.

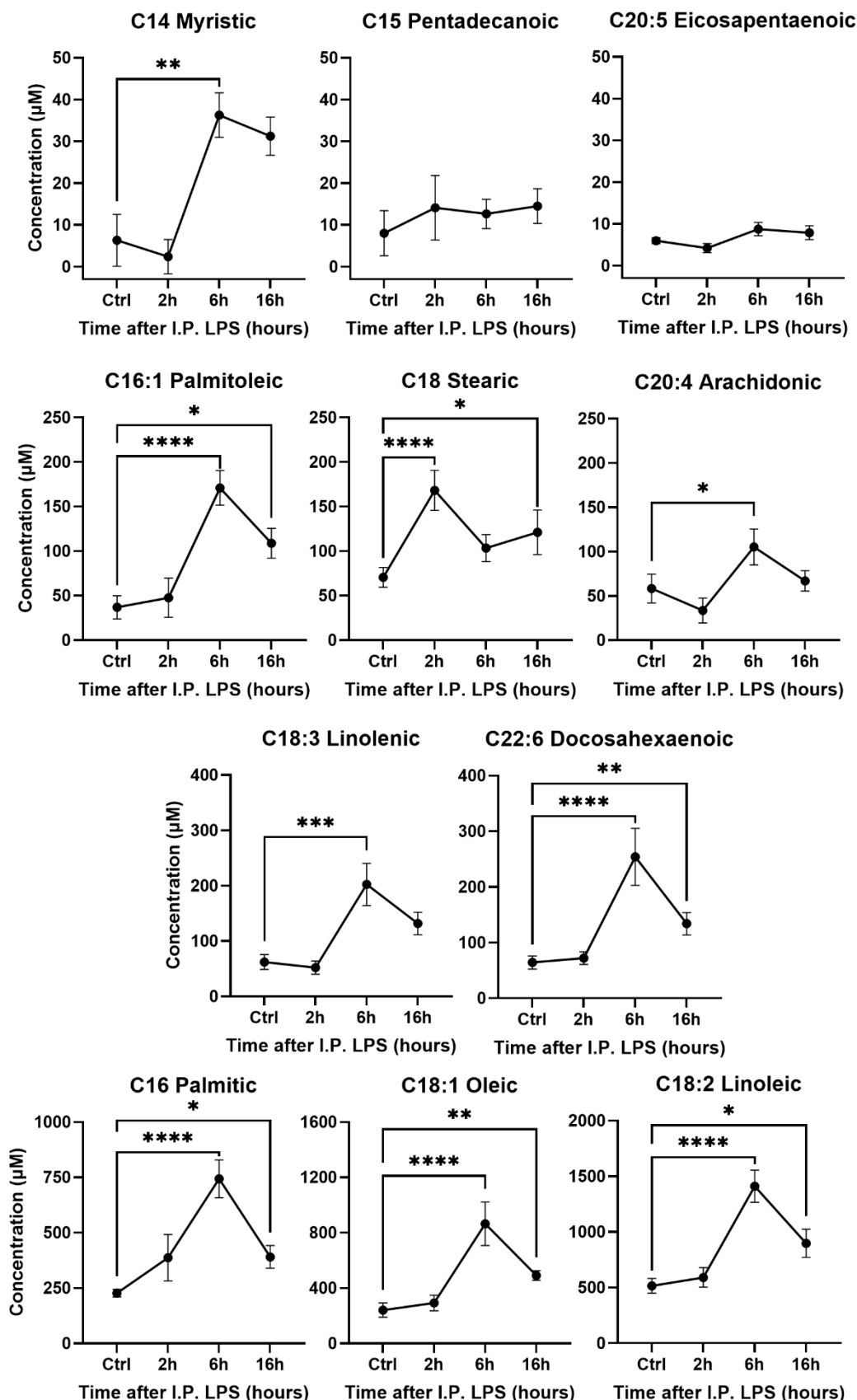


**Figure 3.5, Time-course of different serum LCFA in response to LPS.**

WT mice were injected with 0.5 mg/kg LPS via I.P. for 2, 6 and 16 hours before being sacrificed. Serum was separated from whole blood and LCFA content was analysed using LC-MS. Each individual LCFA measured was plotted. Mean and standard deviation was calculated and shown on the graph (n = 9). A Kruskal-Wallis test with a Dunn's correction for

multiple comparisons was performed, comparing each timepoint against the control group, and significant differences are marked using asterisks (\* =  $p < 0.05$ , \*\* =  $P < 0.01$ , \*\*\* =  $p < 0.001$  and \*\*\*\* =  $p < 0.0001$ ).

Due to the changes seen in the LCFAs in the serum in response to LPS, other blood metabolic markers were analysed. Blood glucose, the primary fuel choice for cellular ATP production, and ketones, produced when excess acetyl-CoA is produced during fatty acid oxidation, were selected as markers for glycolysis and fatty acid oxidation. Blood collected following LPS treatment was analysed using a ketone and glucose monitor (Figure 3.6A). Neither blood glucose levels (Figure 3.6B) or blood ketone levels (Figure 3.6C) significantly changed 2 hours after LPS treatment. However, by 6 hours blood glucose levels had significantly decreased 3-fold and dropped by nearly 10-fold by 16 hours (Figure 3.6B). This is likely due to the limited food intake from mice following LPS treatment. Whilst food intake was not monitored during this study, which is a potential limitation, it has been well documented that even at low doses, LPS causes a significant decrease in food consumption. For example, 4 hours after LPS treatment, food intake is nearly 50% lower compared to control rats. This reduction in food intake in LPS treated rats and mice was still observed at the 24-hour mark, with mice consuming 75% less food compared to controls (547, 548). This may explain the decrease in blood glucose levels seen in response to LPS treatment. Blood ketones significantly increased by 6 hours following LPS treatment but were still within the normal range (Figure 3.6C), and by 16 hours had increased by over 10-fold indicating increased reliance on fatty acid oxidation, with excess acetyl-CoA being produced. However, these measurements only tell us whole-organism trends and are not cell or tissue specific.

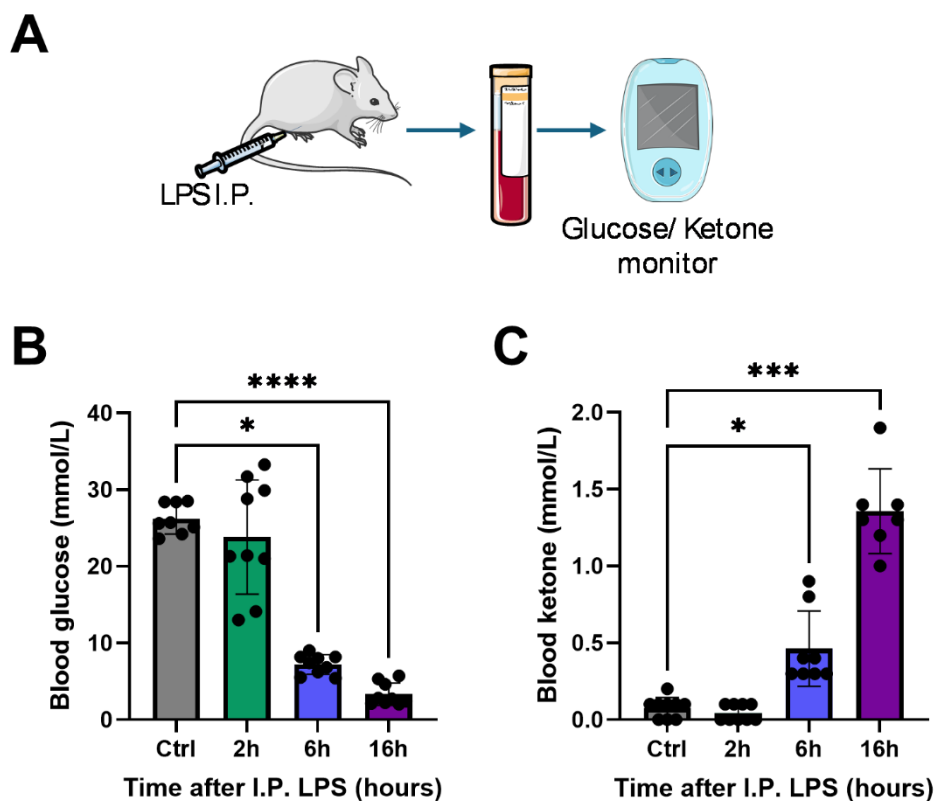


**Figure 3.6, Time-course of blood glucose and ketone levels in response to LPS treatment.**

WT mice were injected with 0.5 mg/kg LPS via I.P. for 2, 6 and 16 hours before being sacrificed. **A)** Glucose and ketone levels within the blood were measured using monitors and test-strips. **B)** Blood glucose levels following LPS treatment. **C)** Blood ketone levels following LPS treatment. Mean and standard deviation was calculated and shown on the graph (n = 9). A Kruskal-Wallis test with a Dunn's correction for multiple comparisons was performed, comparing each timepoint against the control group, and significant differences are marked using asterisks (\* =  $p < 0.05$ , \*\* =  $P < 0.01$ , \*\*\* =  $p < 0.001$  and \*\*\*\* =  $p < 0.0001$ ).

Increased ketogenesis and decreased blood glucose levels have been associated with weight loss. Therefore, mice were weighed before and after LPS treatment to monitor any weight changes. Percentage weight change was calculated by comparing the weight of the mouse at the end relative to their start weight. A value over 100% indicates the mouse gained weight and less than 100% lost weight. No significant weight loss was observed until 16 hours after LPS treatment (Figure 3.7), highlighting that the changes in the metabolic profile including LCFA abundance, blood glucose and blood ketone levels precedes any observable weight loss. The weight loss seen at 16 hours may be caused by a reduction in food or water intake in LPS treated mice, however this was not measured during this study and thus is a potential limitation.

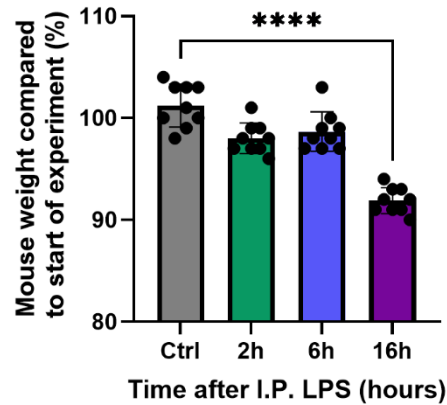


**Figure 3.7, Time-course of monitoring changes in mouse weight in response to LPS treatment.**

WT mice were injected with 0.5 mg/kg LPS via I.P. for 2, 6 and 16 hours before being sacrificed. Mice were weighed at the start of the experiment and again at the end. Percentage change of weight was calculated by comparing the difference between these two weights. Mean and standard deviation was calculated and shown on the graph (n = 9). A Kruskal-Wallis test with a Dunn's correction for multiple comparisons was performed, comparing each timepoint against the control group, and significant differences are marked using asterisks (\* = p < 0.05, \*\* = P < 0.01, \*\*\* = p < 0.001 and \*\*\*\* = p < 0.0001).

The primary source of circulating fatty acids comes from lipolysis, releasing fatty acids from adipose tissue. Therefore, the inguinal fat pad was isolated from the legs of each mouse post sacrifice. The gonadal fat pad surrounding the sex organs in the lower region of the abdomen was also removed (Figure 3.8A). The weights of the dissected fat pads from the mice were then measured and their weight relative to their total body weight was calculated. There was no significant difference in inguinal (Figure 3.8B) or gonadal (Figure 3.8C) at any of the time points measured. This is not unexpected due to the short time points chosen and any significant differences would only be expected at longer time points such as 2-3 days. This is supported by previous studies, which only reported a reduction in adipocyte size after 24-hours in LPS-treated mice (549).

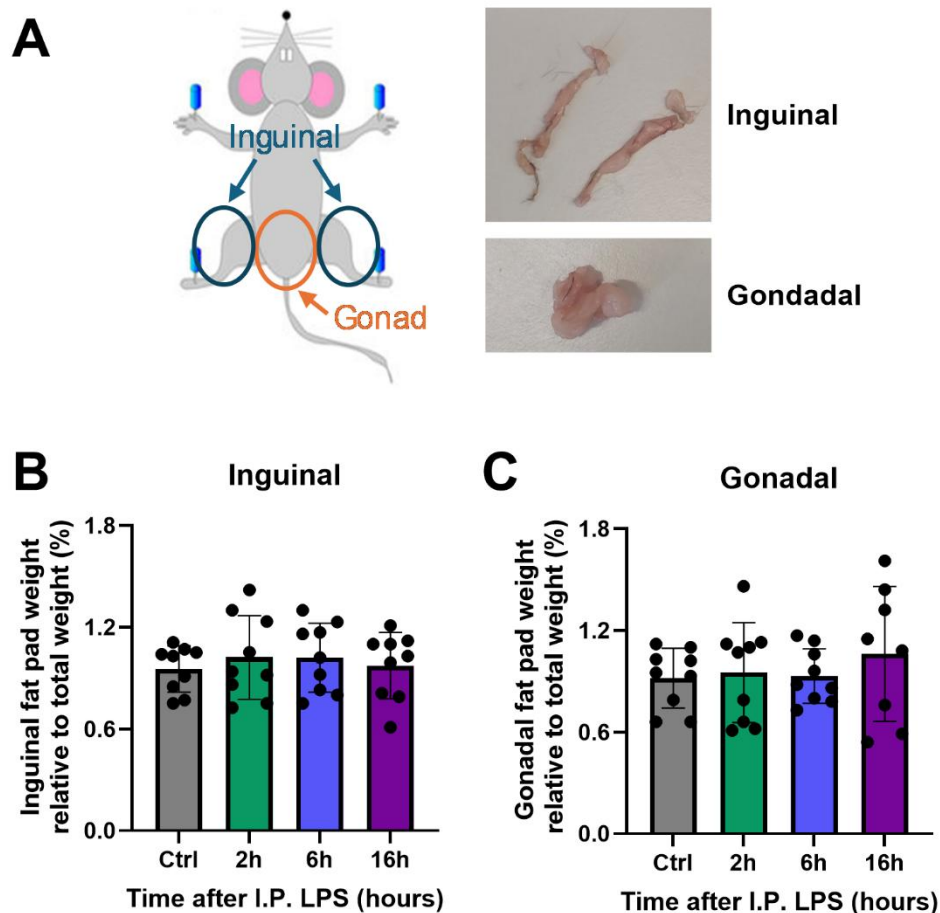


**Figure 3.8, Time-course of monitoring changes in mouse fat pad weight in response to LPS treatment.**

WT mice were injected with 0.5 mg/kg LPS via I.P. for 2, 6 and 16 hours before being sacrificed. **A**) Inguinal and gonadal fat pads were dissected from mice and weighed. The percentage the weight of each fat pad was calculated against total body weight at time of sacrifice. **B**) Inguinal fat pad. **C**) Gonadal fat pad. Mean and standard deviation was calculated and shown on each graph (n = 9). A Kruskal-Wallis test with a Dunn's correction for multiple comparisons was performed, comparing each timepoint against the control group, and significant differences are marked using asterisks (\* = p < 0.05, \*\* = P < 0.01, \*\*\* = p < 0.001 and \*\*\*\* = p < 0.0001).

Adipocytes within WAT are the main store of fat in the body. Therefore, to determine if the increase in circulating LCFAs could be due to increased lipolysis and thus fatty acid release from adipose tissue, RNA was extracted from the isolated inguinal and gonadal fat pads.

Because RT-qPCR data is normalised against a housekeeping gene, it was important to determine the most suitable housekeeping gene for whole fat pad lysate RNA. Therefore, all samples were run against the 3 housekeeping genes which were

available: glyceraldehyde-3-phosphate dehydrogenase (*Gapdh*), hypoxanthine phosphoribosyltransferase (*Hprt*) and ribosomal protein S18 (*Rps18*). The ‘BestKeeper’ method (542) was used to determine which housekeeping had the best stability, which calculates the Pearson correlation between genes. The gene with the highest correlation coefficient and with a standard deviation of Ct values of below 1 was *Rps18* and thus this was chosen as the most suitable housekeeping gene to normalise target gene expression against (Table 3.1).

**Table 3.1, Results of the BestKeeper algorithm to determine housekeeping gene stability for inguinal and gonadal fat pad samples.**

	<i>Gapdh</i>	<i>Hprt</i>	<i>Rps18</i>
<b>Mean Ct value</b>	20.25	28.97	23.20
<b>Standard deviation of Ct values</b>	1.06	2.46	0.93
<b>Correlation coefficient [r]</b>	0.678	0.856	0.952
<b>p-value</b>	0.005	0.001	0.001

Gene expression of two key lipolysis genes was determined. Patatin like domain 2, triacylglycerol lipase (*Pnpla2*) encodes ATGL, the enzyme which catalyses the first step of lipolysis, hydrolysing triglycerides into diacylglycerol and fatty acid. Lipase E (*Lipe*) encodes HSL, responsible for catalysing the hydrolysis of diacylglycerol into monoacylglycerol and fatty acid (550). Thus, both are crucial for the hydrolysis of stored triglycerides into fatty acids. *Pnpla2* and *Lipe* were significantly upregulated in response to LPS in the inguinal adipose tissue (Figure 3.9A). However, neither was significantly altered in gonadal adipose tissue (Figure 3.9B). This difference may be due to fat pad location, as inguinal fat pads are much closer in proximity to bone marrow than gonadal fat pads are, and therefore different adipose tissue may play different roles. Taken together, these results provide evidence that the expression of genes associated with lipolysis increased in inguinal, but not gonadal fat pads, highlighting a potential difference between the different fat pads. However, it should be noted that because only gene expression was assessed, it is difficult to conclude if this increase in lipolytic genes actually contributed towards the increase in LCFAs observed in the early response to LPS, a limitation of this study.

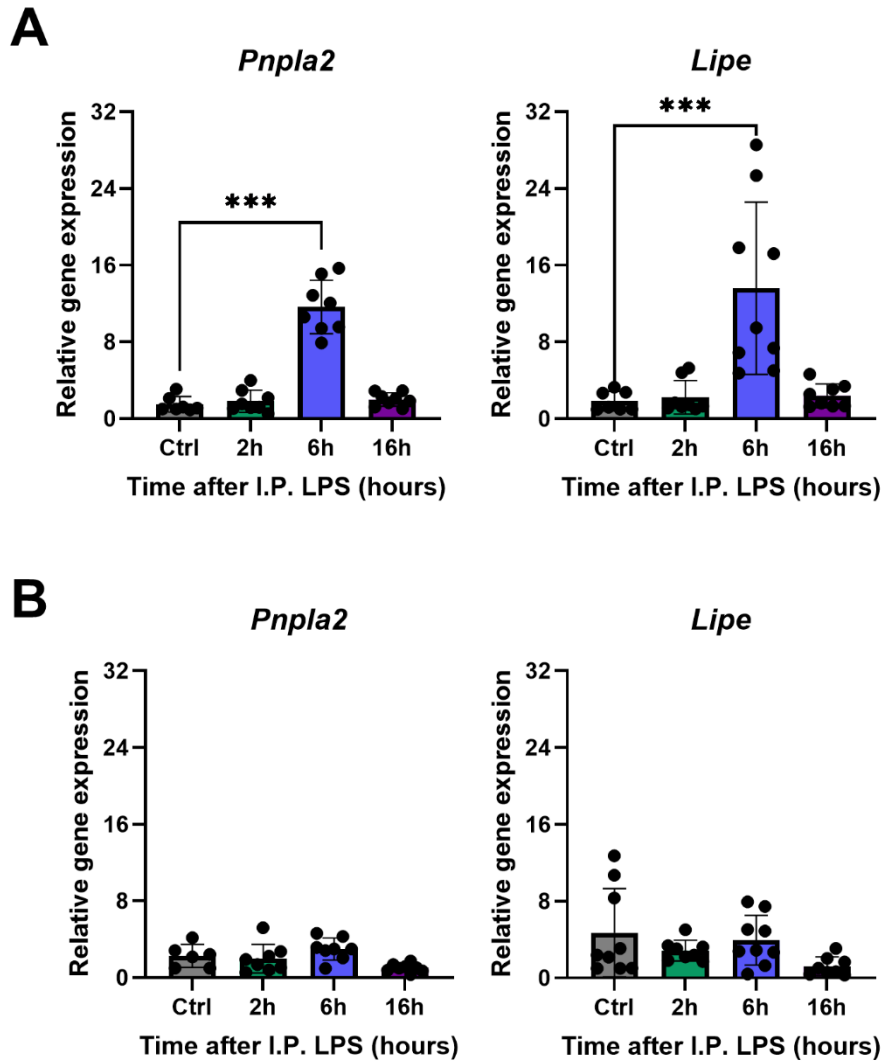


**Figure 3.9, Time-course of lipolysis associated gene expression in inguinal and gonadal fat pads in response to LPS treatment.**

WT mice were injected with 0.5 mg/kg LPS via I.P. for 2, 6 and 16 hours before being sacrificed. RNA was extracted from inguinal and gonadal fat pads and analysed for lipolytic gene expression via RT-qPCR. **A)** Inguinal fat pad gene expression **B)** Gonadal fat pad gene expression. Gene expression was normalised against *Rps18*. Mean and standard deviation was calculated and shown on the graph (n = 9). A Kruskal-Wallis test with a Dunn's correction for multiple comparisons was performed, comparing each timepoint against the control group, and significant differences are marked using asterisks (\* = p < 0.05, \*\* = P < 0.01, \*\*\* = p < 0.001 and \*\*\*\* = p < 0.0001).

When taken together, this data provides evidence that 6 hours after LPS injection, LCFAs significantly increased in the serum of mice. By 16 hours, whilst this increase in LCFAs was still evident, it was not as pronounced. This increase in LCFAs in response to LPS was associated with a reduction in blood glucose levels and an increase in blood ketone levels. Fat pad weight did not significantly change across the time-course, however inguinal fat pads had an increase in lipolytic associated gene expression not seen in gonadal fat pads.

### **3.4 Characterising the role of the liver in circulating LCFA availability in response to LPS**

Whilst lipolysis may be, at least in part, contributing towards the increase in circulating LCFAs in response to LPS, the role of the liver was also explored. In healthy individuals, the majority of fatty acids released by adipocytes are taken up and processed by the liver (551). This is because the liver is the master regulator of fatty acid availability in the circulation. Therefore, the role of the liver within regulating fatty acid availability in response to LPS was investigated.

Firstly, the liver was assessed for any LPS-associated damage that could impact its metabolic response. Fixed liver lobes from mice treated with LPS for 2, 6 and 16 hours were embedded as described in section 2.7.1 of the methods. Livers were then sectioned and stained with haematoxylin and eosin (H&E) to check overall liver cellularity and for areas of necrosis (Figure 3.10). There were no notable differences seen between control mice and mice treated with LPS for 2 and 6 hours. However, there were small patches of necrosis directly surrounding the portal vein in mice 16 hours after LPS treatment, noted with arrows.

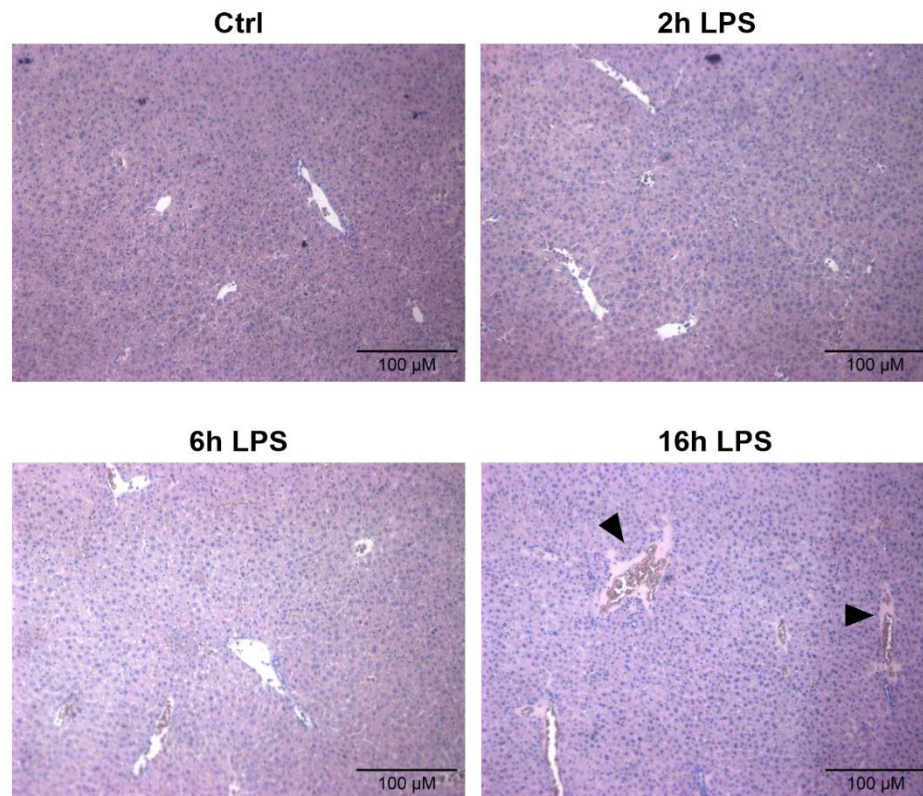


**Figure 3.10, Histological staining of liver tissue to assess histological changes in cellularity in response to LPS.**

WT mice were injected with 0.5 mg/kg LPS via I.P. for 2, 6 and 16 hours before being sacrificed. Liver tissue was fixed, embedded, sectioned and stained for H&E. Representative images are shown for each group, with arrows marking areas of necrosis. Images were taken at 4x magnification with scale bars shown.

Taking into consideration that the largest increase in circulating LCFAs was seen at 6 hours following LPS treatment, and that liver cellularity looked comparable to control mice with no notable necrosis or damage, 6 hours was determined to be the most suitable timepoint to study the effects of LPS treatment on liver metabolism. RNA extracted from whole liver lysate from mice treated with LPS for 6 hours was sent to Novogene (Cambridge, UK) for bulk RNA sequencing. Whilst initial analysis to identify differentially expressed genes (DEGs) and subsequent Kegg pathway enrichment was performed by Novogene, further identification and analysis of the relevant data and genes, as well as overall data interpretation and presentation was done myself. A volcano plot showing the log<sub>2</sub> fold change revealed a similar number of genes were upregulated or downregulated in response to LPS (Figure 3.11A). The genes with the most significant increase in expression were *Saa3*, *Gbp2* and *Cxcl9*, all of which are

known markers of and play an important role in inflammation and infection (552). The most significantly downregulated but relevant genes included *G0s2* and *Cyp7a1*.

Clustermap analysis confirmed that the differences seen in DEGs was between and not within sample groups (Figure 3.11B). Samples were clustered using the  $\log_2(\text{FPKM}+1)$  values. LPS treated mice clustered together, showing similarities within the 3 samples sequenced. Control mice showed an almost opposite clustering effect to LPS treated livers, and thus there was a distinct visual difference between the two groups.

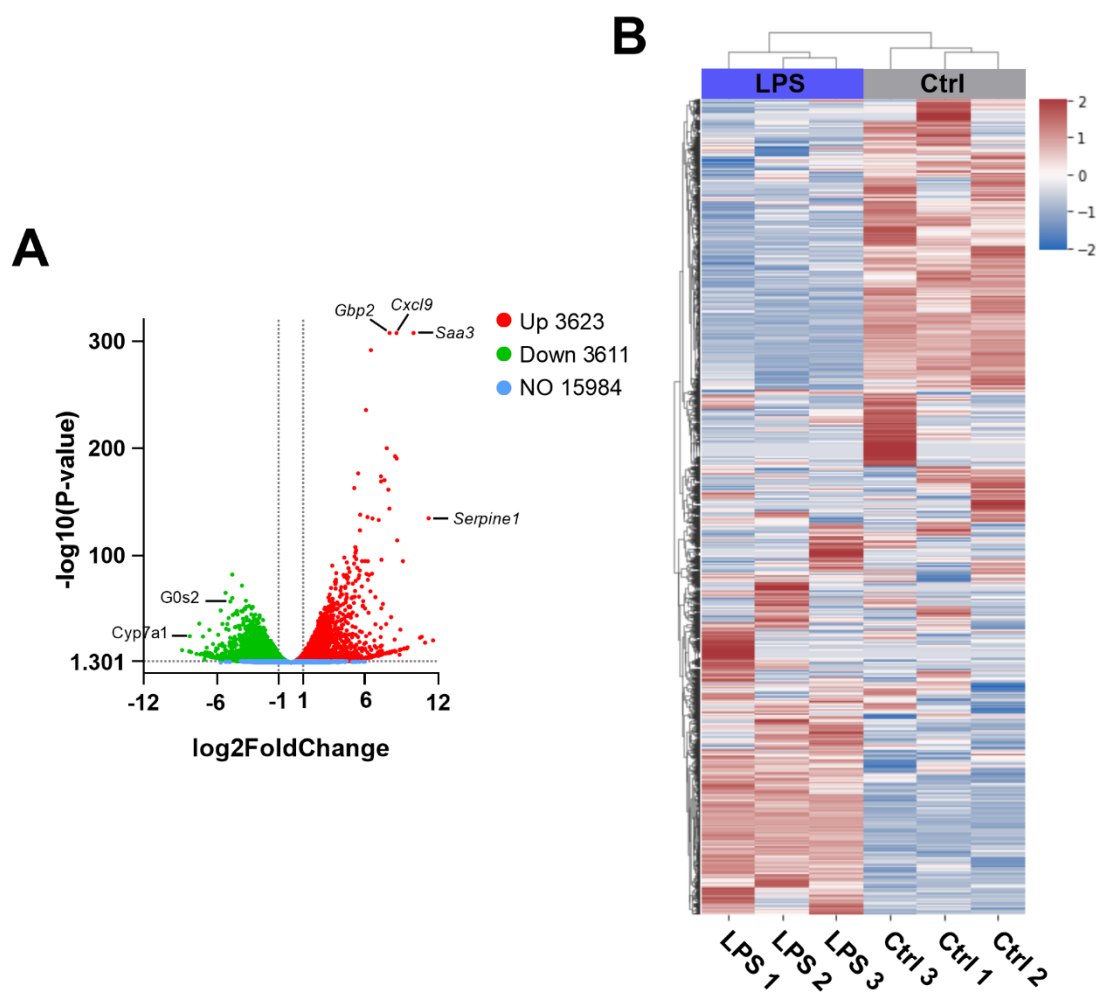


**Figure 3.11, Bulk RNA sequencing revealed distinct differences in liver gene expression between control and LPS treated mice.**

WT mice were injected with 0.5 mg/kg LPS via I.P. for 6 hours before being sacrificed. RNA was extracted from whole liver lysates and sequenced. **A)** Volcano plot of differentially expressed genes by  $\log_2$  fold change. **B)** Clustermap analysis using the  $\log_2(\text{FPKM}+1)$  to visualise the data, (n = 3).

Kegg pathway enrichment analysis was then performed to identify the most upregulated pathways (Figure 3.12). This is done by calculating the number of genes which were upregulated compared to the total number of genes associated with that pathway. Unsurprisingly, the most upregulated pathways were nearly all proinflammatory or infection associated pathways. Many of which were cytokine associated signalling pathways including the TNF, NF $\kappa$ B and MAPK signalling cascades.

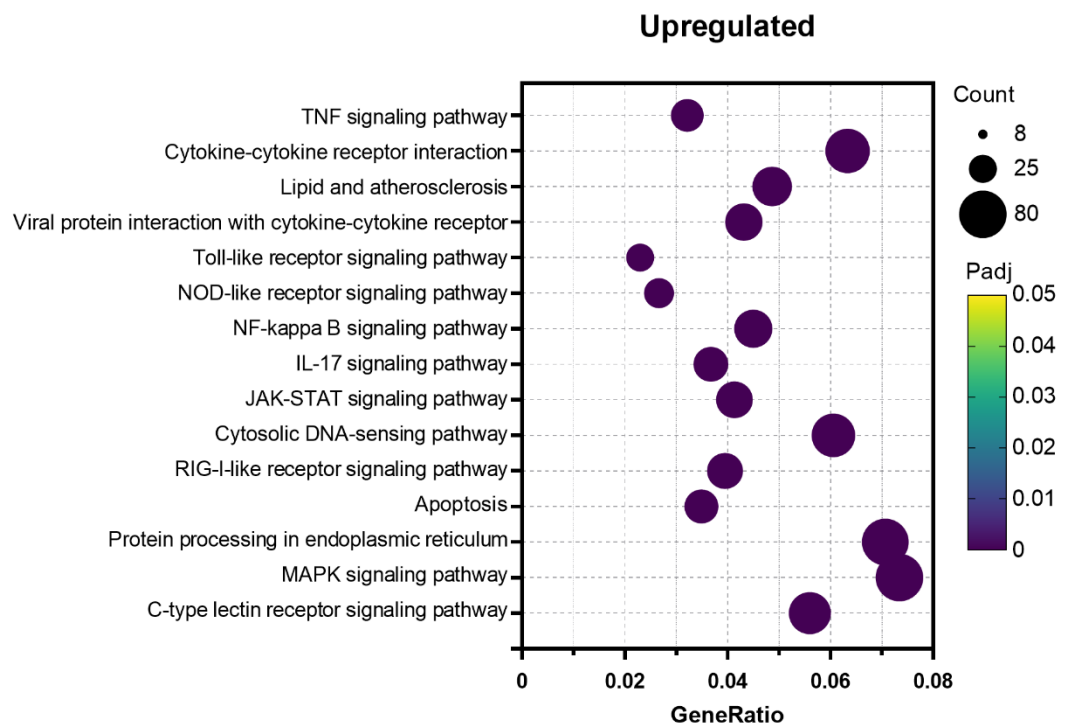


**Figure 3.12, Kegg enrichment analysis of bulk RNA sequencing for the most significantly upregulated pathways in liver gene expression between control and LPS treated mice.**

WT mice were injected with 0.5 mg/kg LPS via I.P. for 6 hours before being sacrificed. RNA was extracted from whole liver lysates and sequenced. Kegg enrichment and pathway analysis of the most significantly upregulated pathways identified in of LPS treated mice compared to control mice, (n = 3).

The majority of the most downregulated pathways in the liver in response to LPS treatment were associated with fatty acid metabolism (Figure 3.13). This included fatty acid biosynthesis and several LCFA specific pathways including linoleic and arachidonic acid metabolism.

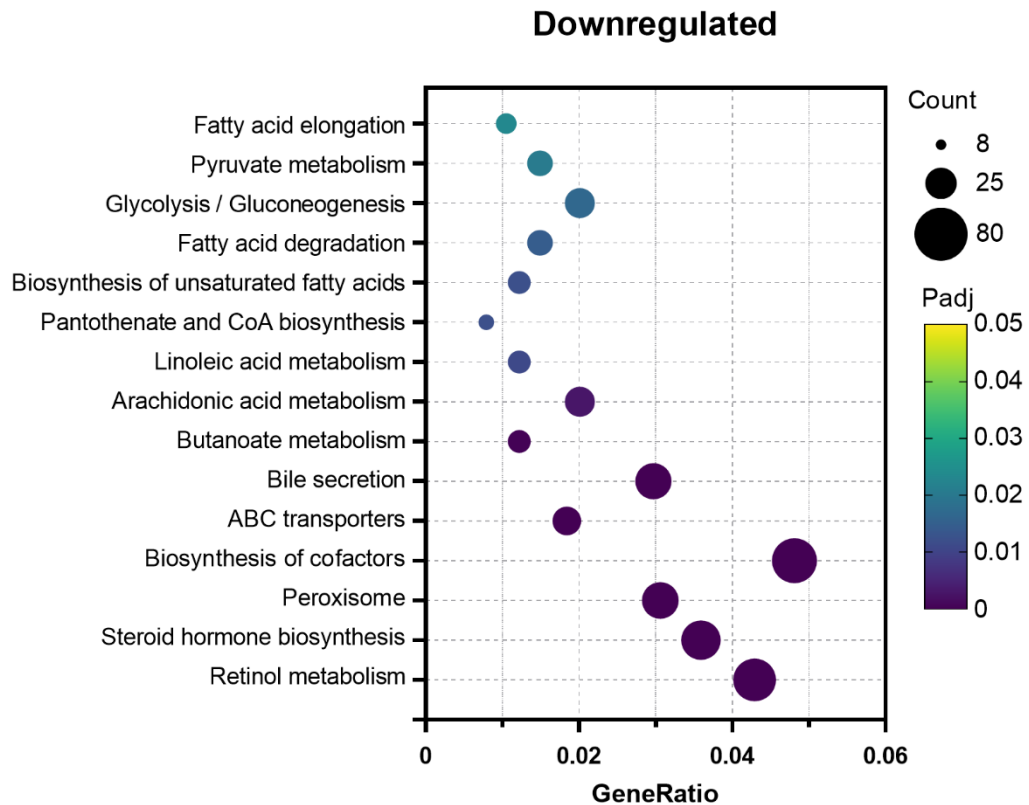


**Figure 3.13, Kegg enrichment analysis of bulk RNA sequencing for the most significantly downregulated pathways in liver gene expression between control and LPS treated mice.**

WT mice were injected with 0.5 mg/kg LPS via I.P. for 6 hours before being sacrificed. RNA was extracted from whole liver lysates and sequenced. Kegg enrichment and pathway analysis of the most significantly downregulated pathways identified in LPS treated mice compared to control mice, (n = 3).

Pathway analysis identified that overall fatty acid metabolism was downregulated in the livers of LPS treated mice, and serum analysis revealed a significant increase in circulating LCFA. Therefore, the expression of fatty acid transport genes known to be important in the liver were checked. Many of these fatty acid transporters were significantly downregulated including *Fabp1*, *Fabp2*, *Slc27a1* and *Slc27a2* (Figure 3.14). This provides evidence that the liver stops taking up fatty acids in response to LPS. However, not all transporter genes were downregulated, for example there was no significant change in *Cd36* or *Lrp1* (low-density lipoprotein receptor-related protein 1) expression. *Fabp5* and *Fabp7* were significantly upregulated in the liver in response to LPS. As well as its role in fatty acid transport, *Fabp7* has been shown to be important in regulating Kupffer cell phagocytosis (553). Additionally, *Fabp5* has

been shown to be upregulated in response to endotoxins such as LPS as part of the inflammatory response and is also thought to regulate macrophage response (554). That being said, the most highly expressed fatty acid transport genes in the liver are *Fabp1*, *Slc27a2* and *Slc27a5*, all of which are LCFA transporters and were significantly downregulated in response to LPS. Taken together, these results demonstrate that the liver downregulates fatty acid metabolism in response to LPS.

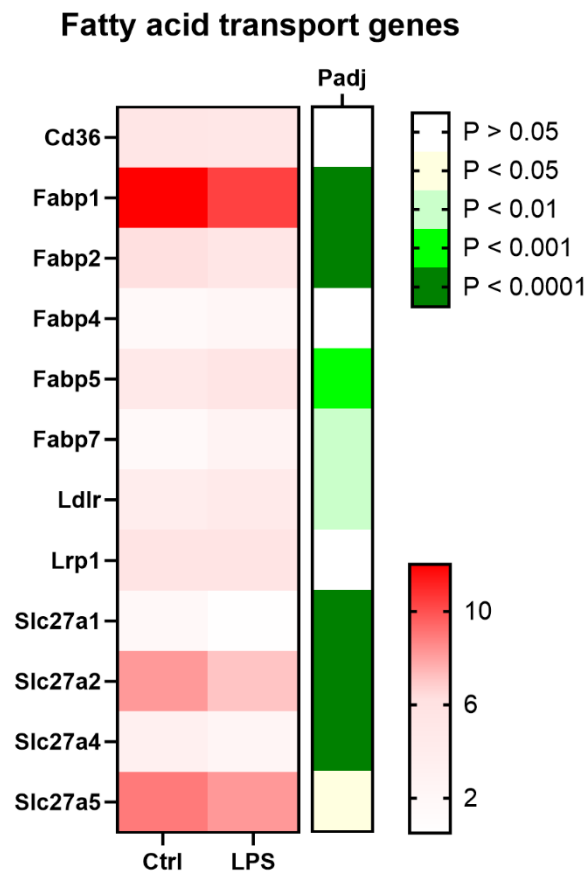


**Figure 3.14, Bulk RNA sequencing revealed distinct differences in liver gene expression of LCFA transporters between control and LPS treated mice.**

WT mice were injected with 0.5 mg/kg LPS via I.P. for 6 hours before being sacrificed. RNA was extracted from whole liver lysates and sequenced. Heatmap of liver specific fatty acid transport proteins using the  $\log_2(\text{FPKM}+1)$  value and adjusted p-value to indicate significance, (n = 3).

Due to the significant upregulation in multiple proinflammatory and immune response associated genes and pathways identified within the liver bulk RNA sequencing, the populations of different liver immune cells were assessed in both control and LPS treated mice. Liver immune cells were isolated from one liver lobe and stained with the antibodies shown below in the gating strategy used (Figure 3.15).

Positive and negative populations were identified using FMO controls. Gating strategy was designed by selecting markers relevant for this study, taking a combination of previous publications into consideration (555-557).

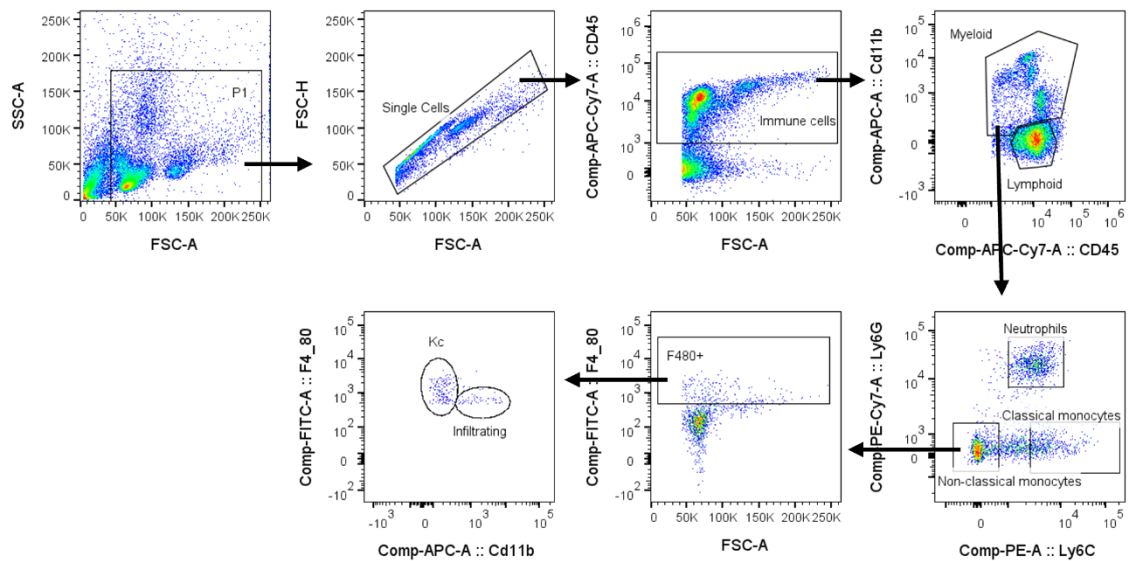


**Figure 3.15, Gating strategy to identify liver immune cells populations.**

WT mice were injected with 0.5 mg/kg LPS via I.P. for 6 hours before being sacrificed. Immune cells isolated from the liver were stained with an antibody panel using markers for lymphoid and myeloid populations. Flow cytometry gating strategy to identify different immune populations.

Total immune cell number significantly decreased in the liver in response to LPS treatment (Figure 3.16). Lymphoid cells also significantly decreased in number, however there was no significant difference between LPS treatment and controls for myeloid cell number. Despite this, the neutrophil cell count per 50,000 isolated liver cells significantly increased in response to LPS.

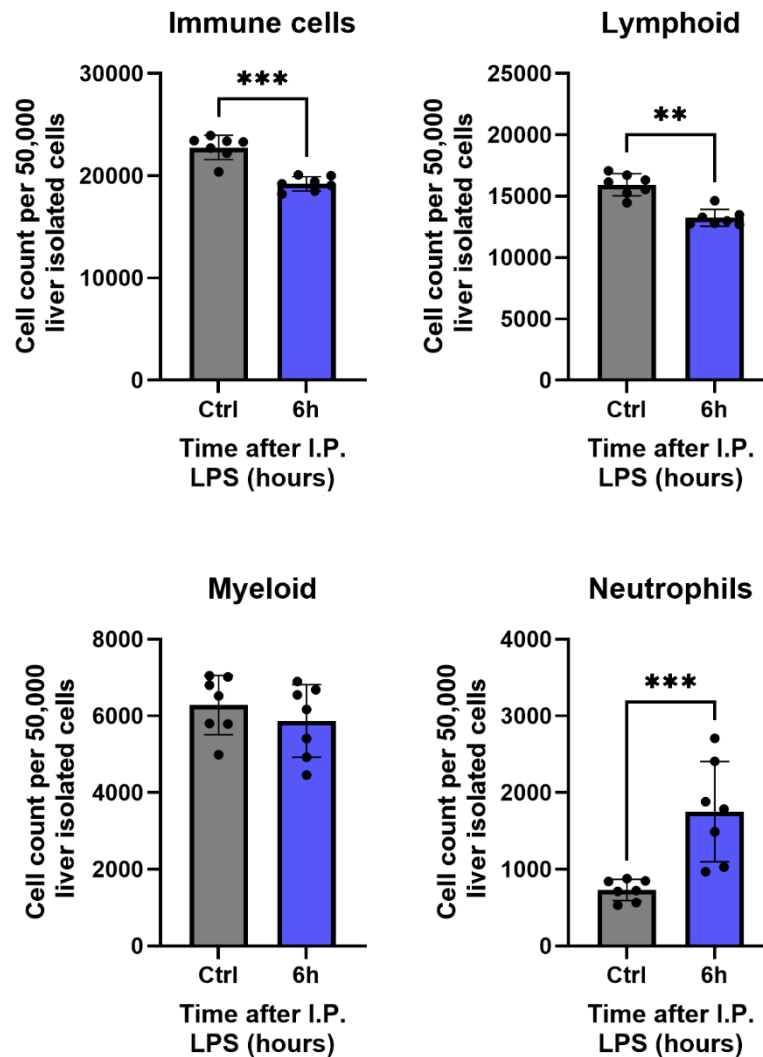


**Figure 3.16, Liver immune cell numbers in response to LPS treatment.**

WT mice were injected with 0.5 mg/kg LPS via I.P. for 6 hours before being sacrificed. Immune cells isolated from the liver were stained with an antibody panel using markers for lymphoid, myeloid and neutrophil populations. Mean and standard deviation was calculated and shown on each graph (n = 7). A Mann-Whitney test was performed comparing control and LPS treated groups, and significant differences are marked using asterisks (\* = p < 0.05, \*\* = P < 0.01, \*\*\* = p < 0.001 and \*\*\*\* = p < 0.0001).

The number of monocytes per 50,000 isolated liver cells also significantly decreased in response to LPS (Figure 3.17). This included a significant reduction in the number of classical monocytes. Classical monocytes are proinflammatory and play an important role in the innate immune response. Opposingly, non-classical monocytes are associated with an anti-inflammatory response (558, 559). Despite a decrease in total monocyte numbers, the number of non-classical monocytes significantly increased in the liver in response to LPS (Figure 3.17).

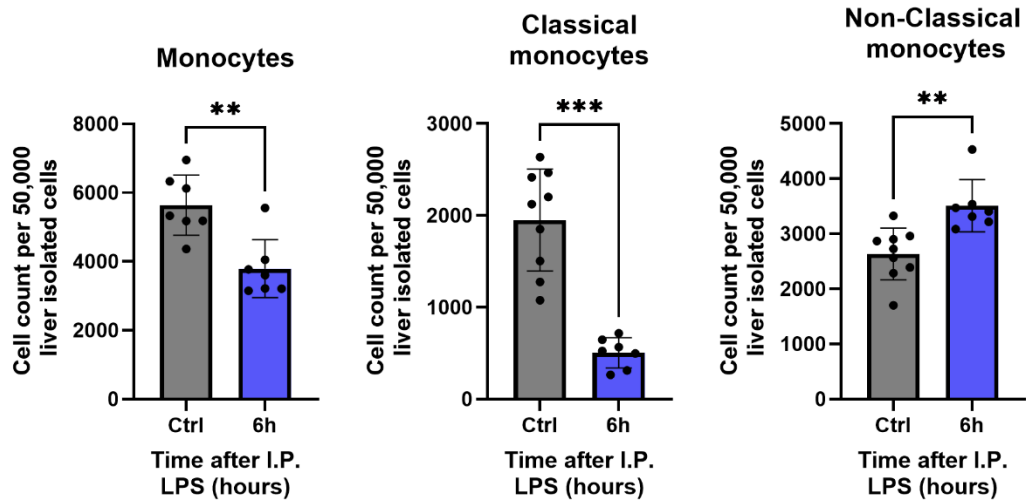


**Figure 3.17, Liver monocyte numbers in response to LPS treatment.**

WT mice were injected with 0.5 mg/kg LPS via I.P. for 6 hours before being sacrificed. Immune cells isolated from the liver were stained with an antibody panel using markers for classical and non-classical monocyte populations. Mean and standard deviation was calculated and shown on the graph (n = 7). A Mann-Whitney test was performed comparing control and LPS treated groups, and significant differences are marked using asterisks (\* = p < 0.05, \*\* = P < 0.01, \*\*\* = p < 0.001 and \*\*\*\* = p < 0.0001).

The number of macrophages per 50,000 isolated liver cells also significantly decreased in response to LPS. This was reflected in a significant decrease in non-tissue resident, or infiltrating, macrophages (Figure 3.18). There was no significant difference in the number of tissue-resident macrophages, more commonly referred to as Kupffer cells.

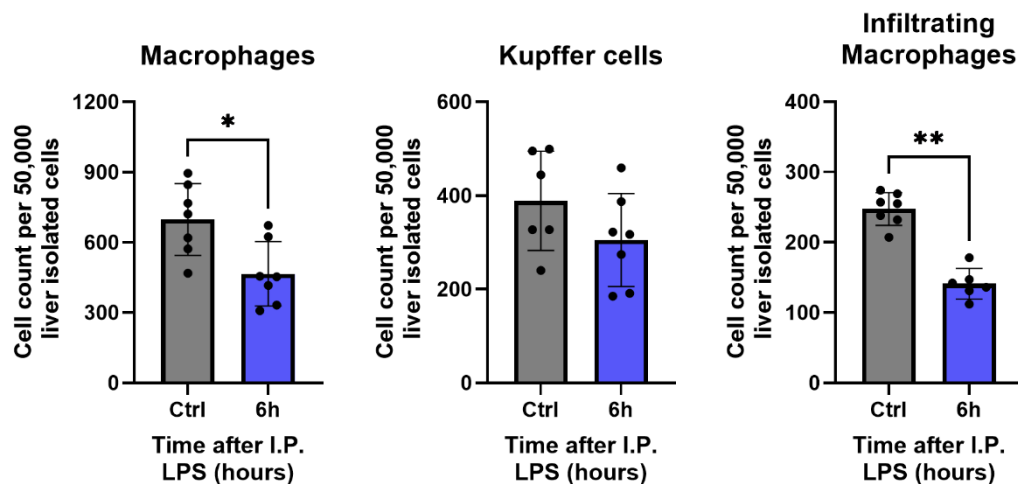


**Figure 3.18, Liver macrophage numbers in response to LPS treatment.**

WT mice were injected with 0.5 mg/kg LPS via I.P. for 6 hours before being sacrificed. Immune cells isolated from the liver were stained with an antibody panel using markers for macrophage populations. Mean and standard deviation was calculated and shown on the graph (n = 7). A Mann-Whitney test was performed comparing control and LPS treated groups, and significant differences are marked using asterisks (\* = p < 0.05, \*\* = P < 0.01, \*\*\* = p < 0.001 and \*\*\*\* = p < 0.0001).

Taken together, this suggest that fatty acid metabolism is significantly downregulated in response to LPS, but that this is not associated with increased liver damage or an increase in immune cell populations. The downregulation of some immune populations was observed in the liver. Therefore, the next step was to understand the kinetics of this downregulation of fatty acid metabolism. Key fatty acid oxidation and metabolism genes were chosen to look at the liver’s response to LPS 2, 6 and 16 hours after LPS treatment. RNA was extracted from whole liver lysates and gene expression was analysed using RT-qPCR.

Because housekeeping suitability is often tissue specific, the most suitable housekeeping gene for whole liver lysate RNA was also assessed. All samples were run against the 3 available housekeeping genes and the ‘BestKeeper’ method (542) was used to determine which housekeeping had the greatest stability. The gene with the highest correlation coefficient and with a standard deviation of Ct values of below 1 was *Rps18* (Table 3.2), and thus this was chosen as the most suitable housekeeping gene to normalise target gene expression against.

**Table 3.2, Results of the BestKeeper algorithm to determine housekeeping gene stability in the liver.**

	<i>Gapdh</i>	<i>Hprt</i>	<i>Rps18</i>
<b>Mean Ct value</b>	20.35	23.24	19.94
<b>Standard deviation of Ct values</b>	0.75	1.10	0.69
<b>Correlation coefficient [r]</b>	0.172	0.787	0.901
<b>p-value</b>	0.244	0.001	0.001

The acyl-Coenzyme A dehydrogenase (*Acadm*) gene encodes for an essential enzyme involved in fatty acid oxidation (560). Acyl-CoA synthetase long-chain family member 1 (*Acs11*) also plays an important part in fatty acid metabolism, including activating and directing LCFAs towards mitochondrial fatty acid oxidation for ATP production (561). *Cpt1a* is essential for transporting fatty acids across the mitochondrial membrane into the mitochondrial matrix to be metabolised. 3-hydroxy-3-methylglutaryl-CoA synthase 2 (*Hmgcs2*) encodes the rate limiting enzyme in ketogenesis and *Hmgcr* encodes the critical enzyme in cholesterol synthesis (562,

563). All of these together provide an important picture of overall liver fatty acid metabolism in response to LPS.

None of the genes selected were significantly downregulated at 2 hours, however all were significantly downregulated in response to LPS by 6 hours apart from *Cpt1a* (Figure 3.19). However, *Cpt1a* was significantly downregulated by 16 hours. Taken together this confirms bulk RNA sequencing data, that liver fatty acid metabolism is significantly downregulated in response to LPS by 6 hours, however this downregulation continues until at least 16 hours after LPS treatment.

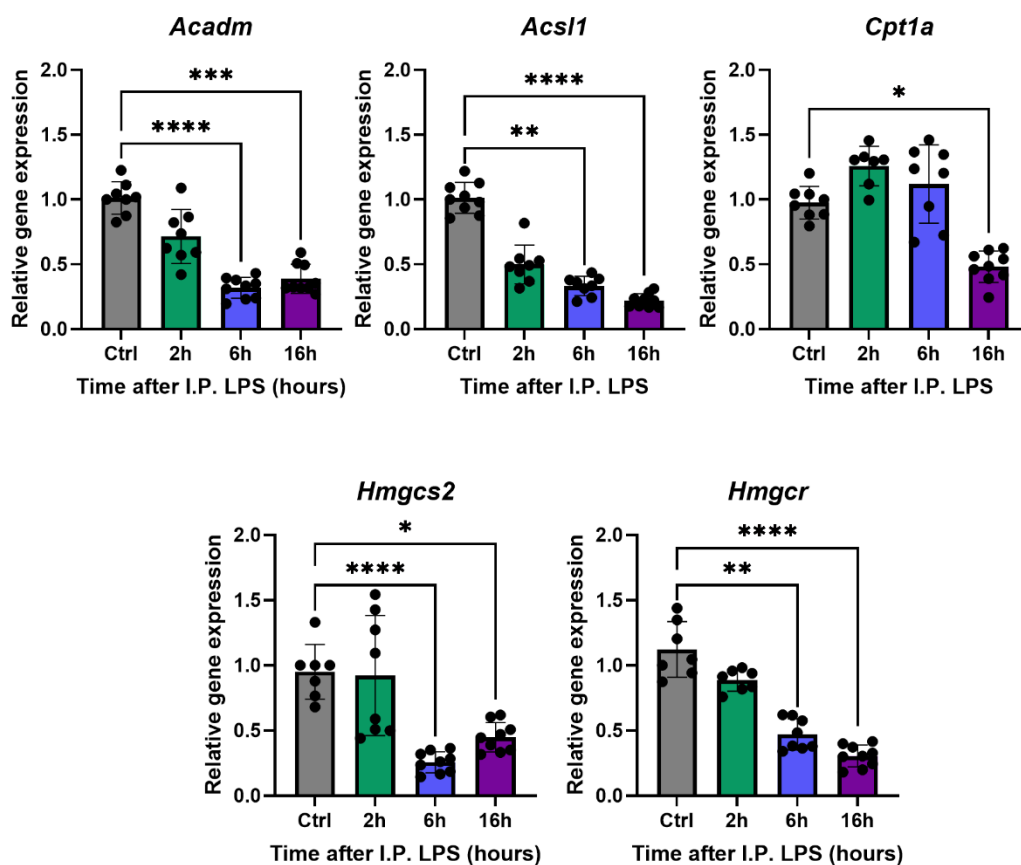


**Figure 3.19, Determining the expression of key fatty acid metabolism genes in the liver in response to LPS over time.**

WT mice were injected with 0.5 mg/kg LPS via I.P. for 2, 6 and 16 hours before being sacrificed. RNA was extracted from whole liver lysates and analysed using RT-qPCR. Gene expression was normalised against *Rps18*. Mean and standard deviation was calculated and shown on the graph (n = 9). A Kruskal-Wallis test with a Dunn's correction for multiple comparisons was performed, comparing each timepoint against the control group, and significant differences are marked using asterisks (\* = p < 0.05, \*\* = P < 0.01, \*\*\* = p < 0.001 and \*\*\*\* = p < 0.0001).

Finally, the gene expression of three key fatty acid transport genes was checked. *Cd36* and *Slc27a2* encode LCFA specific transporter proteins, and *Ldlr* is essential for binding to and removing LDL from the circulation and thus is important in cholesterol and fatty acid metabolism (564). In line with sequencing data, both *Ldlr* and *Slc27a2* were significantly downregulated in response to LPS by 6 hours and expression remained low at 16 hours (Figure 3.20). *Cd36* expression did not significantly change.

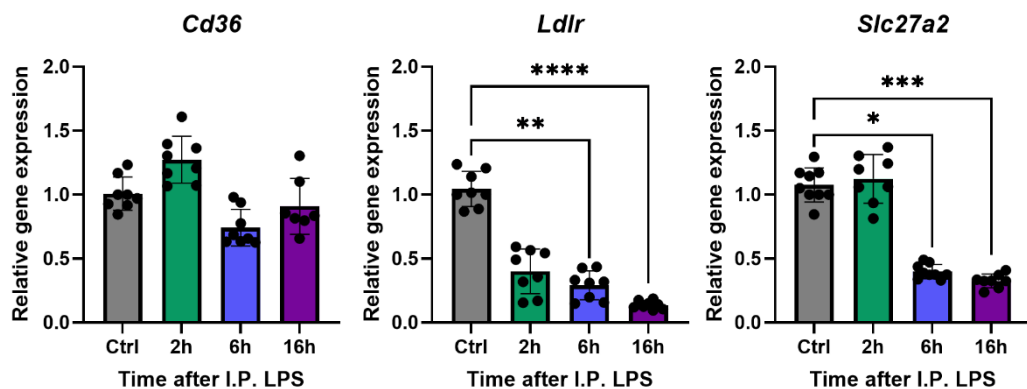


**Figure 3.20, Determining the expression of key fatty acid transport genes in the liver in response to LPS over time.**

WT mice were injected with 0.5 mg/kg LPS via I.P. for 2, 6 and 16 hours before being sacrificed. RNA was extracted from whole liver lysates and analysed using RT-qPCR. Gene expression was normalised against *Rps18*. Mean and standard deviation was calculated and shown on the graph (n = 9). A Kruskal-Wallis test with a Dunn's correction for multiple comparisons was performed, comparing each timepoint against the control group, and significant differences are marked using asterisks (\* = p < 0.05, \*\* = P < 0.01, \*\*\* = p < 0.001 and \*\*\*\* = p < 0.0001).

### 3.5 Summary

In summary, this chapter characterises the fatty acid specific metabolic changes which occur in response to LPS. Results confirmed that HSC expansion occurs 16 hours after LPS treatment and that these HSCs have a greater uptake of the LCFA C16. Furthermore, this chapter determined that circulating LCFAs increased in response to LPS at 6 hours. Using LC-MS, this study characterised the amount each measured LCFA increased by. This increase in LCFA availability occurs alongside an increase in lipolysis associated gene expression from inguinal but not gonadal adipose tissue and a downregulation in the expression of genes associated with liver fatty acid metabolism. The downregulation of genes involved in liver fatty acid metabolism was not associated with increased liver damage or with increased immune cell infiltration. These results highlight the potential importance of the liver and fat pads working together to regulate the availability of LCFAs in response to LPS. It identifies that the liver may be an important mediator in fatty acid availability in response to LPS and thus supports the hypothesis that the regulation of LCFA availability is an important factor in the immune response to LPS. However, it should be noted that in this chapter, metabolism was only assessed by looking at gene expression and thus this may not accurately reflect the true metabolic activity of the liver and fat pads, a limitation of this study.

## 4 Determining the cause of the downregulation of liver fatty acid metabolism in response to LPS

### 4.1 Introduction

Infection has been shown to alter lipid metabolism, reflecting the host's increased energy demands in response to the pathogen. However, the mechanisms underlying this metabolic switch remain unclear. Currently research suggests that liver fatty acid metabolism is regulated by a combination of several factors, including enzymes, hormones, transcription factors and ATP availability (565). The liver plays an important role in regulating circulating free fatty acids by extracting them proportionally to their plasma concentration (566). Studies have shown that the liver removes between 20-30% of each fatty acid from the blood as it circulates through the liver (567, 568). Models using stable isotope tracing have demonstrated that circulating free fatty acids are the largest single source of hepatic fatty acids uptake and storage (436). Thus, the liver plays an essential role in regulating the availability of circulating fatty acids.

The previous chapter provided evidence that LPS treatment increased the availability of circulating LCFAs and significantly downregulated liver fatty acid metabolism associated gene expression. However, the cause of this downregulation in the liver is currently undetermined. Due to the rapid nature of this response, it is less likely that this downregulation is hormone driven, and instead is more likely to be a direct response to LPS or cytokine driven. In general, hormones are considered to be slow acting, however there are some notable exceptions to this including epinephrine, and thus other factors aside from cytokines were also considered.

Hepatocytes are the main cell type within the liver and are responsible for the majority of liver fatty acid metabolism. Thus, they offer an appropriate *in vitro* model to study liver fatty acid metabolism. Therefore, this chapter investigated if hepatocytes are targeted in the downregulation of liver fatty acid metabolism associated gene expression in response to LPS and by what mechanism. This was primarily carried out using two mouse hepatocyte models: a healthy mouse hepatocyte cell line, adult mouse liver 12 weeks old (AML12s) and primary hepatocytes isolated from WT healthy young mice.

## 4.2 Short-term LPS treatment does not downregulate hepatocyte fatty acid metabolism

To investigate if the downregulation of hepatic fatty acid metabolism seen in our LPS *in vivo* models was a direct cause of LPS itself, *in vitro* experiments were performed using two hepatocyte models. Primary hepatocytes were isolated from WT mice by Dr Naiara Beraza and Dr Paula Ruiz. AML12 cells are a WT healthy hepatocyte cell line. Both AML12s cells (Figure 4.1A) and primary hepatocytes (Figure 4.1C) were treated with LPS for 2 hours before RNA was extracted and gene expression was assessed using RT-qPCR. The stability of the 3 available housekeeping genes were assessed in both cell types. *Rps18* was the most suitable housekeeping gene in AML12s, as it had the highest correlation coefficient and a standard deviation of <1 (Table 4.1), whilst *Hprt* was the most stable in primary hepatocytes (Table 4.2).

**Table 4.1, Results of the BestKeeper algorithm to determine housekeeping gene stability for AML12 cells.**

	<i>Gapdh</i>	<i>Hprt</i>	<i>Rps18</i>
Mean Ct value	17.16	20.23	16.94
Standard deviation of Ct values	0.74	1.06	0.85
Correlation coefficient [r]	0.971	0.996	0.982
p-value	0.001	0.001	0.001

**Table 4.2, Results of the BestKeeper algorithm to determine housekeeping gene stability for primary hepatocytes.**

	<i>Gapdh</i>	<i>Hprt</i>	<i>Rps18</i>
Mean Ct value	17.12	20.79	16.55
Standard deviation of Ct values	0.55	0.54	0.55
Correlation coefficient [r]	0.865	0.924	0.800
p-value	0.001	0.001	0.002

Three key marker genes to assess overall hepatic fatty acid metabolism were selected: *Acadm*, *Hmgcr* and *Hmgcs2* which are essential for fatty acid oxidation, cholesterol synthesis and ketogenesis respectively. LPS treatment did not significantly alter any of these three key genes in either AML12 cells (Figure 4.1B) or primary hepatocytes (Figure 4.1D).

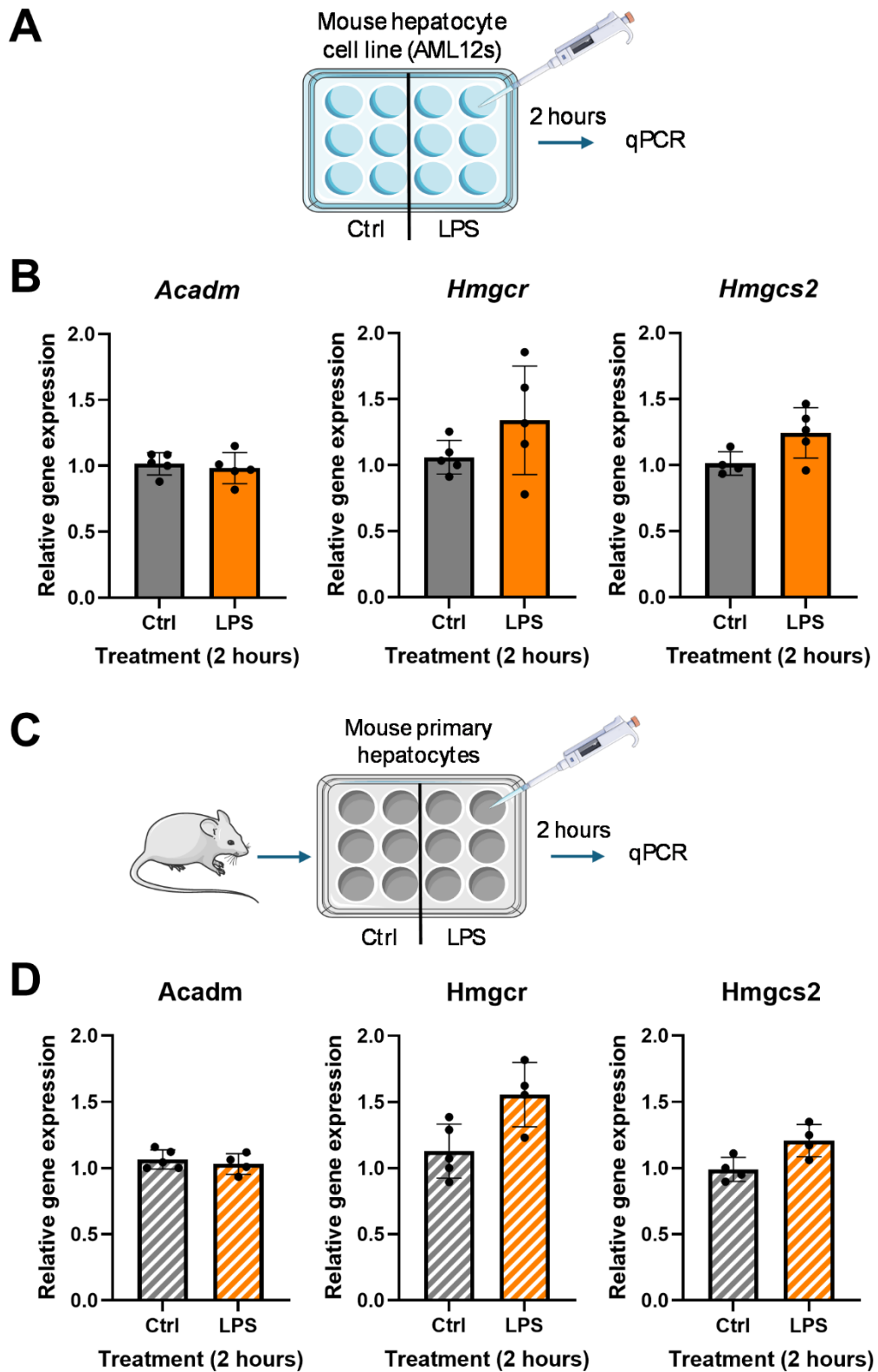


**Figure 4.1, Short-term LPS treatment did not significantly alter hepatic fatty acid metabolism gene expression *in vitro*.**

Hepatocytes were cultured with 100 ng/mL LPS for 2 hours before RNA was extracted and gene expression assessed using qRT-PCR. **A)** Schematic of experimental design for AML12 cells. **B)** AML12 cell gene expression for three key hepatic fatty acid metabolism genes normalised against *Rps18* (n = 5). **C)** Schematic of experimental design for primary hepatocytes. **D)** Primary hepatocyte gene expression for three key hepatic fatty acid metabolism genes normalised against *Hprt* (n = 5). Means and standard deviations were

calculated and are shown on each graph. A Mann-Whitney test was performed, and significant differences are marked using asterisks (\* =  $p < 0.05$ , \*\* =  $P < 0.01$ , \*\*\* =  $p < 0.001$  and \*\*\*\* =  $p < 0.0001$ ).

Whilst fatty acid associated gene expression in hepatocytes was not significantly affected by LPS, it was also important to check if hepatocytes were functionally affected. This was checked due to the bulk RNA sequencing data and liver gene expression presented in the previous chapter, which showed a significant downregulation in liver LCFA transport genes. This suggests that liver LCFA uptake is significantly reduced in LPS treated mice and thus hepatocyte LCFA uptake was assessed. Both AML12 cells and primary hepatocytes were treated with LPS for 1 hour before C16 BODIPY was added to each well. Cells were incubated for another hour before being fixed and counterstained with DAPI to identify nuclei and imaged at x10 magnification (Figure 4.2A). There were no visible differences between C16 uptake in control and LPS treated AML12 cells (Figure 4.2B), or primary hepatocytes (Figure 4.2D). C16 BODIPY fluorescence intensity per hepatocyte was then measured, and this provided quantitative evidence that C16 uptake was comparable between control and LPS treated AML12 cells (Figure 4.2C) and primary hepatocytes (Figure 4.2E). Thus, short-term LPS treatment is unlikely to directly affect hepatocyte LCFA uptake.

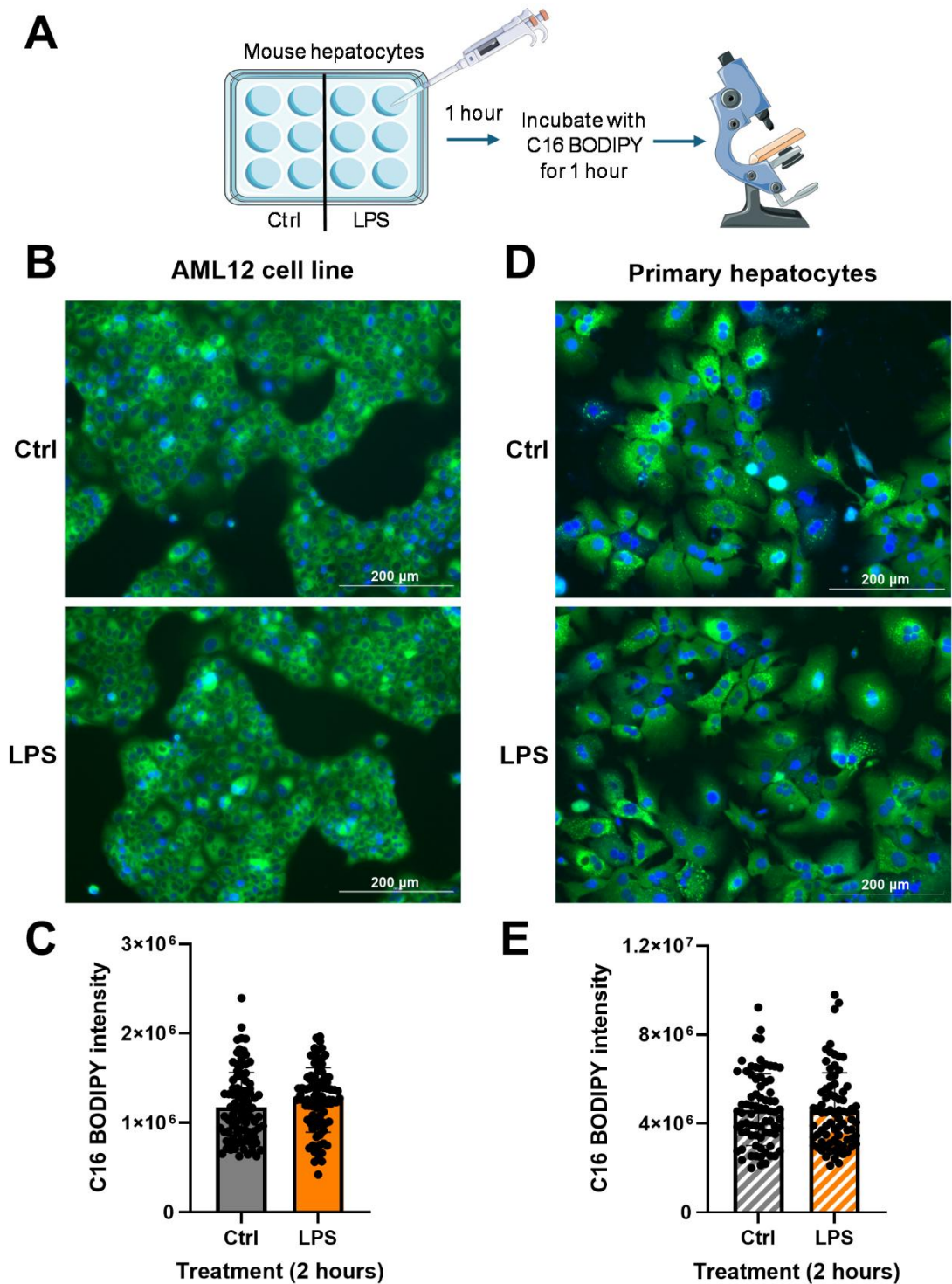


**Figure 4.2, Short-term LPS treatment did not significantly alter hepatic LCFA uptake *in vitro*.**

Hepatocytes were cultured with 100 ng/mL LPS for 1 hour before 1  $\mu$ M C16 BODIPY was added and cells were further incubated for 1 hour before fixing, counter staining with DAPI and imaging. **A)** Schematic of experimental design for AML12 cells and primary hepatocytes. **B)** Representative images of control and LPS treated AML12 cells, DAPI = blue, C16 BODIPY = green at x10 magnification. **C)** BODIPY intensity measured per AML12 cell (n = 100). **D)** Representative images of control and LPS treated primary hepatocytes, DAPI = blue, C16 BODIPY = green at x10 magnification. **E)** BODIPY intensity measured per primary hepatocyte (n = 100). Means and standard deviations were calculated and shown on each graph. A Mann-

Whitney test was performed, and significant differences are marked using asterisks (\* =  $p < 0.05$ , \*\* =  $P < 0.01$ , \*\*\* =  $p < 0.001$  and \*\*\*\* =  $p < 0.0001$ ).

Finally, to assess if short-term LPS treatment affected hepatic mitochondrial respiration when LCFA was the main fuel, a seahorse MitoStresTest was performed. Due to the limited availability of primary hepatocytes, this was only done on AML12 cells. AML12 cells were treated with 100 ng/mL LPS for 2 hours prior to the start of the seahorse assay (Figure 4.3A). Media was removed from each well and replaced with palmitic acid media (seahorse media supplemented with 100  $\mu$ M palmitic acid with no glucose, detailed in 2.5.6 in the methods). This was chosen to specifically test fatty acid associated mitochondrial respiration in response to short-term LPS treatment and not glycolysis. LPS treatment did not affect the cell viability, measured by counting the number of cells per well which survived at the end of the assay (Figure 4.3B). The OCR trace was then normalised to viable cell count before basal, maximal and ATP-linked respiration were calculated. Basal respiration is calculated by subtracting non-mitochondrial oxygen consumption from the initial OCR readings measured at the start of the assay. It describes the energetic demand of the cell under non-stress conditions. ATP-linked respiration describes the cellular oxygen consumption associated with ATP production. Maximal respiration describes the maximum rate of respiration the cell is capable of under stress-conditions. OCR was not visibly altered in LPS treated AML12 cells compared to control (Figure 4.3C), and this resulted in no significant difference in basal and maximal respiration (Figure 4.3D). However, ATP-linked respiration was significantly increased in the LPS treated group (Figure 4.3D).

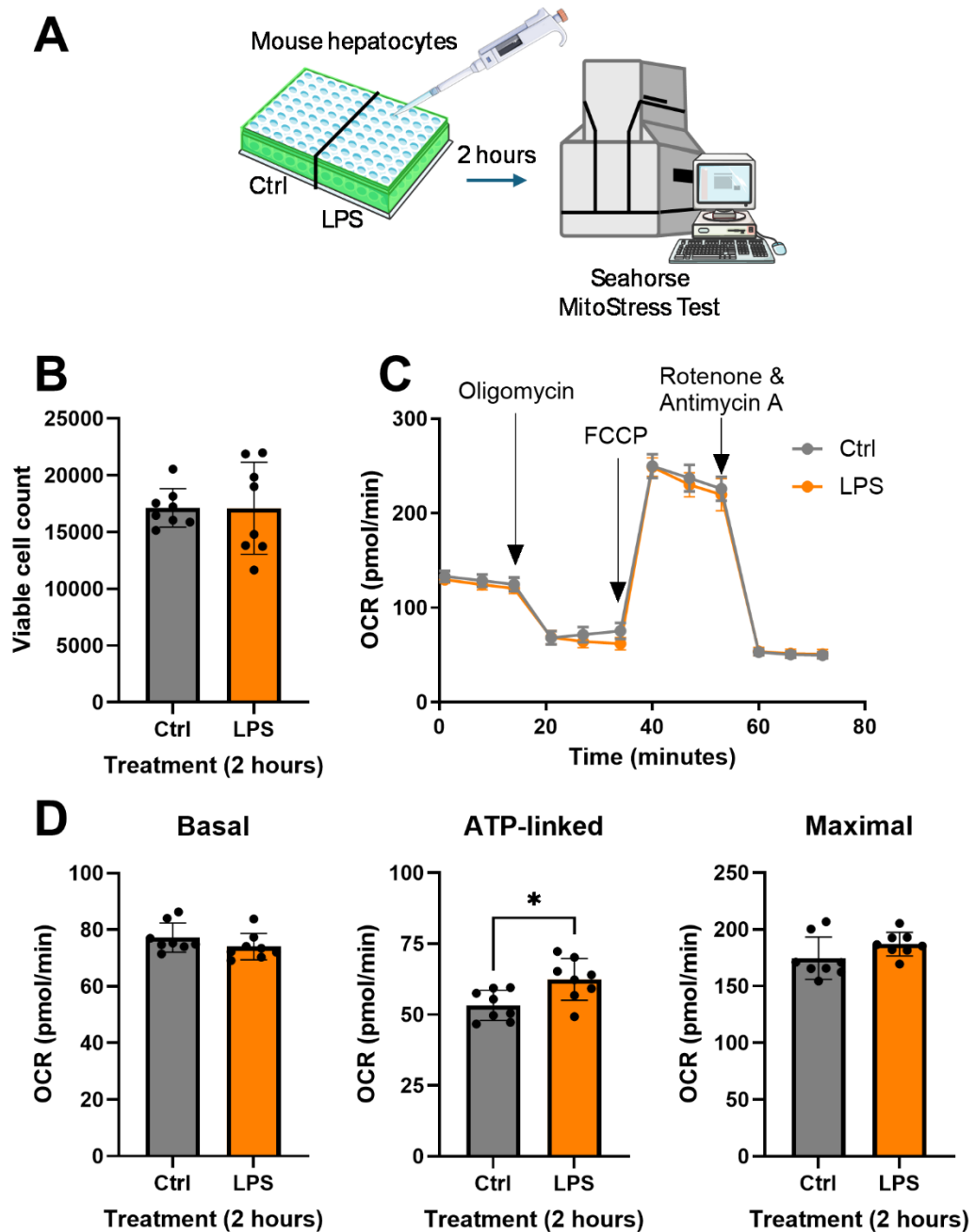


**Figure 4.3, Short-term LPS treatment did not downregulate hepatic fatty acid associated mitochondrial respiration *in vitro*.**

AML12 cells were cultured with 100 ng/mL LPS for 2 hours. **A)** Schematic of experimental of Seahorse MitoStress test. **B)** Viable cell count taken at the end of the assay. **C)** Seahorse tracing of OCR normalised to cell count. **D)** Basal, ATP-linked and maximal respiration calculated from the normalised OCR trace. Means and standard deviations were calculated and are shown on each graph (n = 8). A Mann-Whitney test was performed, and significant differences are marked using asterisks (\* = p < 0.05, \*\* = P < 0.01, \*\*\* = p < 0.001 and \*\*\*\* = p < 0.0001).

Taken together, this data shows that short-term LPS treatment does not significantly alter hepatic fatty acid metabolism. Therefore, the downregulation of liver fatty acid metabolism seen in LPS treated mice is not directly due to LPS itself but another factor or cell type being affected.

### **4.3 Serum from LPS-treated mice downregulated hepatic fatty acid metabolism *in vitro***

To test if the downregulation of liver fatty acid metabolism seen was due to a factor released into the serum in response to LPS, WT mice were treated with LPS for 2 hours before being sacrificed. Serum was separated from whole blood. A 2-hour timepoint was selected because for gene expression to be downregulated in response to LPS *in vivo* by 6 hours, the causative factor would have to be released into the serum quickly to enable it to have enough time induce this downregulation.

Both AML12 cells and primary hepatocytes were treated with serum pooled from 9 control or LPS treated mice for 2 hours before RNA was extracted and gene expression was determined using qRT-PCR using the same 3 fatty acid metabolism marker genes (Figure 4.4A). *Acadm*, *Hmgcr* and *Hmgcs2* were all significantly downregulated in AML12 cells (Figure 4.4B), and primary hepatocytes (Figure 4.4C), treated with serum from LPS-treated mice compared to those treated with serum from control mice.

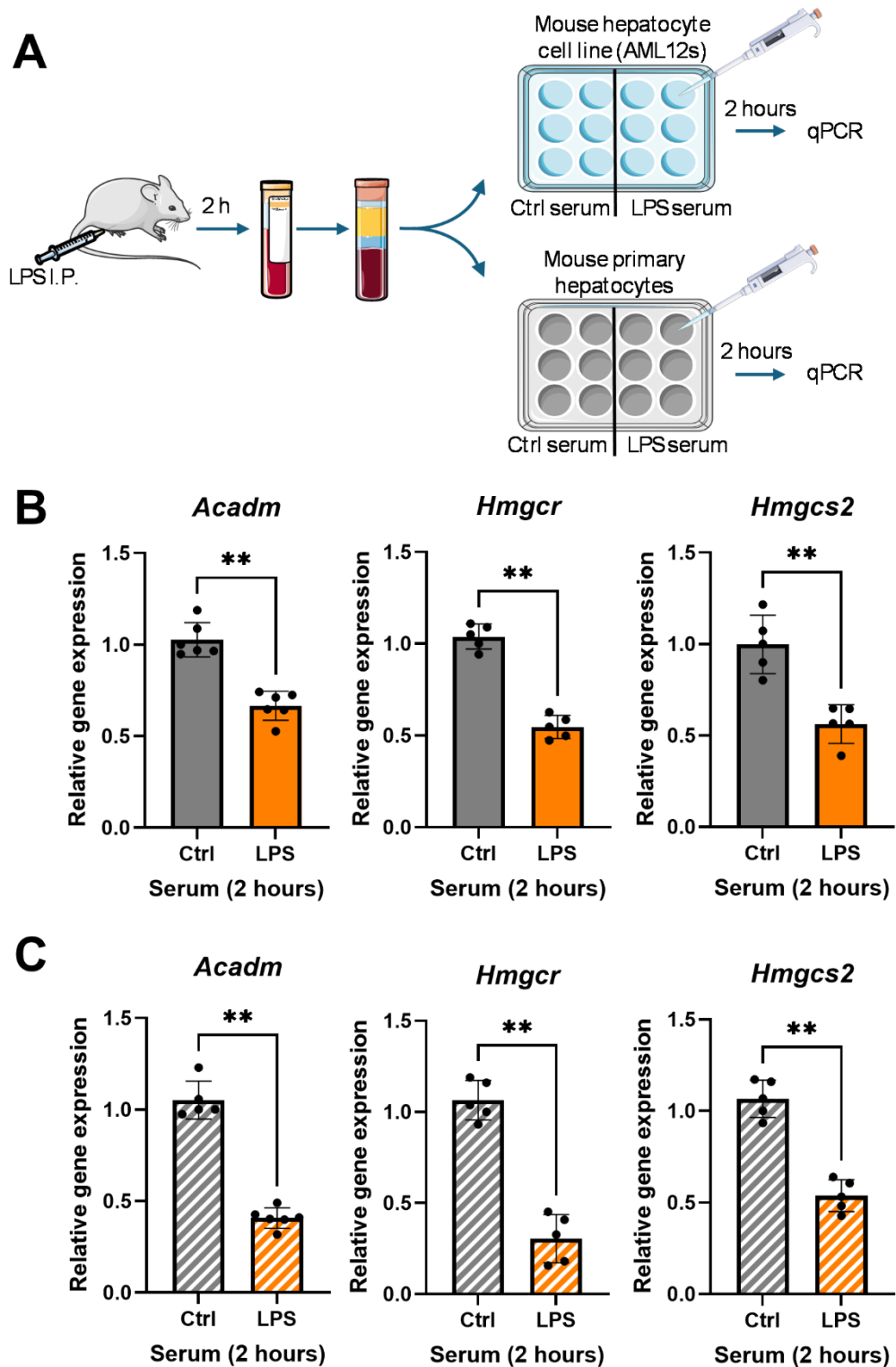


**Figure 4.4, Serum from LPS-treated mice but not control mice downregulated hepatic fatty acid metabolism gene expression *in vitro*.**

Mice were treated with 0.5 mg/kg LPS for 2 hours before being sacrificed. AML12 cells and primary hepatocytes were cultured with serum isolated and pooled from 9 control mice or LPS-treated mice for 2 hours before RNA was extracted and gene expression assessed using qRT-PCR. **A)** Schematic of experimental design. **B)** Gene expression for three key hepatic fatty acid metabolism genes normalised against *Rps18* in AML12 cells (n = 6). **C)** Gene expression for three key hepatic fatty acid metabolism genes normalised against *Hprt* in primary hepatocytes (n = 6). Means and standard deviations were calculated and are shown on each

graph. A Mann-Whitney test was performed, and significant differences are marked using asterisks (\* =  $p < 0.05$ , \*\* =  $P < 0.01$ , \*\*\* =  $p < 0.001$  and \*\*\*\* =  $p < 0.0001$ ).

Next, hepatocyte LCFA uptake was assessed using the same serum model. Both AML12 cells and primary hepatocytes were treated with serum pooled from 9 control or LPS-treated mice for 1 hour before C16 BODIPY was added to each well. Cells were incubated for another hour before being fixed, counterstained with DAPI and imaged. A visible reduction in C16 uptake was observed in AML12 cells (Figure 4.5A) and primary hepatocytes (Figure 4.5C) cultured with serum from LPS-treated mice. Quantification of C16 BODIPY fluorescence intensity per hepatocyte confirmed that serum from an LPS-treated mouse significantly reduced C16 uptake in AML12 cells (Figure 4.5B) and primary hepatocytes (Figure 4.5D).

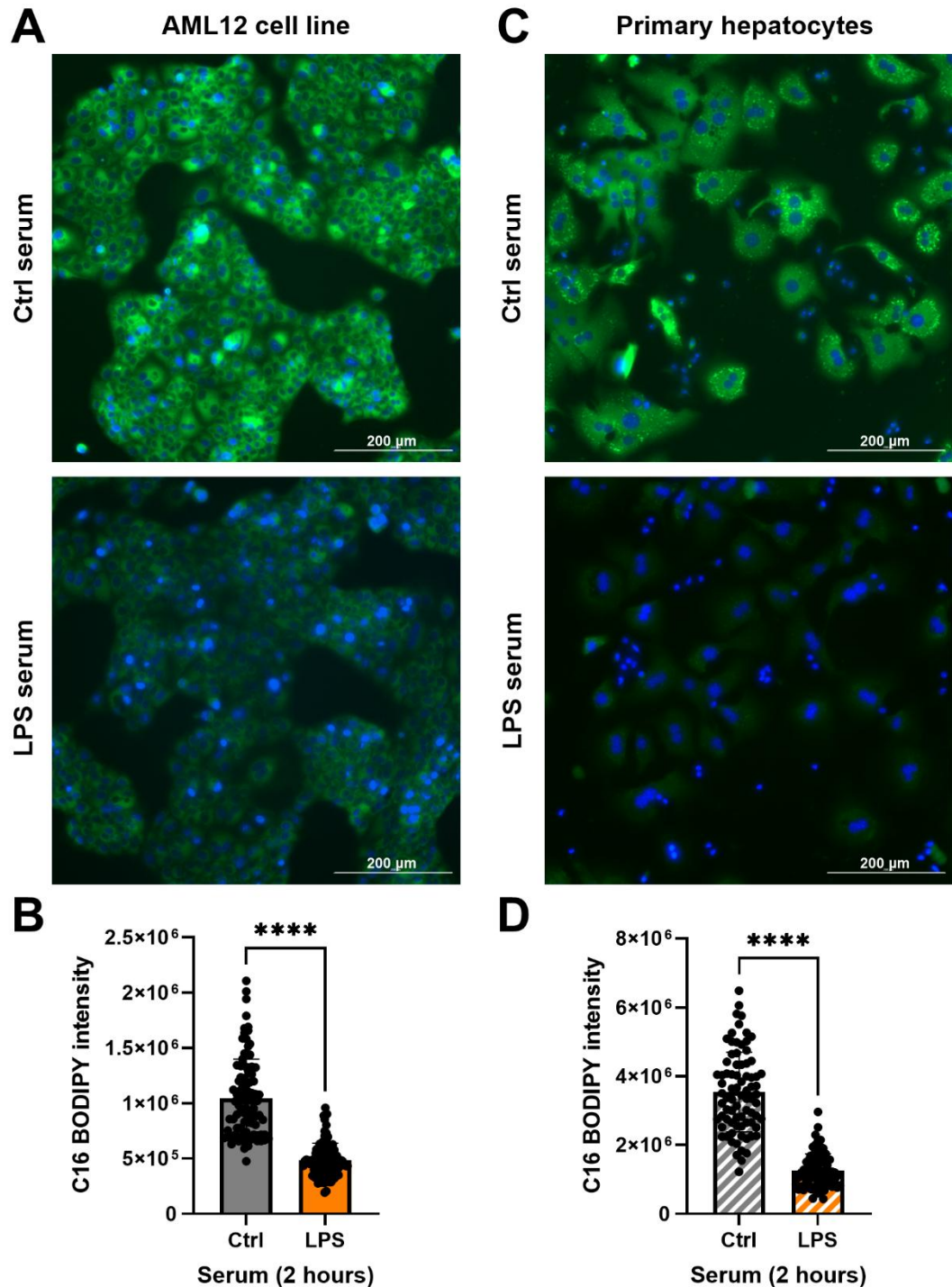


**Figure 4.5, Serum from LPS-treated mice but not control mice downregulated hepatic LCFA uptake *in vitro*.**

Mice were treated with 0.5 mg/kg LPS for 2 hours before being sacrificed. AML12 cells and primary hepatocytes were cultured with serum isolated and pooled from 9 control or LPS-treated mice for 1 hour before 1  $\mu$ M C16 BODIPY was added and cells were further incubated for 1 hour before fixing, counter staining with DAPI and imaging. **A)** Representative images of AML12 cells cultured with control and LPS-treated serum, DAPI = blue, C16 BODIPY = green at x10 magnification. **B)** BODIPY intensity measured per AML12 cell (n = 100). **C)** Representative images of primary hepatocytes cultured with control and LPS-treated serum, DAPI = blue, C16 BODIPY = green at x10 magnification. **D)** BODIPY intensity measured per primary hepatocyte (n = 100). Means and standard deviations were calculated and shown on

each graph. A Mann-Whitney test was performed, and significant differences are marked using asterisks (\* =  $p < 0.05$ , \*\* =  $P < 0.01$ , \*\*\* =  $p < 0.001$  and \*\*\*\* =  $p < 0.0001$ ).

LCFA associated mitochondrial respiration was assessed using both hepatocyte models. AML12 cells and primary hepatocytes were cultured with serum from control or LPS-treated mice for 2 hours prior to the start of the seahorse assay. Media was removed from each well and replaced with palmitic acid seahorse media. Serum from LPS-treated mice did not negatively affect the cell viability in either AML12 cells (Figure 4.6A) or primary hepatocytes (Figure 4.7A). The OCR trace was then normalised to viable cell count for AML12 cells (Figure 4.6B) and primary hepatocytes (Figure 4.7B), revealing marked differences in the trace between control serum treated and LPS-serum treated cells. Basal, maximal and ATP-linked respiration were then calculated. All three measurements were significantly reduced in AML12 cells (Figure 4.6C) and primary hepatocytes (Figure 4.7C) cultured with serum from an LPS-treated mouse. This means that there was a reduction in fatty acid associated mitochondrial ATP production in both stress and non-stress conditions.

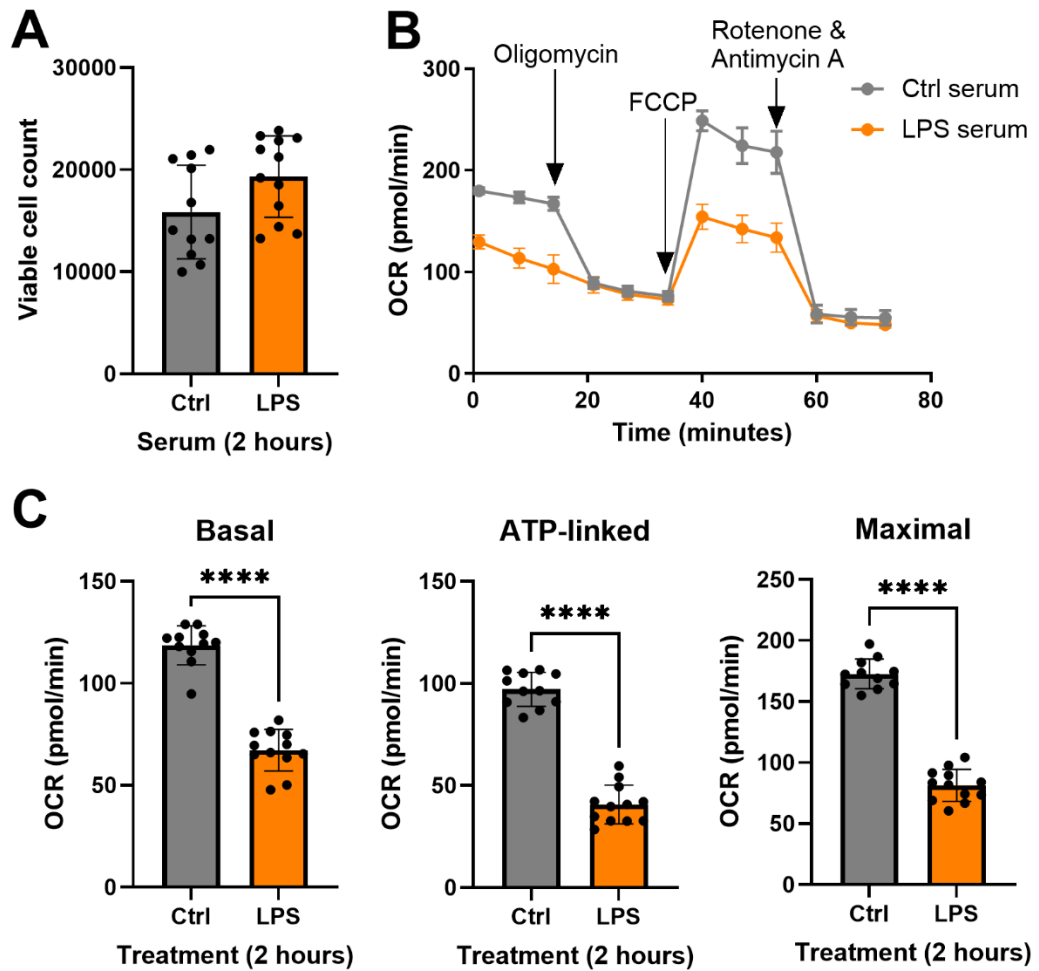


**Figure 4.6, Serum from LPS-treated mice but not control mice downregulated hepatic fatty acid associated mitochondrial respiration *in vitro* in AML12 cells.**

Mice were treated with 0.5 mg/kg LPS for 2 hours before being sacrificed. AML12 cells were cultured with serum isolated from control or LPS-treated mice for 2 hours. **A)** Viable cell count taken at the end of the assay. **B)** Seahorse tracing of OCR normalised to cell count. **C)** Basal, ATP-linked and maximal respiration calculated from the normalised OCR trace. Means and standard deviations were calculated and are shown on each graph (n = 12). A Mann-Whitney test was performed, and significant differences are marked using asterisks (\* = p < 0.05, \*\* = P < 0.01, \*\*\* = p < 0.001 and \*\*\*\* = p < 0.0001).

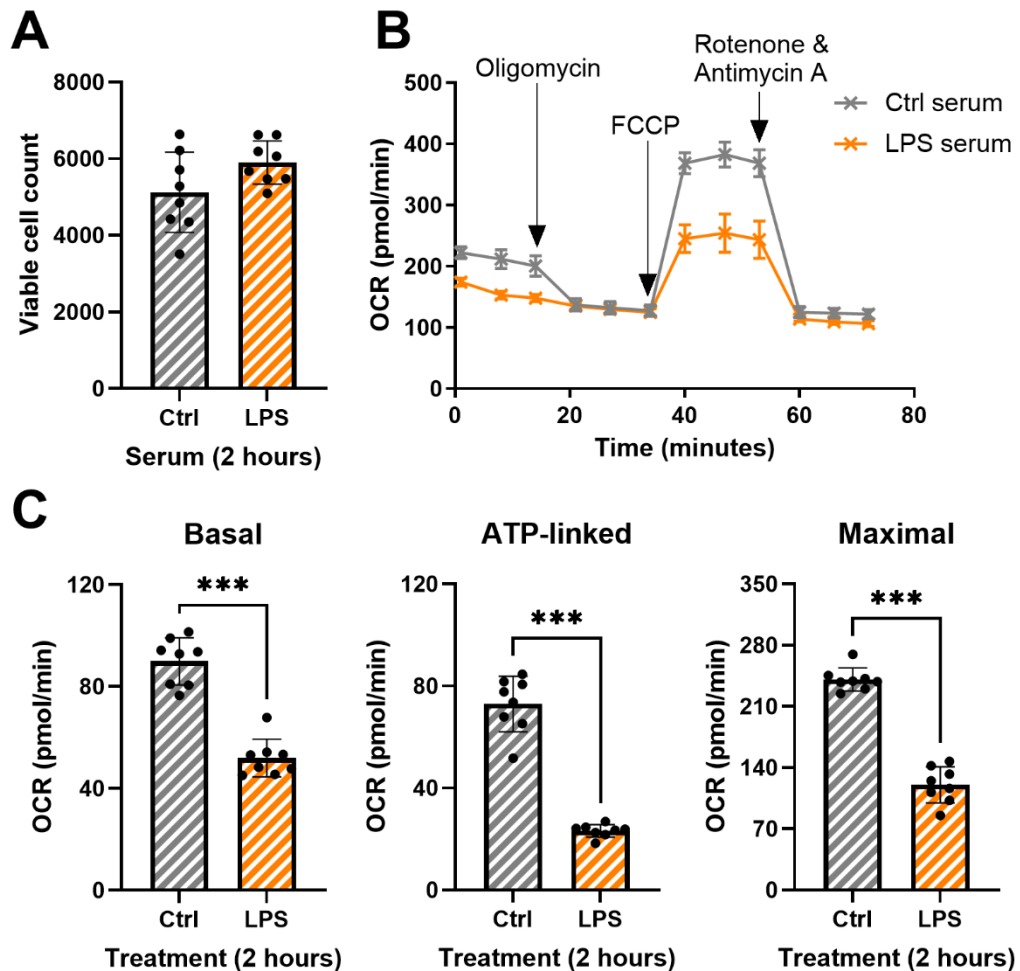


**Figure 4.7, Serum from LPS-treated mice but not control mice downregulated hepatic fatty acid associated mitochondrial respiration *in vitro* in primary hepatocytes.**

Mice were treated with 0.5 mg/kg LPS for 2 hours before being sacrificed. AML12 cells were cultured with serum isolated from control or LPS-treated mice for 2 hours. **A)** Viable cell count taken at the end of the assay. **B)** Seahorse tracing of OCR normalised to cell count. **C)** Basal, ATP-linked and maximal respiration calculated from the normalised OCR trace. Means and standard deviations were calculated and are shown on each graph (n = 8). A Mann-Whitney test was performed, and significant differences are marked using asterisks (\* = p < 0.05, \*\* = P < 0.01, \*\*\* = p < 0.001 and \*\*\*\* = p < 0.0001).

Taken together, these results provide evidence that the serum collected from an LPS-treated mouse but not a control mouse can downregulate hepatic fatty acid metabolism including LCFA uptake and mitochondrial respiration. This suggests that a factor is released into the serum in response to LPS, which then in turn causes the downregulation of liver fatty acid metabolism.

#### **4.4 PAI-1 downregulates hepatocyte fatty acid metabolism**

The immune system is known to be closely linked to metabolic changes and this interaction is often referred to as 'immunometabolism' (569). In response to LPS, the rapid proinflammatory immune response produces many factors including cytokines which are quickly released into the circulation. Within minutes of receptor stimulation, the cytokine production and release are triggered (570). Several cytokines have been shown to affect lipid metabolism including liver fatty acid metabolism. For example, TNF- $\alpha$  has been shown to induce lipolysis and can negatively regulate PPAR $\gamma$ , an important metabolic regulator (571). IL-1 $\beta$  is known to play a role in the inflammatory stress response as well as being a mediator in liver fibrosis and inflammation (572). IL-6 has also been implicated in the regulation of hepatic lipid metabolism. In the liver, lipogenic enzyme expression is increased after administration of exogenous IL-6 (573). Growth factors have also been implicated in the regulation of liver fatty acid metabolism. FGF21 has been shown to positively regulate insulin sensitivity and lipid metabolism (574), with circulating levels of FGF21 positively correlating with triglyceride content (575).

Since the previous experiments identified that a factor(s) released into the serum in response to LPS-treatment could downregulate hepatic fatty acid metabolism, the cytokines and growth factors in the serum were characterised. Serum analysis was performed using a cytokine array kit measuring 96 different factors present in the serum. For this, a mouse was treated with LPS for 90 minutes before blood was collected at sacrifice. One cytokine array membrane was treated with serum from this LPS-treated mouse, and a second membrane was treated with serum collected from a control mouse. This allowed for the identification of cytokines released specifically in response to LPS and filter out those already present in the control mouse serum (Figure 4.8).

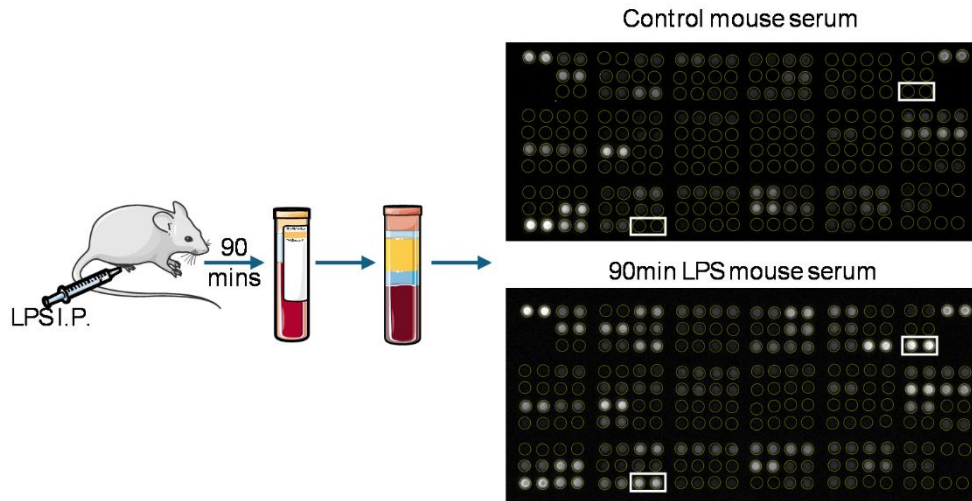


**Figure 4.8, Schematic of cytokine array experimental design.**

A mouse was treated with 0.5 mg/kg LPS for 90 minutes before being sacrificed and serum collected. Cytokine array membranes were treated with serum from a control or LPS-treated mouse to identify differences in the cytokines and growth factors present. Some notable differences are highlighted with white boxes, the left most white box on each membrane marks plasminogen activator inhibitor-1 (PAI-1) and the right most box CXCL2.

The fluorescent intensity of each dot was quantified for control and LPS serum treated membranes. Background intensity was subtracted from the measured intensity, and results were normalised against the reference spots within each membrane. The relative fold-change between the control and LPS serum treated membranes for each factor was then calculated. Results were categorised into chemokines, inflammatory and growth factors (Figure 4.9). The most upregulated cytokine identified in the serum in response to LPS was CXCL2, which increased over 800-fold. The next largest increase was in CXCL1, which increased over 150-times compared to the control membrane. IL-6, C-C motif ligand (CCL)-2, CCL5, CCL20, plasminogen-activator inhibitor 1 (PAI-1) were the next most upregulated, increasing between 20 to 130-fold in LPS treated mice.

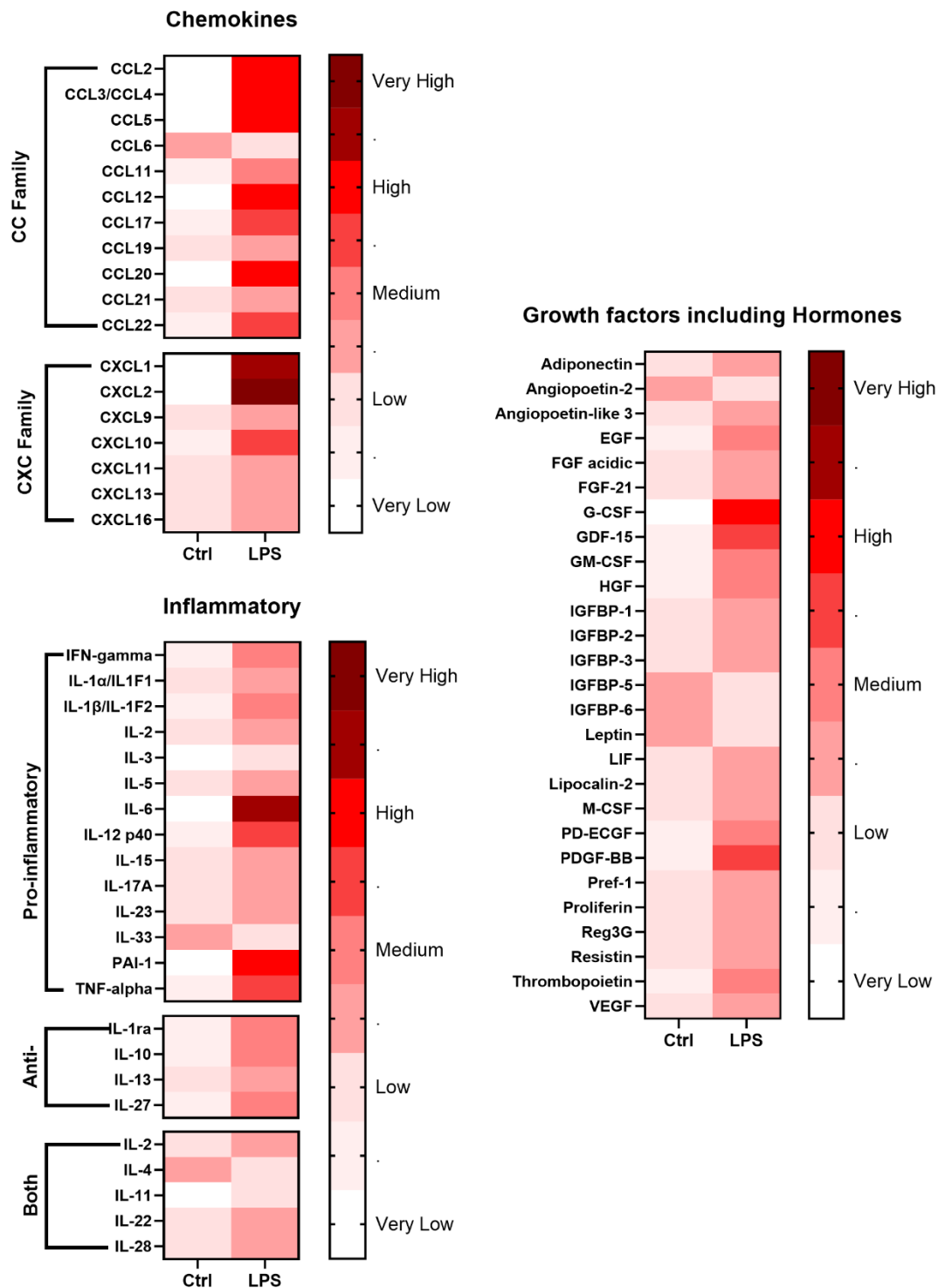


**Figure 4.9, Cytokine release into the serum in response to LPS.**

A mouse was treated with 0.5 mg/kg LPS for 90 minutes before being sacrificed and serum collected. Cytokine array membranes were treated with serum from a control or LPS-treated mouse to identify differences in the cytokines and growth factors present. Heatmap of results split into chemokines, inflammatory cytokines and growth factors.

These top identified cytokines along with TNF- $\alpha$ , which was selected as it was still increased by over 10-fold and has strong links to lipolysis and lipid metabolism, were then selected for further investigation. AML12 cells were treated with these cytokines for 2 hours before RNA was extracted and gene expression of the three key marker genes assessed. Of these cytokines, only PAI-1 decreased *Acadm*, *Hmgcr* and *Hmgcs2* (Figure 4.10). Due to the number of comparisons and thus post-hoc corrections performed when statistically analysing these results, coupled with the low n number, none of these results reached statistical significance.

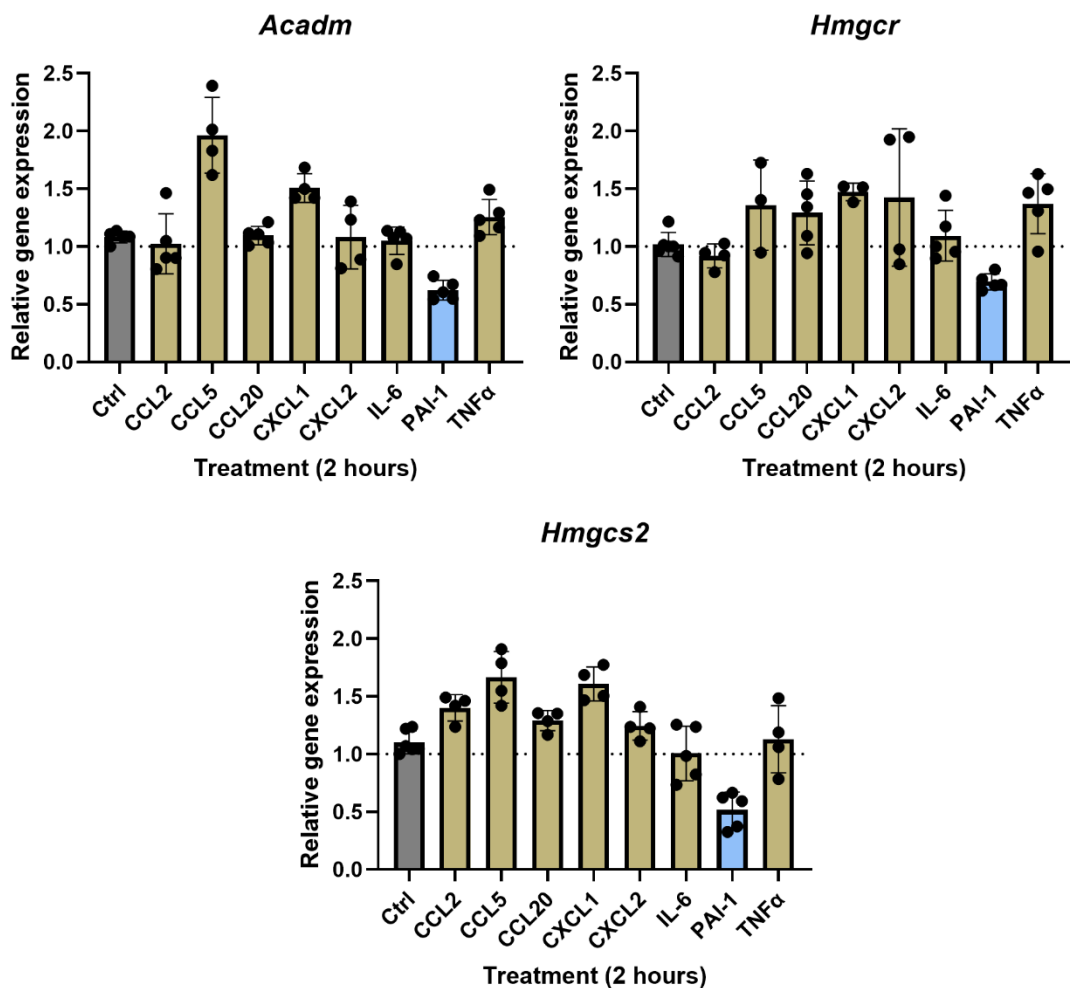


**Figure 4.10, The most increased cytokines were tested on AML12 cells *in vitro* to assess their effect on hepatic fatty acid metabolism.**

AML12 cells were treated with 100 ng/mL of the recombinant mouse protein CCL2, CCL5, CCL20, CXCL1, CXCL2, IL-6, PAI-1 or TNF- $\alpha$  for 2 hours. RNA was extracted and gene expression assessed via qRT-PCR. Gene expression for three key hepatic fatty acid metabolism genes (*Acadm*, *Hmgcr* and *Hmgcs2*) normalised against *Rps18* in AML12 cells (n = 5). A Kruskal-Wallis test with a Dunn's correction for multiple comparisons was performed, comparing each timepoint against the control group, which did not reach statistical significance.

These eight cytokines were also tested on primary hepatocytes to test if these results were repeatable in the second hepatocyte model. Again, only PAI-1 caused the downregulation of these key genes (Figure 4.11). Due to the number of comparisons and thus post-hoc corrections performed when statistically analysing these results, coupled with the low n number, none of these results reached statistical significance.

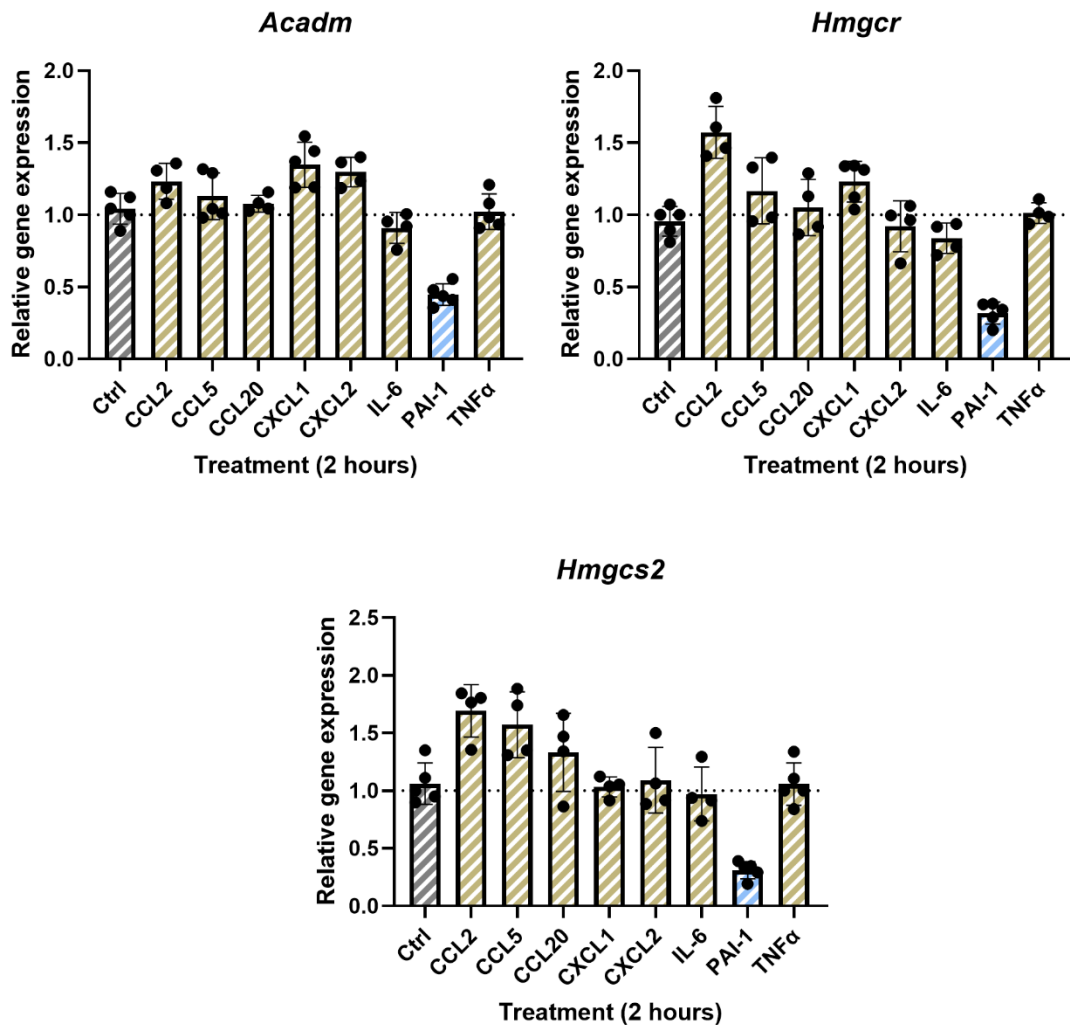


**Figure 4.11, The most increased cytokines were tested on primary hepatocytes *in vitro* to assess their effect on hepatic fatty acid metabolism.**

Primary hepatocytes were treated with 100 ng/mL of the recombinant mouse protein CCL2, CCL5, CCL20, CXCL1, CXCL2, IL-6, PAI-1 or TNF- $\alpha$  for 2 hours. RNA was extracted and gene expression assessed via qRT-PCR. Gene expression for three key hepatic fatty acid metabolism genes (*Acadm*, *Hmgcr* and *Hmgcs2*) normalised against *Hprt* in AML12 cells (n = 5). A Kruskal-Wallis test with a Dunn's correction for multiple comparisons was performed, comparing each timepoint against the control group, which did not reach statistical significance.

To test if the response seen was a dose dependent response, AML12 cells were treated with 20, 50 and 100 ng/mL recombinant mouse PAI-1 protein. Whilst 20 ng/mL did not significantly downregulate the three key genes, 50 ng/mL and 100 ng/mL did downregulate *Acadm*, *Hmgcr* and *Hmgcs2* gene expression (Figure 4.12).

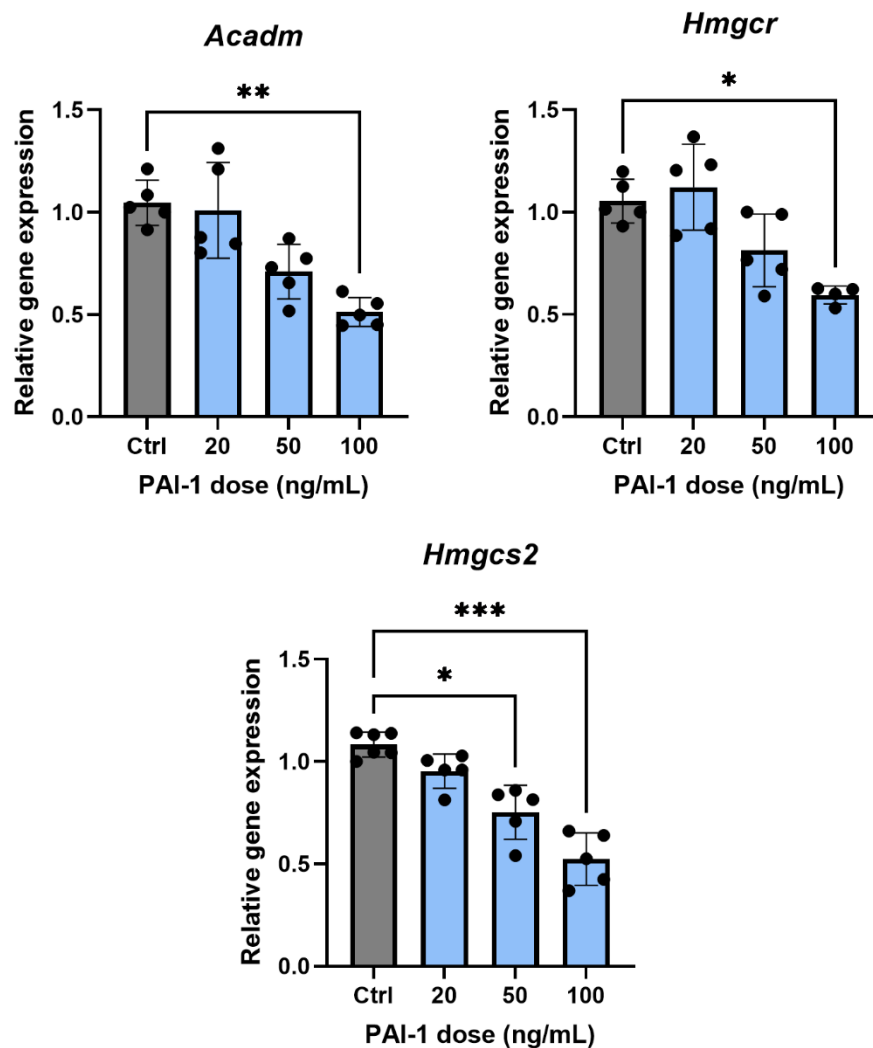


**Figure 4.12, PAI-1 worked in a dose dependent manner to downregulate hepatic fatty acid metabolism.**

AML12 cells were treated with 20, 50 or 100 ng/mL of recombinant mouse PAI-1 protein for 2 hours. RNA was extracted and gene expression assessed via qRT-PCR. Gene expression for three key hepatic fatty acid metabolism genes (*Acadm*, *Hmgcr* and *Hmgcs2*) normalised against *Rps18* (n = 5). A Kruskal-Wallis test with a Dunn's correction for multiple comparisons was performed, comparing each timepoint against the control group, and significant differences are marked using asterisks (\* = p < 0.05, \*\* = P < 0.01, \*\*\* = p < 0.001 and \*\*\*\* = p < 0.0001).

To check if PAI-1 also reduced LCFA uptake in a similar manner to the way LPS-treated serum did, both AML12 cells and primary hepatocytes were treated with 100 ng/mL PAI-1 for 1 hour before C16 BODIPY was added to each well. Cells were incubated for another hour before being fixed, counterstained with DAPI and imaged. A visible reduction in C16 uptake was observed in AML12 cells (Figure 4.13A) and primary hepatocytes (Figure 4.13C) cultured with PAI-1. Quantification of C16 BODIPY fluorescence intensity per hepatocyte confirmed that PAI-1 treated AML12 cells (Figure 4.13B) and primary hepatocytes (Figure 4.13D) had significantly reduced C16 uptake.

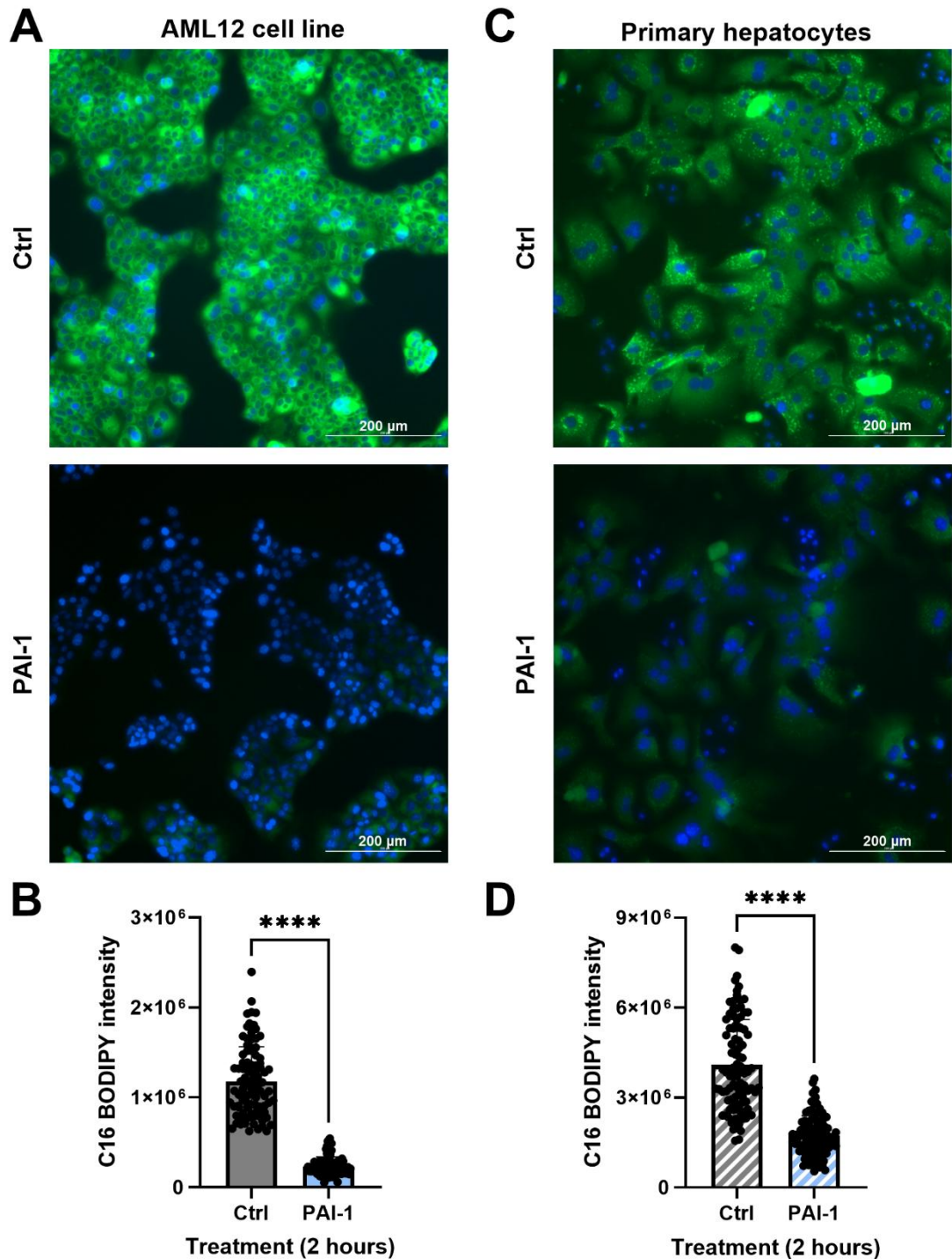


**Figure 4.13, PAI-1 downregulated hepatic LCFA uptake *in vitro*.**

AML12 cells and primary hepatocytes were cultured with 100 ng/mL recombinant mouse PAI-1 protein for 1 hour before 1 $\mu$ M C16 BODIPY was added and cells were further incubated for 1 hour before fixing, counter staining with DAPI and imaging. **A)** Representative images of AML12 cells cultured with PAI-1, DAPI = blue, C16 BODIPY = green at x10 magnification. **B)** BODIPY intensity measured per AML12 cell (n = 100). **C)** Representative images of primary hepatocytes cultured with PAI-1, DAPI = blue, C16 BODIPY = green at x10 magnification. **D)** BODIPY intensity measured per primary hepatocyte (n = 100). Means and standard deviations were calculated and shown on each graph. A Mann-Whitney test was performed, and significant differences are marked using asterisks (\* = p < 0.05, \*\* = P < 0.01, \*\*\* = p < 0.001 and \*\*\*\* = p < 0.0001).

The effect of PAI-1 on AML12 cell and primary hepatocyte fatty acid fuelled mitochondrial respiration was also investigated. Cells were treated with 100 ng/mL recombinant PAI-1 for 2 hours. Media was removed from each well and replaced with palmitic acid seahorse media. PAI-1 treatment did not negatively affect the cell viability in either AML12 cells (Figure 4.14A) or primary hepatocytes (Figure 4.15A). The OCR trace was then normalised to viable cell count for AML12 cells (Figure 4.14B) and primary hepatocytes (Figure 4.15B), revealing reduced OCR in PAI-1 treated cells, similar to that seen in hepatocytes cultured with serum from LPS-treated mice. Basal, maximal and ATP-linked respiration were then calculated. All three measurements were significantly reduced in AML12 cells (Figure 4.14C) and primary hepatocytes (Figure 4.15C) cultured with PAI-1. This means that fatty acid associated mitochondrial ATP production was reduced in both stress and non-stress conditions.

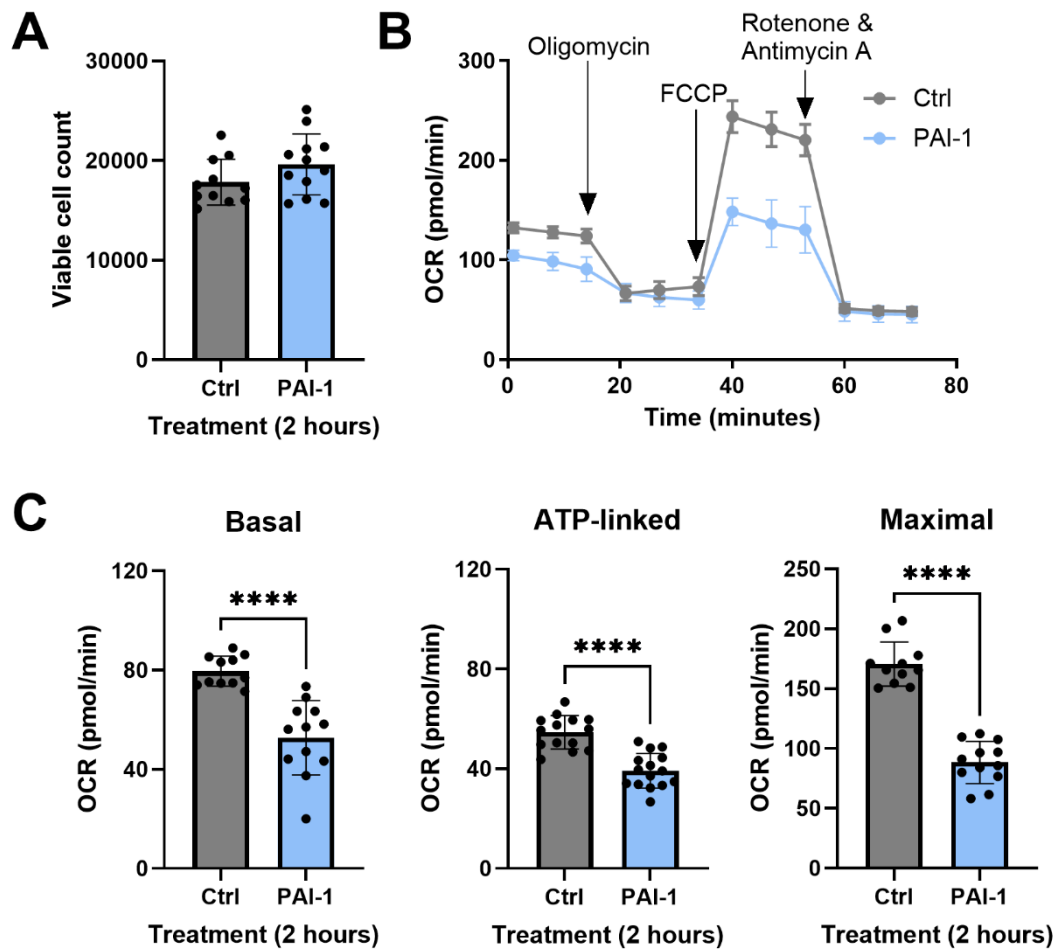


**Figure 4.14, PAI-1 downregulated hepatic fatty acid associated mitochondrial respiration *in vitro* in AML12 cells.**

AML12 cells were cultured with 100 ng/mL recombinant mouse PAI-1 protein for 2 hours before media was removed and replaced with seahorse media supplemented with 100  $\mu$ M C16 (palmitic acid), no glucose. **A**) Viable cell count taken at the end of the assay. **B**) Seahorse tracing of OCR normalised to cell count. **C**) Basal, ATP-linked and maximal respiration calculated from the normalised OCR trace. Means and standard deviations were calculated and are shown on each graph (n = 12). A Mann-Whitney test was performed, and significant differences are marked using asterisks (\* = p < 0.05, \*\* = P < 0.01, \*\*\* = p < 0.001 and \*\*\*\* = p < 0.0001).

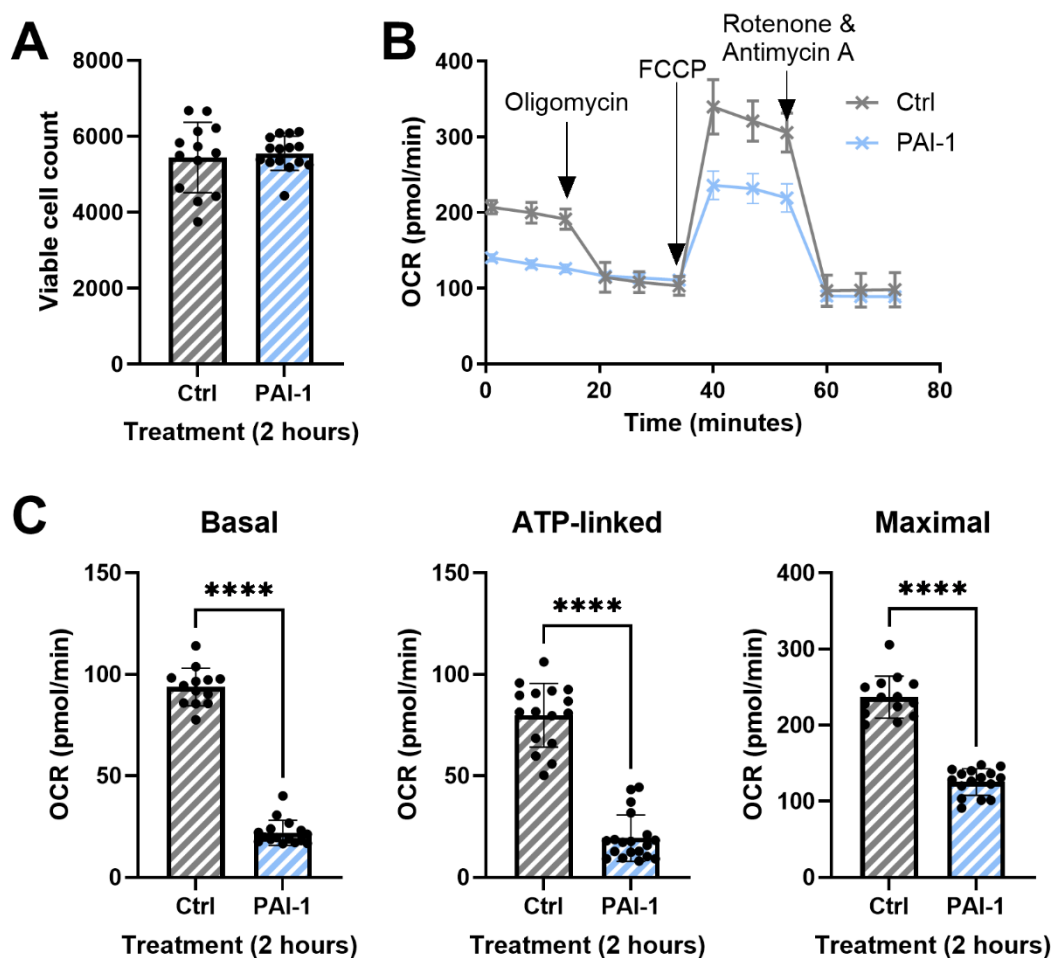


**Figure 4.15, PAI-1 downregulated hepatic fatty acid associated mitochondrial respiration *in vitro* in primary hepatocytes.**

Primary hepatocytes were cultured with 100 ng/mL recombinant mouse PAI-1 protein for 2 hours before media was removed and replaced with seahorse media supplemented with 100  $\mu$ M C16 (palmitic acid), no glucose. **A**) Viable cell count taken at the end of the assay. **B**) Seahorse tracing of OCR normalised to cell count. **C**) Basal, ATP-linked and maximal respiration calculated from the normalised OCR trace. Means and standard deviations were calculated and are shown on each graph (n = 16). A Mann-Whitney test was performed, and significant differences are marked using asterisks (\* = p < 0.05, \*\* = P < 0.01, \*\*\* = p < 0.001 and \*\*\*\* = p < 0.0001).

To test if this reduction in mitochondrial respiration was fatty acid specific or if PAI-1 was downregulating mitochondrial respiration in general, another seahorse MitoStress test was done. This time, following PAI-1 treatment, the media was removed and replaced with glucose supplemented seahorse media with no LCFAs added. Once again, PAI-1 treatment did not negatively impact cell viability in both AML12 cells (Figure 4.16A) or primary hepatocytes (Figure 4.17A). However the OCR

trace did not show any notable differences between PAI-1 treated and control AML12 cells (Figure 4.16B) or primary hepatocytes (Figure 4.17B). When quantified, this resulted in no significant differences between basal, ATP-linked or maximal respiration in AML12 cells (Figure 4.16C) and primary hepatocytes (Figure 4.17C) treated with PAI-1 when given glucose for fuel.

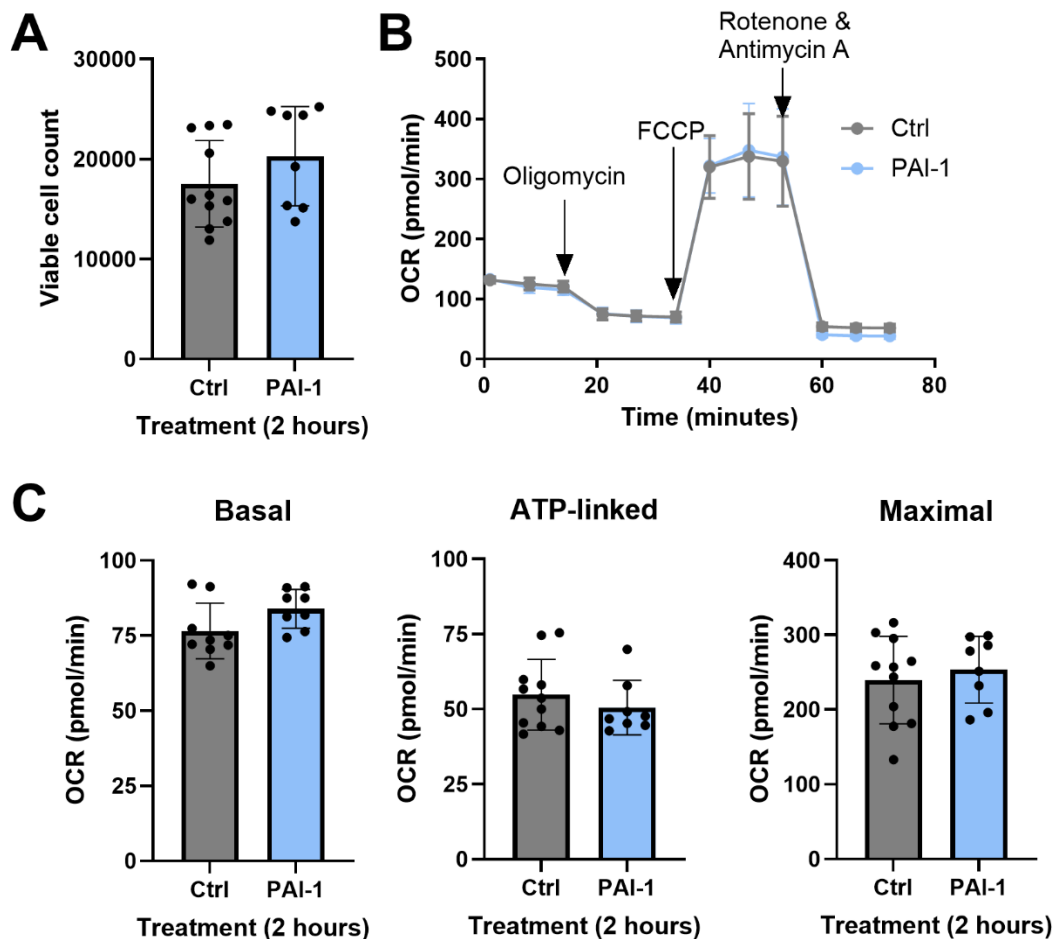


**Figure 4.16, PAI-1 did not downregulate hepatic glucose associated mitochondrial respiration *in vitro* in AML12 cells.**

AML12 cells were cultured with 100 ng/mL recombinant mouse PAI-1 protein for 2 hours before media was removed and replaced with seahorse media supplemented with 100  $\mu$ M glucose, no LCFAs. **A**) Viable cell count taken at the end of the assay. **B**) Seahorse tracing of OCR normalised to cell count. **C**) Basal, ATP-linked and maximal respiration calculated from the normalised OCR trace. Means and standard deviations were calculated and are shown on each graph (n = 9). A Mann-Whitney test was performed, and significant differences are marked using asterisks (\* = p < 0.05, \*\* = P < 0.01, \*\*\* = p < 0.001 and \*\*\*\* = p < 0.0001).

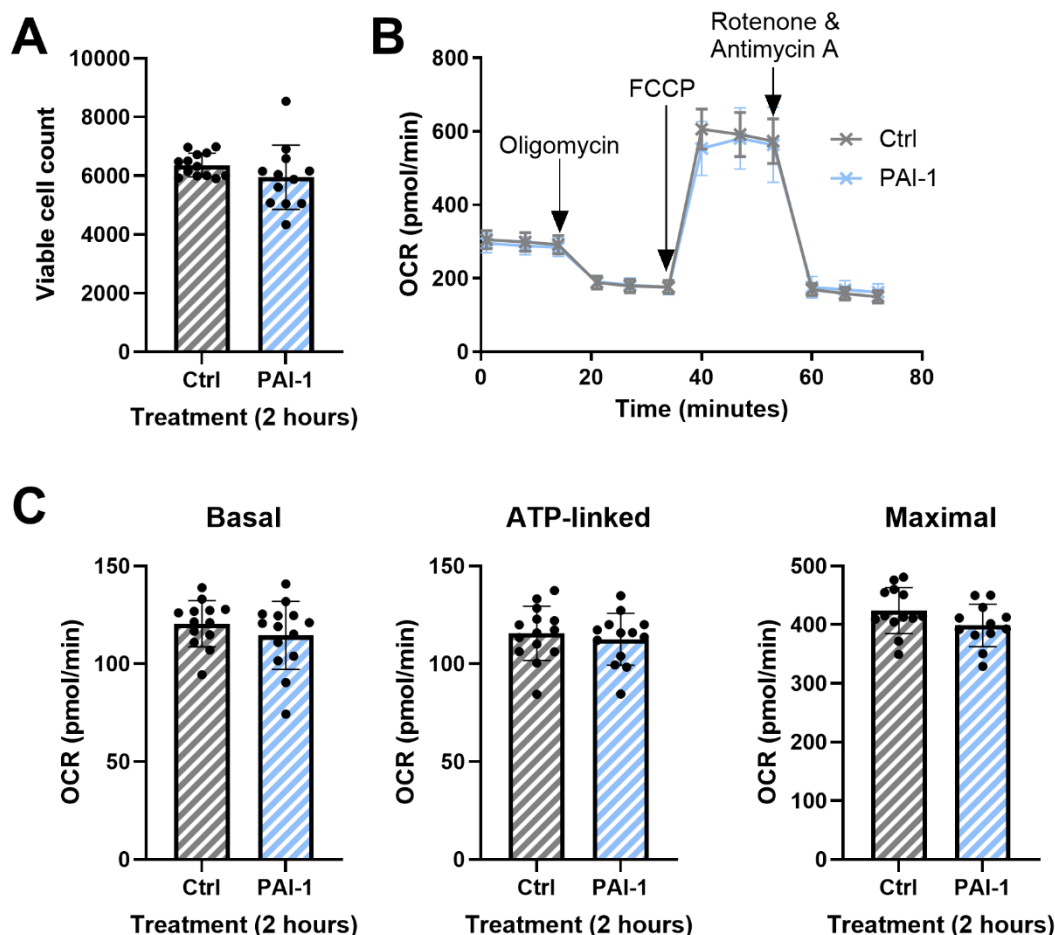


**Figure 4.17, PAI-1 did not downregulate hepatic glucose associated mitochondrial respiration *in vitro* in primary hepatocytes.**

Primary hepatocytes were cultured with 100 ng/mL recombinant mouse PAI-1 protein for 2 hours before media was removed and replaced with seahorse media supplemented with 100  $\mu$ M glucose, no LCFAs. **A)** Viable cell count taken at the end of the assay. **B)** Seahorse tracing of OCR normalised to cell count. **C)** Basal, ATP-linked and maximal respiration calculated from the normalised OCR trace. Means and standard deviations were calculated and are shown on each graph (n = 14). A Mann-Whitney test was performed, and significant differences are marked using asterisks (\* = p < 0.05, \*\* = P < 0.01, \*\*\* = p < 0.001 and \*\*\*\* = p < 0.0001).

In summary these results demonstrate that PAI-1 is one of the most significantly upregulated cytokines present in the serum in response to LPS treatment and was the only one tested which significantly reduced hepatic fatty acid metabolism associated gene expression within 2 hours. Recombinant PAI-1 treatment also reduced LCFA uptake and fatty acid associated hepatic mitochondrial respiration. Interestingly, no effect was seen in hepatocyte mitochondrial respiration when cells were supplemented with glucose and not fatty acids. This indicates that PAI-1 may work in a fatty acid specific manner and not just downregulate metabolism in general, although further work would be needed to confirm this.

#### 4.5 Mice treated with recombinant PAI-1 display a similar phenotype to LPS treated mice

After identifying PAI-1 as the potential cause for the downregulation of hepatic fatty acid metabolism in response to LPS, a PAI-1 ELISA was performed to assess the levels of PAI-1 in mice treated with LPS. This was also done to check the validity of the cytokine array, as a limitation of this array was that it used an n of 1 and results were therefore based off a singular mouse. The PAI-1 ELISA revealed a significant upregulation of PAI-1 in the serum of all mice treated with LPS both at 2 and 6 hours (Figure 4.18). Furthermore, the level of PAI-1 present in the serum after 2 hours was at a similar level to that used to treat hepatocytes *in vitro* (around 100 ng/mL), confirming a clinically relevant dose of PAI-1 was used for *in vitro* experiments.

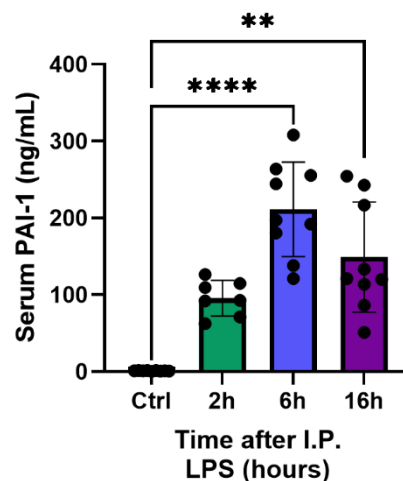


**Figure 4.18, Time-course of total PAI-1 in response to LPS in the serum.**

WT mice were injected with 0.5 mg/kg LPS via I.P. for 2, 6 and 16 hours before being sacrificed. Serum was separated from whole blood and PAI-1 content was analysed using a PAI-1 ELISA. Mean and standard deviation was calculated and shown on the graph (n = 9). A Kruskal-Wallis test with a Dunn's correction for multiple comparisons was performed, comparing each timepoint against the control group, and significant differences are marked using asterisks (\* =  $p < 0.05$ , \*\* =  $P < 0.01$ , \*\*\* =  $p < 0.001$  and \*\*\*\* =  $p < 0.0001$ ).

Next, to further validate PAI-1 as the potential mechanism for the downregulation of hepatic fatty acid metabolism in response to LPS, mice were treated with recombinant mouse PAI-1 *in vivo*. Mice were given 2 doses, one at the start and one after 2 hours due to the short half-life of PAI-1. Mice were sacrificed 4 hours after the start, and samples collected. RNA was extracted from whole liver lysates to assess

liver fatty acid metabolism. *Acadm* and *Hmgcr* gene expression were both significantly downregulated in PAI-1 treated mice (Figure 4.19). *Hmgcs2* did decrease in gene expression but did not reach statistical significance. This could potentially be due to the low dose given, or due to the timepoint.

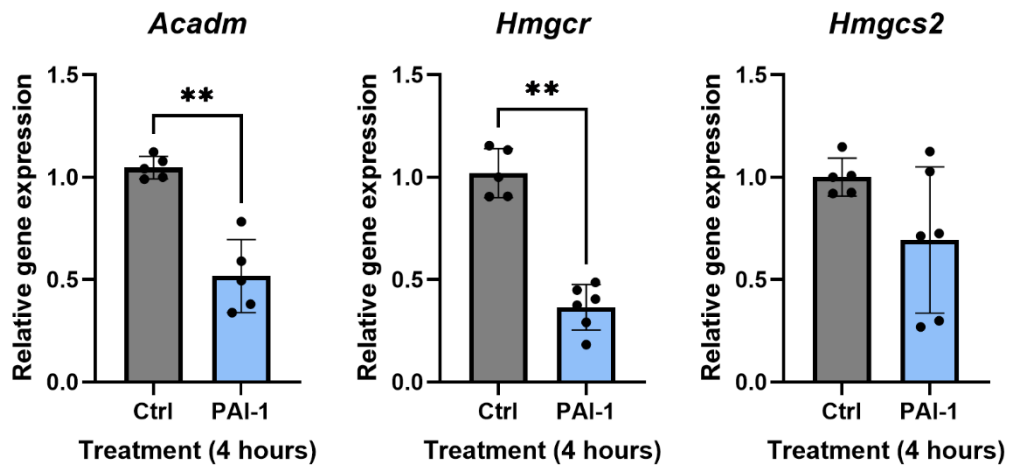


**Figure 4.19, PAI-1 treatment decreased the expression of key liver fatty acid metabolism genes by 4 hours *in vivo*.**

WT mice were injected with 0.05 mg/kg recombinant mouse PAI-1 via I.P. and received a second dose after 2 hours. Mice were sacrificed after 4 hours and RNA extracted from whole liver lysates. Gene expression was normalised against *Rps18* (n = 7). Means and standard deviations were calculated and are shown on each graph. A Mann-Whitney test was performed, and significant differences are marked using asterisks (\* = p < 0.05, \*\* = P < 0.01, \*\*\* = p < 0.001 and \*\*\*\* = p < 0.0001).

LCFA content in the serum was also assessed in these PAI-1 treated mice using LC-MS. Similarities between the two groups was assessed using a PCA plot (Figure 4.20A), which revealed distinct differences in LCFA abundance between control and PAI-1 treated mice. Total serum LCFA concentration was calculated by adding the concentration of each individual LCFA that was measured. Results confirmed that the abundance of LCFAs significantly increased in mice treated with recombinant PAI-1 (Figure 4.20B). Each individual LCFA was then normalised to a control mouse to calculate the relative abundance of each LCFA within the serum (Figure 4.20C). Results show that there was a nearly universal increase in LCFAs in LPS treated mice, with only C18, C20.4 and C20.5 not significantly increasing. At 4 hours, the most significant increase was in C14, myristic acid in PAI-1 treated mice.

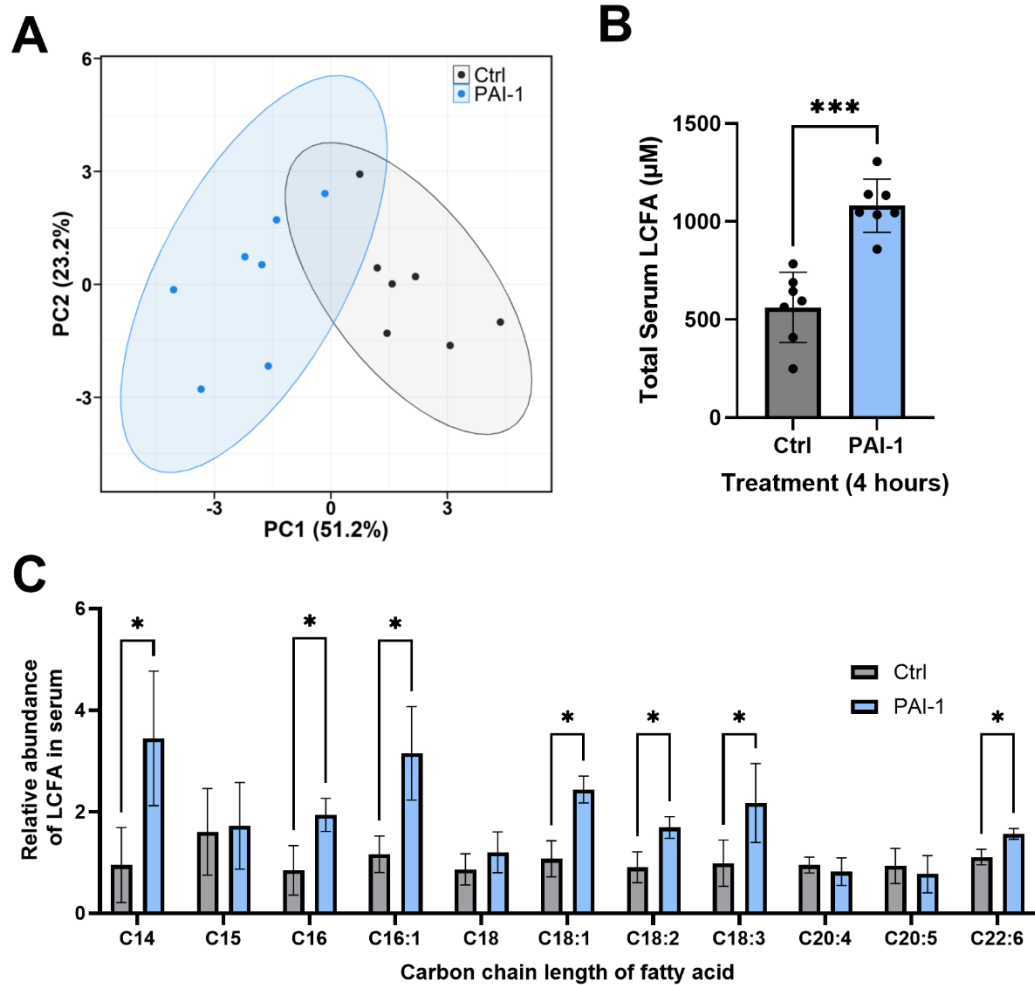


**Figure 4.20, PAI-1 treatment increased serum levels of LCFA by 4 hours *in vivo*.** WT mice were injected with 0.05 mg/kg recombinant mouse PAI-1 via I.P. and received a second dose after 2 hours. Mice were sacrificed after 4 hours. Serum was separated from whole blood and LCFA content was analysed using LC-MS. **A)** PCA plot of serum LCFA abundance from control and PAI-1 treated mice. **B)** Total serum LCFA was calculated by adding the concentration of each individual LCFA measured. **C)** Relative abundance of each LCFA measured in the serum normalised to a control mouse. Mean and standard deviation was calculated and shown on the graph (n = 7). A Mann-Whitney test was performed comparing control and PAI-1 treated groups for each individual LCFA and significant differences are marked using asterisks (\* = p < 0.05, \*\* = P < 0.01, \*\*\* = p < 0.001 and \*\*\*\* = p < 0.0001).

## 4.6 Summary

In summary, this chapter demonstrates that the downregulation of liver fatty acid metabolism in hepatocytes is not caused directly by LPS itself. Instead, a factor is released into the serum in response to LPS. Results identify PAI-1 as one factor which can downregulate hepatic fatty acid metabolism, LCFA uptake and fatty acid specific mitochondrial respiration. Interestingly, glucose associated mitochondrial respiration was not significantly affected by PAI-1 treatment. *In vivo*, treating mice with recombinant PAI-1 downregulated the majority of the fatty acid metabolism genes in the liver, similar to LPS treated mice. Finally, mice directly given recombinant PAI-1 had a significant increase in serum LCFAs. Taken together, this chapter provides evidence for the role of PAI-1 in the downregulation of hepatic fatty acid metabolism and regulation of circulating LCFAs.

## 5 Pharmacological inhibition of PAI-1 prevents LPS-induced downregulation of hepatic liver fatty acid metabolism

### 5.1 Introduction

The previous chapter demonstrated that treating mice with recombinant PAI-1 downregulated liver fatty acid metabolism and increased circulating LCFAs. PAI-1 is most known for the role it plays in regulating blood clotting. It is encoded by the *Serpine1* gene and is a member of the serine-protease inhibitor superfamily discovered in the 1980s (576). PAI-1 inhibits tissue-type plasminogen activator (tPA), which when uninhibited is the enzyme responsible for catalysing the conversion of plasminogen into plasmin. Plasmin is then able to breakdown fibrin within blood clots (577). Thus, PAI-1 plays an important role in preventing the breakdown of fibrin blood clots. Aside from its role in the clotting cascade, PAI-1 is now thought to play an important role in a myriad of other processes. For example, PAI-1 has been associated with inflammation and tissue repair, and thus is closely associated with other proinflammatory cytokines such as IL-6, TNF- $\alpha$  and TGF- $\beta$  (578). Alongside this, PAI-1 is now thought to play a central role in obesity, diabetes and other metabolic syndromes (579).

PAI-1 has also been shown to be a critical mediator in the early immune response to multiple pathogens including *Haemophilus influenzae* and *Mycobacterium tuberculosis* (580, 581). Additionally, high PAI-1 levels have been widely observed in many COVID-19 patients, with PAI-1 levels being shown to independently predict disease severity and COVID-19 mortality rates (582). Despite this, many of these studies are primarily observational. For example, many of these aforementioned studies demonstrate that PAI-1 knockout mice have a reduced ability to clear the infection (580, 581), but do not provide many mechanistic insights as to why.

PAI-1 can be found in multiple forms, including the active, latent and cleaved conformations (583). The active form has a short half-life thought to be between 30 minutes to 2 hours (584), which can be prolonged up to 3-fold by binding to the glycoprotein vitronectin, stabilising PAI-1 (585). Many PAI-1 inhibitors are thought to work by preventing vitronectin from binding to and thus stabilising PAI-1 (586). This

means that the inhibitor bound active PAI-1 is quickly converted into its latent, inactive or cleaved form.

This chapter aims to investigate if pharmacologically inhibiting PAI-1 reverses the downregulation of liver fatty acid metabolism, preventing the accumulation of LCFAs in the serum. Furthermore, it will ascertain if PAI-1 inhibition will affect HSC expansion in response to LPS.

## 5.2 Tiplaxtinin did not reduce circulating PAI-1 in LPS-treated mice

The potent PAI-1 inhibitor Tiplaxtinin (also referred to as PAI-039) was selected as it was the most widely used available PAI-1 inhibitor, with the greatest number of citations. A literature search was conducted to identify studies which used Tiplaxtinin *in vivo*. These studies used doses ranging between 1-100 mg/kg, with the median dose being 10 mg/kg (587-591) and thus this was the dose chosen. WT mice were treated with 10 mg/kg Tiplaxtinin via oral gavage 1 hour prior to LPS I.P. injection, to allow time for the inhibitor to be absorbed into the circulation (Figure 5.1). Mice were sacrificed 6 hours after the final LPS I.P. injection was administered. Alongside these mice, there was an LPS with vehicle only group, a vehicle only group and a Tiplaxtinin only group.

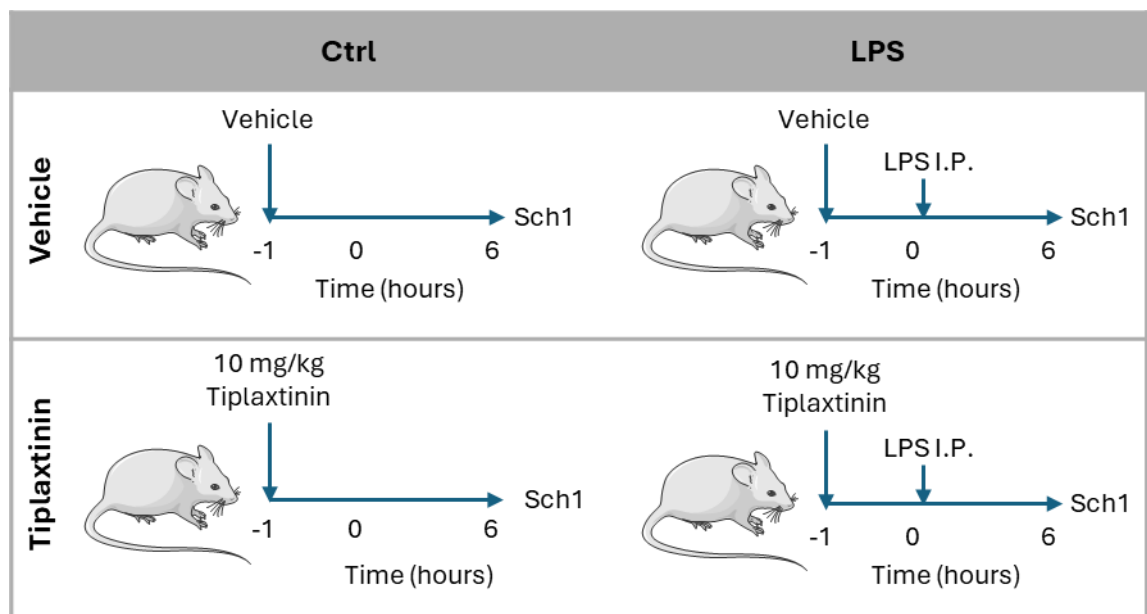


**Figure 5.1, Schematic of Tiplaxtinin with LPS experimental design.**

WT mice pre-treated with 10 mg/kg Tiplaxtinin via oral gavage 1 hour prior to being injected with 0.5 mg/kg LPS via I.P. Mice were sacrificed 6 hours after final LPS I.P. was administered. Mice were split into 4 experimental groups: 1) control mice receiving only the vehicle via oral gavage, 2) Tiplaxtinin only mice who received 10 mg/kg Tiplaxtinin via oral gavage, 3) LPS + vehicle mice who received the vehicle via oral gavage 1 hour prior to 0.5 mg/kg LPS injection via I.P., and 4) LPS + Tiplaxtinin group who received a combination treatment of 10 mg/kg Tiplaxtinin via oral gavage 1 hour prior to 0.5 mg/kg LPS via I.P.

Firstly, serum isolated from whole blood collected at the time of sacrifice was analysed for PAI-1 content using a PAI-1 ELISA. Results showed the amount of PAI-1 present in the serum of the mice given the combined treatment of Tiplaxtinin and LPS was comparable to LPS alone (Figure 5.2). This means that Tiplaxtinin treatment had

no effect on LPS-induced PAI-1 levels. However, it should be noted that the PAI-1 ELISA used measures all PAI-1 protein present in the serum, and does not distinguish between active, latent or cleaved forms.

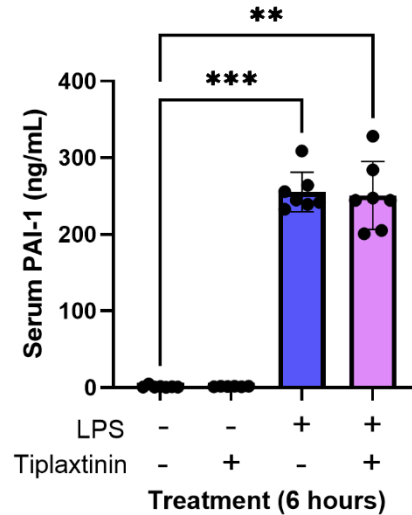


**Figure 5.2, Serum PAI-1 levels in response to LPS both with and without Tiplaxtinin pre-treatment.**

WT mice pre-treated with 10 mg/kg Tiplaxtinin via oral gavage 1 hour prior to being injected with 0.5 mg/kg LPS via I.P. Mice were sacrificed 6 hours after final LPS I.P. was administered. Serum was separated from whole blood and PAI-1 content was analysed using a PAI-1 ELISA. Mean and standard deviation was calculated and shown on the graph (n = 7). A Kruskal-Wallis test with a Dunn's correction for multiple comparisons was performed, comparing each group against the control group, and significant differences are marked using asterisks (\* = p < 0.05, \*\* = P < 0.01, \*\*\* = p < 0.001 and \*\*\*\* = p < 0.0001).

Tiplaxtinin is known to promote the cleavage of PAI-1 (592) and thus it is not totally unexpected that PAI-1 levels did not significantly decrease. Therefore, further analysis was done to assess the effect of Tiplaxtinin pre-treatment on the LPS-induced immune response in mice. Gene expression of RNA extracted from whole liver lysates was analysed. Results showed that pre-treating mice with 10 mg/kg Tiplaxtinin did not prevent the downregulation of key liver fatty acid metabolism genes in response to LPS such as *Acadm*, *Acsl1*, *Hmgcs2* and *Hmgcr* (Figure 5.3). However, *Cpt1a* was significantly downregulated in the Tiplaxtinin only treated group compared to vehicle alone. Despite this, there was no difference in *Ctp1a* gene expression in both LPS treatment groups when compared to vehicle control (Figure 5.3).

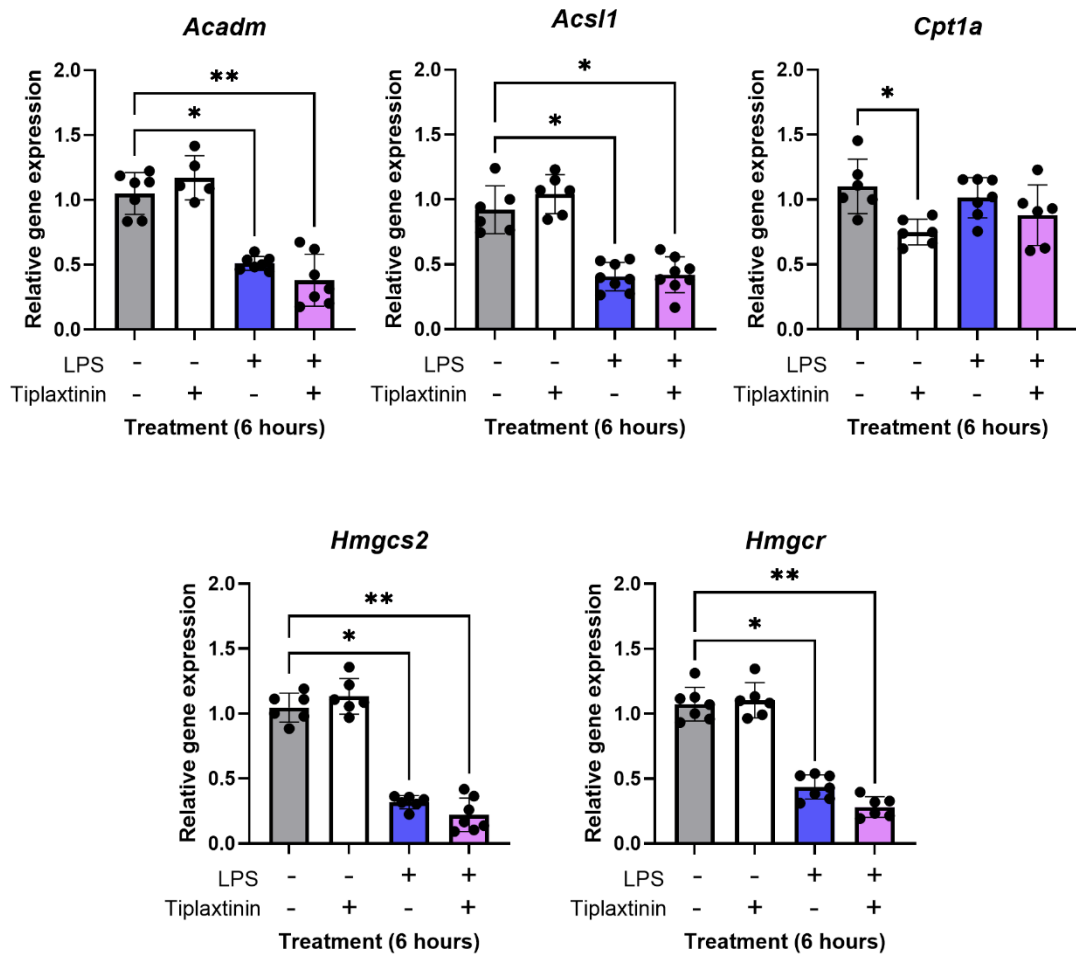


**Figure 5.3, Tiplaxtinin did not affect the LPS-induced downregulation of key liver fatty acid metabolism genes.**

WT mice pre-treated with 10 mg/kg Tiplaxtinin via oral gavage 1 hour prior to being injected with 0.5 mg/kg LPS via I.P. Mice were sacrificed 6 hours after final LPS I.P. was administered. RNA was extracted from whole liver lysates and analysed using RT-qPCR. Gene expression was normalised against *Rps18*. Mean and standard deviation was calculated and shown on each graph (n = 7). A Kruskal-Wallis test with a Dunn's correction for multiple comparisons was performed, comparing each group against the control group, and significant differences are marked using asterisks (\* = p < 0.05, \*\* = P < 0.01, \*\*\* = p < 0.001 and \*\*\*\* = p < 0.0001).

Furthermore, expression of the genes encoding the long-chain fatty acid transporters *Ldlr* and *Slc27a2* were significantly downregulated in the mice pre-treated with Tiplaxtinin prior to LPS administration (Figure 5.4), with no noticeable difference to the LPS vehicle treated group. *Cd36* gene expression did not significantly change across all 4 groups, consistent with earlier findings presented in chapter 1 (Figure 3.19).

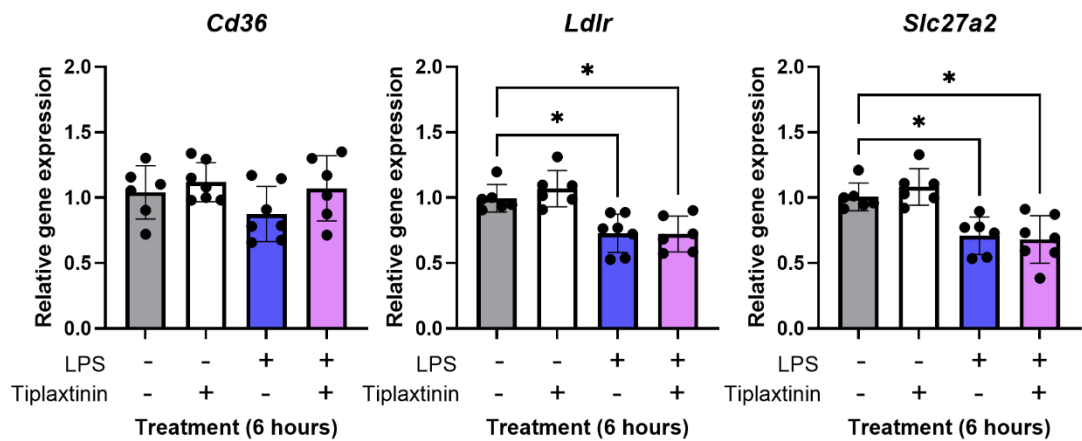


**Figure 5.4, Tiplaxtinin did not affect the LPS-induced downregulation of key liver LCFA transporter genes.**

WT mice pre-treated with 10 mg/kg Tiplaxtinin via oral gavage 1 hour prior to being injected with 0.5 mg/kg LPS via I.P. Mice were sacrificed 6 hours after final LPS I.P. was administered. RNA was extracted from whole liver lysates and analysed using RT-qPCR. Gene expression was normalised against *Rps18*. Mean and standard deviation was calculated and shown on each graph (n = 7). A Kruskal-Wallis test with a Dunn's correction for multiple comparisons was performed, comparing each group against the control group, and significant differences are marked using asterisks (\* = p < 0.05, \*\* = P < 0.01, \*\*\* = p < 0.001 and \*\*\*\* = p < 0.0001).

Serum isolated from whole blood taken at time of sacrifice was analysed using LC-MS to determine the concentration of different circulating LCFAs present in the serum. Results within and between groups were compared using a PCA plot to assess the similarities and differences (Figure 5.5A). The vehicle only and Tiplaxtinin only treatment groups clustered closely together. Whilst the two LPS treated groups (vehicle + LPS and Tiplaxtinin + LPS) also clustered closely together, there was far greater variability between the mice given the combined treatment. Total serum LCFA concentration was calculated by adding the concentration of each individual LCFA that was measured (Figure 5.5B). Both the vehicle + LPS and Tiplaxtinin + LPS groups had significantly increased levels of LCFAs in the serum, which was not unexpected due to the downregulation of liver fatty acid metabolism gene expression observed in both groups. Each individual LCFA was then normalised to a control mouse to calculate the relative abundance of each LCFA within the serum (Figure 5.5C). Results show that there was a universal increase in LCFAs, excluding C15 (pentadecanoic acid) and C20.5 (eicosapentaenoic acid) in the LPS treatment groups, both treated with or without the inhibitor. This result is comparable to the results shown in chapter 1, demonstrating the reproducibility of this LPS model.

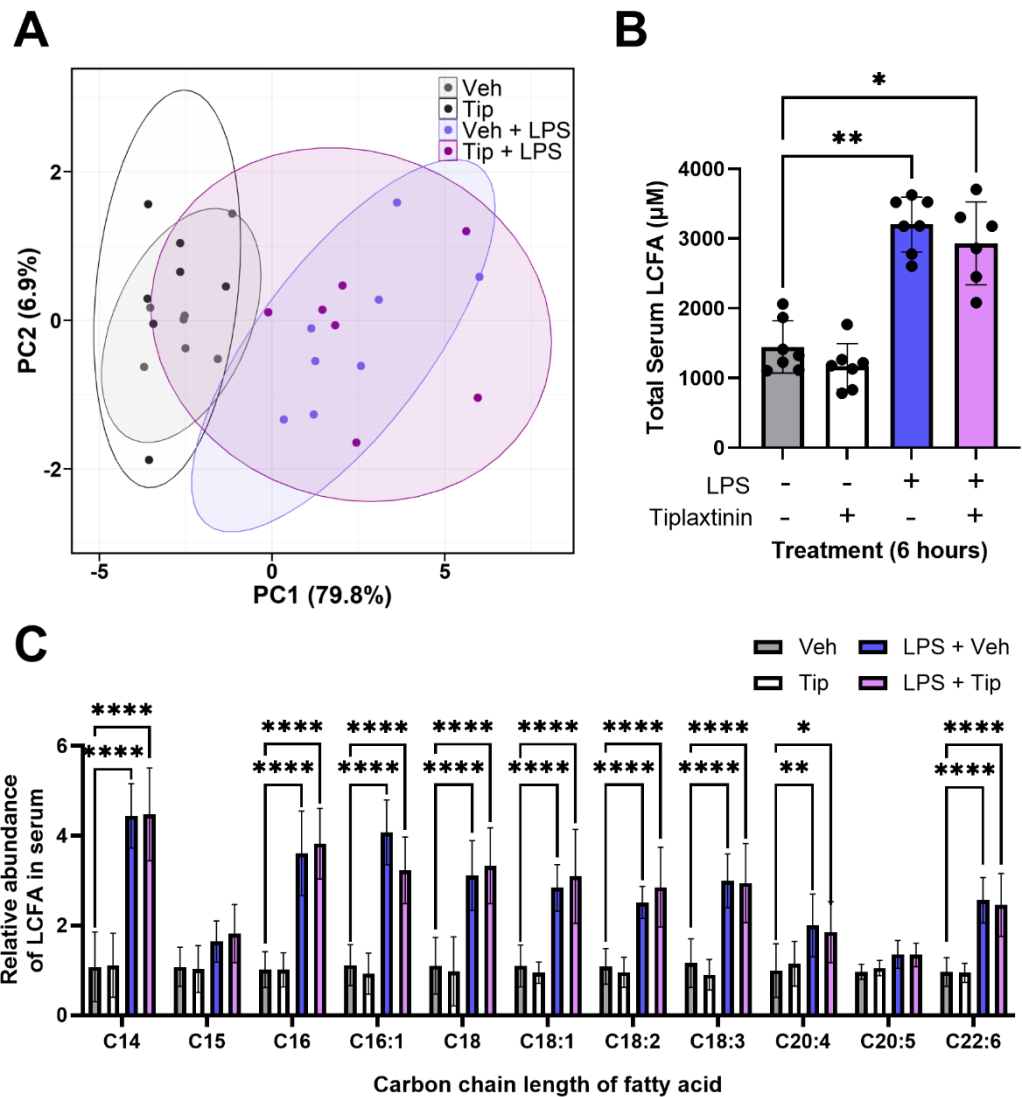


**Figure 5.5, Tiplaxtinin did not alter the LPS-induced increase in serum LCFAs.**

WT mice pre-treated with 10 mg/kg Tiplaxtinin via oral gavage 1 hour prior to being injected with 0.5 mg/kg LPS via I.P. Mice were sacrificed 6 hours after final LPS I.P. was administered. Serum was separated from whole blood and LCFA content was analysed using LC-MS. **A**) PCA plot of serum LCFA abundance from vehicle control, Tiplaxtinin only, LPS + vehicle and LPS + Tiplaxtinin treated mice. **B**) Total serum LCFA was calculated by adding the concentration of each individual LCFA measured. **C**) Relative abundance of each LCFA measured in the serum normalised to a control mouse. Mean and standard deviation was calculated and shown on each graph (n = 7). For B, a Kruskal-Wallis test with a Dunn's correction for multiple comparisons was performed, comparing each group against the control group. For C, a 2way ANOVA with a Dunnett's correction for multiple comparisons was performed comparing each group against the control group for each individual LCFA. Significant differences are marked using asterisks (\* = p < 0.05, \*\* = P < 0.01, \*\*\* = p < 0.001 and \*\*\*\* = p < 0.0001).

Whilst Tiplaxtinin treatment appeared to have no effect on LPS induced downregulation of liver fatty acid metabolism associated gene expression, or on circulating LCFA availability, other parameters were checked including fat pad weight

and blood glucose levels to fully characterise any effects seen. The blood glucose monitor used was designed for to measure appropriate ranges of human blood sugars and thus has a upper range of 33.3 mmol/L. Any reading of above this is noted as high instead of a numerical value and was recorded as the maximum reading of 33.3 mmol/L. Blood glucose levels were significantly decreased in both the vehicle + LPS and Tiplaxtinin + LPS treatment groups (Figure 5.6). There was no significant difference in blood glucose levels between the vehicle and Tiplaxtinin only treatment groups.

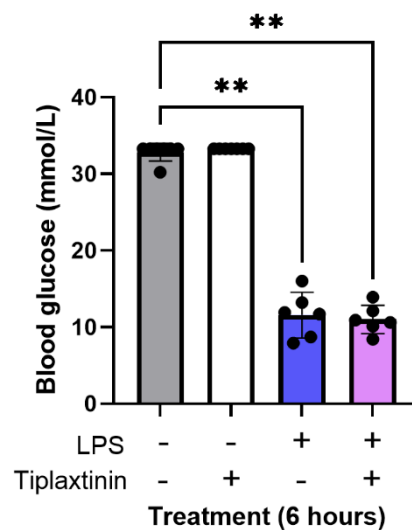


**Figure 5.6, Tiplaxtinin did not affect the LPS-induced downregulation of blood glucose levels.**

WT mice pre-treated with 10 mg/kg Tiplaxtinin via oral gavage 1 hour prior to being injected with 0.5 mg/kg LPS via I.P. Mice were sacrificed 6 hours after final LPS I.P. was administered. Glucose levels within the blood were measured using a blood glucose monitor and test-strips. Mean and standard deviation was calculated and shown on the graph (n = 7). A Kruskal-Wallis test with a Dunn's correction for multiple comparisons was performed, comparing each group against the control group, and significant differences are marked using asterisks (\* = p < 0.05, \*\* = P < 0.01, \*\*\* = p < 0.001 and \*\*\*\* = p < 0.0001).

Additionally, there was no significant difference in both the inguinal and gonadal fat pad weight across all treatment groups (Figure 5.7). This is consistent with earlier findings that fat pad weight did not significantly alter within 6 hours of LPS treatment. Taken together these results demonstrate that Tiplaxtinin did not exhibit any observable effect on LPS-induced metabolic changes *in vivo*.

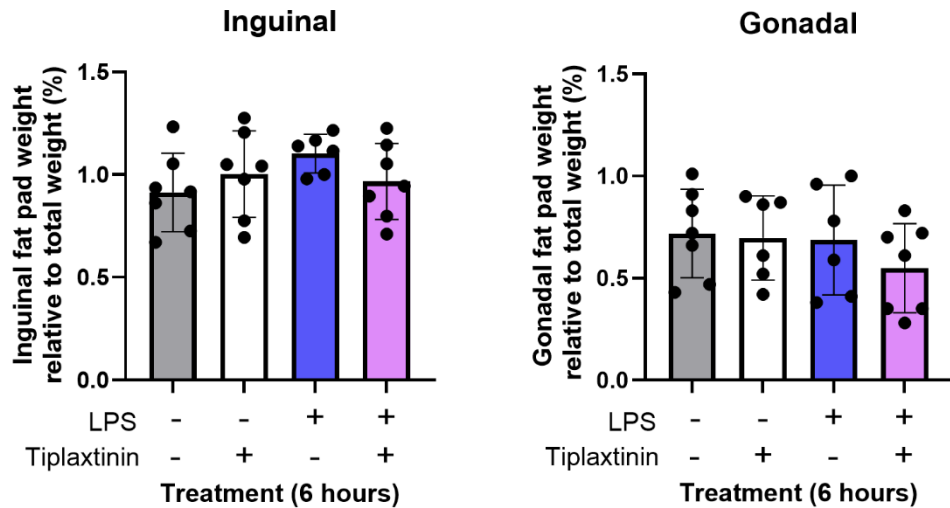


**Figure 5.7, Fat pad weight did not significantly change in Tiplaxtinin or LPS treated mice after 6 hours.**

WT mice pre-treated with 10 mg/kg Tiplaxtinin via oral gavage 1 hour prior to being injected with 0.5 mg/kg LPS via I.P. Mice were sacrificed 6 hours after final LPS I.P. was administered. Inguinal and gonadal fat pads were dissected from mice and weighed. The percentage the weight of each fat pad was calculated against total body weight at time of sacrifice. Mean and standard deviation was calculated and shown on each graph (n = 7). A Kruskal-Wallis test with a Dunn's correction for multiple comparisons was performed, comparing each group against the control group, and significant differences are marked using asterisks (\* = p < 0.05, \*\* = P < 0.01, \*\*\* = p < 0.001 and \*\*\*\* = p < 0.0001).

One potential reason for the unsuccessful result where Tiplaxtinin did not reverse the LPS induced downregulation of liver fatty acid metabolism could be that this dose of Tiplaxtinin had toxic off-target effects. Additionally, there may have been factors affecting Tiplaxtinin's bioavailability or half-life *in vivo*.

### **5.3 Tiplaxtinin partially reverses the downregulation of hepatic fatty acid metabolism *in vitro***

*In vitro* assays using Tiplaxtinin were conducted to determine if this lack of observable difference seen within the *in vivo* model was due to insufficient inhibition of PAI-1, or if there was a compensatory mechanism causing the downregulation of hepatic fatty acid metabolism alongside PAI-1. For this, only the AML12 hepatocyte cell line was used due to the technical complexity and time-intensive nature of isolating primary hepatocytes. Moreover, prior assays showed there were no significant differences between the cell line and primary hepatocytes.

AML12 cells were treated with 0, 25, 50 or 100 ng/mL Tiplaxtinin prior to adding 100 ng/mL of recombinant PAI-1 mouse protein. After 2 hours RNA was extracted, and gene expression was analysed using qRT-PCR for the same 3 key fatty acid metabolism marker genes used previously for *in vitro* experiments (Figure 5.8). In line with previous results, *Acadm*, *Hmgcr* and *Hmgcs2* gene expression were significantly downregulated in hepatocytes treated with PAI-1 alone (Figure 5.8). Whilst 25 ng/mL of Tiplaxtinin did marginally reverse this downregulation, 50 ng/mL showed a more consistent prevention of PAI-1 induced downregulation across all 3 key marker genes. However, the increased variability seen in the 100 ng/mL treatment group could indicate that the high dose had a toxic effect on the cells. To confirm this, a cell viability assay would need to be done.

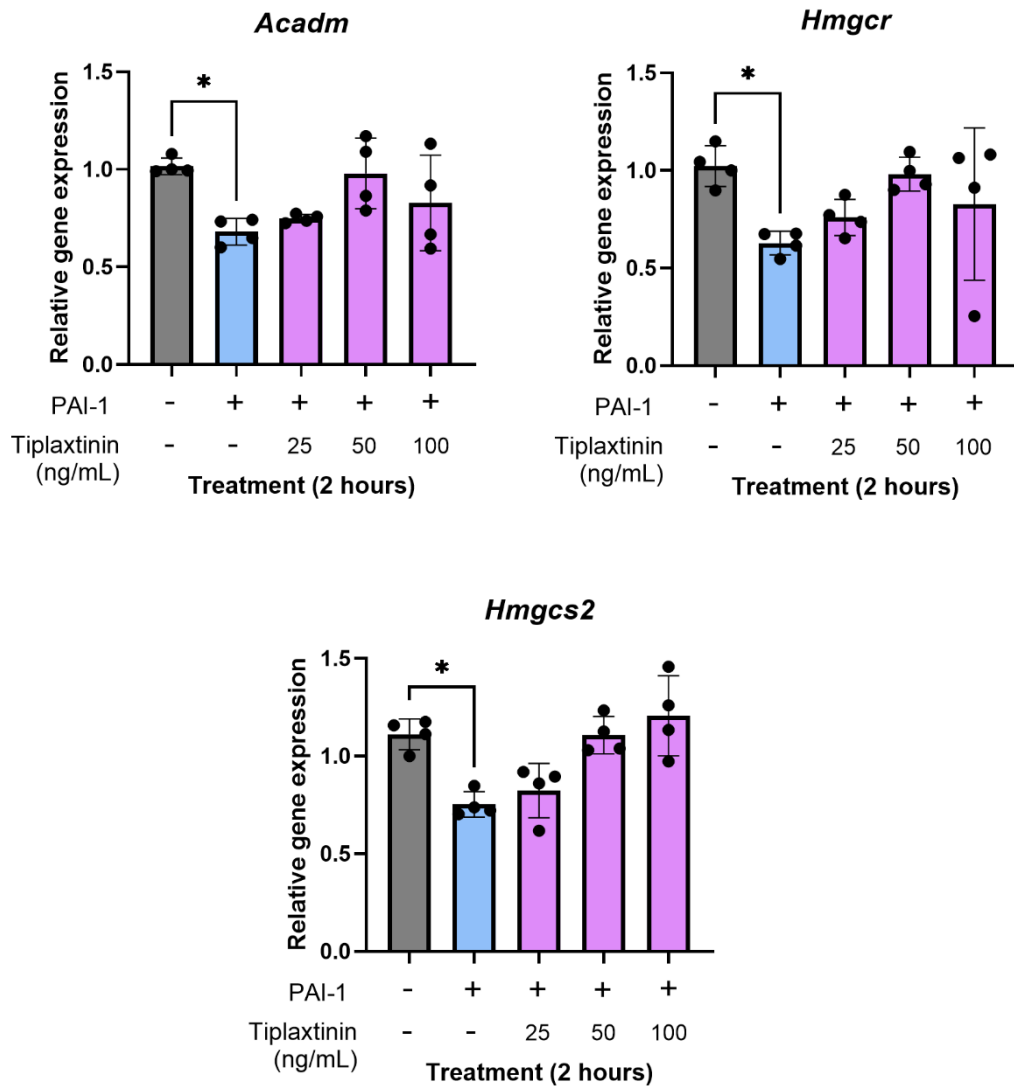


**Figure 5.8, Tiplaxtinin treatment partially reverses PAI-1-induced downregulation of key hepatic fatty acid metabolism gene expression *in vitro* in a dose dependent manner.**

AML12 cells were pre-treated with 0, 25, 50 or 100 ng/mL Tiplaxtinin before 100 ng/mL recombinant PAI-1 mouse protein was added. After 2 hours, RNA was extracted and gene expression assessed using qRT-PCR. AML12 cell gene expression for three key hepatic fatty acid metabolism genes normalised against *Rps18*. Mean and standard deviation was calculated and shown on each graph (n = 4). A Kruskal-Wallis test with a Dunn's correction for multiple comparisons was performed, comparing each group against the control group, and significant differences are marked using asterisks (\* = p < 0.05, \*\* = P < 0.01, \*\*\* = p < 0.001 and \*\*\*\* = p < 0.0001).

Next, this assay was repeated using the optimal dose of 50 ng/mL Tiplaxtinin identified from the previous experiment. This was done to evaluate the reproducibility of this assay, and also to assess the effect of Tiplaxtinin alone on hepatocyte gene expression. In line with previous results, pre-treating hepatocytes with Tiplaxtinin

prevented the downregulation of *Acadm*, *Hmgcr* and *Hmgcs2* gene expression (Figure 5.9). Tiplaxtinin treatment alone did not significantly alter gene expression.

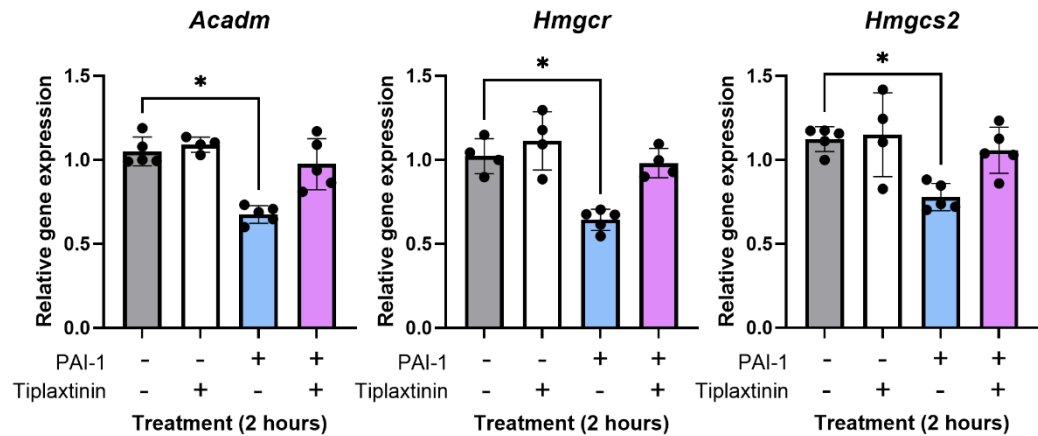


**Figure 5.9, Tiplaxtinin treatment reverses PAI-1-induced downregulation of key hepatic fatty acid metabolism gene expression *in vitro*.**

AML12 cells were pre-treated with 50 ng/mL Tiplaxtinin before 100 ng/mL recombinant PAI-1 mouse protein was added. After 2 hours, RNA was extracted and gene expression assessed using qRT-PCR. AML12 cell gene expression for three key hepatic fatty acid metabolism genes normalised against *Rps18*. Mean and standard deviation was calculated and shown on each graph (n = 5). A Kruskal-Wallis test with a Dunn's correction for multiple comparisons was performed, comparing each group against the control group, and significant differences are marked using asterisks (\* = p < 0.05, \*\* = P < 0.01, \*\*\* = p < 0.001 and \*\*\*\* = p < 0.0001).

To investigate the effect of Tiplaxtinin pre-treatment on hepatocyte LCFA uptake, AML12 cells were treated with recombinant PAI-1 protein with and without 50 ng/mL Tiplaxtinin for 1 hour before C16 BODIPY was added to each well. Cells were incubated for another hour before being fixed, counterstained with DAPI and imaged. A visible reduction in C16 uptake was observed in AML12 cells cultured with PAI-1 regardless of the addition of Tiplaxtinin (Figure 5.10A). However, the combination treatment showed a small but distinguishable increase in C16 uptake into hepatocytes. C16 BODIPY fluorescence intensity per hepatocyte was quantified. This confirmed that the reduction in C16 uptake in hepatocytes given the combined treatment was still significant compared to the control treatment groups (Figure 5.10B). Tiplaxtinin alone did not impact C16 uptake into the AML12 cells or affect the visible number of viable cells. Taken together this data provides evidence that Tiplaxtinin may be able to block some of the effects recombinant PAI-1 protein treatment has on AML12 cells.

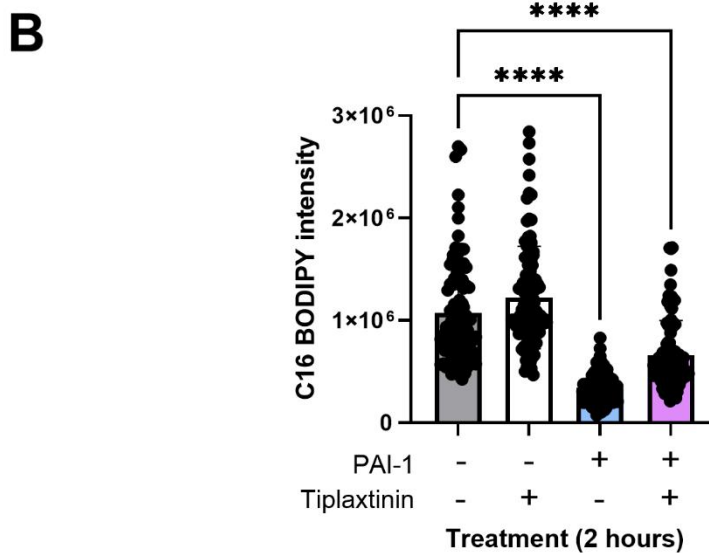
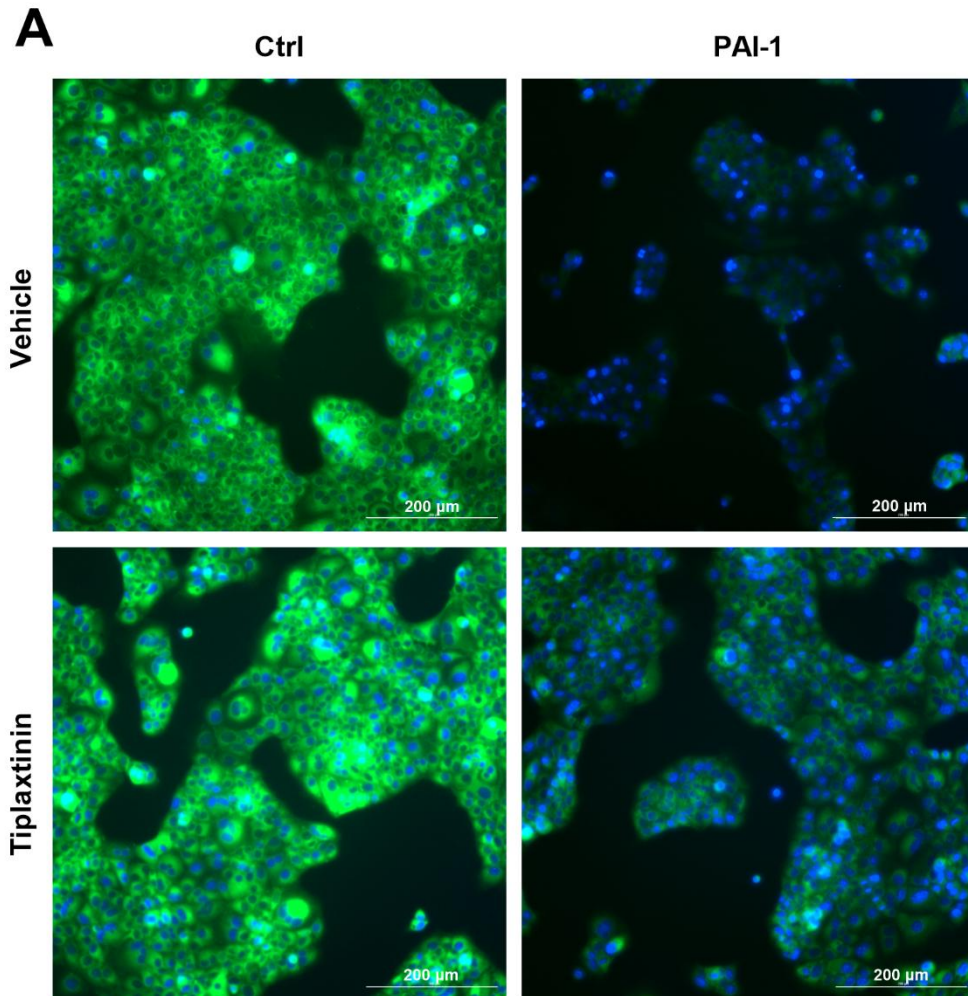


**Figure 5.10, PAI-1-induced reduction in LCFA uptake is not prevented by Tiplaxtinin pre-treatment *in vitro*.**

AML12 cells were pre-treated with 50 ng/mL Tiplaxtinin before 100 ng/mL recombinant PAI-1 mouse protein was added. After 1 hour, 1  $\mu$ M C16 BODIPY was added and cells were further incubated for 1 hour before fixing, counter staining with DAPI and imaging. **A)** Representative images of control, Tiplaxtinin only, LPS only and LPS + Tiplaxtinin treated AML12 cells, DAPI = blue, C16 BODIPY = green at x10 magnification. **B)** BODIPY intensity measured per AML12 cell (n = 100). Means and standard deviations were calculated and shown on the graph. A

Mann-Whitney test was performed, and significant differences are marked using asterisks (\* =  $p < 0.05$ , \*\* =  $P < 0.01$ , \*\*\* =  $p < 0.001$  and \*\*\*\* =  $p < 0.0001$ ).

When taken together, these results were inconclusive. The mouse model using Tiplaxtinin was unsuccessful at preventing the downregulation of liver fatty acid metabolism in response to LPS. However, PAI-1 inhibition using Tiplaxtinin in the hepatocyte cell lines treated with recombinant PAI-1 protein *in vitro* did partially prevent this downregulation. Therefore, in order to further investigate if inhibition of PAI-1 alone by Tiplaxtinin could inhibit the downregulation of hepatic fatty acid metabolism and fatty acid uptake, the *in vitro* model was used with serum isolated from control and LPS treated mice. This is because serum contains several cytokines and factors released in the mouse in response to LPS. Therefore, a serum model was used to help investigate if this difference in results could be due to PAI-1 not being the only factor downregulating hepatic fatty acid metabolism in response to LPS.

For this assay, 50 ng/mL of Tiplaxtinin was added to each well prior to the serum. After 2 hours RNA was extracted, and gene expression was analysed using qRT-PCR for the key marker genes. In line with previous results, *Acadm*, *Hmgcr* and *Hmgcs2* gene expression was significantly downregulated in hepatocytes treated with serum from LPS-treated mice compared to control serum (Figure 5.11). Tiplaxtinin partially prevented the downregulation of gene expression, but not to the same levels of control serum. Hepatocytes treated with both Tiplaxtinin and control serum had significant downregulation of *Hmgcr* gene expression. The combination treatment may therefore be affecting cell viability or having off-target effects.

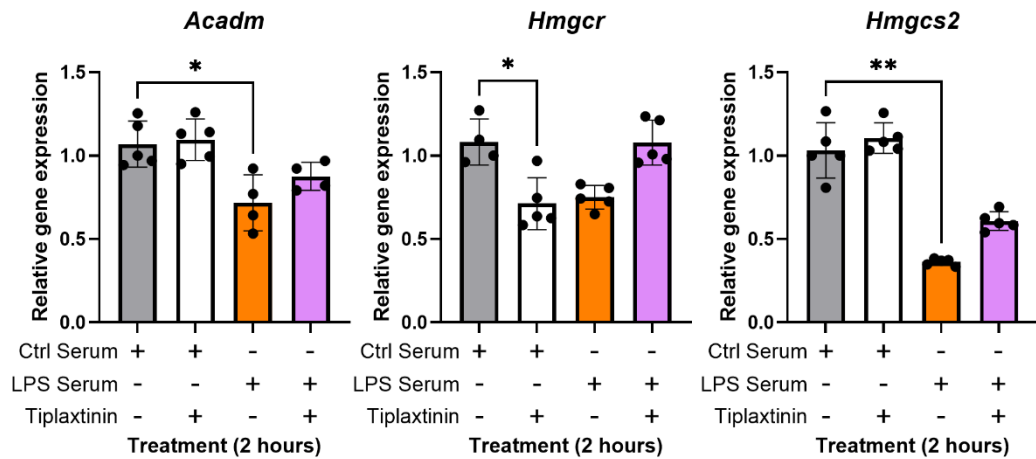


**Figure 5.11, Tiplaxtinin treatment partially reversed the downregulation of key of hepatic fatty acid metabolism genes in response to serum from LPS-treated mice *in vitro*.**

Mice were treated with 0.5 mg/kg LPS for 2 hours before being sacrificed. AML12 cells were pre-treated with 50 ng/mL Tiplaxtinin before being cultured with serum isolated from control mice or LPS-treated mice. After 2 hours, RNA was extracted and gene expression assessed using qRT-PCR. AML12 cell gene expression for three key hepatic fatty acid metabolism genes was normalised against *Rps18*. Mean and standard deviation was calculated and shown on each graph (n = 5). A Kruskal-Wallis test with a Dunn's correction for multiple comparisons was performed, comparing each group against the control group, and significant differences are marked using asterisks (\* = p < 0.05, \*\* = P < 0.01, \*\*\* = p < 0.001 and \*\*\*\* = p < 0.0001).

To investigate the effect of Tiplaxtinin pre-treatment on hepatocyte LCFA uptake in this serum model, AML12 cells were treated with Tiplaxtinin in combination with serum from control or LPS-treated mice for 1 hour before C16 BODIPY was added to each well. A visible reduction in C16 uptake was observed in AML12 cells cultured with LPS-treated mouse serum regardless of the addition of Tiplaxtinin (Figure 5.12A). C16 BODIPY fluorescence intensity per hepatocyte was quantified. Results confirmed that C16 uptake in hepatocytes given the combined treatment was significantly reduced compared to control serum groups (Figure 5.12B). Tiplaxtinin combined with control serum did not impact C16 uptake into the AML12 cells compared to control serum alone.

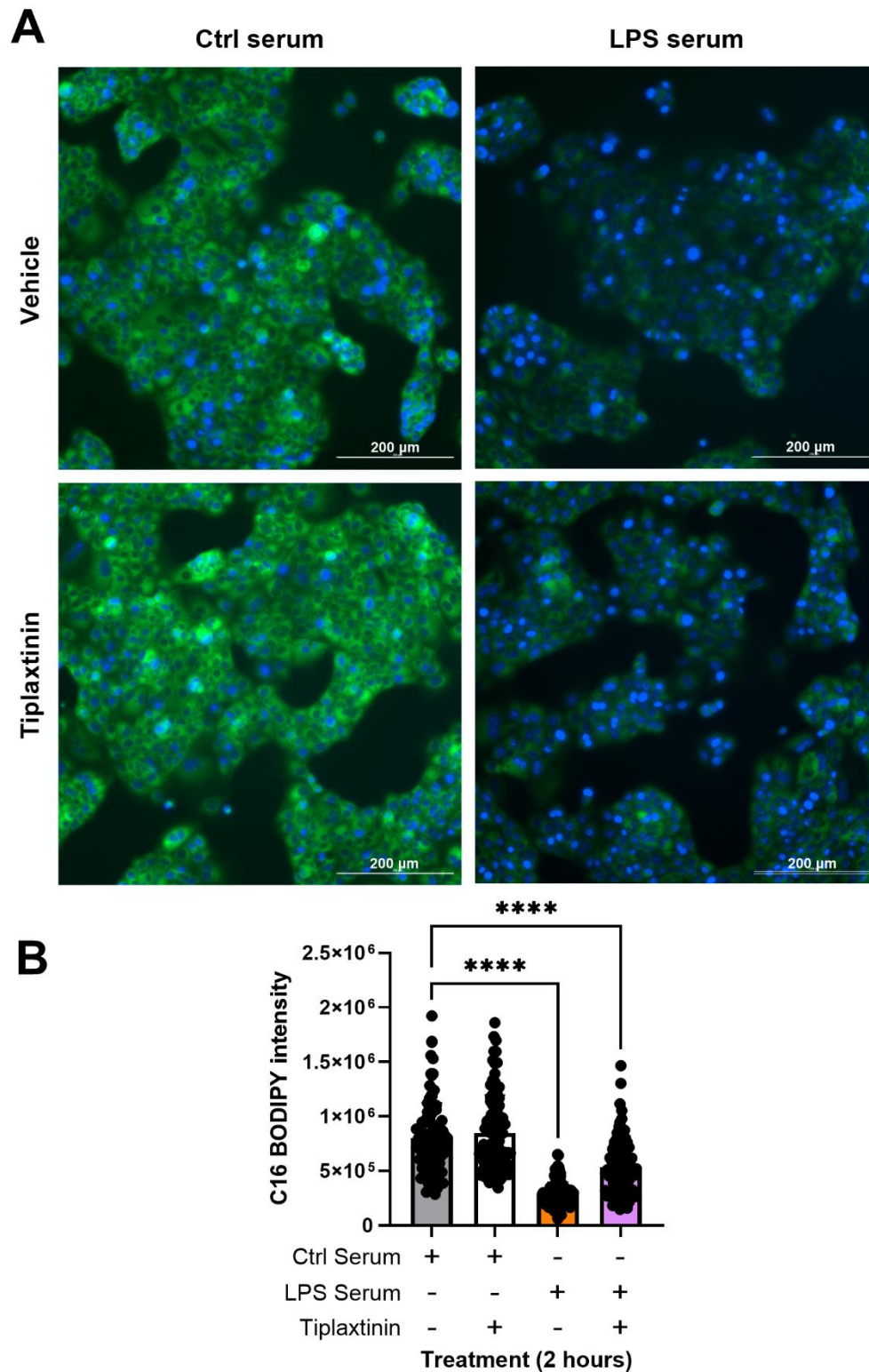


**Figure 5.12, The reduction in LCFA uptake in response to serum from LPS-treated mice was not prevented by Tiplaxtinin pre-treatment *in vitro*.**

Mice were treated with 0.5 mg/kg LPS for 2 hours before being sacrificed. AML12 cells were pre-treated with 50 ng/mL Tiplaxtinin before being cultured with serum isolated from control mice or LPS-treated mice. After 1 hour, 1  $\mu$ M C16 BODIPY was added and cells were further incubated for 1 hour before fixing, counter staining with DAPI and imaging. **A)** Representative images of cells treated with control serum, control serum with Tiplaxtinin, LPS serum and LPS serum with Tiplaxtinin, DAPI = blue, C16 BODIPY = green at x10 magnification. **B)** BODIPY intensity measured per AML12 cell (n = 100). Means and standard deviations were calculated and shown on the graph. A Kruskal-Wallis test with a Dunn's correction for multiple

comparisons was performed, comparing each timepoint against the control group, and significant differences are marked using asterisks (\* =  $p < 0.05$ , \*\* =  $P < 0.01$ , \*\*\* =  $p < 0.001$  and \*\*\*\* =  $p < 0.0001$ ).

Taken together this data provides evidence that Tiplaxtinin may be able to partially block some of the effects of serum from an LPS-treated mouse on hepatic fatty acid metabolism. However, whether this mixed result was due to Tiplaxtinin being unable to effectively inhibit PAI-1 within this pathway or because PAI-1 is not the only factor able to elicit this metabolic downregulation remains to be determined.

#### **5.4 TM5441 reverses PAI-1 induced downregulation of hepatic fatty acid metabolism and LCFA uptake *in vitro*.**

Due to the incomplete response of Tiplaxtinin, an alternative PAI-1 inhibitor was selected. This time, the previous literature was searched for PAI-1 inhibitors specifically used in metabolic associated studies. An interesting study by Levine et al., 2021 demonstrated that PAI-1 inhibition using TM5614 ameliorated hyperlipidaemia in obese mice (593). Unfortunately, this drug is currently patented and is therefore unavailable to buy. Instead, other structural analogues within the TM PAI-1 inhibitor family were explored. TM5441 is a readily available PAI-1 inhibitor which has also been used in metabolic studies. For example, treating mice with TM5441 prevented high fat diet-induced weight gain, increased proinflammatory cytokines and the downregulation of key mitochondrial genes (594). TM5441 and TM5614 share the same molecular formula:  $C_{21}H_{17}ClN_6O_6$ , and core scaffold. In fact, the only difference is the attachment position of the Furan ring to the phenyl ring at position 2 or 3 for TM5614 and TM5441 respectively (Figure 5.13). This is different from Tiplaxtinin, which has a molecular formula of  $C_{24}H_{16}F_3NO_4$ , and thus TM5441 may work via a different mechanism to Tiplaxtinin.

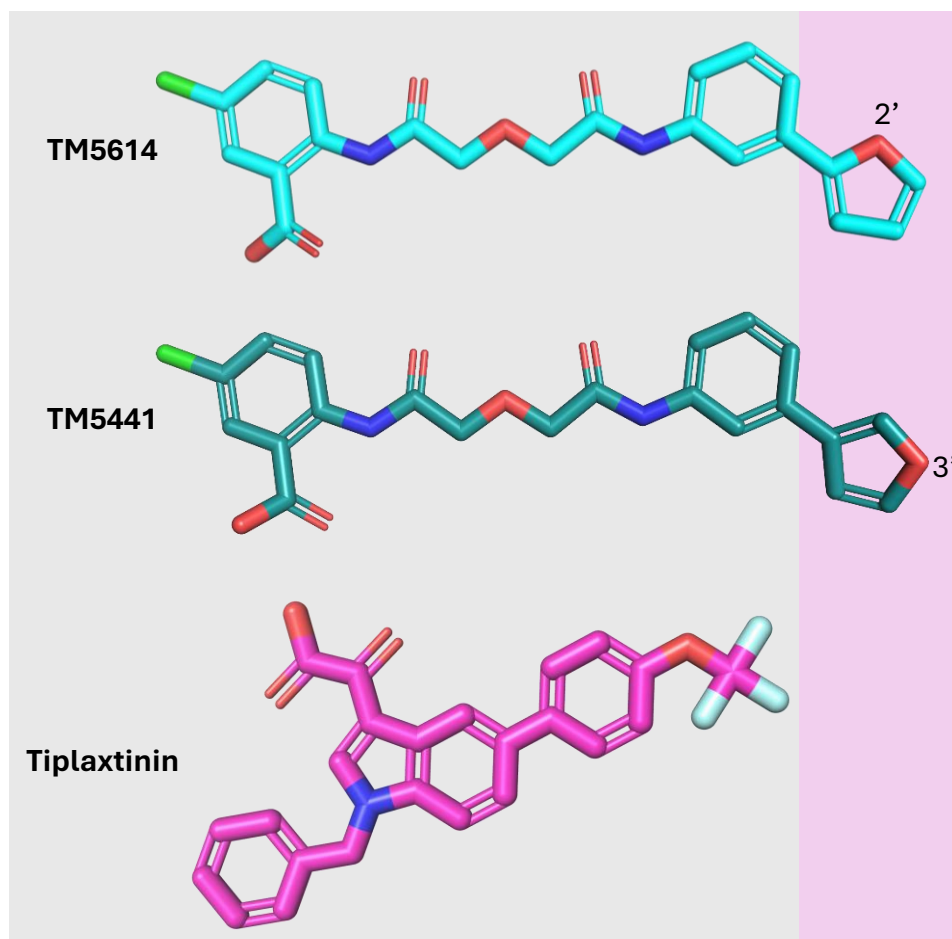


**Figure 5.13, Chemical structure of PAI-1 inhibitors.**

Chemical structures of TM5614, TM5441 and Tiplaxtinin were visualised using the structured data file (PubChem CID 44250551, 44250349 and 6450819 respectively) imported into PyMOL Version 3.1.6.1. The only difference between TM5614 and TM5441 is position of the furan ring (pink box). Oxygen = red, Nitrogen = blue, Chlorine = green, Fluorine = white.

For these reasons TM5441 was selected for further investigation. This drug had a fewer number of citations, especially within cell culture models and therefore, TM5441 was first tested using the AML12 cell line *in vitro*. AML12 cells were treated with 0, 1, 5 or 10  $\mu\text{M}$  TM5441 prior to adding 100 ng/mL of recombinant PAI-1 mouse protein. After 2 hours RNA was extracted, and gene expression was analysed using qRT-PCR for the three key fatty acid metabolism marker genes (Figure 5.14). In line with previous results, *Acadm*, *Hmgcr* and *Hmgcs2* gene expression was significantly downregulated in hepatocytes treated with PAI-1 alone. Whilst 1  $\mu\text{M}$  and 5  $\mu\text{M}$  doses of TM5441 prevented the downregulation of *Acadm* gene expression, this was not consistently seen for *Hmgcr* and *Hmgcs2* gene expression. Pre-treating AML12 cells with 10  $\mu\text{M}$  TM5441 prevented PAI-1-induced downregulation of all 3 genes, and thus was the dose selected going forward.

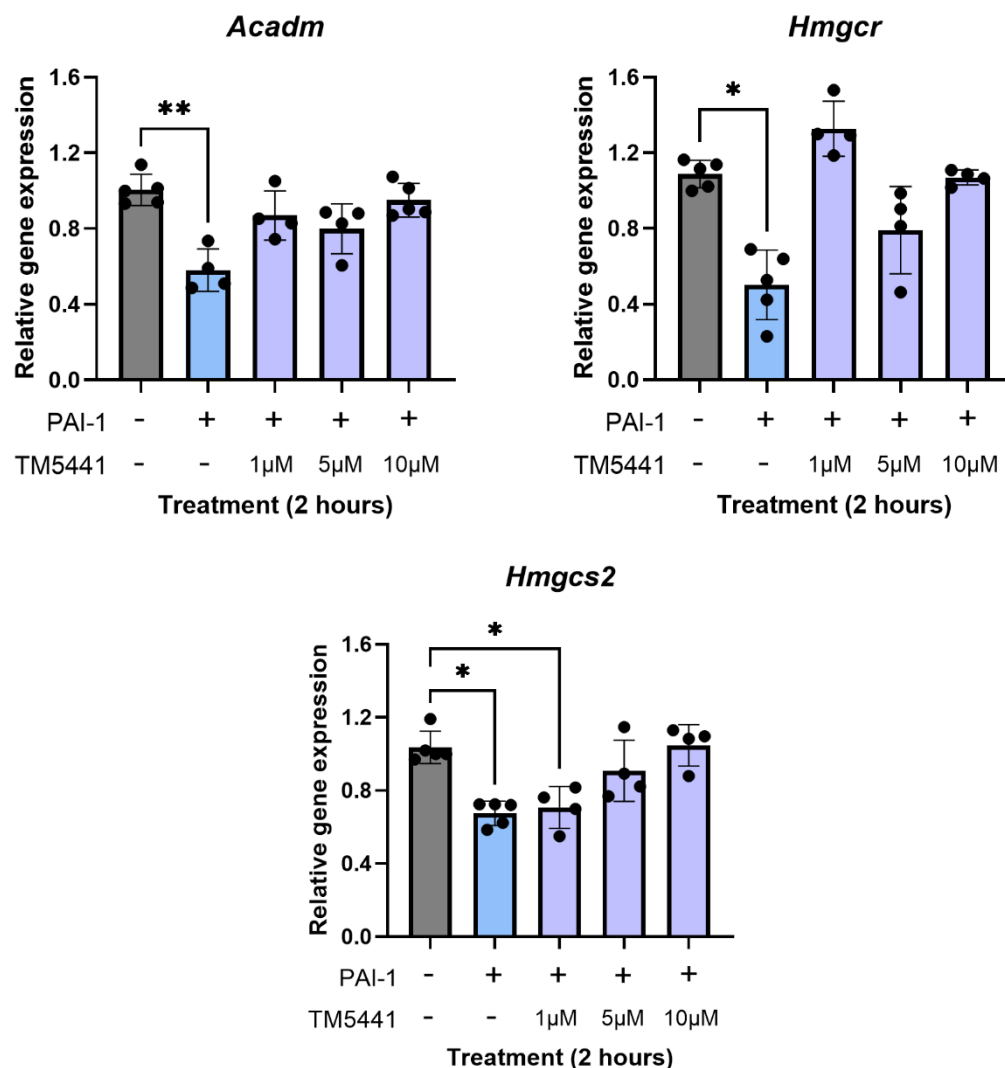


**Figure 5.14, TM5441 treatment reversed PAI-1-induced downregulation of key hepatic fatty acid metabolism gene expression *in vitro* in a dose dependent manner.**

AML12 cells were pre-treated with 0, 1, 5 or 10  $\mu\text{M}$  TM5441 before 100 ng/mL recombinant PAI-1 mouse protein was added. After 2 hours, RNA was extracted and gene expression assessed using qRT-PCR. AML12 cell gene expression for three key hepatic fatty acid metabolism genes normalised against *Rps18*. Mean and standard deviation was calculated and shown on each graph ( $n = 5$ ). A Kruskal-Wallis test with a Dunn's correction for multiple comparisons was performed, comparing each group against the control group, and significant differences are marked using asterisks (\* =  $p < 0.05$ , \*\* =  $P < 0.01$ , \*\*\* =  $p < 0.001$  and \*\*\*\* =  $p < 0.0001$ ).

Next, this assay was repeated to evaluate the reproducibility of TM5441 treatment as well as assess the effect of TM5441 alone on hepatocyte gene expression. In line with previous results, pre-treating hepatocytes with TM5441 blocked the downregulation of *Acadm*, *Hmgcr* and *Hmgcs2* gene expression (Figure 5.15). TM5441 treatment

alone did not significantly alter gene expression, however data did show a slight but not statistically significant reduction in *Hmgcr* and *Hmgcs2* gene expression.

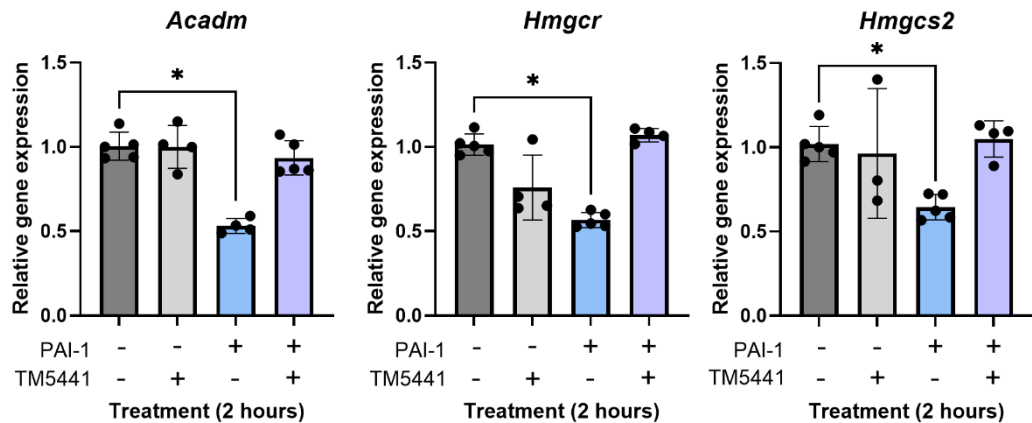


**Figure 5.15, TM5441 treatment reversed PAI-1-induced downregulation of key hepatic fatty acid metabolism gene expression *in vitro*.**

AML12 cells were pre-treated with 10  $\mu$ M before 100 ng/mL recombinant PAI-1 mouse protein was added. After 2 hours, RNA was extracted and gene expression assessed using qRT-PCR. AML12 cell gene expression for three key hepatic fatty acid metabolism genes normalised against *Rps18*. Mean and standard deviation was calculated and shown on each graph (n = 5). A Kruskal-Wallis test with a Dunn's correction for multiple comparisons was performed, comparing each group against the control group, and significant differences are marked using asterisks (\* = p < 0.05, \*\* = P < 0.01, \*\*\* = p < 0.001 and \*\*\*\* = p < 0.0001).

To investigate the effect of pre-treating hepatocytes with TM5441 on LCFA uptake, AML12 cells were treated with recombinant PAI-1 protein with and without 10  $\mu$ M TM5441 for 1 hour before C16 BODIPY was added to each well. A visible reduction in C16 uptake was observed in AML12 cells cultured with PAI-1 without the addition of TM5441 (Figure 5.16A). The combination treatment showed a visible increase in C16 uptake compared to PAI-1 alone, demonstrated by the increased green fluorescence seen. There were no visibly distinguishable differences in C16 uptake or cell number between the control, TM5441 only and combination treatment groups. C16 BODIPY fluorescence intensity per hepatocyte was quantified. This confirmed there was no significant difference in C16 uptake in hepatocytes given the combined treatment compared to the control treatment groups (Figure 5.16B). TM5441 alone did not impact C16 uptake into the AML12 cells.

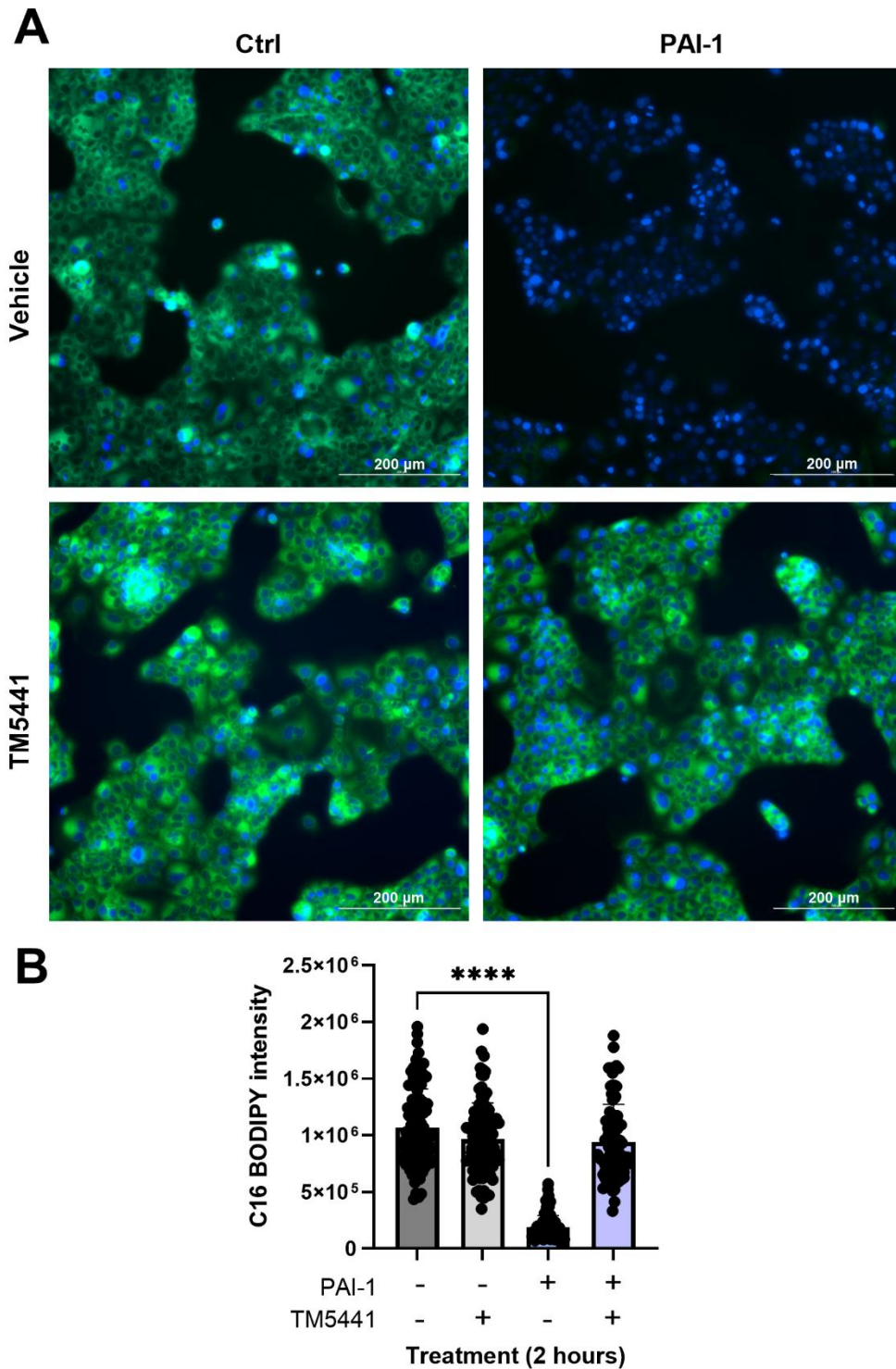


**Figure 5.16, TM5441 prevented PAI-1-induced reduction of LCFA uptake in AML12 cells *in vitro*.**

AML12 cells were pre-treated with 10  $\mu$ M TM5441 before 100 ng/mL recombinant PAI-1 mouse protein was added. After 1 hour, 1  $\mu$ M C16 BODIPY was added and cells were further incubated for 1 hour before fixing, counter staining with DAPI and imaging. **A)** Representative images of control, TM5441 only, LPS only and LPS + TM5441 treated AML12 cells, DAPI = blue, C16 BODIPY = green at x10 magnification. **B)** BODIPY intensity measured per AML12 cell (n = 100). Means and standard deviations were calculated and shown on the graph. A Kruskal-Wallis test with a Dunn's correction for multiple comparisons was performed, comparing each timepoint against the control group, and significant differences are marked using asterisks (\* = p < 0.05, \*\* = P < 0.01, \*\*\* = p < 0.001 and \*\*\*\* = p < 0.0001).

Due to the successful prevention of PAI-1-induced reduction in C16 uptake into AML12 cells by TM5441 pre-treatment, the effect of TM5441 on mitochondrial respiration was investigated. AML12 cells were pre-treated with 10  $\mu$ M TM5441 before 100 ng/mL of recombinant PAI-1 mouse protein was added for 2 hours. Media was removed from each well and replaced with palmitic acid seahorse media. PAI-1, TM5441 or a combination treatment of both did not negatively affect the cell viability of AML12 cells (Figure 5.17A). The OCR trace was then normalised to viable cell count. The OCR trace was not significantly different in the TM5441 only treatment group (Figure 5.17B). Similar to previous findings presented in chapter 2, PAI-1 reduced OCR. However, this reduction was not seen in the combination treatment group. Basal, maximal and ATP-linked respiration were then calculated. There was no significant difference in any of these measurements between the control and TM5441 only treatment groups (Figure 5.17C). As expected, there was a reduction in basal, maximal and ATP-linked respiration in AML12 cells cultured with PAI-1. Notably, this reduction was not seen in the combination treatment group. This indicates that TM5441 pre-treatment prevents the downregulation of fatty acid associated mitochondrial ATP production, in both stress and non-stress conditions in response to PAI-1. Taken together, this data provides evidence that TM5441 effectively prevents PAI-1-induced downregulation of hepatic fatty acid metabolism.

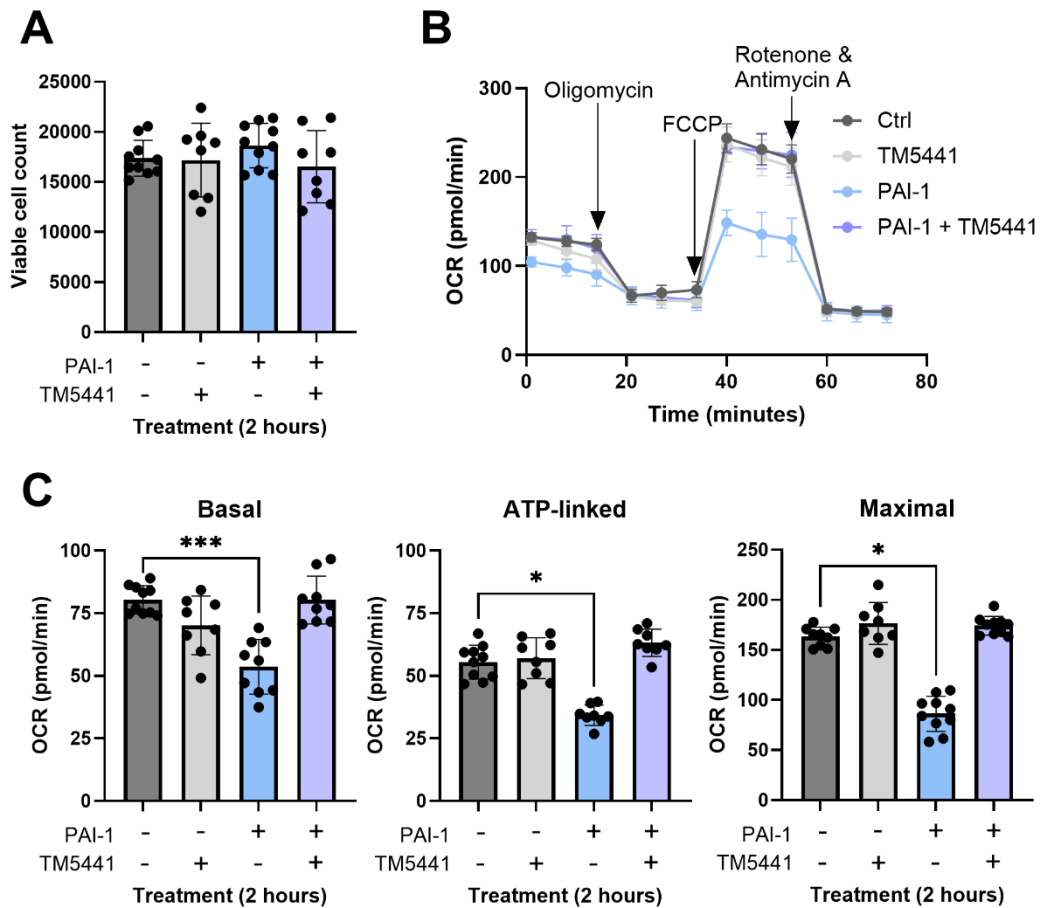


**Figure 5.17, PAI-1 downregulated hepatic fatty acid associated mitochondrial respiration *in vitro* in AML12 cells was reversed by TM5441 treatment.**

AML12 cells were cultured with 10  $\mu$ M TM5441 and 100 ng/mL recombinant mouse PAI-1 protein for 2 hours before media was removed and replaced with seahorse media supplemented with 100  $\mu$ M C16 (palmitic acid), no glucose. **A)** Viable cell count taken at the end of the assay. **B)** Seahorse tracing of OCR normalised to cell count. **C)** Basal, ATP-linked and maximal respiration calculated from the normalised OCR trace. Means and standard deviations were calculated and are shown on each graph (n = 10). A Kruskal-Wallis test with a Dunn's correction for multiple comparisons was performed, comparing each timepoint against the control group, and significant differences are marked using asterisks (\* = p < 0.05, \*\* = P < 0.01, \*\*\* = p < 0.001 and \*\*\*\* = p < 0.0001).

To understand if inhibition of PAI-1 using TM5441 could also prevent the downregulation of hepatic fatty acid uptake and metabolism in response to LPS-treated serum, AML12 cells were treated with serum from control or LPS-treated mice. Serum from LPS-treated mice contains multiple cytokines and factors, and thus this experiment was conducted to characterise the effect of TM5441 pre-treatment on LPS-treated mouse serum. This experiment aimed to help identify if it was solely PAI-1 present in the serum responsible for downregulating hepatic fatty acid metabolism or if it was one of several factors. For this assay, 10  $\mu$ M of TM5441

was added to each well prior to the serum. After 2 hours RNA was extracted, and gene expression was analysed using qRT-PCR for the key marker genes. In line with previous results, *Acadm*, *Hmgcr* and *Hmgcs2* gene expression was all significantly downregulated in hepatocytes treated with serum from LPS-treated mice compared to control serum (Figure 5.18). Pre-treating cells with TM5441 blocked the downregulation of gene expression induced by LPS-treated serum, with gene expression in all 3 genes comparable to the control serum only treatment group. However, it should be noted that TM5441 treatment in combination with control serum significantly downregulated *Hmgcr* gene expression.

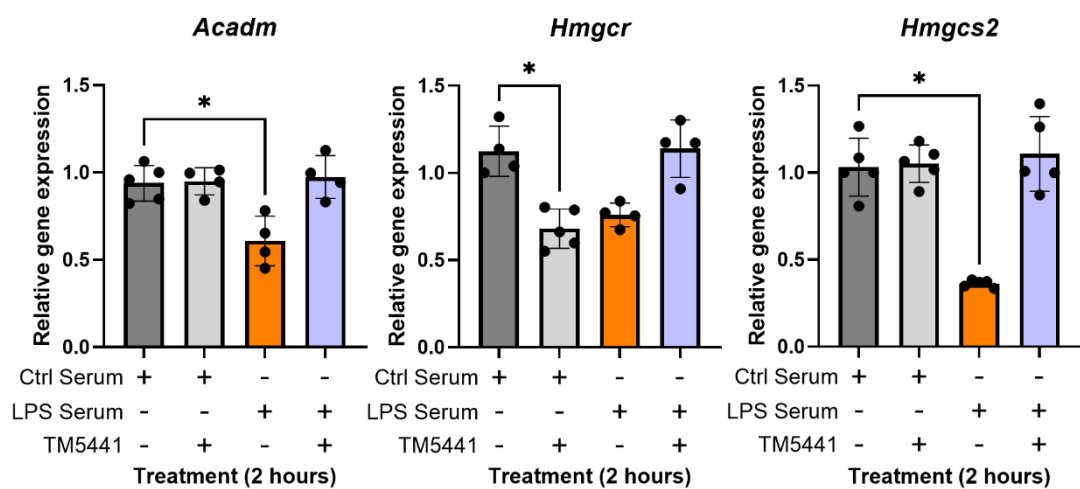


**Figure 5.18, TM5441 treatment prevented the downregulation of key of hepatic fatty acid metabolism genes in response to serum from LPS-treated mice *in vitro*.** Mice were treated with 0.5 mg/kg LPS for 2 hours before being sacrificed. AML12 cells were pre-treated with 10  $\mu$ M TM5441 before being cultured with serum isolated from control mice or LPS-treated mice. After 2 hours, RNA was extracted and gene expression assessed using qRT-PCR. AML12 cell gene expression for three key hepatic fatty acid metabolism genes was normalised against *Rps18*. Mean and standard deviation was calculated and shown on each graph (n = 5). A Kruskal-Wallis test with a Dunn's correction for multiple comparisons was performed, comparing each group against the control group, and significant differences are marked using asterisks (\* = p < 0.05, \*\* = P < 0.01, \*\*\* = p < 0.001 and \*\*\*\* = p < 0.0001).

Next, the effect of pre-treating hepatocytes with TM5441 on LCFA uptake in the presence of serum from LPS-treated mice was investigated. AML12 cells were treated with 10  $\mu$ M TM5441 and either serum isolated from control or LPS-treated mice for 1 hour before C16 BODIPY was added to each well. Cells were incubated for another hour before being fixed, counterstained with DAPI and imaged. As expected, there was a visible reduction in C16 uptake in AML12 cells cultured with serum from

LPS-treated mice without the addition of TM5441 (Figure 5.19A). However, the combination treatment showed visible increase in C16 uptake compared to LPS serum alone, demonstrated by the increased green fluorescence seen. There were no visibly distinguishable differences in C16 uptake or cell number between the control serum, TM5441 with control serum and LPS serum with TM5441 treatment groups. Quantification of C16 BODIPY fluorescence intensity per hepatocyte confirmed there was no significant difference in C16 uptake in hepatocytes given the LPS serum in combination with TM5441 compared to the control serum treatment groups (Figure 5.19B). TM5441 with control serum did not impact C16 uptake into the AML12 cells.

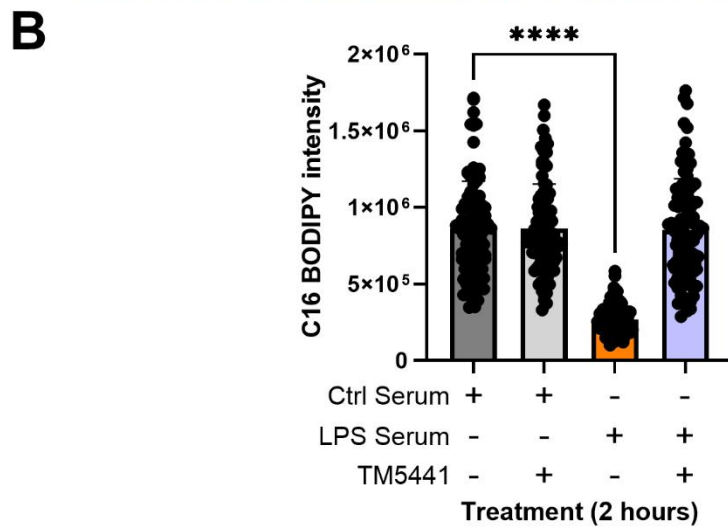
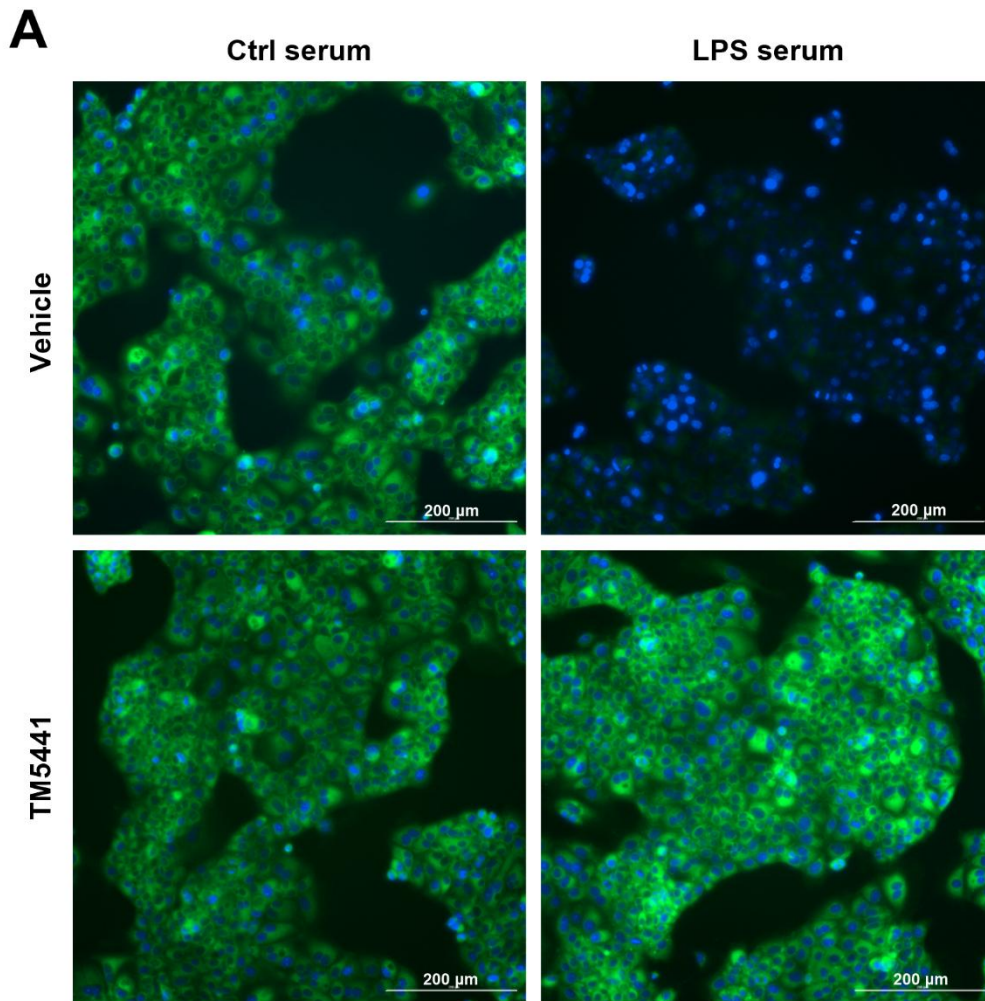


**Figure 5.19, the reduction in LCFA uptake in response to serum from LPS-treated mice was prevented by TM5441 pre-treatment *in vitro*.**

Mice were treated with 0.5 mg/kg LPS for 2 hours before being sacrificed. AML12 cells were pre-treated with 10  $\mu$ M TM5441 before being cultured with serum isolated from control mice or LPS-treated mice. After 1 hour, 1  $\mu$ M C16 BODIPY was added and cells were further incubated for 1 hour before fixing, counter staining with DAPI and imaging. **A)** Representative images of cells treated with control serum, control serum with TM5441, LPS serum and LPS serum with TM5441, DAPI = blue, C16 BODIPY = green at x10 magnification. **B)** BODIPY intensity measured per AML12 cell (n = 100). Means and standard deviations were calculated and shown on the graph. A Kruskal-Wallis test with a Dunn's correction for multiple

comparisons was performed, comparing each timepoint against the control group, and significant differences are marked using asterisks (\* =  $p < 0.05$ , \*\* =  $P < 0.01$ , \*\*\* =  $p < 0.001$  and \*\*\*\* =  $p < 0.0001$ ).

Taken together, this data provides evidence that TM5441 effectively prevents LPS serum-induced downregulation of hepatic fatty acid metabolism gene expression, and hepatic C16 uptake in AML12 cells. This supports the hypothesis that PAI-1 is the main cytokine present in the serum of mice treated with LPS at 2 hours causing the downregulation of hepatic fatty acid metabolism.

## 5.5 TM5441 attenuates LPS-induced downregulation of liver fatty acid metabolism associated gene expression *in vivo*

The next step was to investigate if pre-treating mice with TM5441 *in vivo* could prevent the LPS-induced downregulation of liver fatty acid metabolism and thus reduce the availability of circulating fatty acids. The limited literature, none of which used LPS, identified 10 or 20 mg/kg as a suitable dose of TM5441 in mice (595, 596). The higher dose of 20 mg/kg has been associated with acute hepatotoxicity, whilst the lower dose of 10 mg/kg has not (597). Therefore, a dose of 10 mg/kg TM5441 was selected to ensure the risk of liver damage was minimal. WT mice were treated with 10 mg/kg TM5441 via oral gavage 1 hour prior to LPS I.P. injection to allow time for the inhibitor to be absorbed into the circulation (Figure 5.20). Mice were sacrificed 6 hours after the final LPS I.P. injection was administered. The experimental design is shown below (Figure 5.20). Mice were split into 4 groups: vehicle only, TM5441 only, Vehicle + LPS and TM5441 + LPS.

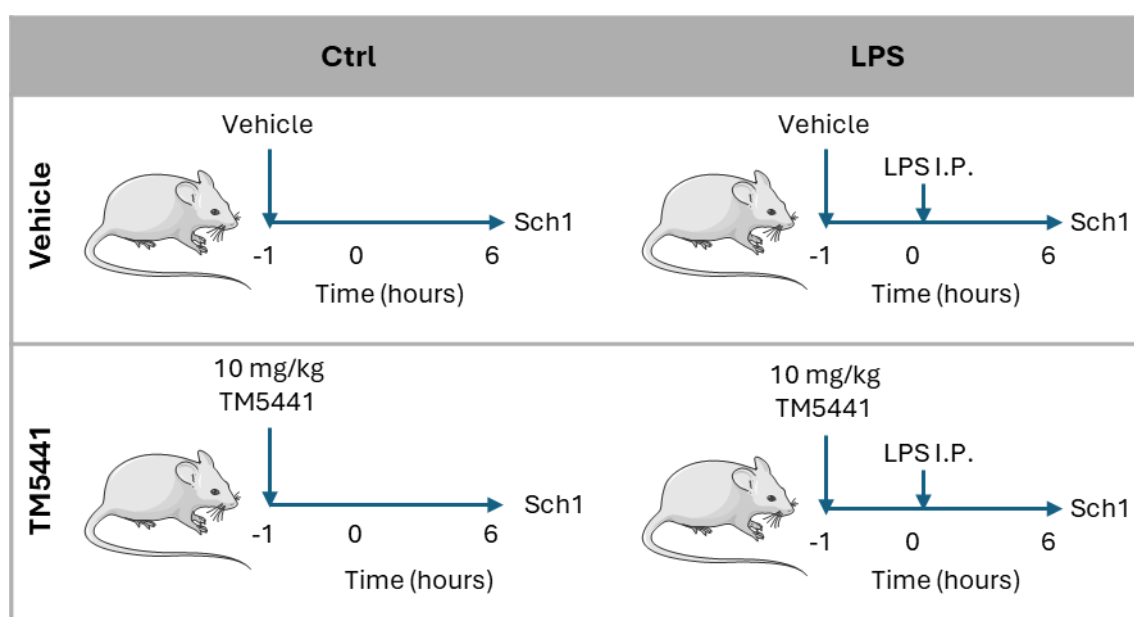


**Figure 5.20, Schematic of TM5441 with LPS experimental design.**

WT mice pre-treated with 10 mg/kg TM5441 via oral gavage 1 hour prior to being injected with 0.5 mg/kg LPS via I.P. Mice were sacrificed 6 hours after final LPS I.P. was administered. Mice were split into 4 experimental groups: 1) control mice receiving only the vehicle via oral gavage, 2) TM5441 only mice who received 10 mg/kg TM5441 via oral gavage, 3) LPS + vehicle mice who received the vehicle via oral gavage 1 hour prior to 0.5 mg/kg LPS injection via I.P., and 4) LPS + TM5441 group who received a combination treatment of 10 mg/kg TM5441 via oral gavage 1 hour prior to 0.5 mg/kg LPS via I.P.

Firstly, serum from the mice was analysed for PAI-1 content using a PAI-1 ELISA. Results showed that pre-treating mice with TM5441 reduced the amount of circulating PAI-1 by nearly half (Figure 5.21). There was no notable difference between the vehicle only and TM5441 only treatment groups.

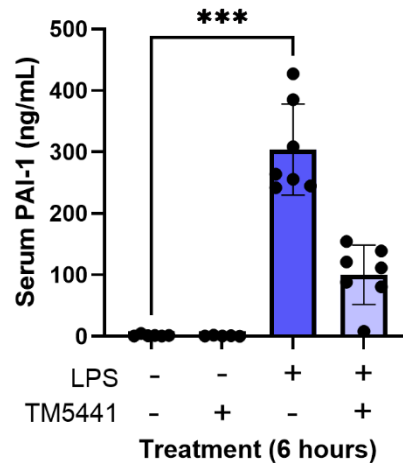


**Figure 5.21, Serum PAI-1 levels decreased in mice pre-treated with TM5441 before LPS administration.**

WT mice pre-treated with 10 mg/kg TM5441 via oral gavage 1 hour prior to being injected with 0.5 mg/kg LPS via I.P. Mice were sacrificed 6 hours after final LPS I.P. was administered. Serum was separated from whole blood and PAI-1 content was analysed using a PAI-1 ELISA. Mean and standard deviation was calculated and shown on the graph (n = 7). A Kruskal-Wallis test with a Dunn's correction for multiple comparisons was performed, comparing each group against the control group, and significant differences are marked using asterisks (\* = p < 0.05, \*\* = P < 0.01, \*\*\* = p < 0.001 and \*\*\*\* = p < 0.0001).

RNA was extracted from whole liver lysates. Pre-treating mice with 10 mg/kg TM5441 prevented the downregulation of key liver fatty acid metabolism genes in response to LPS including *Acadm*, *Acsl1*, *Hmgcs2* and *Hmgcr* (Figure 5.22). In line with previous findings, *Cpt1a* gene expression did not significantly change across treatment groups.

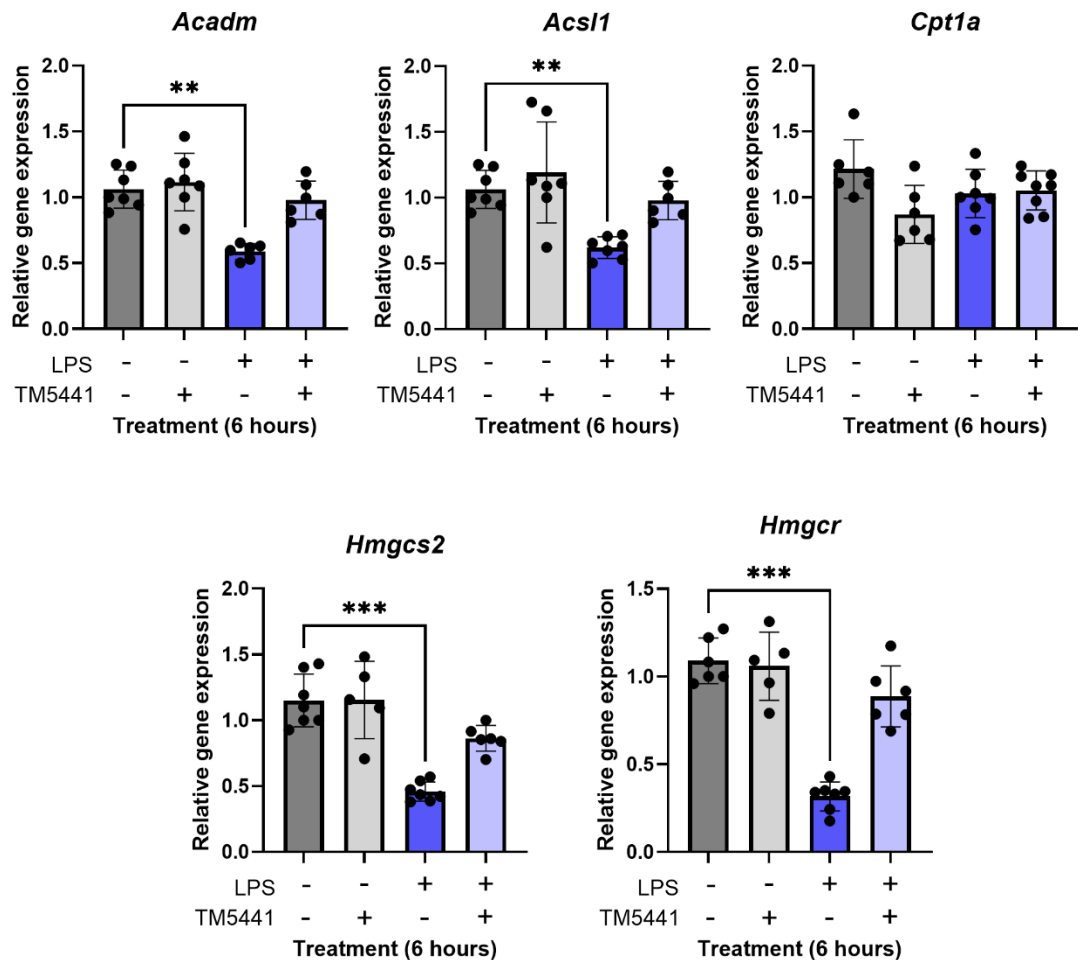


**Figure 5.22, TM5441 prevented the LPS-induced downregulation of key liver fatty acid metabolism genes.**

WT mice pre-treated with 10 mg/kg TM5441 via oral gavage 1 hour prior to being injected with 0.5 mg/kg LPS via I.P. Mice were sacrificed 6 hours after final LPS I.P. was administered. RNA was extracted from whole liver lysates and analysed using RT-qPCR. Gene expression was normalised against *Rps18*. Mean and standard deviation was calculated and shown on each graph (n = 7). A Kruskal-Wallis test with a Dunn's correction for multiple comparisons was performed, comparing each group against the control group, and significant differences are marked using asterisks (\* = p < 0.05, \*\* = P < 0.01, \*\*\* = p < 0.001 and \*\*\*\* = p < 0.0001).

Furthermore, expression of the genes encoding the long-chain fatty acid transporters *Ldlr* and *Slc27a2* were not significantly downregulated in the mice pre-treated with TM5441 prior to LPS administration (Figure 5.23), noticeably increased compared to the LPS vehicle treated group. As expected, *Cd36* gene expression did not significantly change across all 4 groups. In toto, TM5441 prevented the downregulation of liver fatty acid metabolism gene expression in response to LPS.

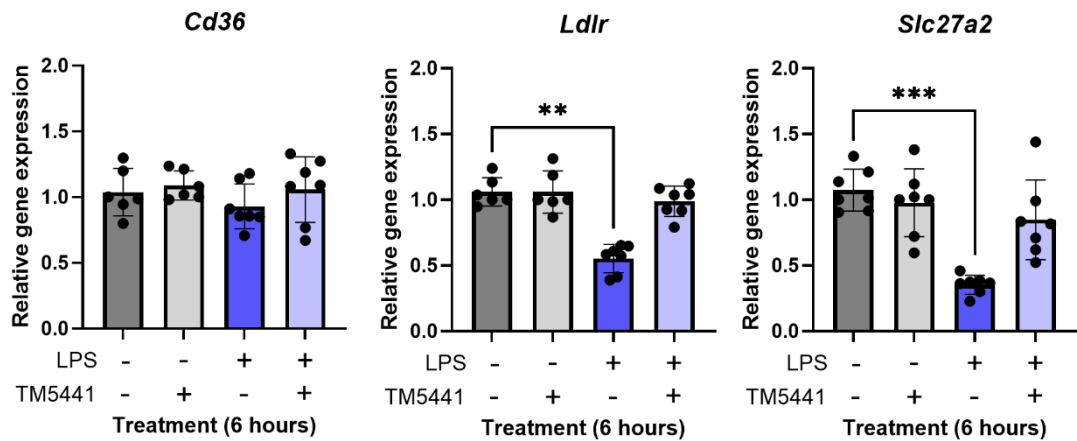


**Figure 5.23, TM5441 reversed the LPS-induced downregulation of key liver LCFA transporter genes.**

WT mice pre-treated with 10 mg/kg TM5441 via oral gavage 1 hour prior to being injected with 0.5 mg/kg LPS via I.P. Mice were sacrificed 6 hours after final LPS I.P. was administered. RNA was extracted from whole liver lysates and analysed using RT-qPCR. Gene expression was normalised against *Rps18*. Mean and standard deviation was calculated and shown on each graph (n = 7). A Kruskal-Wallis test with a Dunn's correction for multiple comparisons was performed, comparing each group against the control group, and significant differences are marked using asterisks (\* = p < 0.05, \*\* = P < 0.01, \*\*\* = p < 0.001 and \*\*\*\* = p < 0.0001).

Next, the serum was analysed using LC-MS to investigate the effect of this on circulating fatty acids. Results within and between groups were compared using a PCA plot to assess the similarities and differences (Figure 5.24A). The combination treatment of TM5441 and LPS clustered closely to the vehicle control and TM5441 only mice, whereas the vehicle with LPS treated mice were more distinctly separate from the other groups. Total serum LCFA concentration was calculated by adding the concentration of each individual LCFA that was measured (Figure 5.24B). LPS treated mice had significantly higher levels of LCFA compared to both controls. The combination treatment of TM5441 and LPS did not have significantly increased levels of serum LCFAs compared to controls. The relative abundance of each LCFA further supported these results. The majority of LCFAs were not significantly upregulated in the combination treatment group (Figure 5.24C). Only C14 (myristic acid), C16.1 (palmitoleic acid) and C22.6 (docosahexaenoic acid) were still significantly upregulated, although to a much lower level than in the LPS only treatment group. This supports the role of the liver in controlling the availability of circulating fatty acids.

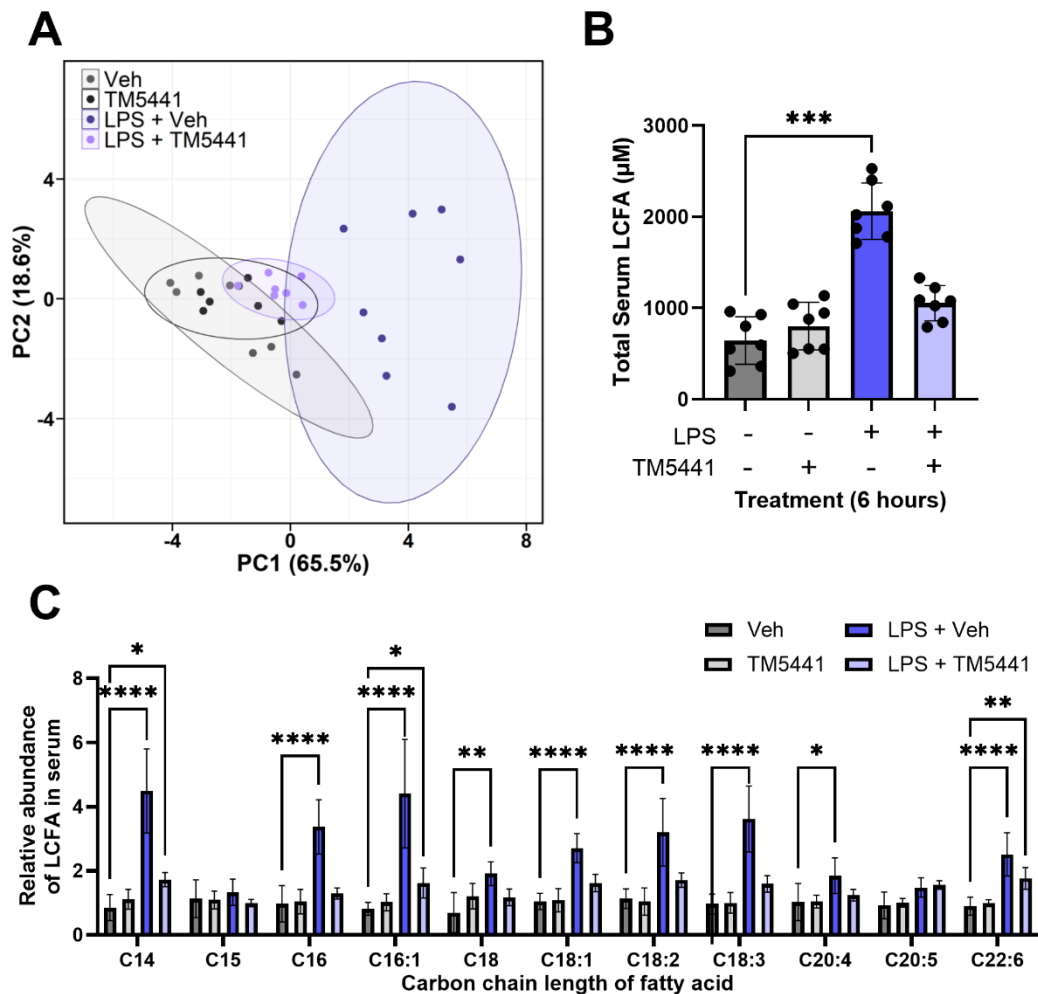


**Figure 5.24, TM5441 prevented the LPS-induced increase in serum LCFAs.**

WT mice pre-treated with 10 mg/kg TM5441 via oral gavage 1 hour prior to being injected with 0.5 mg/kg LPS via I.P. Mice were sacrificed 6 hours after final LPS I.P. was administered. Serum was separated from whole blood and LCFA content was analysed using LC-MS. **A)** PCA plot of serum LCFA abundance from vehicle control, TM5441 only, LPS + vehicle and LPS + TM5441 treated mice. **B)** Total serum LCFA was calculated by adding the concentration of each individual LCFA measured. **C)** Relative abundance of each LCFA measured in the serum normalised to a control mouse. Mean and standard deviation was calculated and shown on each graph (n = 7). For B, a Kruskal-Wallis test with a Dunn's correction for multiple comparisons was performed, comparing each group against the control group. For C, a 2way ANOVA with a Dunnett's correction for multiple comparisons was performed comparing each group against the control group for each individual LCFA. Significant differences are marked using asterisks (\* = p < 0.05, \*\* = P < 0.01, \*\*\* = p < 0.001 and \*\*\*\* = p < 0.0001).

Blood glucose levels were still significantly decreased in both LPS treatment groups (Figure 5.25). This further supports the idea presented in chapter 2 that PAI-1 specifically affects fatty acid metabolism and not just a generic downregulation of metabolism because inhibition of PAI-1 via TM5441 had minimal effect on overall blood glucose levels.

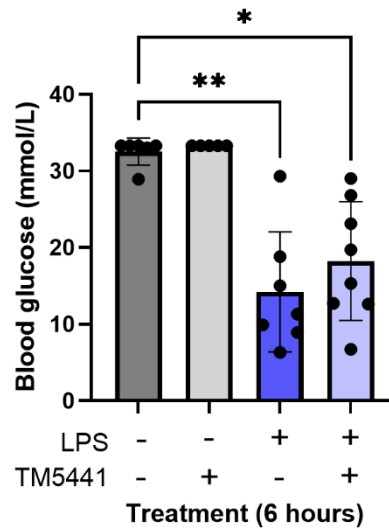


**Figure 5.25, TM5441 did not affect the LPS-induced downregulation of blood glucose levels.**

WT mice pre-treated with 10 mg/kg TM5441 via oral gavage 1 hour prior to being injected with 0.5 mg/kg LPS via I.P. Mice were sacrificed 6 hours after final LPS I.P. was administered. Glucose levels within the blood were measured using a blood glucose monitor and test-strips. Mean and standard deviation was calculated and shown on the graph (n = 7). A Kruskal-Wallis test with a Dunn's correction for multiple comparisons was performed, comparing each group against the control group, and significant differences are marked using asterisks (\* =  $p < 0.05$ , \*\* =  $P < 0.01$ , \*\*\* =  $p < 0.001$  and \*\*\*\* =  $p < 0.0001$ ).

The weight of mice across all 4 groups did not significantly change over the course of the experiment (Figure 5.26). This was not unexpected due to the short 6-hour timepoint.

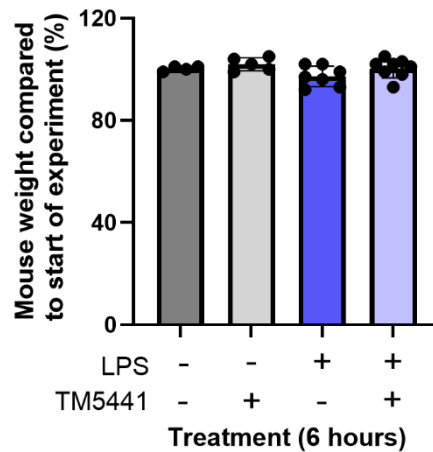


**Figure 5.26, 6-hours of TM5441 did not affect mouse weight.**

WT mice pre-treated with 10 mg/kg TM5441 via oral gavage 1 hour prior to being injected with 0.5 mg/kg LPS via I.P. Mice were sacrificed 6 hours after final LPS I.P. was administered. Mice were weighed at the start of the experiment and again at the end. Percentage change of weight was calculated by comparing the difference between these two weights. Mean and standard deviation was calculated and shown on the graph (n = 7). A Kruskal-Wallis test with a Dunn's correction for multiple comparisons was performed, comparing each timepoint against the control group, and significant differences are marked using asterisks (\* = p < 0.05, \*\* = P < 0.01, \*\*\* = p < 0.001 and \*\*\*\* = p < 0.0001).

The weights of the mice taken at the endpoint of the experiment were then used to calculate the percentage weight of the inguinal and gonadal fat pads relative to total body weight. Again, there was no significant difference in the percentage weight of both the inguinal and gonadal fat pads across all 4 groups (Figure 5.27).

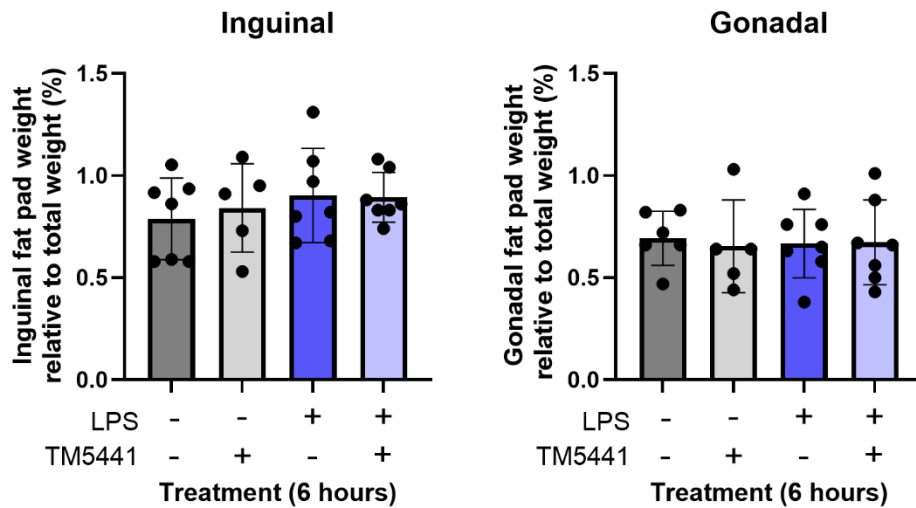


**Figure 5.27, Fat pad weight did not significantly change in TM5441 or LPS treated mice after 6 hours.**

WT mice pre-treated with 10 mg/kg TM5441 via oral gavage 1 hour prior to being injected with 0.5 mg/kg LPS via I.P. Mice were sacrificed 6 hours after final LPS I.P. was administered. Inguinal and gonadal fat pads were dissected from mice and weighed. The percentage the weight of each fat pad was calculated against total body weight at time of sacrifice. Mean and standard deviation was calculated and shown on each graph (n = 7). A Kruskal-Wallis test with a Dunn's correction for multiple comparisons was performed, comparing each group against the control group, and significant differences are marked using asterisks (\* = p < 0.05, \*\* = P < 0.01, \*\*\* = p < 0.001 and \*\*\*\* = p < 0.0001).

To investigate if TM5441 pre-treatment affected liver immune cell populations, liver immune cells were isolated from one liver lobe and stained with the same antibodies and gating strategy as shown in chapter 1. The number of total immune cells per 50,000 isolated liver cells significantly decreased in the liver in response to LPS treatment (Figure 5.28). Lymphoid cells also significantly decreased in number in both LPS treatment groups. Interestingly, compared to vehicle control, there was a significant reduction in myeloid cell number per 50,000 isolated liver cells in the three other groups. This differs to earlier results that 6 hours after LPS myeloid cell number did not significantly change. Despite this, the neutrophil cell count per 50,000 isolated liver cells significantly increased in response to LPS. Whilst the number of neutrophils was still higher in the combination treatment group, it did not reach statistical significance. This provides evidence that PAI-1 inhibition may affect neutrophils infiltration into the liver in response to LPS.

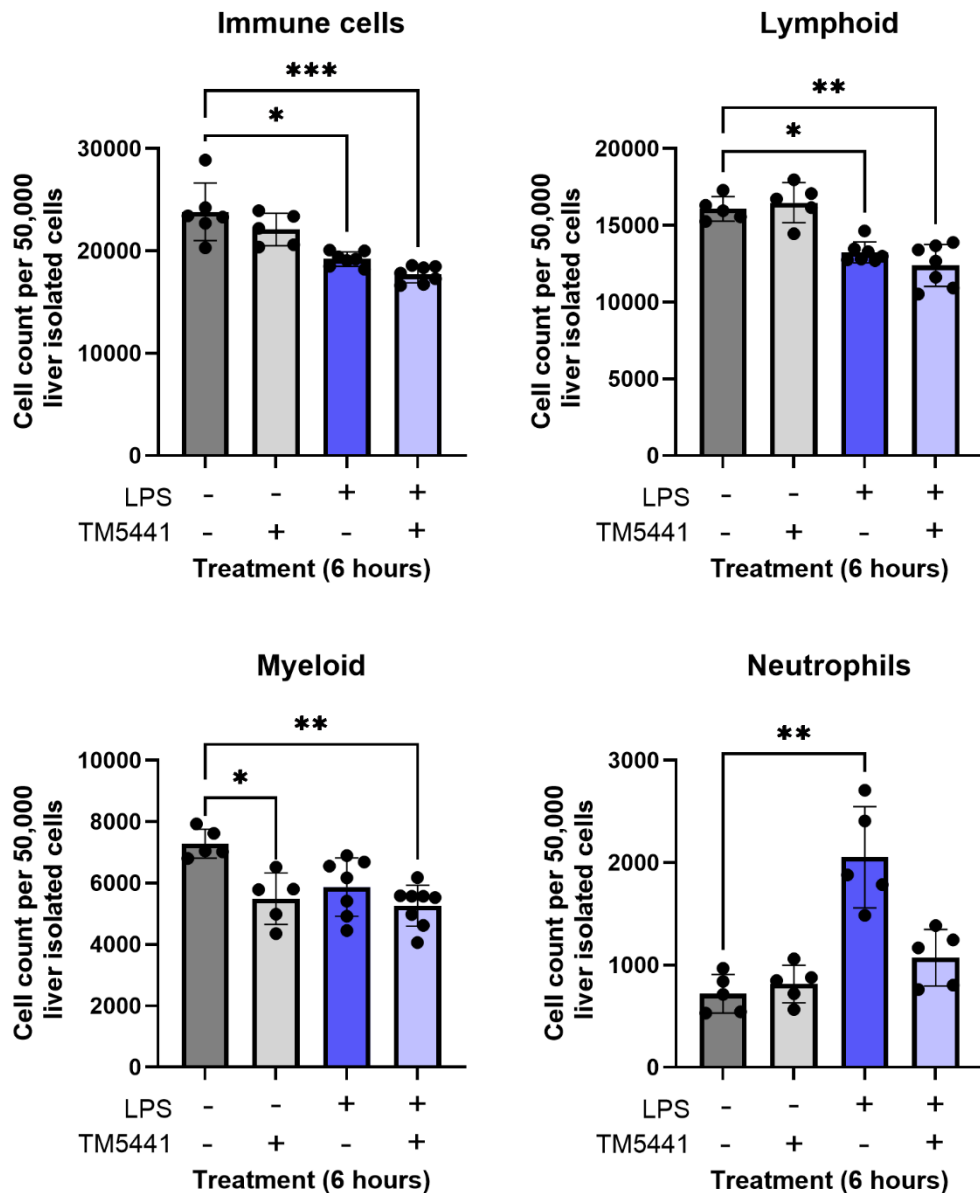


**Figure 5.28, Liver immune cell numbers in response to TM5441 and LPS treatment.**

WT mice pre-treated with 10 mg/kg TM5441 via oral gavage 1 hour prior to being injected with 0.5 mg/kg LPS via I.P. Mice were sacrificed 6 hours after final LPS I.P. was administered. Immune cells isolated from the liver were stained with an antibody panel using markers for lymphoid, myeloid and neutrophil populations. Mean and standard deviation was calculated and shown on each graph (n = 7). A Kruskal-Wallis test with a Dunn's correction for multiple comparisons was performed, comparing each group against the control group, and significant differences are marked using asterisks (\* = p < 0.05, \*\* = P < 0.01, \*\*\* = p < 0.001 and \*\*\*\* = p < 0.0001).

The number of monocytes per 50,000 isolated liver cells also significantly decreased in response to LPS, both with and without TM5441 (Figure 5.29). This included a significant reduction in the number of classical monocytes. Despite a decrease in

total monocyte numbers, the number of non-classical monocytes did not significantly change across the 4 groups. This differs from previously presented results that non-classical monocytes significantly increased 6 hours after LPS administration. This difference could be a result of the oral gavage treatments given to these mice.

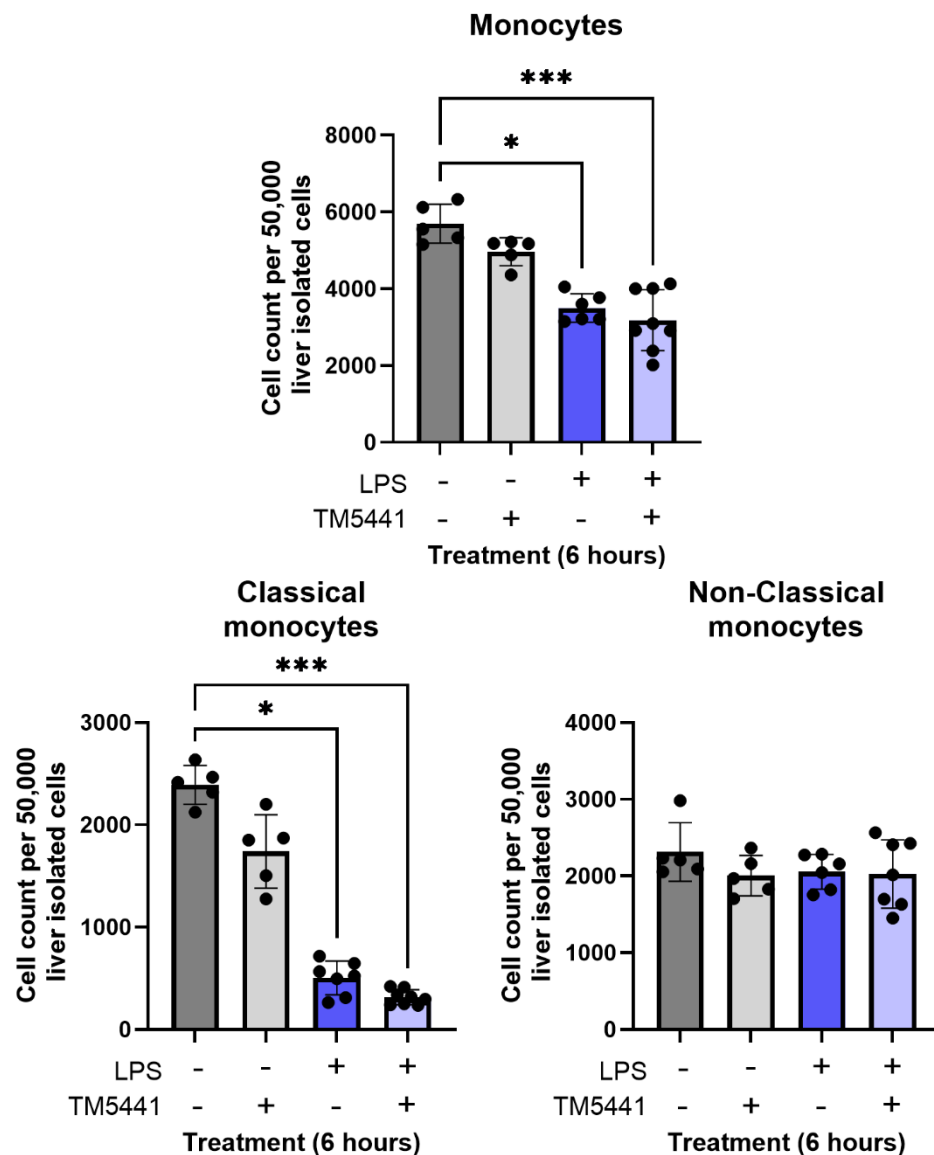


**Figure 5.29, Liver monocyte numbers in response to TM5441 and LPS treatment.** WT mice pre-treated with 10 mg/kg TM5441 via oral gavage 1 hour prior to being injected with 0.5 mg/kg LPS via I.P. Mice were sacrificed 6 hours after final LPS I.P. was administered. Immune cells isolated from the liver were stained with an antibody panel using markers for classical and non-classical monocyte populations. Mean and standard deviation was calculated and shown on each graph (n = 7). A Kruskal-Wallis test with a Dunn's correction for multiple comparisons was performed, comparing each group against the control group, and significant differences are marked using asterisks (\* = p < 0.05, \*\* = P < 0.01, \*\*\* = p < 0.001 and \*\*\*\* = p < 0.0001).

The number of macrophages per 50,000 isolated cells also significantly decreased in response to LPS in groups with, as well as without, TM5441. This was reflected in a significant decrease in non-tissue resident, or infiltrating, macrophages (Figure 5.30). There was no significant difference in the number of tissue-resident macrophages, more commonly referred to as Kupffer cells.

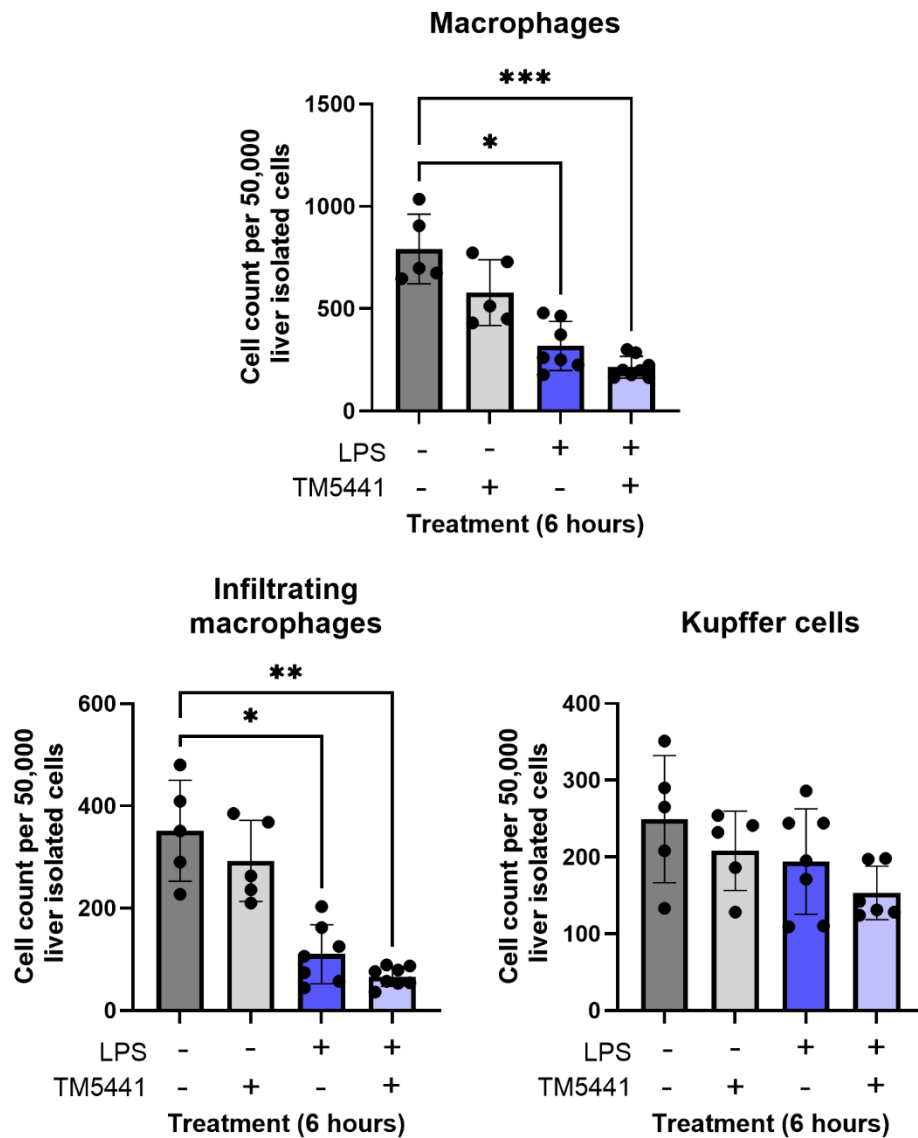


**Figure 5.30, Liver macrophage numbers in response to TM5441 and LPS treatment.**

WT mice pre-treated with 10 mg/kg TM5441 via oral gavage 1 hour prior to being injected with 0.5 mg/kg LPS via I.P. Mice were sacrificed 6 hours after final LPS I.P. was administered. Immune cells isolated from the liver were stained with an antibody panel using markers for macrophage populations. Mean and standard deviation was calculated and shown on each graph (n = 7). A Kruskal-Wallis test with a Dunn's correction for multiple comparisons was performed, comparing each group against the control group, and significant differences are marked using asterisks (\* = p < 0.05, \*\* = P < 0.01, \*\*\* = p < 0.001 and \*\*\*\* = p < 0.0001).

Taken together, these results demonstrate that TM5441 treatment prevented the downregulation of genes associated with liver fatty acid metabolism in response to LPS treatment. This was associated with normal levels of circulating LCFAs, comparable to control mice at 6 hours, in mice treated with a combination of both TM5441 and LPS. However, the LPS only group still had a significant increase in circulating LCFAs present in the serum. TM5441 treatment did not affect blood glucose levels, which still significantly decreased in both the LPS only and combination treatment groups. Furthermore, TM5441 in combination with LPS did not significantly alter the population of liver immune cells compared to LPS treatment alone. The exception to this was that the number of neutrophils did not significantly increase in response to LPS in the combination treatment group. This signifies that TM5441 treatment may affect neutrophils within the liver.

## 5.6 Pre-treating mice with TM5441 impacted HSC expansion in response to LPS in the bone marrow

Finally, because inhibition of PAI-1 by TM5441 treatment significantly reduced the amount of circulating LCFAs in response to LPS, the consequences of PAI-1 inhibition on HSC expansion was investigated. For this, the same experimental design was used, however the endpoint was extended to 16 hours. This was done to allow time for HSC expansion to occur in response to LPS. Firstly, metabolic parameters were assessed to identify if TM5441 retained its therapeutic efficacy at a 16-hour timepoint. PAI-1 levels in the serum were assessed using a PAI-1 ELISA, which showed that TM5441 reduced serum PAI-1 levels in the mice by around 50% (Figure 5.31). This would indicate that one dose of TM5441 was still effective at reducing circulating PAI-1 levels in mice over a longer time period.

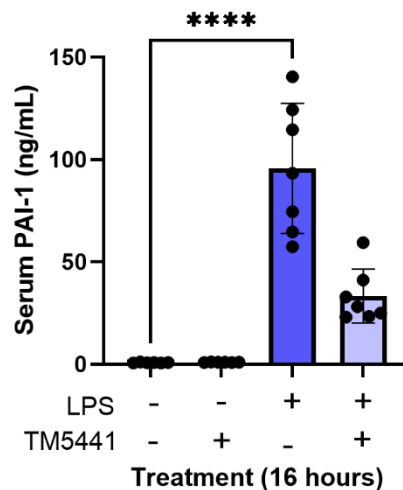


**Figure 5.31, Serum PAI-1 levels decreased in mice pre-treated with TM5441 before LPS administration at 16 hours.**

WT mice pre-treated with 10 mg/kg TM5441 via oral gavage 1 hour prior to being injected with 0.5 mg/kg LPS via I.P. Mice were sacrificed 16 hours after final LPS I.P. was administered. Serum was separated from whole blood and PAI-1 content was analysed using a PAI-1 ELISA. Mean and standard deviation was calculated and shown on the graph ( $n = 7$ ). A Kruskal-Wallis test with a Dunn's correction for multiple comparisons was performed, comparing each group against the control group, and significant differences are marked using asterisks ( $* = p < 0.05$ ,  $** = P < 0.01$ ,  $*** = p < 0.001$  and  $**** = p < 0.0001$ ).

RNA was extracted from whole liver lysates. Similarly to the 6-hour timepoint, pre-treating mice with 10 mg/kg TM5441 prevented the downregulation of key liver fatty acid metabolism genes in response to LPS including *Acadm*, *Hmgcs2*, *Hmgcr* and

*Cpt1a* 16 hours after LPS injection (Figure 5.32). The downregulation of *Cpt1a* at this 16-hour timepoint is consistent with findings presented in chapter 1. *Acs1l* gene expression was still significantly downregulated in the combination treatment group, although expression was still higher than in the LPS + vehicle treatment group. In fact all genes shown here were slightly decreased in the combination treatment group compared to the controls. This could be due to the fact that only 1 dose of TM5441 was given and by 16 hours it could no longer be viable and active. However further investigations on the drugs kinetics would be needed to confirm this.

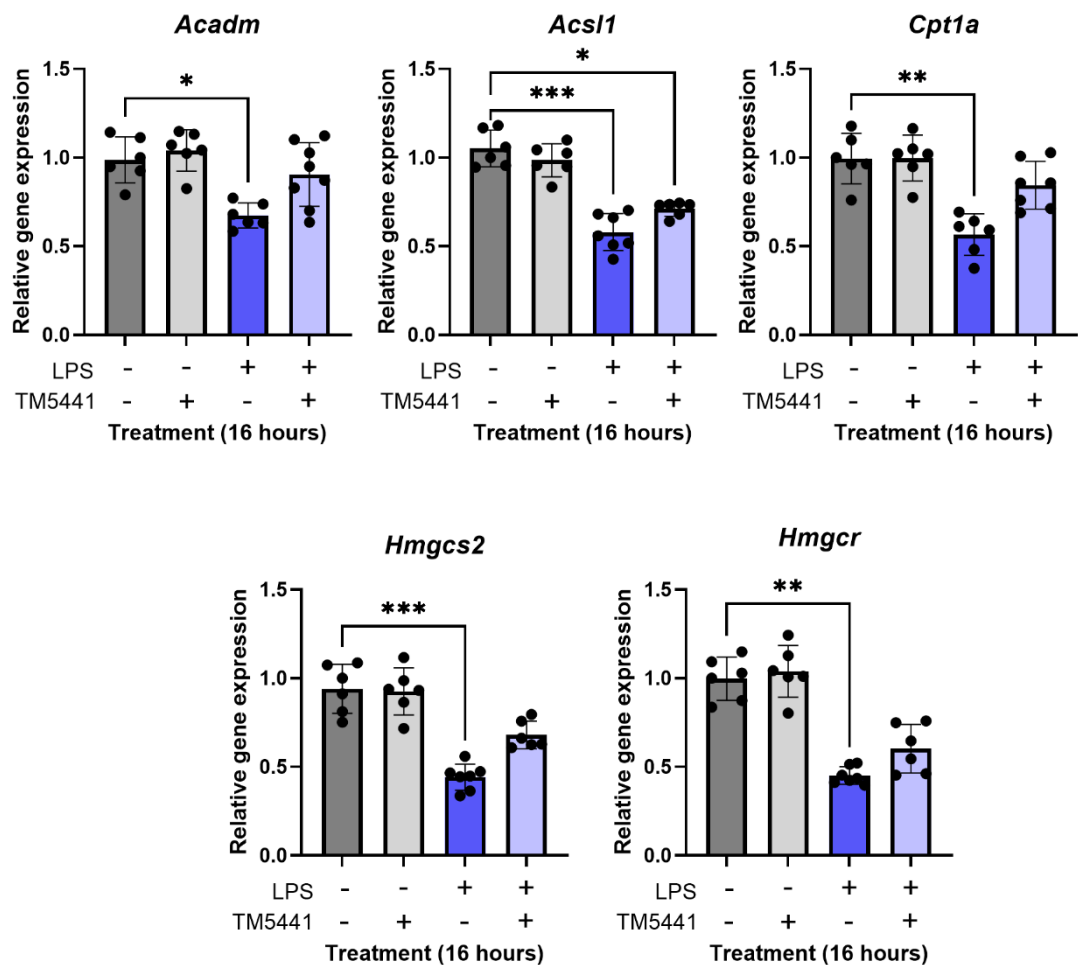


**Figure 5.32, TM5441 partially prevented the LPS-induced downregulation of key liver fatty acid metabolism genes at 16 hours.**

WT mice pre-treated with 10 mg/kg TM5441 via oral gavage 1 hour prior to being injected with 0.5 mg/kg LPS via I.P. Mice were sacrificed 16 hours after final LPS I.P. was administered. RNA was extracted from whole liver lysates and analysed using RT-qPCR. Gene expression was normalised against *Rps18*. Mean and standard deviation was calculated and shown on each graph (n = 7). A Kruskal-Wallis test with a Dunn's correction for multiple comparisons was performed, comparing each group against the control group, and significant differences are marked using asterisks (\* = p < 0.05, \*\* = P < 0.01, \*\*\* = p < 0.001 and \*\*\*\* = p < 0.0001).

Furthermore, expression of the gene encoding the long-chain fatty acid transporter *Slc27a2* was not significantly downregulated in the mice pre-treated with TM5441 prior to LPS administration at the 16-hour timepoint (Figure 5.33). Both *Ldlr* and *Slc27a2* gene expression noticeably increased compared to the LPS vehicle treated group, but were still lower than the control groups. *Ldlr* gene expression was still significantly lower in the combination treatment group than in the controls. Again, this could be due to the reduced bioavailability of TM5441 by the 16-hour mark. As expected, *Cd36* gene expression did not significantly change across all 4 groups. Overall, TM5441 prevented the downregulation most of the liver fatty acid metabolism genes in response to LPS at 16 hours.

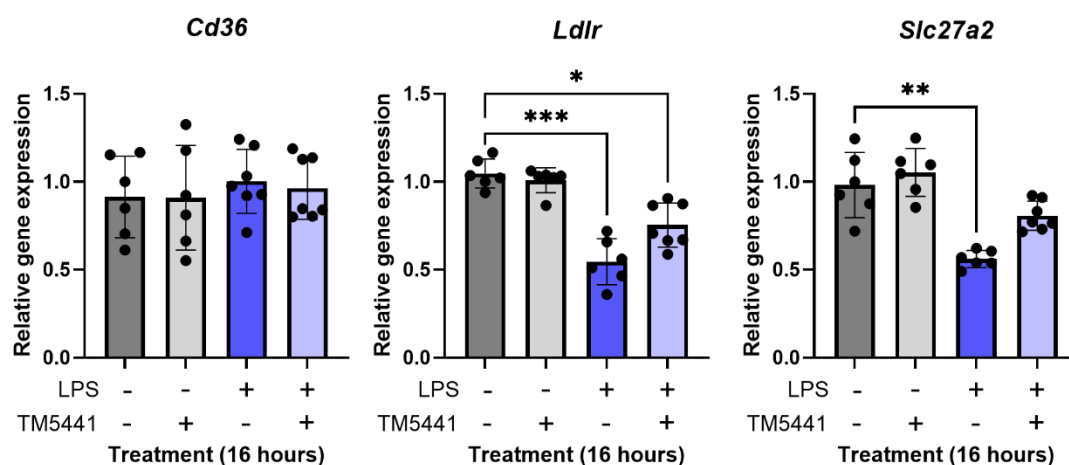


**Figure 5.33, TM5441 partially reversed the LPS-induced downregulation of key liver LCFA transporter genes at 16 hours.**

WT mice pre-treated with 10 mg/kg TM5441 via oral gavage 1 hour prior to being injected with 0.5 mg/kg LPS via I.P. Mice were sacrificed 16 hours after final LPS I.P. was administered. RNA was extracted from whole liver lysates and analysed using RT-qPCR. Gene expression was normalised against *Rps18*. Mean and standard deviation was calculated and shown on each graph (n = 7). A Kruskal-Wallis test with a Dunn's correction for multiple comparisons was performed, comparing each group against the control group, and significant differences are marked using asterisks (\* = p < 0.05, \*\* = P < 0.01, \*\*\* = p < 0.001 and \*\*\*\* = p < 0.0001).

Next, the serum was analysed using LC-MS to investigate the effect of TM5441 pre-treatment on circulating fatty acids 16 hour after LPS administration. Results within and between groups were compared using a PCA plot to assess the similarities and differences (Figure 5.34A). The combination treatment of TM5441 with LPS clustered closely to the vehicle control and TM5441 only mice, whereas the vehicle with LPS treated mice were more distinctly separate from the other groups. Total serum LCFA

concentration was calculated by adding the concentration of each individual LCFA that was measured (Figure 5.34B). LPS treated mice had significantly higher levels of LCFA compared to both controls. The combination treatment of TM5441 and LPS did not have significantly increased levels of serum LCFAs compared to controls. The relative abundance of each LCFA further supported these results. The majority of LCFAs were not significantly upregulated in the combination treatment group (Figure 5.34C). Only C18 (stearic acid), was still significantly upregulated, although to a much lower level than in the LPS only treatment group. Interestingly, alongside C15 (pentadecanoic acid), C20.4 (arachidonic acid) and C20.5 (eicosapentaenoic acid) were not significantly altered across all 4 treatment groups. However overall, the reduction in serum LCFAs supports the role of the liver in controlling the availability of circulating fatty acids.

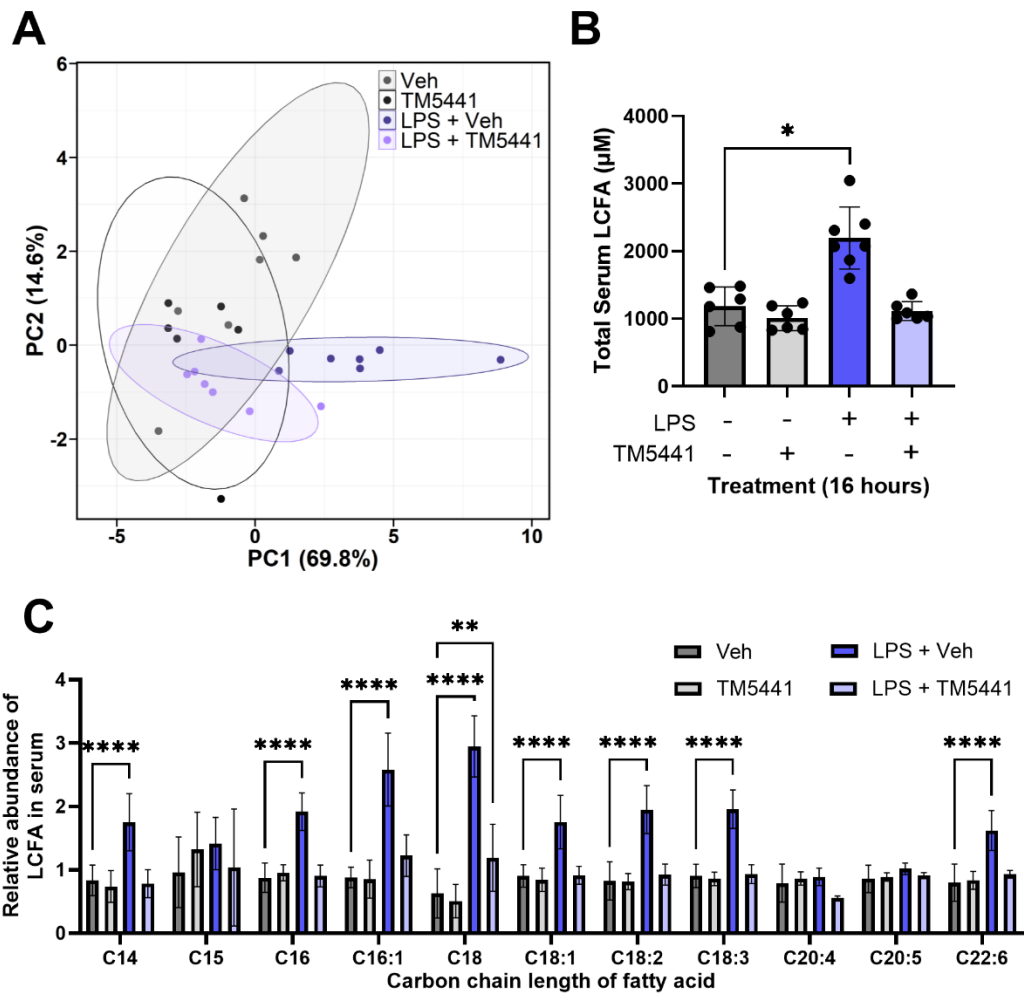


**Figure 5.34, TM5441 prevented the LPS-induced increase in serum LCFAs at 16 hours.**

WT mice pre-treated with 10 mg/kg TM5441 via oral gavage 1 hour prior to being injected with 0.5 mg/kg LPS via I.P. Mice were sacrificed 16 hours after final LPS I.P. was administered. Serum was separated from whole blood and LCFA content was analysed using LC-MS. **A)** PCA plot of serum LCFA abundance from vehicle control, TM5441 only, LPS + vehicle and LPS + TM5441 treated mice. **B)** Total serum LCFA was calculated by adding the concentration of each individual LCFA measured. **C)** Relative abundance of each LCFA measured in the serum normalised to a control mouse. Mean and standard deviation was calculated and shown on each graph (n = 7). For B, a Kruskal-Wallis test with a Dunn's correction for multiple comparisons was performed, comparing each group against the control group. For C, a 2way ANOVA with a Dunnett's correction for multiple comparisons was performed comparing each group against the control group for each individual LCFA. Significant differences are marked using asterisks (\* = p < 0.05, \*\* = P < 0.01, \*\*\* = p < 0.001 and \*\*\*\* = p < 0.0001).

Blood glucose levels were still significantly reduced in both LPS treatment groups (Figure 5.35). This provides evidence that PAI-1 inhibition using TM5441 did not affect the reduction in blood glucose levels in response to LPS, further supporting the idea that PAI-1 is not responsible for regulating blood glucose levels.

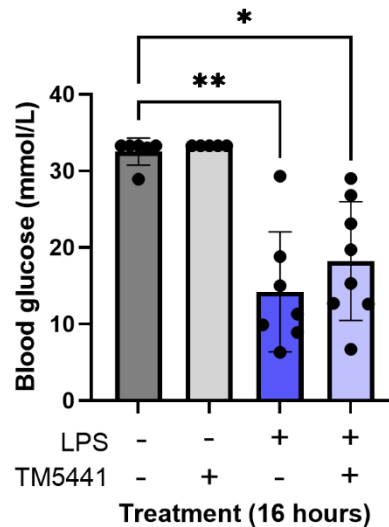


**Figure 5.35, There were no significant differences in blood glucose levels in TM5441 treated mice compared to LPS alone at 16 hours.**

WT mice pre-treated with 10 mg/kg TM5441 via oral gavage 1 hour prior to being injected with 0.5 mg/kg LPS via I.P. Mice were sacrificed 16 hours after final LPS I.P. was administered. Glucose levels within the blood were measured using a blood glucose monitor and test-strips. Mean and standard deviation was calculated and shown on the graph (n = 7). A Kruskal-Wallis test with a Dunn's correction for multiple comparisons was performed, comparing each group against the control group, and significant differences are marked using asterisks (\* =  $p < 0.05$ , \*\* =  $P < 0.01$ , \*\*\* =  $p < 0.001$  and \*\*\*\* =  $p < 0.0001$ ).

Both groups of mice treated with LPS still lost a significant amount of bodyweight by 16 hours compared to their starting weight (Figure 5.36). This means that TM5441 had no effect on LPS-induced weight loss within this mouse model. This could potentially be due to the mice still feeling unwell and not wanting to eat, however food intake would have to be monitored to confirm this.

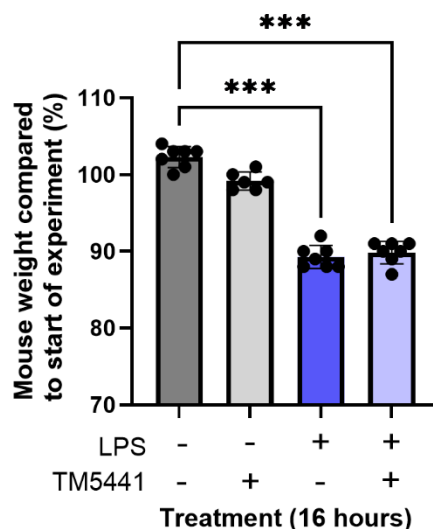


**Figure 5.36, Weight loss was similar in LPS treated mice and mice treated with both TM5441 and LPS at 16 hours.**

WT mice pre-treated with 10 mg/kg TM5441 via oral gavage 1 hour prior to being injected with 0.5 mg/kg LPS via I.P. Mice were sacrificed 16 hours after final LPS I.P. was administered. Mice were weighed at the start of the experiment and again at the end. Percentage change of weight was calculated by comparing the difference between these two weights. Mean and standard deviation was calculated and shown on the graph (n = 7). A Kruskal-Wallis test with a Dunn's correction for multiple comparisons was performed, comparing each timepoint against the control group, and significant differences are marked using asterisks (\* = p < 0.05, \*\* = P < 0.01, \*\*\* = p < 0.001 and \*\*\*\* = p < 0.0001).

Finally, the effect of TM5441 pre-treatment on immune cell populations in response to LPS was investigated. First, the impact on HSC expansion was assessed. Bone marrow was extracted from femurs and tibias by centrifugation and stained with antibodies for HSPC markers. The same gating strategy used to identify LSKs, MPPs and HSCs as shown in chapter 1 (Figure 3.1). As expected, the population of LSKs, MPPs and HSC per 100,000 bone marrow cells all significantly increased in response to LPS stimulation after 16 hours (Figure 5.37). However, interestingly, the combination treatment groups where mice were pre-treated with TM5441 prior to LPS injection did not have the same increase in HSC count per 100,000 bone marrow cells. This provides evidence that reducing the availability of circulating fatty acids may impact the ability for HSCs to expand. However, further investigation would be needed to prove that TM5441 treatment was not directly affecting HSCs themselves. Despite the reduced HSC count, LSK and MPP counts per 100,000 bone marrow cells were both still significantly increased in the combination treatment group. This would indicate that TM5441 itself or the reduced availability of LCFAs impacted only HSCs within the bone marrow.

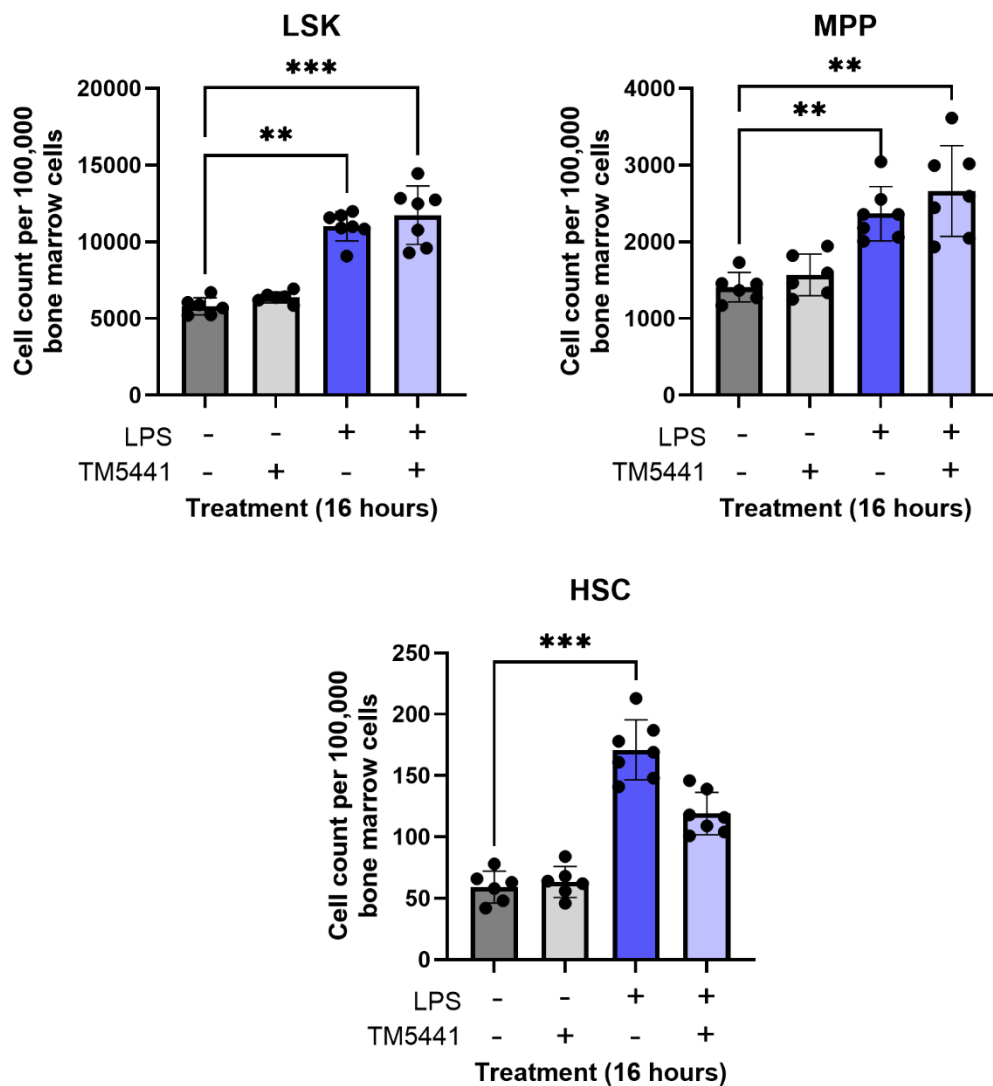


**Figure 5.37, TM5441 partially prevents the LPS induced increase in the proportion of HSPCs in the bone marrow.**

WT mice pre-treated with 10 mg/kg TM5441 via oral gavage 1 hour prior to being injected with 0.5 mg/kg LPS via I.P. Mice were sacrificed 16 hours after final LPS I.P. was administered. Isolated bone marrow cells were stained with an antibody panel using markers for LSK, MPP and HSC populations. Number of LSKs, MPPs and HSCs per 100,000 BM cells were recorded in control and LPS treated mice with and without TM5441 (n = 7). Means and standard deviations were calculated and shown on each graph. A Kruskal-Wallis test with a Dunn's correction for multiple comparisons was performed, comparing each timepoint against the control group, and significant differences are marked using asterisks (\* = p < 0.05, \*\* = P < 0.01, \*\*\* = p < 0.001 and \*\*\*\* = p < 0.0001).

Whilst HSC expansion is a hallmark of the immune response to acute infection, the ability of the HSC to take up LCFAs is also important. Therefore, it was investigated if TM5441 affected HSCs' ability to take up LCFAs. Isolated bone marrow was incubated with C16-tagged BODIPY (palmitic acid) before being washed and stained with the same HSC antibody panel. The same gating strategy as was used to identify the HSC population and a histogram of BODIPY fluorescent intensity revealed a

distinct difference in C16 uptake between control and LPS treated mice, indicating that LPS treated HSCs had increased LCFA uptake (Figure 5.38A). Due to washing off any excess BODIPY stain, any remaining fluorescence indicates C16 taken up directly into the cell. The MFI of BODIPY of the HSC population was measured for each sample (Figure 5.38B). Results demonstrate a significant increase in palmitic acid uptake by HSCs in response to LPS, in both the LPS only and combination treatment groups. This suggests that HSCs have an increased reliance and need for LCFAs during expansion in response to LPS. Interestingly, HSCs from mice treated with both TM5441 and LPS did not take up as much palmitic acid as the LPS only treatment. This may indicate that TM5441 treatment may affect HSCs themselves. Further investigation would be needed to assess if TM5441 treatment directly affects HSCs themselves and that reduction in HSC expansion is not just due to the reduction of LCFA availability to fuel HSCs.

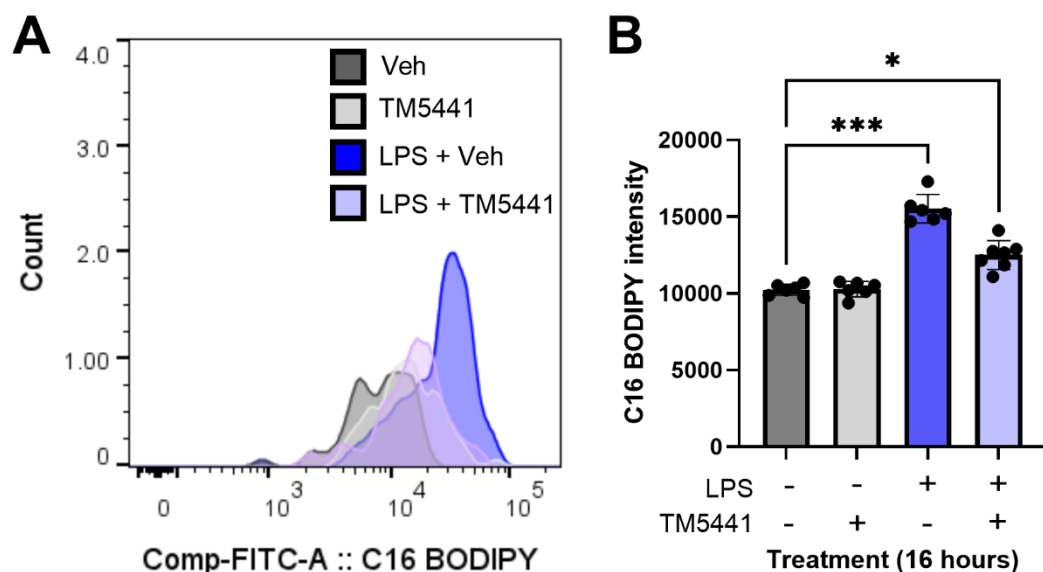


**Figure 5.38, LPS increases HSC palmitic acid uptake in HSCs with and without TM5441.**

WT mice pre-treated with 10 mg/kg TM5441 via oral gavage 1 hour prior to being injected with 0.5 mg/kg LPS via I.P. Mice were sacrificed 16 hours after final LPS I.P. was administered. **A)** Representative flow cytometry histogram of HSC C16 BODIPY uptake in control and LPS treated mice with and without TM5441. **B)** Median fluorescent intensity of BODIPY in HSCs in control and LPS treated mice with and without TM5441 (n = 7). Mean and standard deviation was calculated and shown on the graph. A Kruskal-Wallis test with a Dunn's correction for multiple comparisons was performed, comparing each timepoint against the control group, and significant differences are marked using asterisks (\* = p < 0.05, \*\* = P < 0.01, \*\*\* = p < 0.001 and \*\*\*\* = p < 0.0001).

To investigate the impact of reduced HSC expansion on immune cell populations within the peripheral blood as well as mature blood cell production in the bone marrow, lysed peripheral blood and isolated bone marrow was stained with antibodies to identify monocytes (CD11b+, Ly6G-), neutrophils, CD11b+, Ly6G+), T cells (CD4+ or CD8+) and B cells (CD19+). The gating strategy is shown in Figure 5.39 using peripheral blood samples, but the same gating strategy was used to analyse bone marrow as well.

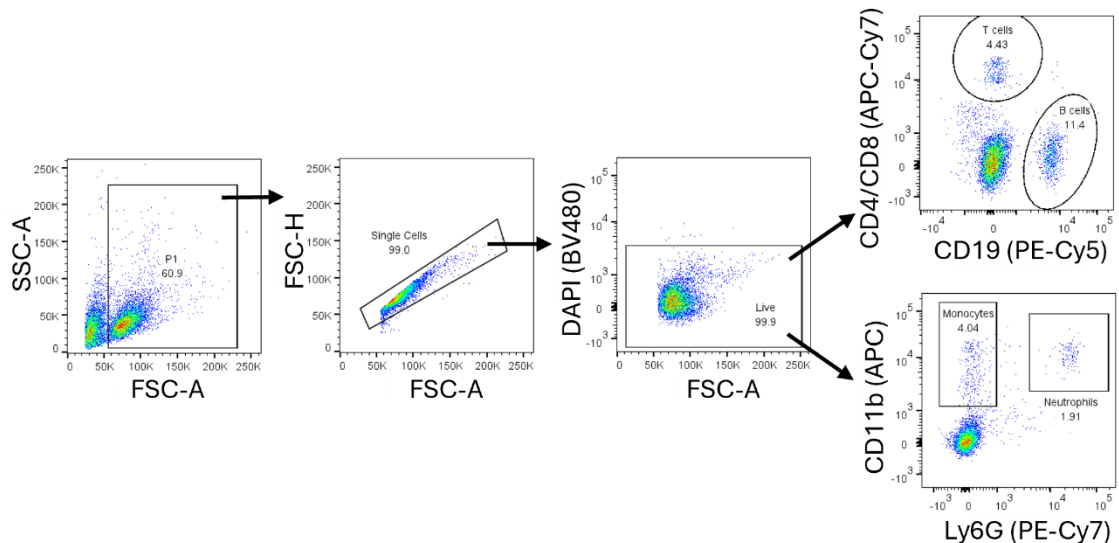


**Figure 5.39, Gating strategy for mature immune cell populations in the peripheral blood and bone marrow.**

Flow cytometry gating strategy for mature immune cells in the bone marrow and peripheral blood monocular cells in the blood.

Cell counts were calculated based on 100,000 bone marrow cells collected. The number of monocytes, neutrophils and T cells per 100,000 bone marrow cells all significantly decreased in response to LPS, regardless of the addition of TM5441 (Figure 5.40). The number of B cells did not significantly change across all 4 groups. This result indicates that at the 16-hour timepoint, the reduction of HSC expansion did not affect mature cell populations within the bone marrow.

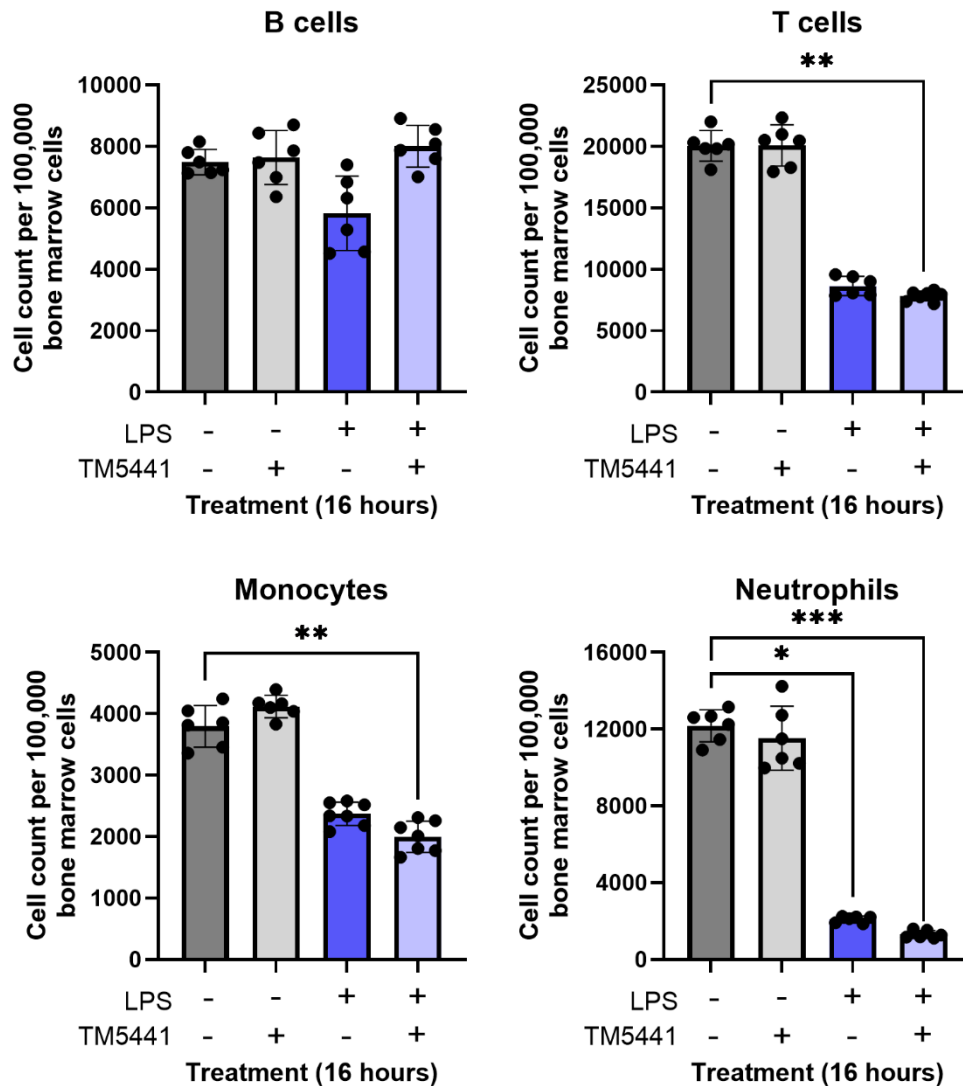


**Figure 5.40, Bone marrow mature immune cells in response to TM5441 and LPS treatment at 16 hours.**

WT mice pre-treated with 10 mg/kg TM5441 via oral gavage 1 hour prior to being injected with 0.5 mg/kg LPS via I.P. Mice were sacrificed 16 hours after final LPS I.P. was administered. Isolated bone marrow cells were stained with an antibody panel using markers for monocytes (CD11b+, Ly6G-), neutrophils, CD11b+, Ly6G+), T cells (CD4+ or CD8+) and B cells (CD19+). Mean and standard deviation was calculated and shown on each graph (n = 7). A Kruskal-Wallis test with a Dunn's correction for multiple comparisons was performed, comparing each group against the control group, and significant differences are marked using asterisks (\* =  $p < 0.05$ , \*\* =  $P < 0.01$ , \*\*\* =  $p < 0.001$  and \*\*\*\* =  $p < 0.0001$ ).

Peripheral blood collected at endpoint was analysed via flow cytometry to assess the number of circulating mature blood cell populations. Results shown are relative to the total number of nucleated blood cells collected over 30 seconds to ensure that any red blood cells that were not successfully lysed did not affect the nucleated cell number and skew results. Results show that 16 hours after LPS administration there was a reduction in B and T cells (Figure 5.41). This supports the wider literature that

B and T cell populations in the peripheral blood decrease in response to LPS (598). The addition of TM5441 did not alter this, and both populations were still significantly decreased in the combination treatment group. Mice treated with LPS had a significant increase in neutrophils within peripheral blood, with a mean neutrophil count of 338 in the LPS only treatment group compared to 102 in the control. However, this increase in peripheral blood neutrophil count was visibly lower in the combination treatment group, with a mean of 254 compared to 106 in the TM5441 only treatment group. LPS had no impact on the population of monocytes. Results indicate that inhibiting PAI-1 using TM5441 may have affected LPS-induced changes to peripheral blood neutrophil population, without affecting B cells, T cells and monocytes. Therefore, PAI-1 could play an important role in neutrophils' response to LPS. Despite this, further experiments would be needed to properly explore PAI-1's role in neutrophil regulation in response to LPS.

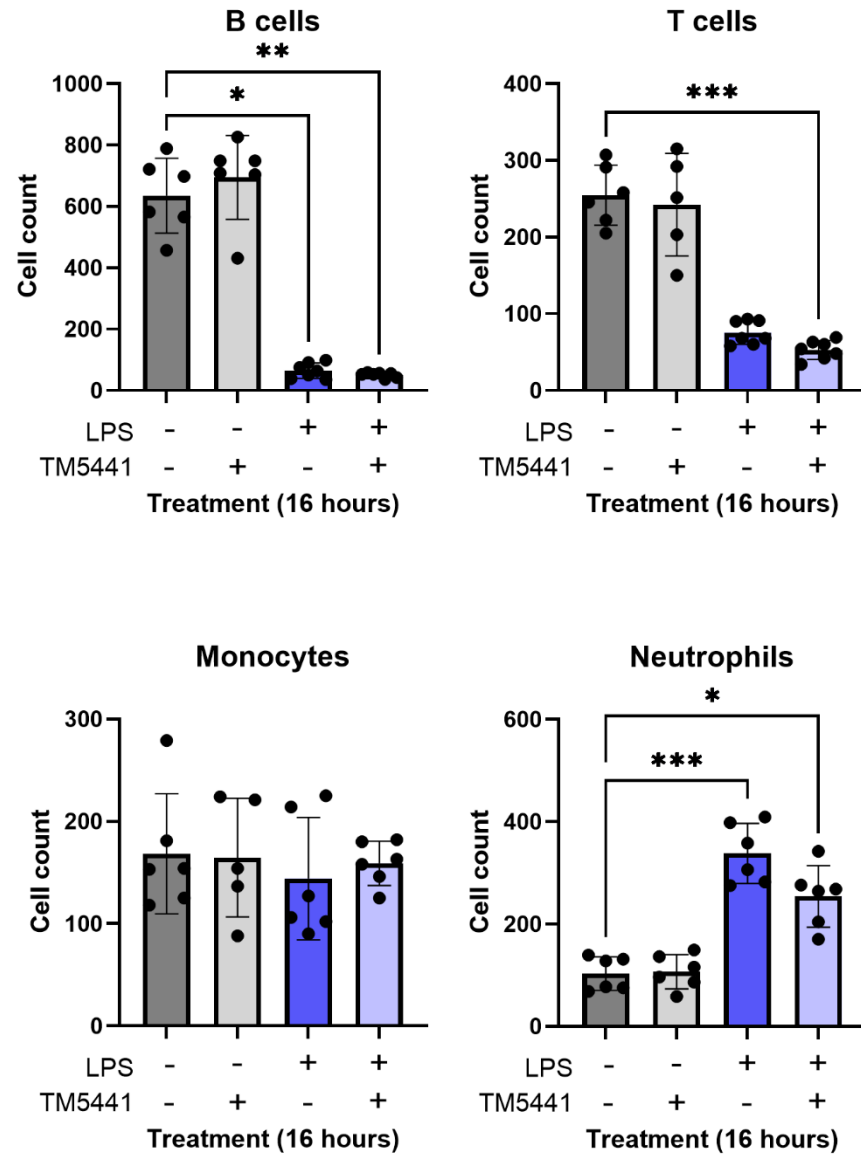


**Figure 5.41, Peripheral blood mature immune cells in response to TM5441 and LPS treatment at 16 hours.**

WT mice pre-treated with 10 mg/kg TM5441 via oral gavage 1 hour prior to being injected with 0.5 mg/kg LPS via I.P. Mice were sacrificed 16 hours after final LPS I.P. was administered. Peripheral blood was stained with an antibody panel using markers for monocytes (CD11b+, Ly6G-), neutrophils, (CD11b+, Ly6G+), T cells (CD4+ or CD8+) and B cells (CD19+). Mean and standard deviation was calculated and shown on each graph (n = 7). A Kruskal-Wallis test with a Dunn's correction for multiple comparisons was performed, comparing each group against the control group, and significant differences are marked using asterisks (\* = p < 0.05, \*\* = P < 0.01, \*\*\* = p < 0.001 and \*\*\*\* = p < 0.0001).

Taken together, these results demonstrate that PAI-1 inhibition using TM5441 does not affect LPS-induced changes to mature bone marrow and peripheral blood mononuclear cells. The exception to this is that TM5441 decreased the number of neutrophils within the peripheral blood. This indicates that PAI-1 may play an important role in the neutrophil response to infection.

## 5.7 Summary

In the third chapter of this thesis, the data presented demonstrates that pre-treating mice with the PAI-1 inhibitor TM5441, but not Tiplaxtinin, prevented the LPS-induced downregulation of liver fatty acid metabolism associated gene expression at 6 hours. Treatment with TM5441 prior to LPS resulted in a reduction of serum PAI-1 compared to LPS alone, whereas Tiplaxtinin treatment had no effect of LPS induced PAI-1 serum levels at 6 hours. TM5441 also partially prevented the increase of circulating LCFAs in response to LPS, most likely as a result of the reversal of liver fatty acid downregulation. At 6 hours, TM5441 treatment ameliorated the LPS-induced increase in the proportion of neutrophils within the liver. TM5441 treatment alone may also affect the population of monocytes and macrophages within the liver at 6 hours. T5441 also partially prevented the increase of circulating LCFAs in response to LPS.

At 16 hours, this prevention of increased availability of circulating LCFAs corresponded with a reduction in bone marrow HSC expansion. Whilst C16 BODIPY uptake experiments demonstrated that HSCs treated with a combination of TM5441 and LPS still had an increased ability to take up LCFAs, it was lower than HSCs treated with LPS alone. This may indicate that TM5441 treatment may also affect the HSCs. Neutrophil count per 100,000 bone marrow cells still significantly decreased in the combination treatment group. However, there was no longer a significant increase in neutrophils found in the peripheral blood of mice treated with both TM5441 and LPS compared to LPS treatment alone. This provides evidence that PAI-1 may play a role in the neutrophil immune response.

Taken together, the data presented provides evidence for the role of PAI-1 in the downregulation of liver fatty acid uptake and metabolism, leading to the increased availability of circulating fatty acids in response to LPS. Inhibiting PAI-1 using TM5441 prevented this increase in circulating LCFAs and resulted in a reduction in HSC expansion in response to LPS.

## 6 Platelets play an important role in the LPS-induced PAI-1 response

### 6.1 Introduction

Whilst many cell types are able to synthesise PAI-1, including macrophages, adipocytes, liver cells, fibroblasts and megakaryocytes, it is primarily stored in platelets (576). It is estimated that up to 90% of PAI-1 is stored in platelets inside  $\alpha$ -granules (599, 600). These  $\alpha$ -granules also store its cofactor vitronectin (601, 602). Platelets are also able to synthesise high levels of PAI-1 (603). Studies have suggested that only up to 5% of PAI-1 stored with platelets is stored in its active form (600). Thus, it remains debated if platelets are able to release large amounts of active PAI-1 or not. However, Huebner et al., 2018 demonstrated that treating platelets with thrombin triggers them to rapidly release active PAI-1, this prevents the breakdown of fibrin clots through  $\alpha$ -degranulation (599).

It is unclear if platelets can be directly activated by LPS itself. Whilst platelets express the LPS receptor TLR4, they do not express the coreceptor CD14, which is required for LPS-induced TLR4 endocytosis (604). TLR4 needs CD14 in order to recognise LPS (605). However, it has been shown that platelets can absorb CD14 from the surrounding plasma to aid LPS/TLR4 signalling (606).

The ability for platelets to respond to LPS is controversial. Therefore, this chapter aims to investigate if platelets play an important role in regulating the availability of circulating LCFAs in response to LPS infection. Experiments were performed to investigate if platelets were an important source of PAI-1 in the acute immune response to LPS. This was done through a mixture of *ex vivo* experiments, assessing if platelets can release PAI-1 in response to LPS stimulation, as well as the *in vivo* experiments to explore the impact of platelet depletion on the LPS induced immune response.

## 6.2 Platelets release PAI-1 when stimulated with LPS

First, it was investigated if platelets could release PAI-1 when stimulated with LPS. In order to choose an appropriate timepoint for this experiment, a small-scale pilot experiment was done to investigate how long it took for PAI-1 levels to increase in the serum of mice treated with LPS. For this, mice were injected with LPS for 0, 30, 60, 90 or 120 minutes, with 2 mice allocated to each group (Figure 6.1). The final endpoint chosen was 2 hours because the cytokine array presented in chapter 2 demonstrated that serum PAI-1 increased in mice treated with LPS for 90 minutes.

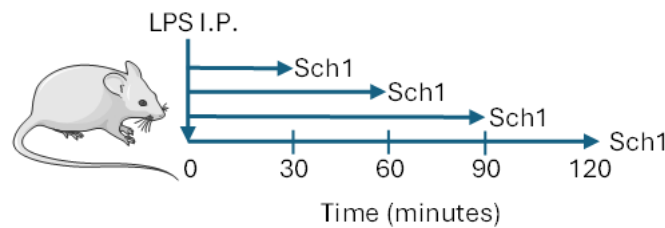


**Figure 6.1, Schematic of pilot experiment assessing speed of PAI-1 release in response to LPS.**

Experimental design of pilot study. WT mice treated with 0.5 mg/kg LPS via I.P. Mice were sacrificed 30, 60, 90 or 120 minutes after LPS was administered.

A PAI-1 ELISA was performed on serum collected from mice during sacrifice. Results show that PAI-1 levels start to increase at 60 minutes after LPS was administered, reaching levels around 5-times greater than in control mice (Figure 6.2). However, PAI-1 levels dramatically increased 90 minutes after LPS administration to more than 50 times to levels found in controls.

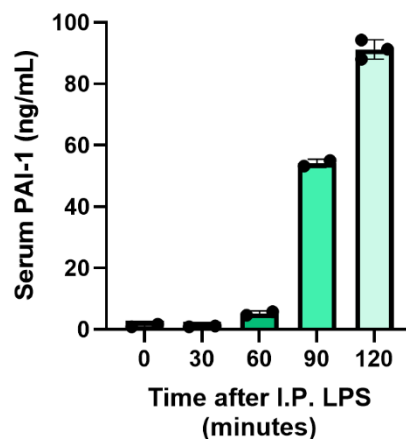


**Figure 6.2, Serum PAI-1 levels in response to LPS over a short time course.**

WT mice treated with 0.5 mg/kg LPS via I.P. Mice were sacrificed 30, 60, 90 or 120 minutes after LPS was administered. Serum was separated from whole blood and PAI-1 content was analysed using a PAI-1 ELISA. Mean and standard deviation was calculated and shown on the graph (n = 2). No statistical analysis was performed due to small sample sizes.

Using the previous results as a guideline for an appropriate timepoint, platelet rich plasma was isolated from whole blood collected from WT control mice. Cells were counted and seeded at a density of 500,000 cells. Platelets were treated with 100 ng/mL LPS for either 30 or 60 minutes before supernatant was collected from all samples including the controls, and analysed for PAI-1 content using an ELISA. Whilst control platelets released small amounts of PAI-1, platelets treated with LPS released significantly more PAI-1 (Figure 6.3). This result indicates that platelets can directly release PAI-1 in response to LPS.

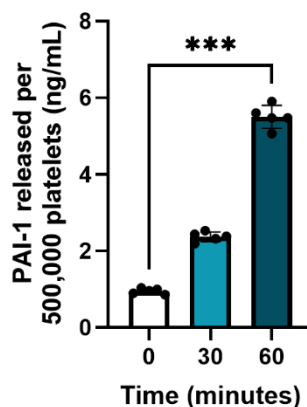


**Figure 6.3, Platelets isolated from WT mice release PAI-1 when stimulated with LPS.**

Whole blood was collected from WT healthy mice. Platelet rich plasma was isolated, and platelets were counted and seeded at a density of 500,000 cells. Platelets were then treated with 100 ng/mL LPS for 30 or 60 minutes before supernatant was collected and analysed for PAI-1 content using an ELISA. Mean and standard deviation was calculated and shown on the graph (n = 5). A Kruskal-Wallis test with a Dunn's correction for multiple comparisons was performed, comparing each group against the control group, and significant differences are marked using asterisks (\* = p < 0.05, \*\* = P < 0.01, \*\*\* = p < 0.001 and \*\*\*\* = p < 0.0001).

Taken together, this provides evidence that platelets can rapidly release PAI-1 in response to LPS. However, further work would be needed to investigate the mechanism behind this. Additionally, whilst this does demonstrate that *ex vivo* platelets can release PAI-1 in response to LPS, it does not necessarily mean that LPS directly causes PAI-1 release from platelets *in vivo*.

### 6.3 Depleting platelets partially reverses LPS-induced downregulation of liver fatty acid metabolism

As platelets are the main store of PAI-1 and they can release PAI-1 in response to LPS stimulation, the importance of platelets in the regulation of fatty acid availability in response to LPS was investigated. For this, platelets were depleted from WT mice using R300 anti-CD42 antibody, which has been proven to effectively deplete platelets from mice for at least 48 hours (607). This antibody was administered via the tail vein by Dr Charlotte Hellmich. Mice were left overnight to allow full depletion of platelets before 0.5 mg/kg LPS was administered to mice via I.P. After 6 hours, mice were sacrificed, and samples collected (Figure 6.4).

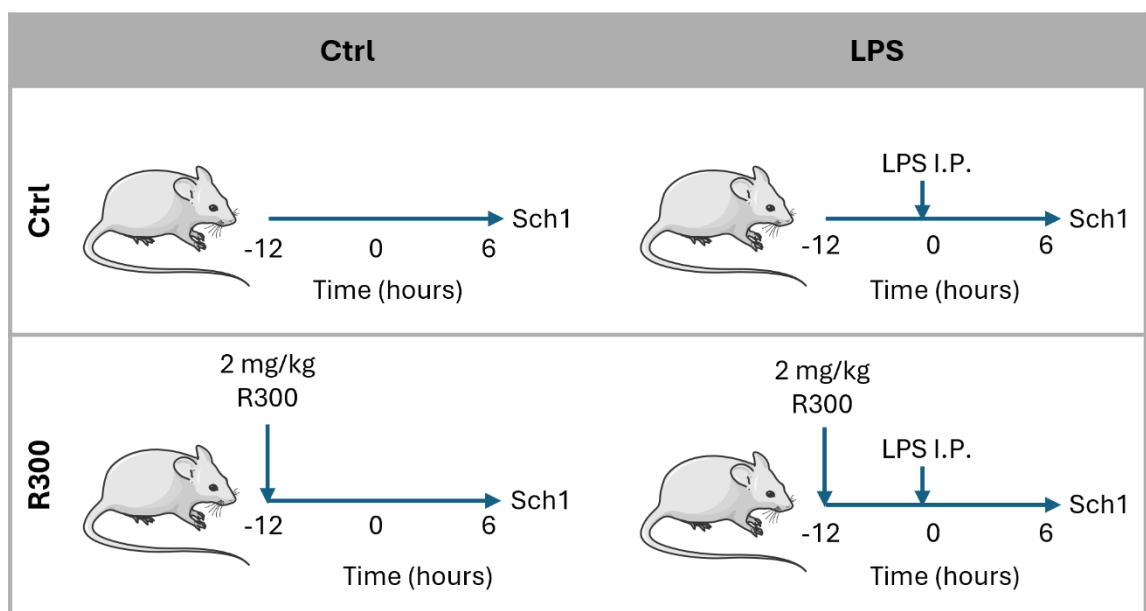


**Figure 6.4, Schematic of experimental design for platelet depletion prior to LPS infection.**

WT mice pre-treated with 2 mg/kg R300 anti-CD42 antibody via tail vein I.V. 12 hours prior to being injected with 0.5 mg/kg LPS via I.P. Mice were sacrificed 6 hours after final LPS I.P. was administered. Mice were split into 4 experimental groups: 1) control mice, 2) Platelet depleted control mice, 3) LPS only, and 4) Platelet depleted mice treated with LPS.

Firstly, peripheral blood was stained with CD41 as a marker for platelets and Ter119 to exclude red blood cells. Flow cytometry analysis was done to confirm platelet depletion using the gating strategy shown below (Figure 6.5). Sphero beads were used to confirm the presence of antibodies even in the platelet depleted groups. Sphero beads are blank, unstained beads ranging between 6.0 – 6.4  $\mu\text{m}$  in size. These were added as a positive control to confirm the presence of the antibodies in all groups, even in those with no platelets present.

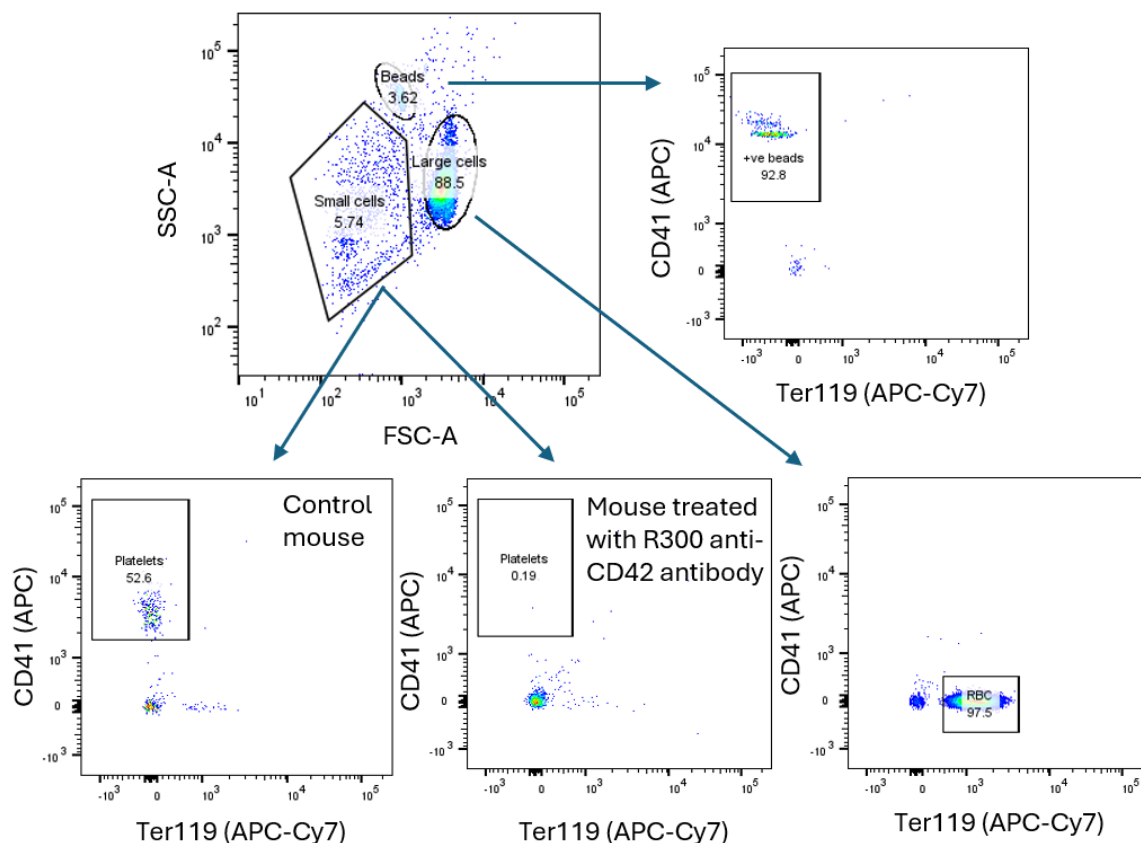


**Figure 6.5, Gating strategy used to quantify the number of platelets within the peripheral blood.**

WT mice pre-treated with 2 mg/kg R300 anti-CD42 antibody via tail vein I.V. 12 hours prior to being injected with 0.5 mg/kg LPS via I.P. Peripheral blood was collected in EDTA tubes to prevent clotting, diluted and Sphero control beads were added before the sample was stained for CD41 (platelets) and Ter119 (red blood cells). Samples were flowed for 60 seconds on medium flow rate (35  $\mu$ L/min). Platelets were identified by their small size, CD41+ and Ter119-.

Results confirmed that mice treated with R300 overnight had been successfully depleted of platelets within their peripheral blood (Figure 6.6). Additionally, there was no significant difference in the number of platelets per  $\mu$ L of blood in control and LPS treated mice. This indicates that LPS does not have an effect on the number of platelets in the peripheral blood at 6 hours.

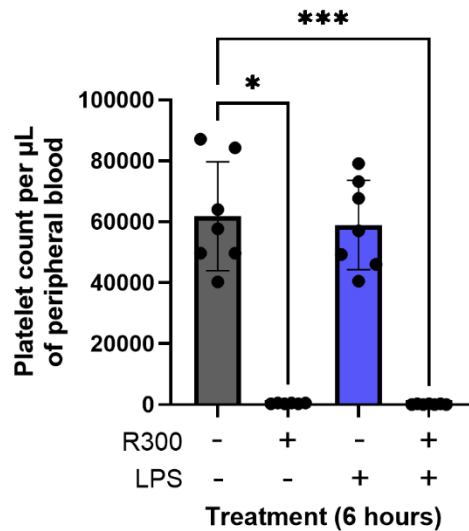


**Figure 6.6, R300 treatment successfully depleted platelets from the peripheral blood of mice.**

WT mice pre-treated with 2 mg/kg R300 anti-CD42 antibody via tail vein I.V. 12 hours prior to being injected with 0.5 mg/kg LPS via I.P. Peripheral blood was collected in EDTA tubes to prevent clotting, diluted and the sample was stained for CD41 (platelets) and Ter119 (red blood cells). Samples were flowed for 60 seconds on medium flow rate (35  $\mu\text{L}/\text{min}$ ). CD41+ Ter119- cells were identified as platelets, and the number of platelets per  $\mu\text{L}$  of blood was calculated based on flow rate and platelet count. Mean and standard deviation was calculated and shown on the graph (n = 7). A Kruskal-Wallis test with a Dunn's correction for multiple comparisons was performed, comparing each group against the control group, and significant differences are marked using asterisks (\* = p < 0.05, \*\* = P < 0.01, \*\*\* = p < 0.001 and \*\*\*\* = p < 0.0001).

Next, liver gene expression was assessed. The LPS-induced downregulation of *Acadm*, *Acs11*, *Hmgcs2* and *Hmgcr* expression was partially attenuated in platelet depleted mice (Figure 6.7). This provides evidence that platelets play a role in the LPS-driven downregulation of liver fatty acid metabolism. Platelet depletion alone did not impact the expression of these genes. In line with previous results, *Ctp1a* expression remained unchanged across all treatment groups.

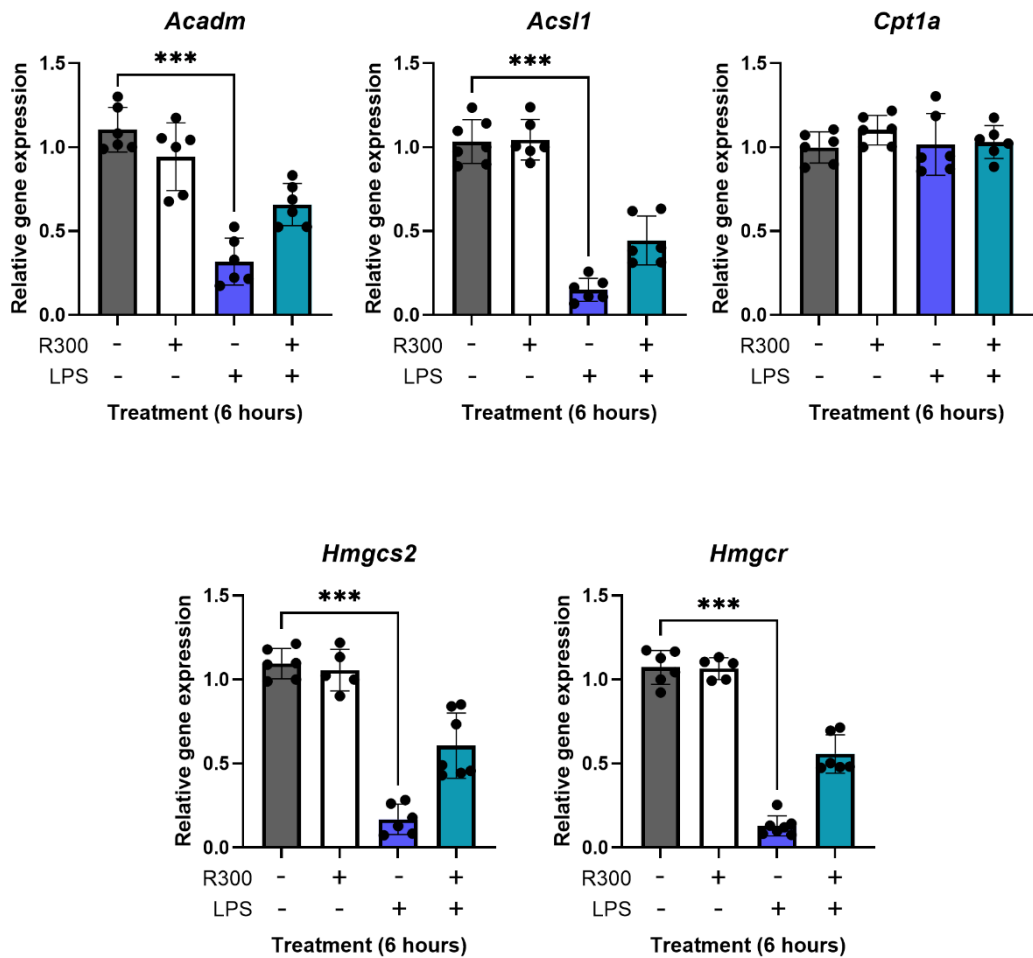


**Figure 6.7, Depleting platelets prior to LPS treatment partially prevented the downregulation of key liver fatty acid metabolism genes.**

WT mice pre-treated with 2 mg/kg R300 anti-CD42 antibody via tail vein I.V. 12 hours prior to being injected with 0.5 mg/kg LPS via I.P. Mice were sacrificed 6 hours after final LPS I.P. was administered. RNA was extracted from whole liver lysates and analysed using RT-qPCR. Gene expression was normalised against *Rps18*. Mean and standard deviation was calculated and shown on each graph (n = 7). A Kruskal-Wallis test with a Dunn's correction for multiple comparisons was performed, comparing each group against the control group, and significant differences are marked using asterisks (\* = p < 0.05, \*\* = P < 0.01, \*\*\* = p < 0.001 and \*\*\*\* = p < 0.0001).

Furthermore, the gene expression of the fatty acid transporters *Ldlr* and *Slc27a2* were also partially restored in the combination treatment group (Figure 6.8). This further demonstrates the importance of platelets in regulating the livers response to LPS. *Cd36* expression was unaffected in the platelet depleted mice.

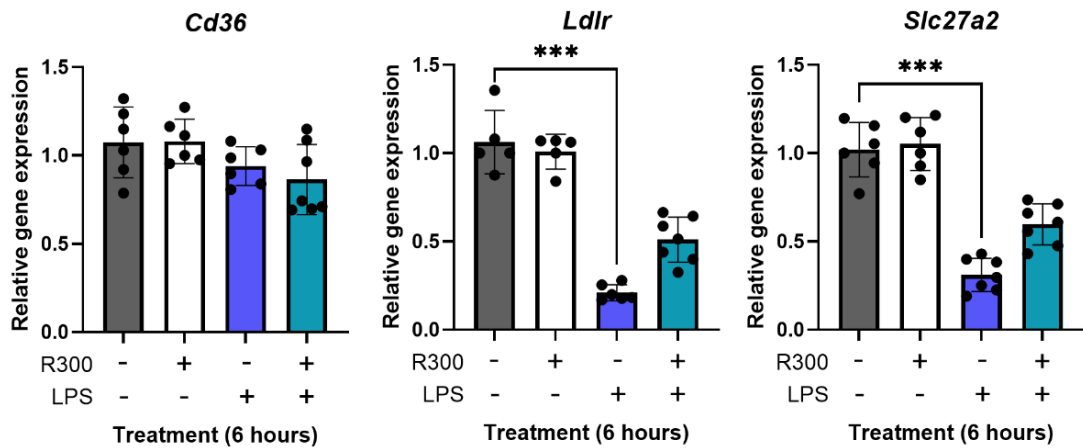


**Figure 6.8, Depleting platelets prior to LPS treatment partially prevented the downregulation of key liver LCFA transporter genes.**

WT mice pre-treated with 2 mg/kg R300 anti-CD42 antibody via tail vein I.V. 12 hours prior to being injected with 0.5 mg/kg LPS via I.P. Mice were sacrificed 6 hours after final LPS I.P. was administered. RNA was extracted from whole liver lysates and analysed using RT-qPCR. Gene expression was normalised against *Rps18*. Mean and standard deviation was calculated and shown on each graph ( $n = 7$ ). A Kruskal-Wallis test with a Dunn's correction for multiple comparisons was performed, comparing each group against the control group, and significant differences are marked using asterisks (\* =  $p < 0.05$ , \*\* =  $P < 0.01$ , \*\*\* =  $p < 0.001$  and \*\*\*\* =  $p < 0.0001$ ).

Due to the partial restoration of liver fatty acid metabolism gene expression in the platelet depleted mice treated with LPS, the levels of circulating LCFA in the serum was assessed using LC-MS. A PCA plot was used to visualise the overall relationships both between and within groups (Figure 6.9A). Control and platelet depleted mice clustered closely together. LPS treated mice clustered furthest away from the control group, indicating the biggest difference in LCFA content and composition compared to controls. Platelet depleted mice treated with LPS clustered between the control and LPS only treated groups, indicating that they may have an intermediary phenotype. Total serum LCFA concentrations confirmed this (Figure 6.9B). There was no difference in total LCFA content in the control and platelet depleted mice. LPS treated mice had a significant increase in serum LCFAs. However, platelet depleted mice treated with LPS did not have significantly increased serum total LCFAs compared to control or platelet depleted mice. The relative abundance of each LCFA measured also further confirmed this (Figure 6.9C). Whilst C14 (myristic acid), C16 (palmitic acid), C16.1 (palmitoleic acid), C18.2 (linoleic acid) and C22.6 (docosahexaenoic acid) were all still significantly increased in the serum of LPS-treated platelet depleted mice compared to control mice, they were all noticeably lower than levels found in the LPS only treated mice. Taken together, these results

implicate the importance of platelets in the regulation of LCFA availability in response to LPS.

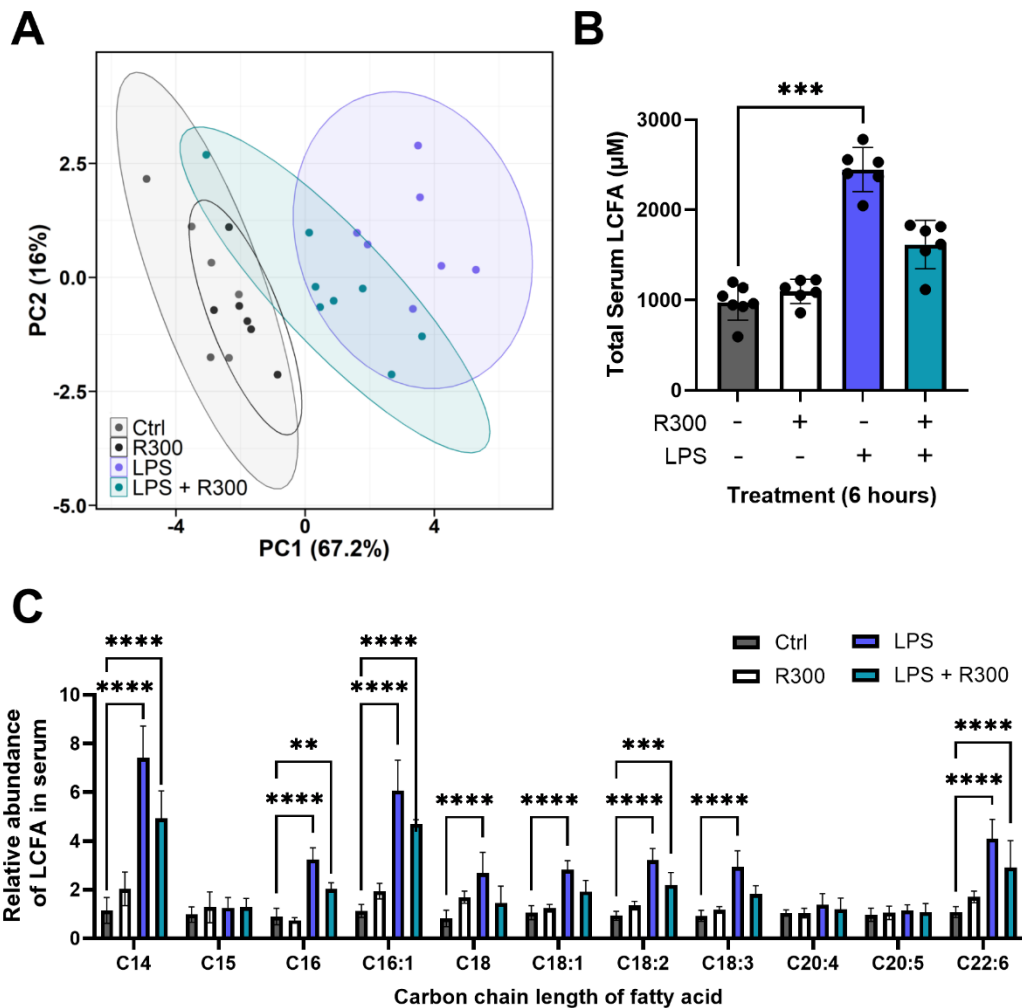


**Figure 6.9, Depleting platelets prior to LPS injection partially prevented the increase of serum LCFAs.**

WT mice pre-treated with 2 mg/kg R300 anti-CD42 antibody via tail vein I.V. 12 hours prior to being injected with 0.5 mg/kg LPS via I.P. Mice were sacrificed 6 hours after final LPS I.P. was administered. Serum was separated from whole blood and LCFA content was analysed using LC-MS. **A**) PCA plot of serum LCFA abundance from control, platelet depleted control mice (R300), LPS-treated mice and platelet depleted mice treated with LPS (LPS + R300). **B**) Total serum LCFA was calculated by adding the concentration of each individual LCFA measured. **C**) Relative abundance of each LCFA measured in the serum normalised to a control mouse. Mean and standard deviation was calculated and shown on each graph (n = 7). For B, a Kruskal-Wallis test with a Dunn's correction for multiple comparisons was performed, comparing each group against the control group. For C, a 2way ANOVA with a Dunnett's correction for multiple comparisons was performed comparing each group against the control group for each individual LCFA. Significant differences are marked using asterisks (\* = p < 0.05, \*\* = P < 0.01, \*\*\* = p < 0.001 and \*\*\*\* = p < 0.0001).

Next, PAI-1 content within the serum was calculated using an ELISA. Results showed that the levels of PAI-1 decreased by nearly 40 % in the platelet depleted group compared to the LPS only group, with a mean of 283 ng/mL, SD  $\pm$  50 in the LPS only group compared to 176 ng/mL, SD  $\pm$  50 in the platelet depleted LPS treated group (Figure 6.10). This provides further evidence that platelets are important in the release of PAI-1 in response to acute LPS infection. However, PAI-1 levels were still fairly high in the LPS-treated platelet depleted mice. This could explain why the LPS-induced phenotype was only partially and not fully reversed in platelet depleted LPS-treated mice.

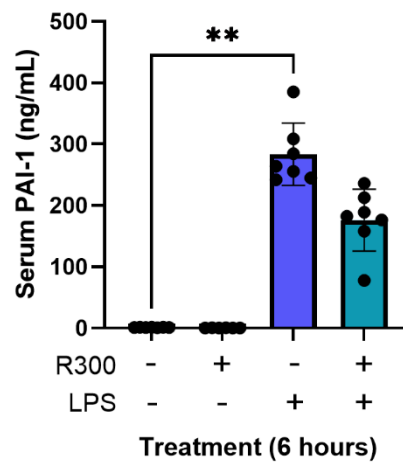


**Figure 6.10, Serum PAI-1 levels were reduced in platelet depleted mice treated with LPS.**

WT mice pre-treated with 2 mg/kg R300 anti-CD42 antibody via tail vein I.V. 12 hours prior to being injected with 0.5 mg/kg LPS via I.P. Mice were sacrificed 6 hours after final LPS I.P. was administered. Serum was separated from whole blood and PAI-1 content was analysed using a PAI-1 ELISA. Mean and standard deviation was calculated and shown on the graph (n = 7). A Kruskal-Wallis test with a Dunn's correction for multiple comparisons was performed, comparing each group against the control group, and significant differences are marked using asterisks (\* = p < 0.05, \*\* = P < 0.01, \*\*\* = p < 0.001 and \*\*\*\* = p < 0.0001).

Whilst platelets are the main source of stored PAI-1, multiple other tissues can synthesise PAI-1 in response to stimuli including inflammation (576). Both adipose tissue and liver tissue are large producers of PAI-1. Therefore, the expression of *Serpine1*, the gene encoding PAI-1, in the liver was checked. Results show that 6 hours after LPS infection, LPS-treated mice had more than a 100-fold increase in *Serpine1* gene expression, with a mean relative gene expression of 140.94, SD  $\pm$  51.62 compared to 2.34, SD  $\pm$  1.25 in the control group (Figure 6.11). However, in the platelet depleted mice relative gene expression was visibly higher, with a mean of 233.38, SD  $\pm$  51.89 compared to 0.95, SD  $\pm$  0.14 in the platelet depleted only mice.

This result may demonstrate that in the absence of platelets, other tissues compensate and produce more PAI-1 in order to create the appropriate immune response. However, further investigations would be needed to confirm this theory.

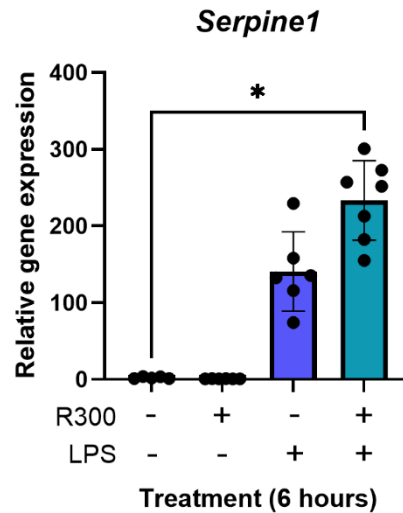


**Figure 6.11, Depleting platelets prior to LPS treatment increased the expression of the gene encoding PAI-1 in the liver.**

WT mice pre-treated with 2 mg/kg R300 anti-CD42 antibody via tail vein I.V. 12 hours prior to being injected with 0.5 mg/kg LPS via I.P. Mice were sacrificed 6 hours after final LPS I.P. was administered. RNA was extracted from whole liver lysates and analysed using RT-qPCR. Gene expression was normalised against *Rps18*. Mean and standard deviation was calculated and shown on the graph (n = 7). A Kruskal-Wallis test with a Dunn's correction for multiple comparisons was performed, comparing each group against the control group, and significant differences are marked using asterisks (\* = p < 0.05, \*\* = P < 0.01, \*\*\* = p < 0.001 and \*\*\*\* = p < 0.0001).

In addition, other markers were measured in this model to assess the impact of platelet depletion. Blood glucose levels were significantly decreased in both LPS treated groups (Figure 6.12). Although not significant, there was also a notable reduction in blood glucose levels in the platelet depleted control mice. This implicates platelets in the regulation of blood glucose levels.

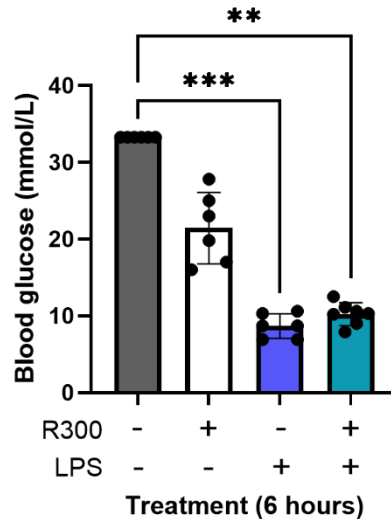


**Figure 6.12, Depleting platelets from mice prior to LPS treatment did not affect the LPS-induced downregulation of blood glucose levels.**

WT mice pre-treated with 2 mg/kg R300 anti-CD42 antibody via tail vein I.V. 12 hours prior to being injected with 0.5 mg/kg LPS via I.P. Mice were sacrificed 6 hours after final LPS I.P. was administered. Glucose levels within the blood were measured using a blood glucose monitor and test-strips. Mean and standard deviation was calculated and shown on the graph (n = 7). A Kruskal-Wallis test with a Dunn's correction for multiple comparisons was performed, comparing each group against the control group, and significant differences are marked using asterisks (\* = p < 0.05, \*\* = P < 0.01, \*\*\* = p < 0.001 and \*\*\*\* = p < 0.0001).

The weight of mice was measured prior to platelet depletion and again at experiment endpoint. Neither LPS nor platelet depletion significantly affected mouse weight, with no notable weight change across all 4 groups (Figure 6.13).

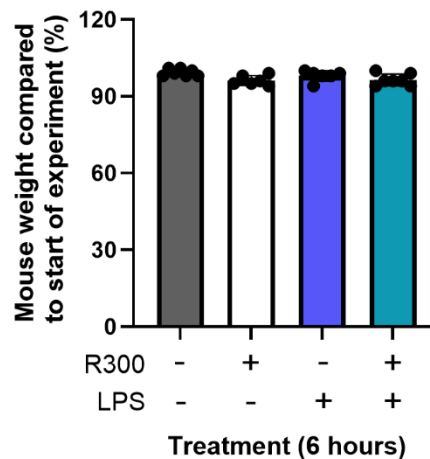


**Figure 6.13, Short-term platelet depletion did not affect mouse weight.**

WT mice pre-treated with 2 mg/kg R300 anti-CD42 antibody via tail vein I.V. 12 hours prior to being injected with 0.5 mg/kg LPS via I.P. Mice were weighed at the start of the experiment and again at the end. Percentage change of weight was calculated by comparing the difference between these two weights. Mean and standard deviation was calculated and shown on the graph (n = 7). A Kruskal-Wallis test with a Dunn's correction for multiple comparisons was performed, comparing each timepoint against the control group, and significant differences are marked using asterisks (\* = p < 0.05, \*\* = P < 0.01, \*\*\* = p < 0.001 and \*\*\*\* = p < 0.0001).

Platelet depletion also had no impact on inguinal and gonadal fat pad weight in proportion to total bodyweight (Figure 6.14).

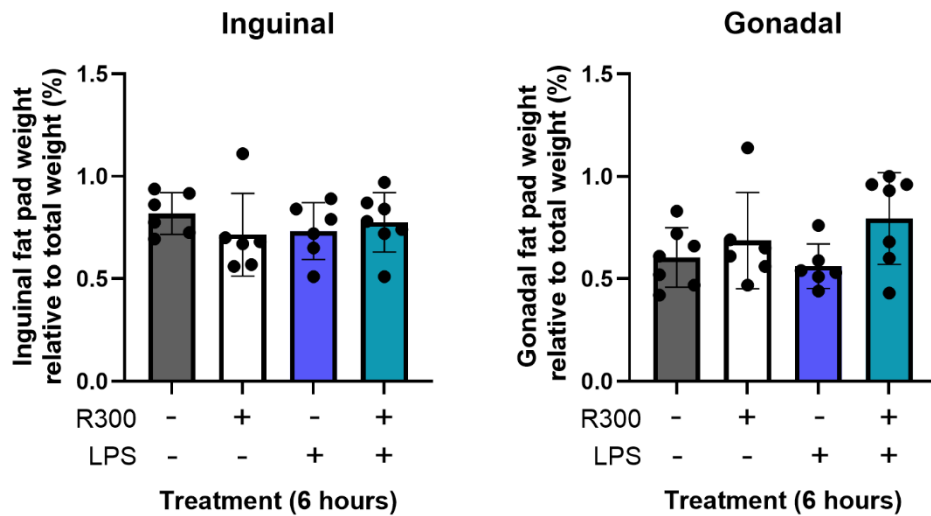


**Figure 6.14, Short-term platelet depletion did not significantly affect fat pad weight.**

WT mice pre-treated with 2 mg/kg R300 anti-CD42 antibody via tail vein I.V. 12 hours prior to being injected with 0.5 mg/kg LPS via I.P. Mice were sacrificed 6 hours after final LPS I.P. was administered. Inguinal and gonadal fat pads were dissected from mice and weighed. The percentage the weight of each fat pad was calculated against total body weight at time of sacrifice. Mean and standard deviation was calculated and shown on each graph (n = 7). A Kruskal-Wallis test with a Dunn's correction for multiple comparisons was performed, comparing each group against the control group, and significant differences are marked using asterisks (\* = p < 0.05, \*\* = P < 0.01, \*\*\* = p < 0.001 and \*\*\*\* = p < 0.0001).

Finally, the populations of liver immune cells were studied to assess the impact of platelet depletion on liver immune cells. Total immune cell number per 50,000 events significantly decreased in the liver in response to LPS treatment in both control and platelet depleted mice (Figure 6.15). Lymphoid cells only significantly decreased in number in LPS treated mice. This decrease was not seen in the platelet depleted mice treated with LPS. Similarly, there was a significant increase in neutrophils per 50,000 isolated liver cells in the LPS treated mice. Whilst there was an increase in neutrophils in both the platelet depleted controls and platelet depleted mice treated with LPS, neither reached statistical significance and this was visibly lower than in the LPS control treated mice. Therefore, platelet depletion may affect neutrophil populations within the liver, regardless of LPS. Myeloid cell number per 50,000 isolated liver cells did not significantly change across all 4 groups.

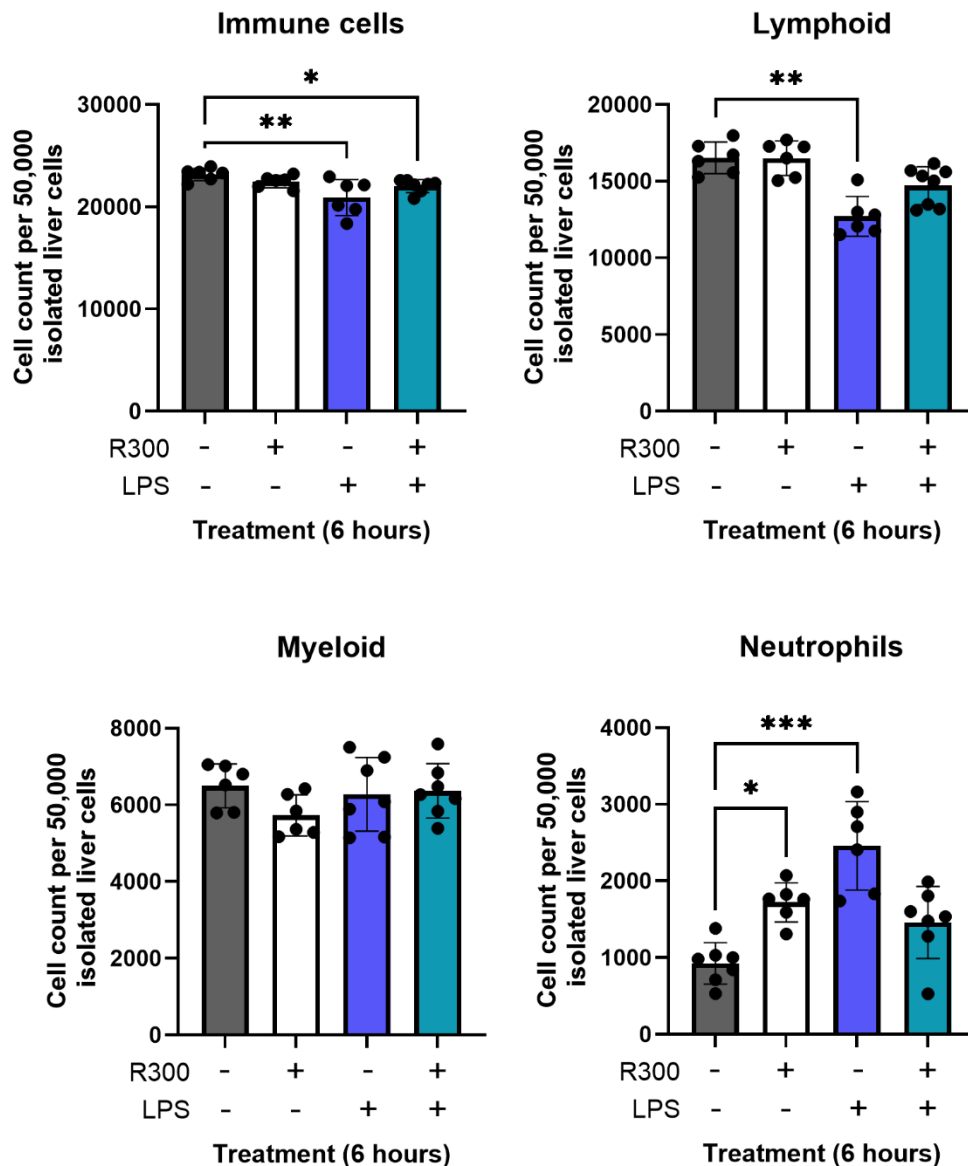


**Figure 6.15, Liver immune cell numbers in response to platelet depletion and LPS treatment.**

WT mice pre-treated with 2 mg/kg R300 anti-CD42 antibody via tail vein I.V. 12 hours prior to being injected with 0.5 mg/kg LPS via I.P. Mice were sacrificed 6 hours after final LPS I.P. was administered. Immune cells isolated from the liver were stained with an antibody panel using markers for lymphoid, myeloid and neutrophil populations. Mean and standard deviation was calculated and shown on each graph (n = 7). A Kruskal-Wallis test with a Dunn's correction for multiple comparisons was performed, comparing each group against the control group, and significant differences are marked using asterisks (\* = p < 0.05, \*\* = P < 0.01, \*\*\* = p < 0.001 and \*\*\*\* = p < 0.0001).

The number of monocytes per 50,000 isolated liver cells was also significantly decreased in platelet depleted and LPS treated mice (Figure 6.16). This indicates that both platelet depletion and LPS affects the population of monocytes within the liver. Within this monocyte population, there was a significant decrease in classical monocytes in both the control and platelet depleted mice treated with LPS. Classical

monocytes play a role in the inflammatory response and thus this indicates that inflammation may be lower in the platelet depleted control mice, however further investigation would be needed to support this idea. Platelet depletion alone had no impact on classical monocytes in the liver. Interestingly, there was a significant reduction in non-classical monocytes within platelet depleted control mice. Because non-classical monocytes are associated with anti-inflammatory responses, this could implicate a role for platelets within this. There was a visible but non-significant increase in non-classical monocytes in response to LPS which was not seen in platelet depleted mice treated with LPS. This further highlights a potential role for platelets in the non-classical monocyte population within the liver.

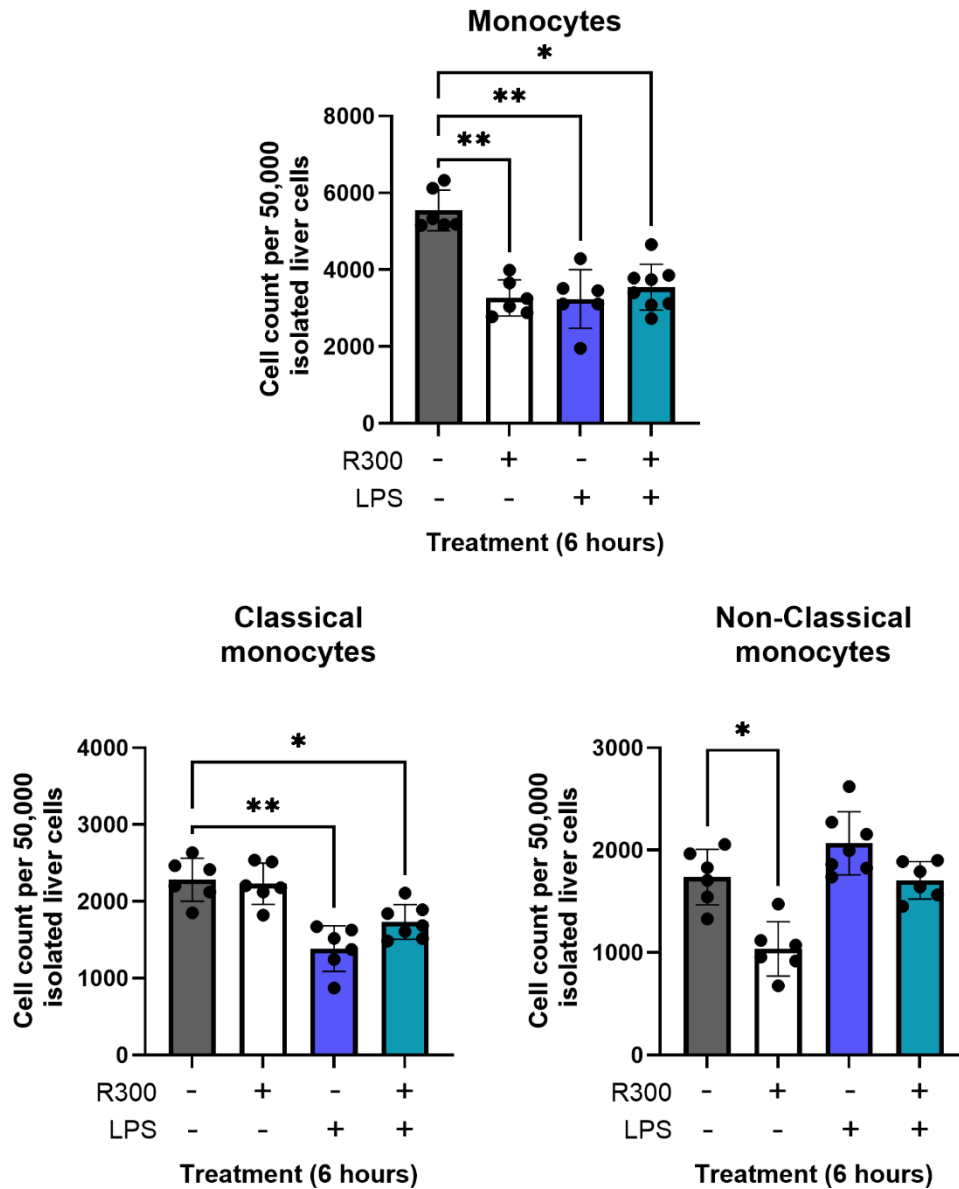


**Figure 6.16, Liver monocyte numbers in response to platelet depletion and LPS treatment.**

WT mice pre-treated with 2 mg/kg R300 anti-CD42 antibody via tail vein I.V. 12 hours prior to being injected with 0.5 mg/kg LPS via I.P. Mice were sacrificed 6 hours after final LPS I.P. was administered. Immune cells isolated from the liver were stained with an antibody panel using markers for classical and non-classical monocyte populations. Mean and standard deviation was calculated and shown on each graph (n = 7). A Kruskal-Wallis test with a Dunn's correction for multiple comparisons was performed, comparing each group against the control group, and significant differences are marked using asterisks (\* = p < 0.05, \*\* = P < 0.01, \*\*\* = p < 0.001 and \*\*\*\* = p < 0.0001).

The population of macrophages per 50,000 isolated liver cells was also significantly downregulated in both platelet depleted mice and mice treated with LPS (Figure 6.17). This could indicate that platelet depletion affects liver macrophage populations. In line with this, there was a reduction in the number of infiltrating macrophages in the liver in the platelet depleted mice, however this did not reach

statistical significance. The number of infiltrating macrophages per 50,000 isolated liver cells was even lower in LPS-treated mice. The reduction was similar in mice with platelet depletion treated with LPS. Finally, whilst LPS treatment alone did not affect the number of Kupffer cells, both groups with platelet depleted mice had a significant reduction in the number of Kupffer cells.

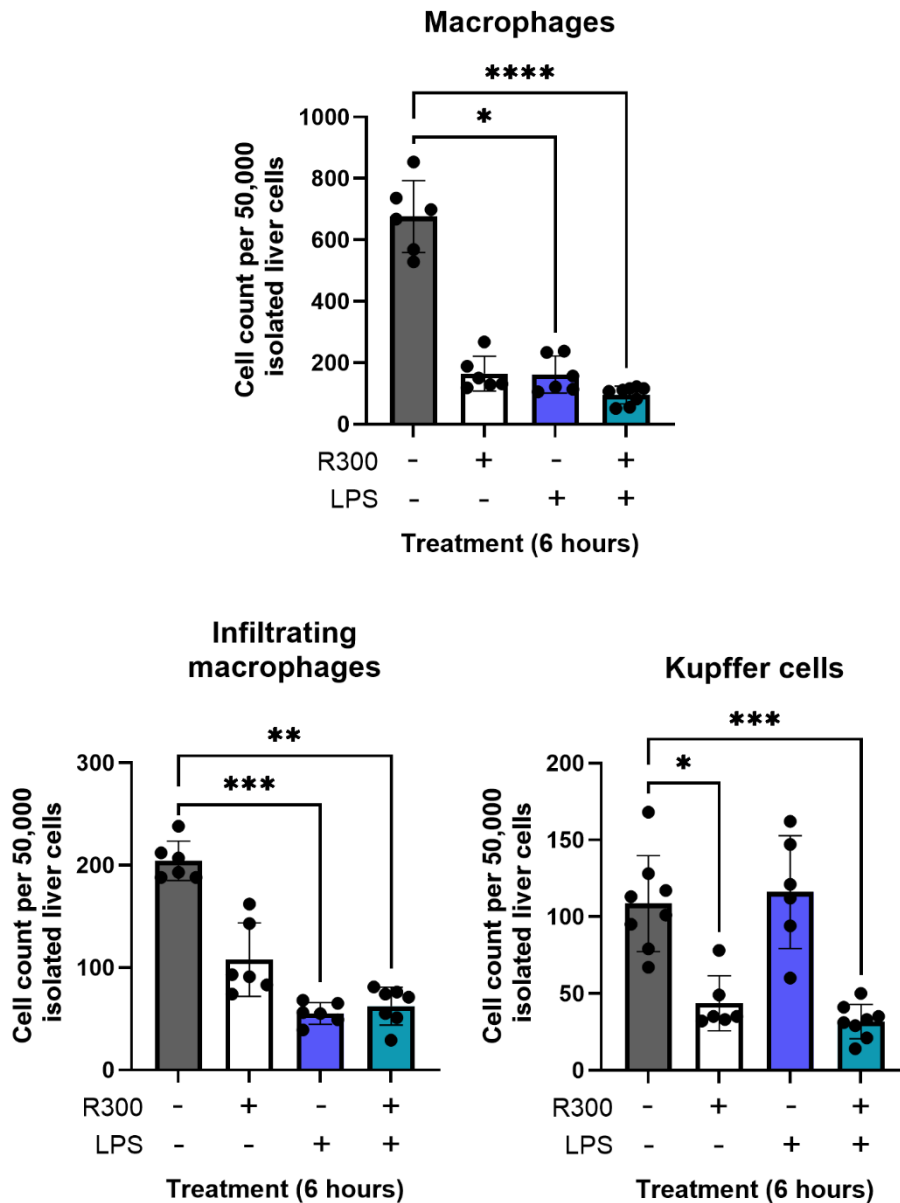


**Figure 6.17, Liver macrophage numbers in response to platelet depletion and LPS treatment.**

WT mice pre-treated with 2 mg/kg R300 anti-CD42 antibody via tail vein I.V. 12 hours prior to being injected with 0.5 mg/kg LPS via I.P. Mice were sacrificed 6 hours after final LPS I.P. was administered. Immune cells isolated from the liver were stained with an antibody panel using markers for macrophage populations. Mean and standard deviation was calculated and shown on each graph (n = 7). A Kruskal-Wallis test with a Dunn's correction for multiple comparisons was performed, comparing each group against the control group, and significant differences are marked using asterisks (\* = p < 0.05, \*\* = P < 0.01, \*\*\* = p < 0.001 and \*\*\*\* = p < 0.0001).

Taken together, this data supports the role of platelets in the initial immune response to LPS infection. Platelet depletion did not affect mouse body or fatpad weight. There were some changes to the population of liver immune cells associated with platelet depletion, such as a reduction in the populations of monocytes and macrophages. Whilst limited, other studies have demonstrated that neutrophil depletion actually resulted in an increase in the population of macrophages within the liver (608). This indicates that the reduction of macrophages within the liver in response to platelet depletion may be specific to platelet depletion and not just a response to cell depletion in general. Depleting platelets prior to LPS infection partially reduced the increase in neutrophil numbers within the liver.

Given the importance of platelets in regulating the availability of circulating LCFAs in response to LPS infection, it was investigated if the PAI-1 inhibitor TM5441 affected the number of platelets. There was no significant difference in platelet count in mice treated with TM5441 both with and without LPS compared to control mice (Figure 6.18). This result indicates that TM5441 targets PAI-1 itself without affecting platelet count.

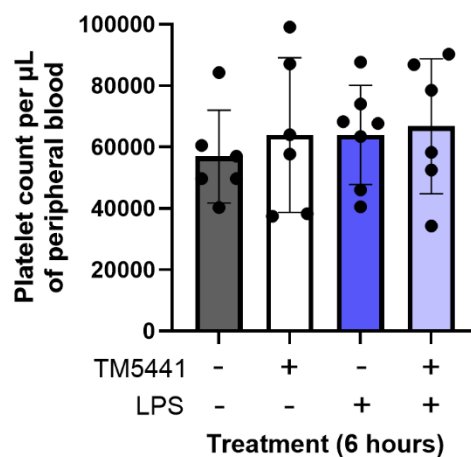


**Figure 6.18, TM5441 did not affect platelet number in the peripheral blood of mice.**

WT mice pre-treated with 10 mg/kg TM5441 via oral gavage 1 hour prior to being injected with 0.5 mg/kg LPS via I.P. Mice were sacrificed 6 hours after final LPS I.P. was administered. Peripheral blood was collected in EDTA tubes to prevent clotting, diluted and the sample was stained for CD41 (platelets) and Ter119 (red blood cells). Samples were flowed for 60 seconds on medium flow rate (35 µL/min). CD41+ Ter119- cells were identified as platelets, and the number of platelets per µL of blood was calculated based on flow rate and platelet count. Mean and standard deviation was calculated and shown on the graph (n = 7). A Kruskal-Wallis test with a Dunn's correction for multiple comparisons was performed, comparing each group against the control group, and significant differences are marked using asterisks (\* = p < 0.05, \*\* = P < 0.01, \*\*\* = p < 0.001 and \*\*\*\* = p < 0.0001).

## **6.4 Summary**

In summary, this chapter demonstrates the importance of platelets in the initial response to LPS infection. Platelets can release PAI-1 in response to LPS within 60 minutes of stimulation. Depleting platelets prior to LPS treatment resulted in a marked reduction in serum levels of PAI-1. This reduction of PAI-1 in platelet depleted mice was associated with a partial reversal of the downregulation of key liver fatty acid metabolism genes. Platelet depleted mice had a notable reduction in total levels of circulating LCFAs.

## 7 Discussion

### 7.1 General Discussion

Despite representing only a small minority of cells within the bone marrow, HSCs are responsible for indirectly producing over 500 billion blood cells every day through the tightly controlled process of haematopoiesis (609). However, in times of stress such as infection, a state of emergency haematopoiesis is triggered. During this, the demand for immune cells increases by nearly ten-fold (610). In order to cope with this demand, the population of HSCs expand (611). This allows for a rapid and robust innate immune response to occur, generating vast amounts of immune cells, in particular leukocytes over a short-time period (612). However, the switch from steady state to emergency haematopoiesis creates a substantial increase in metabolic demands. For example, during emergency haematopoiesis, HSCs increase mitochondrial oxidative phosphorylation to boost ATP production (613). FAO has been shown to be a crucial part of HSC expansion (614). Increased LCFA uptake into HSCs via CD36 is critical for enabling HSC activation and re-entry into the cell cycle. Therefore, to fuel HSC's need for fatty acids, especially LCFAs, the levels of circulating fatty acids increase in response to infection. Whilst this increase in circulating fatty acids has been widely demonstrated using multiple models of bacterial and viral infections (421, 533), the kinetics and mechanistic control of this increase remains unclear. By understanding the mechanisms underpinning a healthy immune response, findings can be applied to better understand if they become dysregulated in diseases such as ageing and cancer.

In this thesis, the data presented demonstrates that circulating LCFAs significantly increased by 6 hours after LPS was administered. This increase in LCFA levels was associated with the downregulation of liver fatty acid metabolism genes, and a reduction in hepatocyte LCFA uptake. PAI-1 was identified as one factor able to rapidly induce this downregulation of key genes involved in liver fatty acid metabolism, resulting in increased availability of circulating LCFAs. This increase in circulating LCFAs is associated with increased LCFA uptake into HSCs and their subsequent expansion. Additionally, this thesis identified the importance of platelets in this immune response.

## **7.2 Key findings**

### **7.2.1 Circulating LCFAs increase in response to LPS**

Data presented in this thesis provides evidence that within 6 hours of LPS administration, the levels of circulating LCFAs significantly increases. This increase has been previously well described. However, the kinetics behind the increase in LCFAs in response to infection were previously undefined and thus represent a novel finding of this thesis. Circulating levels of free fatty acids have been shown to rise dramatically during infection in both animal models and human studies (421, 533, 534, 544). This includes both gram positive and gram negative bacteria, viral, and parasitic infections. Infection associated alterations to serum lipid levels is thought to be proportional to infection severity. Clinically, serum levels of palmitic acid may negatively correlate with disease severity of certain viruses including H7N9 influenza (615) and COVID-19 (616). Mouse models using LPS as a bacterial infection mimic and *S. Typhimurium* also demonstrate similar findings, showing increased serum free fatty acids in response to infection (421). However, the majority of these publications, especially clinical studies, measured serum fatty acid levels once the innate immune response was already fully underway, often days after the initial infection occurred. Therefore, the kinetics of this increase was previously undetermined. This highlights the novelty of this finding, that within 6 hours of LPS treatment, LCFA levels significantly increased in the serum of mice. However, further work would be needed to establish the kinetics of this response in bacterial and viral infections.

### **7.2.2 LPS induces a downregulation of genes associated with liver fatty acid metabolism**

LPS treatment within mice induced a downregulation of key genes involved in liver fatty acid metabolism. The liver is a crucial organ involved in the regulation of circulating fatty acids, including LCFA availability. The liver takes up circulating fatty acids in proportion to their concentration within the blood (567, 568). In this study, bulk-RNA sequencing, supported by RT-qPCR analysis of gene expression from liver tissue, identified a significant downregulation of several metabolic pathways important in fatty acid metabolism in response to LPS. This included pathways associated with fatty acid synthesis and elongation. Further gene expression analysis

also identified the downregulation of several LCFA transporters in response to LPS. This downregulation of hepatic LCFA uptake and metabolism offers a potential explanation to why the levels of circulating LCFAs increased. For example, several metabolic disorders which affect the liver including diabetes and obesity increase the risk of MASLD (617). During MASLD, there is an excessive accumulation of lipids within the liver (618). This results in a reduction in hepatic fatty acid uptake, contributing to increased concentrations of circulating fatty acids in the blood, a hallmark of this condition (545). Whilst limited, some studies have demonstrated that infection can decrease FAO in several organs, including the heart and kidney (619), as well as tissues such as the diaphragm (620). Mice treated with a high dose (5 mg/kg) of LPS for 16 hours had a nearly 40% reduction in the FAO of LCFAs in the diaphragm muscle. This was associated with a significant downregulation of several key fatty acid metabolism genes including *Acsl1* and *Cd36* (620). Similarly, another study demonstrated that LPS treatment decreased renal FAO by 40% in mice, finding a similar downregulation of FAO associated gene expression within the kidney (619). Taken together, these studies provide evidence to support the findings of this thesis, that LPS can induce the downregulation of several key genes involved in liver fatty acid metabolism.

This thesis provides evidence that this downregulation of fatty acid metabolism associated gene expression within the liver is not a direct response to LPS itself. Treating hepatocytes *in vitro* with LPS had no effect on key fatty acid metabolism gene expression, palmitic acid uptake or fatty acid associated mitochondrial respiration. Instead, using serum models, it was determined that a factor released into the serum of these mice treated with LPS caused the downregulation of hepatic fatty acid metabolism associated gene expression. The two aforementioned studies used mouse models to study the effects of LPS on the kidney and diaphragm muscle, and thus did not determine if LPS itself was directly causing the reduction in FAO seen (619, 620). However, a study looking at the effect of LPS on adipose tissue also found that genes associated with adipose tissue triglyceride biosynthesis was downregulated in mice treated with LPS. Despite this, *in vitro* models of adipocyte cells lines treated with LPS did not show the same downregulation. Instead, the study found adipocytes treated with that TNF- $\alpha$ , IL-1 $\beta$  and IFN $\gamma$ , but not IL-6, induced the

same downregulation of triglyceride biosynthesis associated genes (544). These findings support the data presented in this thesis, that LPS does not directly induce the downregulation of liver fatty acid metabolism. Instead, the inflammation associated with the infection response is at least partly responsible.

### **7.2.3 PAI-1 regulates liver fatty acid metabolism and increases the availability of LCFAs**

This thesis provides evidence that PAI-1 levels significantly increase within 90 minutes of mice being injected with LPS. Previous studies have implicated a role for PAI-1 in the early immune response. For example, PAI-1 knockout mice had a reduced ability to clear *Haemophilus influenzae* and *Mycobacterium tuberculosis* infections compared to control mice (580, 581). Additionally, high PAI-1 levels have been widely observed in many COVID-19 patients, with PAI-1 levels being shown to independently predict disease severity and COVID-19 mortality rates (582). High levels of PAI-1 have also been observed in septic patients (621).

PAI-1 has been linked to several metabolic conditions, including obesity, cerebrovascular and cardiovascular disease. For example, PAI-1 has been shown to be significantly increased in obese individuals, with PAI-1 levels positively correlating with decreased sensitivity to insulin and increased visceral fat (622, 623). Furthermore, diabetic mice treated with a novel PAI-1 inhibitor called PAItrap3 had improved metabolic function and reduced triglyceride levels (624). Data collected as part of the Study of Women's Health Across the Nation, termed the SWAN study, showed that increased levels of blood PAI-1 was associated with increased risk of cardiovascular and metabolic complications (625). This was the case even when confounding factors including age and BMI were accounted for. Elevated PAI-1 has also been associated with increased risk of atherosclerosis (626). Furthermore, a sustained increase in blood PAI-1 levels has been observed during the acute phase of ischemic strokes in patients (627) and has been linked to other cerebrovascular conditions (628). The majority of conditions associated with increased levels of PAI-1 have also been associated with immune dysregulation, increased risk of infection and a weaker immune response. Obesity (432), diabetes (629), stroke (630), and cardiovascular disease (631) have all been associated not only with an increased risk of infection, but also with a worse recovery after an infection. Perhaps PAI-1 can

provide the link between the already altered lipid metabolism and the diminished infection response.

In some of these conditions, particularly those associated with vascular tissues, this increase in PAI-1 has been linked to impaired fibrinolytic activity. For example, obesity increases the risk of atherosclerosis. One major component of atherosclerotic plaques is fibrin. The elevated PAI-1 in obese individuals would prevent the breakdown of this fibrin, resulting in increased plaque formation and size. Similarly obesity, alongside atherosclerosis and diabetes, also massively increases the risk of stroke, which again is thought to be linked to fibrinolytic activity. However, whilst this is the main impact of elevated PAI-1 studied in these conditions, it does not mean this is the only effect PAI-1 has in these conditions. For example, many of these diseases majorly affect many metabolic pathways, including lipid metabolism. Thus, the role of PAI-1 within this requires greater investigation, including what causes this increase in circulating PAI-1.

Outside of infection, higher levels of PAI-1 have been associated with poor prognosis in breast cancer (632). In fact, several cancers have been shown to upregulate PAI-1 (633). Alongside this, many cancers including haematological cancers have adapted to use fatty acids as an energy source (634). Several mechanisms that control free fatty acid uptake and metabolism are altered in cancer cells to support their survival. In models of triple negative breast cancer, PAI-1 activated the ERK signalling cascade and promoted mitochondrial fragmentation (635). Pharmacological inhibition of PAI-1 using Tiplaxtinin prevented PAI-1 induced ERK activation and prevented cell migration. PAI-1 has also been shown to be elevated in patients with multiple myeloma (636). Reducing PAI-1 levels by silencing Stomatin-like protein 2 (known to be overexpressed in other cancers), prevented multiple myeloma cell proliferation (637). Thus, too much PAI-1 may be detrimental for patient outcomes in both infection and cancer.

Metabolically, other studies support this thesis' findings, that PAI-1 can alter hepatic fatty acid metabolism. For example, Levine et al., 2021 provided evidence that PAI-1 is a critical regulator of hepatic lipid metabolism, by directly regulating numerous genes associated with lipid homeostasis including PCSK9 and FGF21 (593).

Inhibition of PAI-1 using TM5614 in obese mice prevented obesity associated hyperlipidaemia, further supporting the role of PAI-1 in regulating fatty acid metabolism. Additionally, PAI-1 levels have been shown to be elevated in patients with MASLD, further providing a link between PAI-1 and liver fatty acid metabolism. Not only that, but studies have demonstrated that plasma PAI-1 levels are more strongly associated with PAI-1 expression in the liver than in adipose tissue, and this was further correlated with hepatic fat accumulation, referred to as hepatic steatosis (638). This same study also proposed that liver steatosis induced TNF dysregulation could be part of the signalling cascade leading to increased PAI-1 expression in the liver. Pharmacological and genetic inhibition of PAI-1 prevented obesity induced hepatic steatosis, however did not affect obesity associated hepatic inflammation and fibrosis (639). This further supports the specificity of PAI-1 in regulating hepatic fatty acid metabolism and not just hepatic inflammation in general.

#### **7.2.4 PAI-1 may work specifically to downregulate hepatocyte fatty acid metabolism without affecting glucose metabolism.**

The results presented in this thesis identify PAI-1's ability to induce the downregulation of hepatic fatty acid metabolism, including reduced LCFA uptake using both *in vivo* and *in vitro* models. *In vitro*, hepatocytes treated with PAI-1 had reduced fatty acid associated mitochondrial respiration under both normal and stressed conditions. Whilst the literature supporting this is limited, some studies have shown that PAI-1 can alter mitochondrial oxygen production under stress conditions. However, this effect was not seen under resting steady state conditions (640). Furthermore, PAI-1 knockout mice had reduced mitochondrial depolarisation and increased smooth muscle death when oxidative stress was induced by hydrogen peroxide (640). It should be noted that both of these studies used oxidative stress to model stroke pathology, and thus were not specifically investigating metabolism. However, results from studies such as these can provide crucial insights into a variety of other pathways and diseases linked to PAI-1. Furthermore, mouse models of obesity have demonstrated that PAI-1 has been directly linked to adipocyte inflammation and downregulation of genes involved in mitochondrial biogenesis and function (594).

Interestingly, in this thesis, in hepatocytes fuelled with glucose instead of palmitic acid, recombinant PAI-1 was unable to induce the same downregulation of mitochondrial respiration. This provides evidence that PAI-1 may specifically target hepatic fatty acid metabolism and not just metabolism in general. Wider literature can support these findings. In triple negative breast cancer cell lines, PAI-1 promoted glycolysis over oxidative phosphorylation, increasing extracellular acidification rate (ECAR) (635). Furthermore, inhibiting glycolysis in bone marrow derived macrophages reduced PAI-1 secretion by nearly 50% (641). Both of these studies provide a link between PAI-1 and reliance on glycolysis. In multiple myeloma, downregulating PAI-1 expression reduced myeloma cell glucose consumption, and subsequent lactate production (637), further highlighting this link that PAI-1 levels are associated with increased glucose consumption. This also highlights one of the limitations of this thesis. Whether or not PAI-1 downregulated hepatic fatty acid metabolism without affecting glycolysis could have been investigated further. For example, the effect of glucose uptake into hepatocytes treated with PAI-1 could have been explored using a similar BODIPY assay. Moreover, this increased reliance of cells on glucose in response to PAI-1 may also partially explain the decrease in glucose levels seen in mice treated with LPS presented in this thesis. However, glucose regulation is complex and pharmacological inhibition of PAI-1 did not reverse this reduction in blood glucose levels.

#### **7.2.5 PAI-1 inhibition using TM5441 but not Tiplaxtinin prevented LPS-induced increase in circulating LCFAs**

In this study, pre-treating mice with the PAI-1 inhibitor TM5441 prevented the downregulation of liver fatty acid metabolism in response to LPS. This resulted in a decrease in circulating LCFAs. However, pre-treating mice with a different PAI-1 inhibitor called Tiplaxtinin did not show the same effect. One reason for this could be that Tiplaxtinin has been shown to promote PAI-1 cleavage (592). Cleavage of PAI-1 has been shown to impede the anti-proteolytic activity of PAI-1 and thus its effect on preventing the breakdown of fibrin blood clots. However, this anti-proteolytic activity may not be important in PAI-1's role in the acute immune response to LPS. Studies using Tiplaxtinin have demonstrated using Western blotting that total PAI-1 protein does not decrease, and instead the ratio of cleaved PAI-1 to active PAI-1 increases

(592). On the other hand, in experiments which used TM5441, Western blotting revealed a decrease in total PAI-1 protein, regardless of conformation (594). Data presented in this thesis supports these studies, as total serum PAI-1 content in mice treated with LPS and a combination of LPS and Tiplaxtinin was comparable. However, serum PAI-1 content was significantly lower in mice treated with both TM5441 and LPS compared to mice treated with LPS alone. This may indicate that TM5441 targets PAI-1 protein degradation, although the mechanism of action for TM5441 remains unclear. With little data confirming the binding site for Tiplaxtinin and none for TM5441, protein-ligand structure predictions were performed using Boltz-2 (*Rowan Scientific*. <https://www.rowansci.com> - accessed 2025-07-25). Boltz-2 is an open-source deep learning model which can be used to predict protein-ligand structures using protein-ligand co-folding (642). Boltz-2 is a stochastic model that will produce different structures each time a prediction is run. Multiple runs predicted Tiplaxtinin binding to PAI-1 in the same place each time, in the pocket just above the vitronectin binding site (Figure 7.1). However, when predictions were run for PAI-1 with TM5441, 50% of them predicted the same binding site as Tiplaxtinin, whilst the other 50% predicted TM5441 binds to PAI-1 lower down, specifically within the same binding site vitronectin has been shown to bind (643). Whilst this is only predictive software, if TM5441 and Tiplaxtinin bind to two different regions of PAI-1, this could potentially explain the differences observed within this study.

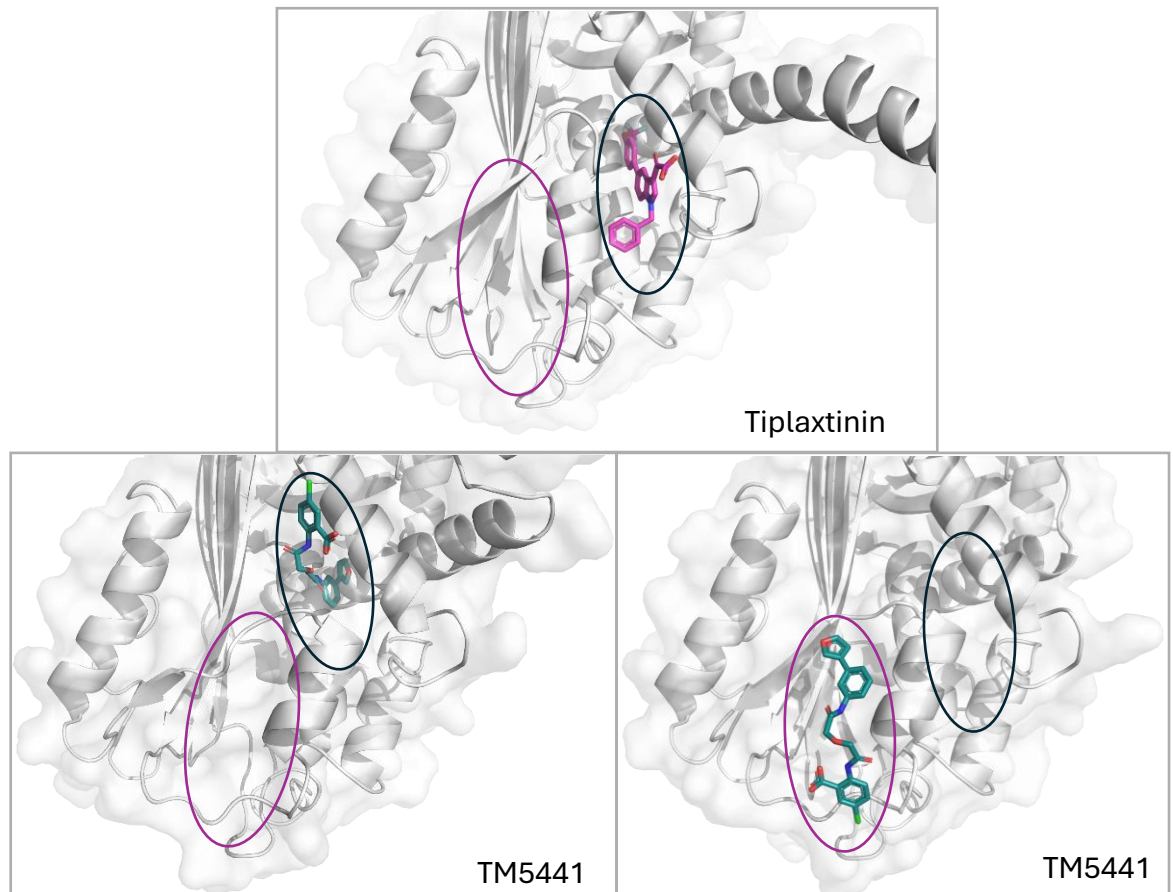


**Figure 7.1, Predicted binding site for Tiplaxtinin and TM5441.**

Boltz-2 was used to predict protein-ligand structures using protein-ligand co-folding for Tiplaxtinin and TM5441.

Other studies also support the potential role of TM5441 in inhibiting metabolic processes linked to PAI-1. For example, HepG2 cells, a hepatocellular carcinoma cell line, treated with TM5441 inhibited PAI-1-induced mitochondrial dysfunction and lipid accumulation (644). In mice, TM5441 prevented high-fat diet associated weight gain and improved insulin resistance (594). TM5441 treatment also normalised the dysregulation of JNK and Akt phosphorylation in adipose tissue and improved mitochondrial fitness. PAI-1 knockout mice fed a control diet had no difference in food intake or weight gain compared to WT mice. However, food intake was decreased in PAI-1 knockout mice fed a high-fat diet compared to WT mice, which resulted in a suppression in diet-associated weight gain (645). WT mice treated with TM5441 showed a similar result. Taken together, these results provide supporting evidence to the data presented in this thesis: that TM5441 can effectively inhibit PAI-

1 and reverse some of the metabolic associated phenotypes associated with elevated PAI-1. The data presented in this thesis could be significantly strengthened by using a PAI-1 knockout mouse model to further support these findings.

#### **7.2.6 PAI-1 inhibition impaired HSC expansion in response to LPS**

This thesis provides evidence that inhibiting PAI-1 with TM5441 results in a reduced expansion of HSCs in response to LPS at 16 hours. HSC expansion in response to infection has been well documented (421). To cope with the rapid expansion of HSCs during emergency haematopoiesis, HSCs increase their energy production by switching from low ATP-yielding glycolysis to high ATP-yielding mitochondrial oxidative phosphorylation (613). It is this metabolic switch which provides enough energy to enable rapid HSC expansion and differentiation into downstream progeny to increase the immune cell pool and effectively clear the infection. The expression of CD36 on HSCs significantly increases in response to infection (421). This allows HSCs to increase their fatty acid uptake. CD36 mediated LCFA uptake is so crucial for HSC expansion that loss of CD36 prevented fatty acid uptake into HSCs, impairing HSC cycling and expansion (420, 421). Furthermore, loss of CD36 has also been shown to directly affect the rate of FAO (422), highlighting the importance of LCFA uptake into HSCs to fuel ATP production.

Therefore, the reduction in HSC expansion demonstrated in this thesis is likely to be directly related to the prevention of LCFA accumulation within the serum by PAI-1 inhibition. Because HSCs no longer have the necessary fuel to drive rapid ATP production, this may slow HSCs ability to replicate and expand. Long-term HSCs have been shown to only increase uptake of LCFAs, and not MCFAs or SCFAs in response to LPS (421). Using palmitate tracing and subsequent metabolomic analysis has further demonstrated that HSCs and their progenitors specifically engage in LCFA associated FAO (546). Despite this, short-term HSCs have been shown to increase both SCFA and LCFA uptake in response to LPS (421). This highlights another limitation of this thesis, that the expansion of different subpopulations of HSCs was not assessed. Additional markers could have been added to the HSC flow cytometry panel to further subdivide the HSC population into long and short-term HSCs. Even so, CD36 expression on HSCs is critical for HSC

expansion, which is specifically a LCFA transport protein. Thus, it can be concluded that LCFAs are essential for HSC expansion. In fact, the proliferative capacity of HSCs has been directly linked to the availability of fatty acids. Increasing the serum content, which contains an abundance of LCFAs, in the media of cultured HSCs increased their proliferation (646). Conversely, HSCs cultured in serum-free media, which would have extremely low LCFA content, had significantly reduced HSC expansion even when cytokines known to induce HSC proliferation were added. The small amount of expansion seen was then shown to be due to the HSC itself synthesising the necessary LCFAs (646). Taken together, this provides evidence that HSCs require LCFAs to expand, and that reducing LCFA availability by PAI-1 inhibition may potentially be the cause of the reduction of HSC expansion in response to LPS.

Interestingly, this thesis demonstrated that whilst PAI-1 inhibition using TM5441 reduced HSC expansion in response to LPS, this was not the case for bone marrow LSK or MPP cells. Both the population of LSKs and MPPs per 100,000 bone marrow cells still significantly increased in response to LPS even with PAI-1 inhibition. One potential explanation for this, is that LSKs expand independently of HSCs. However, studies have demonstrated that CD36 knockout mice have impaired LSK and MPP expansion in response to LPS (421). This implies that CD36, and thus LCFA uptake, is crucial for LSKs and MPPs as well. In steady state, the population of HSCs is maintained by balancing differentiation and proliferation (647). During the initial phase of emergency haematopoiesis, this balance switches to favour proliferation over differentiation (311, 648). This results in an increase in HSC numbers. Once enough HSCs have been produced and the infection is under control, the scale is flipped and differentiation is favoured to produce the remaining immune cells required, whilst allowing the population of HSCs to return to pre-infection numbers (648). Therefore, an alternative explanation for increased LSK and MPP populations in the absence of HSC expansion, is that when the supply of LCFAs for HSCs is lower than the demand, the rate of HSC proliferation under stress is lower. This may then shift the balance towards HSC differentiation. Overtime, higher rates of HSC differentiation compared to proliferation would result in a reduction of HSC expansion without impacting the production of LSKs and MPPs. However, the role that PAI-1 plays on HSCs themselves, along with any effects TM5441 may have on

HSCs still needs to be fully characterised to confirm if it is the reduction of circulating LCFAs alone which is impacting this LPS-induced HSC expansion presented in this thesis.

### **7.2.7 Platelets release PAI-1 when stimulated with LPS**

Results in this thesis provide evidence that platelets can directly release PAI-1 in response to LPS. Whilst platelets express the LPS receptor TLR4, they do not express CD14, which is thought to be an essential component of the TLR4 signalling cascade, important to enable TLR4 to recognise and bind LPS (649). Thus, it has been widely debated whether or not LPS can directly activate platelets (650). Despite this, plenty of studies have reported that LPS can indeed directly active platelets, through a TLR4/MyD88 dependent pathway (651). For example, it has been demonstrated that LPS can induce  $\alpha$ -degranulation within platelets. Increased expression of granule-stored proteins was detected on the surface of these platelets within 1 hour of LPS exposure, which further increased when stimulated for longer (652). This provides evidence that platelets can indeed be activated by LPS, and allow the release of factors and proteins stored within their  $\alpha$ -granules.

Some of the controversy around LPS-induced platelet activation may come from the method used to isolate platelets. For example, it has been shown that platelets can absorb CD14 from the surrounding plasma to aid LPS/TLR4 signalling (606). However, if the surrounding plasma has been removed from the platelets during the isolation protocol, then there may be no availability of CD14 to enable platelet activation by LPS. For this thesis, platelets were isolated and kept in their platelet rich plasma, meaning that the platelets would still have access to any CD14 readily present in the plasma.

Platelets retain the mRNA and machinery to synthesise large amounts of PAI-1 (600). Whilst literature is incredibly limited as to if platelets can release PAI-1 in response to LPS, there is a larger body of evidence proving that activating platelets using factors associated with acute stress induces the rapid release of PAI-1. For example, studies have demonstrated that treating platelets with thrombin triggers them to rapidly release active PAI-1, this prevents the breakdown of fibrin clots through  $\alpha$ -degranulation (599). Additionally, hypoxic stress has been shown to increase platelet

PAI-1 synthesis and release PAI-1 through extracellular vesicle shedding (653). Collectively, studies such as these provide evidence that PAI-1 can be synthesised and released from platelets in response to acute stress.

Whilst the exact mechanism behind PAI-1 release from platelets is not yet fully understood, platelets are not the only cell type able to produce PAI-1. Thus, other cell types can provide mechanistic insights which may be relevant to platelets. In models using LPS, studies have shown that LPS-induced PAI-1 expression was accompanied with an upregulation of microRNA-19b in human aortic endothelial cells. Treating cells with anti-microRNA-19b significantly decreased LPS induced PAI-1 expression (654). MicroRNAs are a type of short, non-coding RNA which often play an important role in regulating gene expression. Additionally, treating these endothelial cells with a STAT-3 inhibitor also attenuated LPS-stimulated PAI-1 expression (654). Mechanistically, LCFAs themselves have also been shown to affect PAI-1 secretion from certain cell types. For example, treating endothelial cells with oleic (C18.1), linoleic (C18.2), linolenic (C18.3) and eicosapentaenoic acid (C20.5) significantly increased the amount of PAI-1 secreted by cells (655). However interestingly, palmitic (C16) and stearic acid (C18) had no effect on endothelial cell PAI-1 secretion. This may indicate a feedback mechanism, that PAI-1 helps increase circulating LCFAs, which in turn drives other cells and tissues to produce PAI-1. Taken together, this provides some insight into the potential mechanism of LPS-induced PAI-1 expression.

### **7.2.8 Platelet depletion partially ameliorates the LPS-induced increase in circulating LCFAs**

In this thesis, the data presented demonstrates there is a dramatic spike in serum PAI-1 within 90 minutes of LPS treatment. Whilst many tissues are able to synthesise PAI-1, platelets are the most obvious source of this PAI-1. This is because platelets are able to store large amounts of PAI-1, which can then be rapidly released when needed. The data presented in this thesis supports the importance of platelets in LPS-induced PAI-1 release. Depleting platelets from mice prior to LPS treatment resulted in a significant reduction in plasma PAI-1 levels. This was associated with a

partial prevention in the downregulation of liver fatty acid metabolism, and a reduction in circulating LCFAs in response to LPS.

The role of platelets in increasing blood PAI-1 levels may be unique to infection and subsequent immune response. Obesity and diabetes have been associated with increased levels of blood PAI-1. However, platelets isolated from these individuals did not have any increase in platelet *Serpine1* gene expression (the gene encoding PAI-1), nor PAI-1 protein levels compared to healthy controls (603). Furthermore, it has been stipulated that adipose tissue is the main contributor of elevated PAI-1 levels in these metabolic disorders. Obesity is strongly associated with chronic low-grade inflammation, which includes elevated levels of TGF- $\beta$  (656). Using both *in vivo* and *in vitro* models, adding TGF- $\beta$  increased adipocyte *Serpine1* expression, which correlated with increased plasma PAI-1 (657). Adipocyte-derived PAI-1 is predominantly expressed from visceral fat and is released into the blood in proportional to visceral fat mass (658). On the other hand, acute triggers such as trauma and hypoxia have been shown to cause platelets to rapidly release large quantities of PAI-1 (653). Thus, different cell-types synthesising and releasing PAI-1 may play different roles in PAI-1 production depending on if it is an acute or chronic response.

Clinical findings further support the importance of platelets in the innate immune response to infection. For instance, thrombocytopenia has been associated with impaired immune function and increased susceptibility to more serious infections (659). Furthermore, patients suffering from the autoimmune disease immune thrombocytopenia (ITP) are more vulnerable to infections (659). In ITP, the immune system inappropriately attacks and destroys platelets, resulting in low platelet numbers (660). One explanation to why ITP patients are at an increased risk of infections is that due to low platelet numbers, they do not have the reserve of PAI-1 normally stored within platelets to rapidly increase serum PAI-1 levels to the required levels. This could affect the liver's ability to downregulate hepatic fatty acid metabolism and increase circulating LCFAs to fuel emergency haematopoiesis. However, ITP patients have been shown to have elevated levels of PAI-1 compared to both healthy individuals and chemotherapy induced thrombocytopenic patients (661). This could imply that PAI-1 is released from platelets when targeted by the

immune system during ITP. Adding to this, a high proportion of ITP patients suffer from hyperlipidaemia as well as other metabolic diseases including cardiovascular and cerebrovascular disease (662). A study characterising serum lipid levels in ITP patients found that NEFA levels (circulating free fatty acids) were high, with a mean of 51.3 mmol/L (663). Although this study did not report the NEFA in healthy individuals, other studies have reported healthy controls to have a fasting NEFA of between 0.5-1.3 mmol/L (664, 665). Thus, when considered together this provides a potential link between elevated PAI-1 levels and increased circulating fatty acids in individuals with ITP. Interestingly, sustained ITP has been shown to increase the number of functional long-term HSCs, although this study did not check PAI-1 or NEFA levels (666). Perhaps increased PAI-1 due to platelet destruction results in increased NEFAs and this in turn leads to expansion of long-term HSCs, although no study has directly investigated this and thus this can only be hypothesised.

### **7.2.9 PAI-1 and immune cells**

Finally, this thesis provided evidence that inhibition of PAI-1 using TM5441 reduced the LPS-induced increase in liver neutrophils. At 6 hours, LPS resulted in a significant increase in liver neutrophils, however this was not seen in mice pre-treated with TM5441. This may be linked to the reduction PAI-1 levels in the combination treatment group compared to LPS alone. Studies have demonstrated that PAI-1 can inhibit neutrophil apoptosis, prolonging neutrophil survival (667). PAI-1 has been shown to play a key role in the inflammatory response following an ischaemic event, directing neutrophils to the site of injury (668). Furthermore, PAI-1 has been shown to regulate neutrophil infiltration into the colon during inflammatory bowel disease via NF- $\kappa$ B (669). A different study investigating chronic obstructive pulmonary disease treated mice with TM5441. They also observed a reduction in neutrophil count within the lungs of mice treated with TM5441 compared to mice treated with cigarette smoke extract alone (670). Collectively, studies such as these provide evidence for the link between PAI-1 and neutrophil infiltration in response to inflammation, and support the findings of this thesis.

Data presented in this thesis also demonstrated that depleting platelets prior to LPS treatment had the same reduction in LPS-induced neutrophil infiltration into the liver.

Again, this was associated with a reduction in serum PAI-1 levels. Platelets have been shown to interact with neutrophils during infection and inflammation (671). For example, LPS induced degranulation and P-selectin expression in platelets. This promoted neutrophil binding. Neutrophils are an important cell within the innate immune response, able to trap pathogens via the release of neutrophil extracellular traps as well as phagocytose them (672). Platelet-neutrophil interactions have been shown to be key within this inflammatory response, aiding neutrophil activation (673). Thus, it is not surprising that depleting platelets prior to LPS lead to a reduction in neutrophil infiltration into the liver in response to LPS. Interestingly, the findings in this thesis included that neutrophil numbers within the liver also significantly increased in platelet depleted mice compared to healthy controls. Whether or not this is due to the loss of platelets themselves, to the subsequent reduction in PAI-1 levels or a combination of both warrants further investigation. Data presented in this thesis would indicate that it is likely a combination of both the platelet itself as well as the PAI-1 released contributing towards liver neutrophil infiltration in response to LPS.

### 7.3 Limitations

Although the data presented in this study provided new insights into the regulation of LCFA availability in response to LPS, there are several important limitations to consider. One major limitation to this thesis is the sole use of LPS as an infection mimic. To confirm that these findings are relevant to infection in general, key experiments would need to be repeated using alternative models of infection, such as *S. Typhimurium*. Whilst there were initially plans to do this, due to time constraints these experiments were unfortunately not performed. *In vivo* experiments were planned in accordance with home office guidelines and careful consideration of the 3Rs (Replacement, Reduction and Refinement). Therefore, experiments using *S. Typhimurium* were planned in conjunction with the use of PAI-1 inhibitors to maximise experimental potential. However, due to the first PAI-1 inhibitor selected (Tiplaxtinin) being unsuccessful, the subsequently planned *S. Typhimurium* experiments were delayed until an appropriate inhibitor was identified. Experiments using the alternative PAI-1 inhibitor (TM5441) in combination with LPS were only performed right at the end of this project and thus there was unfortunately no time to conduct the planned *S. Typhimurium* experiments. Whilst this is not ideal, LPS has been shown to be an effective method to model infection and thus the findings of this thesis are still important.

Another considerable limitation is the reliance of this project on gene expression to characterise liver fatty acid metabolism. Liver bulk-RNA sequencing demonstrated that the gene expression of multiple fatty acid transporters was significantly downregulated in response to LPS treatment. However, it would have been valuable to perform some immunohistochemical analysis of liver sections to visualise if this gene downregulation correlated with a reduction in LCFA transport protein. This would have complemented the *in vitro* assays, measuring C16 BODIPY uptake into hepatocytes, whilst providing valuable insights into LCFA protein expression in the liver *in vivo*.

Adding to this, whilst many of the *in vitro* experiments were performed using both the hepatocyte cell line (AML12s) and primary hepatocytes, unfortunately due to the difficulties in obtaining primary hepatocytes, none of the PAI-1 inhibitor experiments

were done using primary hepatocytes. Whilst this is a limitation of this project, the hepatocyte cell line and primary hepatocytes appeared to react in very similar ways and thus this strengthens the argument that the AML12 cell line is an appropriate model of mouse hepatocytes in the absence of the availability of primary hepatocytes.

Another factor not fully explored in this project is the effect of PAI-1 and PAI-1 inhibition on HSCs themselves. Whilst the literature is incredibly limited, there are a few studies which implicate PAI-1 in HSC engraftment success. HSCs treated with a PAI-1 inhibitor prior to transplantation showed an increased engraftment level compared to untreated HSCs (674). It would have been interesting to explore the effect of PAI-1 on HSCs themselves. However, the primary aim of this project was to characterise how the availability of LCFAs is regulated in response to infection and thus these experiments were not prioritised.

Finally, a considerable limitation of this study is that it does not consider the impact of PAI-1 inhibition on recovery following infection. It would have been interesting to explore if PAI-1 inhibition delayed or prevented infection recovery. Again, the primary aim of this project was to study the initial acute response to infections and for this reason the experiments characterising the recovery phase were not prioritised. Again, because LPS is only a bacterial mimic, it would be more suitable to study recovery following infection using alternative models such as *S. Typhimurium*.

## 7.4 Future work

The main aims and objectives of this study were addressed in this thesis. However, as is often the case with research, there are still many interesting questions left and some key important experiments that could have been done to further strengthen this project. The main and most obvious would be to perform both LPS and *S. Typhimurium* experiments using PAI-1 knockout mice. Whilst PAI-1 knockout mice are available to purchase, buying and shipping new mouse strains is expensive. Therefore, due to the high costs, this project did not use them. However, if PAI-1 knockout strains had been available during this project, several key experiments would have been done. Firstly, do levels of circulating LCFAs increase in the serum of PAI-1 knockout mice treated with LPS? If these knockout mice have impaired downregulation of hepatic fatty acid metabolism, and subsequently reduced availability of LCFAs in response to infection, similar to results seen in mice pre-treated with a PAI-1 inhibitor, then it would be interesting to characterise if this has a knock-on effect on HSC expansion. Furthermore, PAI-1 knockout mice would be ideal to study whether loss of PAI-1 affects recovery following infection and/or infection severity.

Finally, the other important next experiments which warrant further investigation would be to identify the mechanism of action. Whilst this project identified PAI-1 as the causative factor downregulating hepatic fatty acid metabolism in response to LPS, it did not identify the mechanism by which this occurs. Using the bulk-RNA sequencing data along with experiments already done, candidates of master regulators of fatty acid metabolism could be identified. Further experiments could then be done, both *in vivo* and *in vitro*, pharmacologically targeting the most likely candidate(s), either agonising or antagonising it depending if it was up or downregulated in response to infection. If possible, genetic knockdown models, either using siRNAs or a liver specific knockout mouse model for that gene could then be done to confirm these findings. Finally experiments such as phospho-arrays could be performed to identify the signalling pathway involved in the downregulation of hepatic fatty acid metabolism in response to infection. This could then be confirmed using drugs to target that specific pathway. Taken together, these experiments could provide the mechanistic insight into how PAI-1 induces the downregulation of liver

fatty acid metabolism in response to infection, a key element currently missing from this project.

## 7.5 Conclusion

In conclusion, this thesis provides evidence that 6 hours after LPS infection, several key liver fatty acid uptake and metabolism genes are significantly downregulated. This corresponds with a significant increase in the availability of circulating LCFAs. *In vitro* assays using hepatocytes demonstrated that circulating cytokines released in response to LPS caused this downregulation of hepatic fatty acid metabolism. A cytokine array of serum from LPS-treated mice revealed significant upregulation of several cytokines and chemokines. Of these, only PAI-1 significantly decreased LCFA uptake and metabolism in hepatocytes and reduce hepatocyte fatty acid associated mitochondrial respiration. Furthermore, mice treated with recombinant PAI-1 showed significantly increased circulating LCFAs and decreased liver fatty acid metabolism genes.

Pharmacological inhibition of PAI-1 using TM5441 prevented the downregulation of hepatic fatty acid metabolism both *in vitro* and *in vivo*, resulting in a reduction in the availability of circulating LCFAs in response to LPS. Subsequently, pre-treating mice with TM5441 prior to LPS injection resulted in a significant reduction in HSC expansion normally seen in response to LPS. Furthermore, this project identifies platelets as an important producer of PAI-1 in the acute immune response to LPS. Up to 90% of PAI-1 is stored in platelets. This thesis demonstrates that platelets can rapidly release PAI-1 in response to LPS. Depleting platelets from mice prior to LPS infection resulted in a significant reduction in circulating PAI-1 levels. This partially reversed the downregulation of hepatic fatty acid metabolism and reduced the availability of circulating LCFAs.

Overall, the data presented in this thesis provides new insights into the metabolic changes occurring in response to LPS, which regulates the availability of circulating LCFAs necessary to fuel HSC expansion during emergency haematopoiesis.

## 8 References

1. Sambrook P, Kelly P, Eisman J. Bone mass and ageing. *Baillieres Clin Rheumatol.* 1993;7(3):445-57.
2. Kim J, Bixel MG. Intravital Multiphoton Imaging of the Bone and Bone Marrow Environment. *Cytometry A.* 2020;97(5):496-503.
3. Petrtyl M, Hert J, Fiala P. Spatial organization of the haversian bone in man. *J Biomech.* 1996;29(2):161-9.
4. Hwang S, Panicek DM. Magnetic resonance imaging of bone marrow in oncology, Part 2. *Skeletal Radiol.* 2007;36(11):1017-27.
5. Tikhonova AN, Dolgalev I, Hu H, Sivaraj KK, Hoxha E, Cuesta-Dominguez A, et al. The bone marrow microenvironment at single-cell resolution. *Nature.* 2019;569(7755):222-8.
6. Romaniuk A, Lyndina Y, Sikora V, Lyndin M, Karpenko L, Gladchenko O, et al. Structural features of bone marrow. *Interv Med Appl Sci.* 2016;8(3):121-6.
7. Lafage-Proust MH, Roche B, Langer M, Cleret D, Vanden Bossche A, Olivier T, et al. Assessment of bone vascularization and its role in bone remodeling. *Bonekey Rep.* 2015;4:662.
8. Craft CS, Li Z, MacDougald OA, Scheller EL. Molecular differences between subtypes of bone marrow adipocytes. *Curr Mol Biol Rep.* 2018;4(1):16-23.
9. Roche B, David V, Vanden-Bossche A, Peyrin F, Malaval L, Vico L, et al. Structure and quantification of microvascularisation within mouse long bones: what and how should we measure? *Bone.* 2012;50(1):390-9.
10. Pino AM, Rodriguez JP. Is fatty acid composition of human bone marrow significant to bone health? *Bone.* 2019;118:53-61.
11. Gurkan UA, Akkus O. The mechanical environment of bone marrow: a review. *Ann Biomed Eng.* 2008;36(12):1978-91.
12. Raissaki M, Demetriou S, Spanakis K, Skiadas C, Katzilakis N, Velivassakis EG, et al. Multifocal bone and bone marrow lesions in children - MRI findings. *Pediatr Radiol.* 2017;47(3):342-60.
13. Malkiewicz A, Dziedzic M. Bone marrow reconversion - imaging of physiological changes in bone marrow. *Pol J Radiol.* 2012;77(4):45-50.
14. Horowitz MC, Berry R, Holtrup B, Sebo Z, Nelson T, Fretz JA, et al. Bone marrow adipocytes. *Adipocyte.* 2017;6(3):193-204.
15. Ho MS, Medcalf RL, Livesey SA, Traianedes K. The dynamics of adult haematopoiesis in the bone and bone marrow environment. *Br J Haematol.* 2015;170(4):472-86.
16. Kumar R, Godavarthy PS, Krause DS. The bone marrow microenvironment in health and disease at a glance. *J Cell Sci.* 2018;131(4).
17. Calvi LM, Link DC. Cellular complexity of the bone marrow hematopoietic stem cell niche. *Calcif Tissue Int.* 2014;94(1):112-24.
18. Busch C, Nyamondo K, Wheadon H. Complexities of modeling the bone marrow microenvironment to facilitate hematopoietic research. *Exp Hematol.* 2024;135:104233.
19. Carpenter RS, Maryanovich M. Systemic and local regulation of hematopoietic homeostasis in health and disease. *Nat Cardiovasc Res.* 2024;3(6):651-65.

20. Palis J, Yoder MC. Yolk-sac hematopoiesis: the first blood cells of mouse and man. *Exp Hematol*. 2001;29(8):927-36.
21. McGrath KE, Palis J. Hematopoiesis in the yolk sac: more than meets the eye. *Exp Hematol*. 2005;33(9):1021-8.
22. Wittamer V, Bertrand JY. Yolk sac hematopoiesis: does it contribute to the adult hematopoietic system? *Cell Mol Life Sci*. 2020;77(20):4081-91.
23. Dzierzak E, Medvinsky A, de Bruijn M. Qualitative and quantitative aspects of haematopoietic cell development in the mammalian embryo. *Immunol Today*. 1998;19(5):228-36.
24. Christensen JL, Wright DE, Wagers AJ, Weissman IL. Circulation and chemotaxis of fetal hematopoietic stem cells. *PLoS Biol*. 2004;2(3):E75.
25. Anthony BA, Link DC. Regulation of hematopoietic stem cells by bone marrow stromal cells. *Trends Immunol*. 2014;35(1):32-7.
26. Seita J, Weissman IL. Hematopoietic stem cell: self-renewal versus differentiation. *Wiley Interdiscip Rev Syst Biol Med*. 2010;2(6):640-53.
27. Sun J, Ramos A, Chapman B, Johnnidis JB, Le L, Ho YJ, et al. Clonal dynamics of native haematopoiesis. *Nature*. 2014;514(7522):322-7.
28. Velten L, Haas SF, Raffel S, Blaszkiewicz S, Islam S, Hennig BP, et al. Human haematopoietic stem cell lineage commitment is a continuous process. *Nat Cell Biol*. 2017;19(4):271-81.
29. Challen GA, Boles N, Lin KK, Goodell MA. Mouse hematopoietic stem cell identification and analysis. *Cytometry A*. 2009;75(1):14-24.
30. Laurenti E, Gottgens B. From haematopoietic stem cells to complex differentiation landscapes. *Nature*. 2018;553(7689):418-26.
31. Gorgens A, Radtke S, Mollmann M, Cross M, Durig J, Horn PA, et al. Revision of the human hematopoietic tree: granulocyte subtypes derive from distinct hematopoietic lineages. *Cell Rep*. 2013;3(5):1539-52.
32. Ng AP, Alexander WS. Haematopoietic stem cells: past, present and future. *Cell Death Discov*. 2017;3:17002.
33. Ceredig R, Rolink AG, Brown G. Models of haematopoiesis: seeing the wood for the trees. *Nat Rev Immunol*. 2009;9(4):293-300.
34. Manso BA, Rodriguez YBA, Forsberg EC. From Hematopoietic Stem Cells to Platelets: Unifying Differentiation Pathways Identified by Lineage Tracing Mouse Models. *Cells*. 2024;13(8).
35. Sanjuan-Pla A, Macaulay IC, Jensen CT, Woll PS, Luis TC, Mead A, et al. Platelet-biased stem cells reside at the apex of the haematopoietic stem-cell hierarchy. *Nature*. 2013;502(7470):232-6.
36. Wilson A, Trumpp A. Bone-marrow haematopoietic-stem-cell niches. *Nat Rev Immunol*. 2006;6(2):93-106.
37. Aljagthmi AA, Abdel-Aziz AK. Hematopoietic stem cells: Understanding the mechanisms to unleash the therapeutic potential of hematopoietic stem cell transplantation. *Stem Cell Res Ther*. 2025;16(1):60.
38. Cosgrove J, Hustin LSP, de Boer RJ, Perie L. Hematopoiesis in numbers. *Trends Immunol*. 2021;42(12):1100-12.
39. Takizawa H, Regoes RR, Boddupalli CS, Bonhoeffer S, Manz MG. Dynamic variation in cycling of hematopoietic stem cells in steady state and inflammation. *J Exp Med*. 2011;208(2):273-84.

40. Osawa M, Hanada K, Hamada H, Nakauchi H. Long-term lymphohematopoietic reconstitution by a single CD34-low/negative hematopoietic stem cell. *Science*. 1996;273(5272):242-5.
41. Yang L, Bryder D, Adolfsson J, Nygren J, Mansson R, Sigvardsson M, et al. Identification of Lin(-)Sca1(+)kit(+)CD34(+)Flt3- short-term hematopoietic stem cells capable of rapidly reconstituting and rescuing myeloablated transplant recipients. *Blood*. 2005;105(7):2717-23.
42. Kiel MJ, Yilmaz OH, Iwashita T, Yilmaz OH, Terhorst C, Morrison SJ. SLAM family receptors distinguish hematopoietic stem and progenitor cells and reveal endothelial niches for stem cells. *Cell*. 2005;121(7):1109-21.
43. Romo-Rodriguez R, Pelayo R, Ramirez-Ramirez D. Cell therapy in pediatric blood diseases. *Front Med (Lausanne)*. 2025;12:1591287.
44. Sugiyama-Finnis A, Yamazaki S. Culturing Potential: advances in ex vivo cell culture systems for haematopoietic cell-based regenerative therapies. *Regen Ther*. 2025;30:403-14.
45. Bernitz JM, Kim HS, MacArthur B, Sieburg H, Moore K. Hematopoietic Stem Cells Count and Remember Self-Renewal Divisions. *Cell*. 2016;167(5):1296-309 e10.
46. Ibneeva L, Grinenko T. Dissecting dormancy and quiescence in hematopoietic stem cells. *Frontiers in Hematology*. 2024;3.
47. Wilson A, Laurenti E, Oser G, van der Wath RC, Blanco-Bose W, Jaworski M, et al. Hematopoietic stem cells reversibly switch from dormancy to self-renewal during homeostasis and repair. *Cell*. 2008;135(6):1118-29.
48. Foudi A, Hochedlinger K, Van Buren D, Schindler JW, Jaenisch R, Carey V, et al. Analysis of histone 2B-GFP retention reveals slowly cycling hematopoietic stem cells. *Nat Biotechnol*. 2009;27(1):84-90.
49. Cheshier SH, Morrison SJ, Liao X, Weissman IL. In vivo proliferation and cell cycle kinetics of long-term self-renewing hematopoietic stem cells. *Proc Natl Acad Sci U S A*. 1999;96(6):3120-5.
50. Boyle C, Lansdorp PM, Edelstein-Keshet L. Predicting the number of lifetime divisions for hematopoietic stem cells from telomere length measurements. *iScience*. 2023;26(7):107053.
51. Zhang L, Mack R, Breslin P, Zhang J. Molecular and cellular mechanisms of aging in hematopoietic stem cells and their niches. *J Hematol Oncol*. 2020;13(1):157.
52. Johnson C, Belluschi S, Laurenti E. Beyond "to divide or not to divide": Kinetics matters in hematopoietic stem cells. *Exp Hematol*. 2020;92:1-10 e2.
53. Qiu J, Papatsenko D, Niu X, Schaniel C, Moore K. Divisional history and hematopoietic stem cell function during homeostasis. *Stem Cell Reports*. 2014;2(4):473-90.
54. Hsu P, Qu CK. Metabolic plasticity and hematopoietic stem cell biology. *Curr Opin Hematol*. 2013;20(4):289-94.
55. Vannini N, Girotra M, Naveiras O, Nikitin G, Campos V, Giger S, et al. Specification of haematopoietic stem cell fate via modulation of mitochondrial activity. *Nat Commun*. 2016;7:13125.
56. Flach J, Milyavsky M. Replication stress in hematopoietic stem cells in mouse and man. *Mutat Res*. 2018;808:74-82.

57. Hughes MR, Canals Hernaez D, Cait J, Refaeli I, Lo BC, Roskelley CD, et al. A sticky wicket: Defining molecular functions for CD34 in hematopoietic cells. *Exp Hematol.* 2020;86:1-14.
58. Al-Amoodi AS, Li Y, Al-Ghuneim A, Allehaibi H, Isaoglou I, Esau LE, et al. Refining the migration and engraftment of short-term and long-term HSCs by enhancing homing-specific adhesion mechanisms. *Blood Adv.* 2022;6(15):4373-91.
59. Cheng H, Zheng Z, Cheng T. New paradigms on hematopoietic stem cell differentiation. *Protein Cell.* 2020;11(1):34-44.
60. Emmons R, Niemiro GM, De Lisio M. Hematopoiesis with Obesity and Exercise: Role of the Bone Marrow Niche. *Exerc Immunol Rev.* 2017;23:82-95.
61. Liu L, Papa EF, Dooner MS, Machan JT, Johnson KW, Goldberg LR, et al. Homing and long-term engraftment of long- and short-term renewal hematopoietic stem cells. *PLoS One.* 2012;7(2):e31300.
62. Hicks MR, Pyle AD. The emergence of the stem cell niche. *Trends Cell Biol.* 2023;33(2):112-23.
63. Schofield R. The relationship between the spleen colony-forming cell and the haemopoietic stem cell. *Blood Cells.* 1978;4(1-2):7-25.
64. Xie Y, Yin T, Wiegraebe W, He XC, Miller D, Stark D, et al. Detection of functional haematopoietic stem cell niche using real-time imaging. *Nature.* 2009;457(7225):97-101.
65. Asada N, Kunisaki Y, Pierce H, Wang Z, Fernandez NF, Birbrair A, et al. Differential cytokine contributions of perivascular haematopoietic stem cell niches. *Nat Cell Biol.* 2017;19(3):214-23.
66. Yin T, Li L. The stem cell niches in bone. *J Clin Invest.* 2006;116(5):1195-201.
67. Orford KW, Scadden DT. Deconstructing stem cell self-renewal: genetic insights into cell-cycle regulation. *Nat Rev Genet.* 2008;9(2):115-28.
68. Mann Z, Sengar M, Verma YK, Rajalingam R, Raghav PK. Hematopoietic Stem Cell Factors: Their Functional Role in Self-Renewal and Clinical Aspects. *Front Cell Dev Biol.* 2022;10:664261.
69. Jones DL, Wagers AJ. No place like home: anatomy and function of the stem cell niche. *Nat Rev Mol Cell Biol.* 2008;9(1):11-21.
70. Shi G, Zhang P, Zhang X, Li J, Zheng X, Yan J, et al. The spatiotemporal heterogeneity of the biophysical microenvironment during hematopoietic stem cell development: from embryo to adult. *Stem Cell Res Ther.* 2023;14(1):251.
71. Perlin JR, Sporrij A, Zon LI. Blood on the tracks: hematopoietic stem cell-endothelial cell interactions in homing and engraftment. *J Mol Med (Berl).* 2017;95(8):809-19.
72. Li H, Luo Q, Shan W, Cai S, Tie R, Xu Y, et al. Biomechanical cues as master regulators of hematopoietic stem cell fate. *Cell Mol Life Sci.* 2021;78(16):5881-902.
73. Boulais PE, Frenette PS. Making sense of hematopoietic stem cell niches. *Blood.* 2015;125(17):2621-9.
74. Kwon M, Kim BS, Yoon S, Oh SO, Lee D. Hematopoietic Stem Cells and Their Niche in Bone Marrow. *Int J Mol Sci.* 2024;25(13).
75. Doan PL, Chute JP. The vascular niche: home for normal and malignant hematopoietic stem cells. *Leukemia.* 2012;26(1):54-62.
76. He N, Zhang L, Cui J, Li Z. Bone marrow vascular niche: home for hematopoietic stem cells. *Bone Marrow Res.* 2014;2014:128436.

77. Qian J, Shao X, Bao H, Fang Y, Guo W, Li C, et al. Identification and characterization of cell niches in tissue from spatial omics data at single-cell resolution. *Nat Commun.* 2025;16(1):1693.
78. Takubo K, Goda N, Yamada W, Iriuchishima H, Ikeda E, Kubota Y, et al. Regulation of the HIF-1alpha level is essential for hematopoietic stem cells. *Cell Stem Cell.* 2010;7(3):391-402.
79. Felker S, Shrestha A, Bailey J, Pillis DM, Siniard D, Malik P. Differential CXCR4 expression on hematopoietic progenitor cells versus stem cells directs homing and engraftment. *JCI Insight.* 2022;7(9).
80. Fang X, Fang X, Mao Y, Ciechanover A, Xu Y, An J, et al. A novel small molecule CXCR4 antagonist potently mobilizes hematopoietic stem cells in mice and monkeys. *Stem Cell Res Ther.* 2021;12(1):17.
81. Nagasawa T. CXC chemokine ligand 12 (CXCL12) and its receptor CXCR4. *J Mol Med (Berl).* 2014;92(5):433-9.
82. Sugiyama T, Kohara H, Noda M, Nagasawa T. Maintenance of the hematopoietic stem cell pool by CXCL12-CXCR4 chemokine signaling in bone marrow stromal cell niches. *Immunity.* 2006;25(6):977-88.
83. Nie Y, Han YC, Zou YR. CXCR4 is required for the quiescence of primitive hematopoietic cells. *J Exp Med.* 2008;205(4):777-83.
84. Zhang Y, Depond M, He L, Foudi A, Kwarteng EO, Lauret E, et al. CXCR4/CXCL12 axis counteracts hematopoietic stem cell exhaustion through selective protection against oxidative stress. *Sci Rep.* 2016;6:37827.
85. Wiesner C, Nabha SM, Dos Santos EB, Yamamoto H, Meng H, Melchior SW, et al. C-kit and its ligand stem cell factor: potential contribution to prostate cancer bone metastasis. *Neoplasia.* 2008;10(9):996-1003.
86. Molineux G, Migdalska A, Szmikowski M, Zsebo K, Dexter TM. The effects on hematopoiesis of recombinant stem cell factor (ligand for c-kit) administered in vivo to mice either alone or in combination with granulocyte colony-stimulating factor. *Blood.* 1991;78(4):961-6.
87. Whetton AD, Graham GJ. Homing and mobilization in the stem cell niche. *Trends Cell Biol.* 1999;9(6):233-8.
88. Driessen RL, Johnston HM, Nilsson SK. Membrane-bound stem cell factor is a key regulator in the initial lodgment of stem cells within the endosteal marrow region. *Exp Hematol.* 2003;31(12):1284-91.
89. Ding L, Saunders TL, Enikolopov G, Morrison SJ. Endothelial and perivascular cells maintain haematopoietic stem cells. *Nature.* 2012;481(7382):457-62.
90. Omatsu Y, Sugiyama T, Kohara H, Kondoh G, Fujii N, Kohno K, et al. The essential functions of adipo-osteogenic progenitors as the hematopoietic stem and progenitor cell niche. *Immunity.* 2010;33(3):387-99.
91. Machlus KR, Italiano JE, Jr. The incredible journey: From megakaryocyte development to platelet formation. *J Cell Biol.* 2013;201(6):785-96.
92. Patel SR, Hartwig JH, Italiano JE, Jr. The biogenesis of platelets from megakaryocyte proplatelets. *J Clin Invest.* 2005;115(12):3348-54.
93. Day RB, Link DC. Megakaryocytes in the hematopoietic stem cell niche. *Nat Med.* 2014;20(11):1233-4.
94. Pascetti E, Floren M, Fernandes TDS, Anastasio C, Doyle L, Gillette J. Tetraspanin CD82 regulates transforming growth factor-beta signaling in hematopoietic stem and progenitor cells. *Mol Biol Cell.* 2025;36(7):br19.

95. Norozi F, Shahrabi S, Hajizamani S, Saki N. Regulatory role of Megakaryocytes on Hematopoietic Stem Cells Quiescence by CXCL4/PF4 in Bone Marrow Niche. *Leuk Res.* 2016;48:107-12.
96. Rozenova K, Jiang J, Donaghy R, Aressy B, Greenberg RA, Tong W. MERIT40 deficiency expands hematopoietic stem cell pools by regulating thrombopoietin receptor signaling. *Blood.* 2015;125(11):1730-8.
97. Bruns I, Lucas D, Pinho S, Ahmed J, Lambert MP, Kunisaki Y, et al. Megakaryocytes regulate hematopoietic stem cell quiescence through CXCL4 secretion. *Nat Med.* 2014;20(11):1315-20.
98. Zhao M, Perry JM, Marshall H, Venkatraman A, Qian P, He XC, et al. Megakaryocytes maintain homeostatic quiescence and promote post-injury regeneration of hematopoietic stem cells. *Nat Med.* 2014;20(11):1321-6.
99. Kono H, Rock KL. How dying cells alert the immune system to danger. *Nat Rev Immunol.* 2008;8(4):279-89.
100. Mosser DM, Edwards JP. Exploring the full spectrum of macrophage activation. *Nat Rev Immunol.* 2008;8(12):958-69.
101. Winkler IG, Sims NA, Pettit AR, Barbier V, Nowlan B, Helwani F, et al. Bone marrow macrophages maintain hematopoietic stem cell (HSC) niches and their depletion mobilizes HSCs. *Blood.* 2010;116(23):4815-28.
102. McCabe A, Zhang Y, Thai V, Jones M, Jordan MB, MacNamara KC. Macrophage-Lineage Cells Negatively Regulate the Hematopoietic Stem Cell Pool in Response to Interferon Gamma at Steady State and During Infection. *Stem Cells.* 2015;33(7):2294-305.
103. Bisht K, Tay J, Wellburn RN, McGirr C, Fleming W, Nowlan B, et al. Bacterial Lipopolysaccharides Suppress Erythroblastic Islands and Erythropoiesis in the Bone Marrow in an Extrinsic and G-CSF-, IL-1-, and TNF-Independent Manner. *Front Immunol.* 2020;11:583550.
104. Levesque JP, Summers KM, Millard SM, Bisht K, Winkler IG, Pettit AR. Role of macrophages and phagocytes in orchestrating normal and pathologic hematopoietic niches. *Exp Hematol.* 2021;100:12-31 e1.
105. Gao Q, Wang L, Wang S, Huang B, Jing Y, Su J. Bone Marrow Mesenchymal Stromal Cells: Identification, Classification, and Differentiation. *Front Cell Dev Biol.* 2021;9:787118.
106. Calvi LM, Link DC. The hematopoietic stem cell niche in homeostasis and disease. *Blood.* 2015;126(22):2443-51.
107. Dazzi F, Ramasamy R, Glennie S, Jones SP, Roberts I. The role of mesenchymal stem cells in haemopoiesis. *Blood Rev.* 2006;20(3):161-71.
108. Mendez-Ferrer S, Michurina TV, Ferraro F, Mazloom AR, MacArthur BD, Lira SA, et al. Mesenchymal and haematopoietic stem cells form a unique bone marrow niche. *Nature.* 2010;466(7308):829-34.
109. Morrison SJ, Scadden DT. The bone marrow niche for haematopoietic stem cells. *Nature.* 2014;505(7483):327-34.
110. Qian H, Buza-Vidas N, Hyland CD, Jensen CT, Antonchuk J, Mansson R, et al. Critical role of thrombopoietin in maintaining adult quiescent hematopoietic stem cells. *Cell Stem Cell.* 2007;1(6):671-84.
111. Arai F, Hirao A, Ohmura M, Sato H, Matsuoka S, Takubo K, et al. Tie2/angiopoietin-1 signaling regulates hematopoietic stem cell quiescence in the bone marrow niche. *Cell.* 2004;118(2):149-61.

112. Taichman RS, Emerson SG. Human osteoblasts support hematopoiesis through the production of granulocyte colony-stimulating factor. *J Exp Med*. 1994;179(5):1677-82.
113. Jung Y, Wang J, Schneider A, Sun YX, Koh-Paige AJ, Osman NI, et al. Regulation of SDF-1 (CXCL12) production by osteoblasts; a possible mechanism for stem cell homing. *Bone*. 2006;38(4):497-508.
114. Visnjic D, Kalajic Z, Rowe DW, Katavic V, Lorenzo J, Aguila HL. Hematopoiesis is severely altered in mice with an induced osteoblast deficiency. *Blood*. 2004;103(9):3258-64.
115. Kiel MJ, Acar M, Radice GL, Morrison SJ. Hematopoietic stem cells do not depend on N-cadherin to regulate their maintenance. *Cell Stem Cell*. 2009;4(2):170-9.
116. Nombela-Arrieta C, Pivarnik G, Winkel B, Canty KJ, Harley B, Mahoney JE, et al. Quantitative imaging of haematopoietic stem and progenitor cell localization and hypoxic status in the bone marrow microenvironment. *Nat Cell Biol*. 2013;15(5):533-43.
117. Lo Celso C, Fleming HE, Wu JW, Zhao CX, Miake-Lye S, Fujisaki J, et al. Live-animal tracking of individual haematopoietic stem/progenitor cells in their niche. *Nature*. 2009;457(7225):92-6.
118. Raaijmakers MH, Mukherjee S, Guo S, Zhang S, Kobayashi T, Schoonmaker JA, et al. Bone progenitor dysfunction induces myelodysplasia and secondary leukaemia. *Nature*. 2010;464(7290):852-7.
119. Galan-Diez M, Kousteni S. A bone marrow niche-derived molecular switch between osteogenesis and hematopoiesis. *Genes Dev*. 2018;32(5-6):324-6.
120. Sugiyama T, Omatsu Y, Nagasawa T. Niches for hematopoietic stem cells and immune cell progenitors. *Int Immunol*. 2019;31(1):5-11.
121. Zhou BO, Yue R, Murphy MM, Peyer JG, Morrison SJ. Leptin-receptor-expressing mesenchymal stromal cells represent the main source of bone formed by adult bone marrow. *Cell Stem Cell*. 2014;15(2):154-68.
122. Comazzetto S, Murphy MM, Berto S, Jeffery E, Zhao Z, Morrison SJ. Restricted Hematopoietic Progenitors and Erythropoiesis Require SCF from Leptin Receptor+ Niche Cells in the Bone Marrow. *Cell Stem Cell*. 2019;24(3):477-86 e6.
123. Fazeli PK, Horowitz MC, MacDougald OA, Scheller EL, Rodeheffer MS, Rosen CJ, et al. Marrow fat and bone--new perspectives. *J Clin Endocrinol Metab*. 2013;98(3):935-45.
124. Justesen J, Stenderup K, Ebbesen EN, Mosekilde L, Steiniche T, Kassem M. Adipocyte tissue volume in bone marrow is increased with aging and in patients with osteoporosis. *Biogerontology*. 2001;2(3):165-71.
125. Sebo ZL, Rendina-Ruedy E, Ables GP, Lindskog DM, Rodeheffer MS, Fazeli PK, et al. Bone Marrow Adiposity: Basic and Clinical Implications. *Endocr Rev*. 2019;40(5):1187-206.
126. Ambrosi TH, Scialdone A, Graja A, Gohlke S, Jank AM, Bocian C, et al. Adipocyte Accumulation in the Bone Marrow during Obesity and Aging Impairs Stem Cell-Based Hematopoietic and Bone Regeneration. *Cell Stem Cell*. 2017;20(6):771-84 e6.
127. Naveiras O, Nardi V, Wenzel PL, Hauschka PV, Fahey F, Daley GQ. Bone-marrow adipocytes as negative regulators of the haematopoietic microenvironment. *Nature*. 2009;460(7252):259-63.

128. Belaid-Choucair Z, Lepelletier Y, Poncin G, Thiry A, Humblet C, Maachi M, et al. Human bone marrow adipocytes block granulopoiesis through neuropilin-1-induced granulocyte colony-stimulating factor inhibition. *Stem Cells*. 2008;26(6):1556-64.
129. Ghode SS, Bajaj MS, Kulkarni RS, Limaye LS, Shouche YS, Kale VP. Neuropilin-1 Is an Important Niche Component and Exerts Context-Dependent Effects on Hematopoietic Stem Cells. *Stem Cells Dev*. 2017;26(1):35-48.
130. Kaigler D, Krebsbach PH, West ER, Horger K, Huang YC, Mooney DJ. Endothelial cell modulation of bone marrow stromal cell osteogenic potential. *FASEB J*. 2005;19(6):665-7.
131. Tura O, Skinner EM, Barclay GR, Samuel K, Gallagher RC, Brittan M, et al. Late outgrowth endothelial cells resemble mature endothelial cells and are not derived from bone marrow. *Stem Cells*. 2013;31(2):338-48.
132. Rafii S, Butler JM, Ding BS. Angiocrine functions of organ-specific endothelial cells. *Nature*. 2016;529(7586):316-25.
133. Itkin T, Gur-Cohen S, Spencer JA, Schajnovitz A, Ramasamy SK, Kusumbe AP, et al. Distinct bone marrow blood vessels differentially regulate haematopoiesis. *Nature*. 2016;532(7599):323-8.
134. Gunsilius E. Evidence from a leukemia model for maintenance of vascular endothelium by bone-marrow-derived endothelial cells. *Adv Exp Med Biol*. 2003;522:17-24.
135. Li Y, Wu A, Jin X, Shen H, Zhao C, Yi X, et al. DDO1002, an NRF2-KEAP1 inhibitor, improves hematopoietic stem cell aging and stress response. *Life Med*. 2024;3(6):lnae043.
136. Wang Q, Qian W, Han Y, Mao Y, Gao Z, Chen Y, et al. Ferumoxytol promotes haematopoietic stem cell post-injury regeneration as a reactive oxygen species scavenger. *Nat Nanotechnol*. 2025;20(7):959-69.
137. Comazzetto S, Shen B, Morrison SJ. Niches that regulate stem cells and hematopoiesis in adult bone marrow. *Dev Cell*. 2021;56(13):1848-60.
138. Himburg HA, Termini CM, Schluskel L, Kan J, Li M, Zhao L, et al. Distinct Bone Marrow Sources of Pleiotrophin Control Hematopoietic Stem Cell Maintenance and Regeneration. *Cell Stem Cell*. 2018;23(3):370-81 e5.
139. Xu C, Gao X, Wei Q, Nakahara F, Zimmerman SE, Mar J, et al. Stem cell factor is selectively secreted by arterial endothelial cells in bone marrow. *Nat Commun*. 2018;9(1):2449.
140. Greenbaum A, Hsu YM, Day RB, Schuettpelz LG, Christopher MJ, Borgerding JN, et al. CXCL12 in early mesenchymal progenitors is required for haematopoietic stem-cell maintenance. *Nature*. 2013;495(7440):227-30.
141. Winkler IG, Barbier V, Nowlan B, Jacobsen RN, Forristal CE, Patton JT, et al. Vascular niche E-selectin regulates hematopoietic stem cell dormancy, self renewal and chemoresistance. *Nat Med*. 2012;18(11):1651-7.
142. Zhang J, Niu C, Ye L, Huang H, He X, Tong WG, et al. Identification of the haematopoietic stem cell niche and control of the niche size. *Nature*. 2003;425(6960):836-41.
143. Kiel MJ, Morrison SJ. Uncertainty in the niches that maintain haematopoietic stem cells. *Nat Rev Immunol*. 2008;8(4):290-301.
144. Morikawa T, Takubo K. Hypoxia regulates the hematopoietic stem cell niche. *Pflugers Arch*. 2016;468(1):13-22.

145. Simsek T, Kocabas F, Zheng J, Deberardinis RJ, Mahmoud AI, Olson EN, et al. The distinct metabolic profile of hematopoietic stem cells reflects their location in a hypoxic niche. *Cell Stem Cell*. 2010;7(3):380-90.
146. Eliasson P, Rehn M, Hammar P, Larsson P, Sirenko O, Flippin LA, et al. Hypoxia mediates low cell-cycle activity and increases the proportion of long-term-reconstituting hematopoietic stem cells during in vitro culture. *Exp Hematol*. 2010;38(4):301-10 e2.
147. Hermitte F, Brunet de la Grange P, Belloc F, Praloran V, Ivanovic Z. Very low O<sub>2</sub> concentration (0.1%) favors G<sub>0</sub> return of dividing CD34<sup>+</sup> cells. *Stem Cells*. 2006;24(1):65-73.
148. Ivanovic Z, Dello Sbarba P, Trimoreau F, Faucher JL, Praloran V. Primitive human HPCs are better maintained and expanded in vitro at 1 percent oxygen than at 20 percent. *Transfusion*. 2000;40(12):1482-8.
149. Broxmeyer HE, O'Leary HA, Huang X, Mantel C. The importance of hypoxia and extra physiologic oxygen shock/stress for collection and processing of stem and progenitor cells to understand true physiology/pathology of these cells ex vivo. *Curr Opin Hematol*. 2015;22(4):273-8.
150. Mantel CR, O'Leary HA, Chitteti BR, Huang X, Cooper S, Hangoc G, et al. Enhancing Hematopoietic Stem Cell Transplantation Efficacy by Mitigating Oxygen Shock. *Cell*. 2015;161(7):1553-65.
151. Capitano ML, Mohamad SF, Cooper S, Guo B, Huang X, Gunawan AM, et al. Mitigating oxygen stress enhances aged mouse hematopoietic stem cell numbers and function. *J Clin Invest*. 2021;131(1).
152. Zou P, Yoshihara H, Hosokawa K, Tai I, Shinmyozu K, Tsukahara F, et al. p57(Kip2) and p27(Kip1) cooperate to maintain hematopoietic stem cell quiescence through interactions with Hsc70. *Cell Stem Cell*. 2011;9(3):247-61.
153. Imanirad P, Solaimani Kartalaei P, Crisan M, Vink C, Yamada-Inagawa T, de Pater E, et al. HIF1alpha is a regulator of hematopoietic progenitor and stem cell development in hypoxic sites of the mouse embryo. *Stem Cell Res*. 2014;12(1):24-35.
154. Pedersen M, Lofstedt T, Sun J, Holmquist-Mengelbier L, Pahlman S, Ronnstrand L. Stem cell factor induces HIF-1alpha at normoxia in hematopoietic cells. *Biochem Biophys Res Commun*. 2008;377(1):98-103.
155. Kirito K, Fox N, Komatsu N, Kaushansky K. Thrombopoietin enhances expression of vascular endothelial growth factor (VEGF) in primitive hematopoietic cells through induction of HIF-1alpha. *Blood*. 2005;105(11):4258-63.
156. Loeffler D, Schroeder T. Symmetric and asymmetric activation of hematopoietic stem cells. *Curr Opin Hematol*. 2021;28(4):262-8.
157. Watanuki S, Kobayashi H, Sorimachi Y, Yamamoto M, Okamoto S, Takubo K. ATP turnover and glucose dependency in hematopoietic stem/progenitor cells are increased by proliferation and differentiation. *Biochem Biophys Res Commun*. 2019;514(1):287-94.
158. Kierans SJ, Taylor CT. Regulation of glycolysis by the hypoxia-inducible factor (HIF): implications for cellular physiology. *J Physiol*. 2021;599(1):23-37.
159. Basheeruddin M, Qausain S. Hypoxia-Inducible Factor 1-Alpha (HIF-1alpha): An Essential Regulator in Cellular Metabolic Control. *Cureus*. 2024;16(7):e63852.
160. Jang YY, Sharkis SJ. A low level of reactive oxygen species selects for primitive hematopoietic stem cells that may reside in the low-oxygenic niche. *Blood*. 2007;110(8):3056-63.

161. Lynch J, Troadec E, Fung TK, Gladysz K, Virely C, Lau PNI, et al. Hematopoietic stem cell quiescence and DNA replication dynamics maintained by the resilient beta-catenin/Hoxa9/Prmt1 axis. *Blood*. 2024;143(16):1586-98.
162. Ito K, Suda T. Metabolic requirements for the maintenance of self-renewing stem cells. *Nat Rev Mol Cell Biol*. 2014;15(4):243-56.
163. Fang H, Yu E, Liu C, Eapen C, Cheng C, Hu T. Metabolic landscape and rewiring in normal hematopoiesis, leukemia and aging. *Semin Cancer Biol*. 2025.
164. Takubo K, Nagamatsu G, Kobayashi CI, Nakamura-Ishizu A, Kobayashi H, Ikeda E, et al. Regulation of glycolysis by Pdk functions as a metabolic checkpoint for cell cycle quiescence in hematopoietic stem cells. *Cell Stem Cell*. 2013;12(1):49-61.
165. Sutendra G, Michelakis ED. Pyruvate dehydrogenase kinase as a novel therapeutic target in oncology. *Front Oncol*. 2013;3:38.
166. Zhu X, Long D, Zabalawi M, Ingram B, Yoza BK, Stacpoole PW, et al. Stimulating pyruvate dehydrogenase complex reduces itaconate levels and enhances TCA cycle anabolic bioenergetics in acutely inflamed monocytes. *J Leukoc Biol*. 2020;107(3):467-84.
167. Harris RA, Bowker-Kinley MM, Huang B, Wu P. Regulation of the activity of the pyruvate dehydrogenase complex. *Adv Enzyme Regul*. 2002;42:249-59.
168. Woolbright BL, Rajendran G, Harris RA, Taylor JA, 3rd. Metabolic Flexibility in Cancer: Targeting the Pyruvate Dehydrogenase Kinase:Pyruvate Dehydrogenase Axis. *Mol Cancer Ther*. 2019;18(10):1673-81.
169. Wierenga ATJ, Cunningham A, Erdem A, Lopera NV, Brouwers-Vos AZ, Pruis M, et al. HIF1/2-exerted control over glycolytic gene expression is not functionally relevant for glycolysis in human leukemic stem/progenitor cells. *Cancer Metab*. 2019;7:11.
170. Suda T, Takubo K, Semenza GL. Metabolic regulation of hematopoietic stem cells in the hypoxic niche. *Cell Stem Cell*. 2011;9(4):298-310.
171. Morganti C, Cabezas-Wallscheid N, Ito K. Metabolic Regulation of Hematopoietic Stem Cells. *Hemasphere*. 2022;6(7):e740.
172. Wang YH, Israelsen WJ, Lee D, Yu VWC, Jeanson NT, Clish CB, et al. Cell-state-specific metabolic dependency in hematopoiesis and leukemogenesis. *Cell*. 2014;158(6):1309-23.
173. Ito K, Hirao A, Arai F, Takubo K, Matsuoka S, Miyamoto K, et al. Reactive oxygen species act through p38 MAPK to limit the lifespan of hematopoietic stem cells. *Nat Med*. 2006;12(4):446-51.
174. Ito K, Carracedo A, Weiss D, Arai F, Ala U, Avigan DE, et al. A PML-PPAR-delta pathway for fatty acid oxidation regulates hematopoietic stem cell maintenance. *Nat Med*. 2012;18(9):1350-8.
175. DeBerardinis RJ, Thompson CB. Cellular metabolism and disease: what do metabolic outliers teach us? *Cell*. 2012;148(6):1132-44.
176. Walsh CT, Tu BP, Tang Y. Eight Kinetically Stable but Thermodynamically Activated Molecules that Power Cell Metabolism. *Chem Rev*. 2018;118(4):1460-94.
177. Kamerlin SC, Warshel A. On the energetics of ATP hydrolysis in solution. *J Phys Chem B*. 2009;113(47):15692-8.
178. Nicholls JWF, Chin JP, Williams TA, Lenton TM, O'Flaherty V, McGrath JW. On the potential roles of phosphorus in the early evolution of energy metabolism. *Front Microbiol*. 2023;14:1239189.

179. Pickart CM, Jencks WP. Energetics of the calcium-transporting ATPase. *J Biol Chem.* 1984;259(3):1629-43.
180. Ruprecht JJ, King MS, Zogg T, Aleksandrova AA, Pardon E, Crichton PG, et al. The Molecular Mechanism of Transport by the Mitochondrial ADP/ATP Carrier. *Cell.* 2019;176(3):435-47 e15.
181. Mrnjavac N, Martin WF. GTP before ATP: The energy currency at the origin of genes. *Biochim Biophys Acta Bioenerg.* 2025;1866(1):149514.
182. Treberg JR, Quinlan CL, Brand MD. Evidence for two sites of superoxide production by mitochondrial NADH-ubiquinone oxidoreductase (complex I). *J Biol Chem.* 2011;286(31):27103-10.
183. Chi H, Bhosale G, Duchen MR. Assessing the Redox Status of Mitochondria Through the NADH/FAD(2)(+) Ratio in Intact Cells. *Methods Mol Biol.* 2022;2497:313-8.
184. Bangsbo J, Gollnick PD, Graham TE, Juel C, Kiens B, Mizuno M, et al. Anaerobic energy production and O<sub>2</sub> deficit-debt relationship during exhaustive exercise in humans. *J Physiol.* 1990;422:539-59.
185. Li X, Yang Y, Zhang B, Lin X, Fu X, An Y, et al. Lactate metabolism in human health and disease. *Signal Transduct Target Ther.* 2022;7(1):305.
186. McCommis KS, Finck BN. Mitochondrial pyruvate transport: a historical perspective and future research directions. *Biochem J.* 2015;466(3):443-54.
187. Fang D, Maldonado EN. VDAC Regulation: A Mitochondrial Target to Stop Cell Proliferation. *Adv Cancer Res.* 2018;138:41-69.
188. Gray LR, Rauckhorst AJ, Taylor EB. A Method for Multiplexed Measurement of Mitochondrial Pyruvate Carrier Activity. *J Biol Chem.* 2016;291(14):7409-17.
189. Herrmann JM, Riemer J. The intermembrane space of mitochondria. *Antioxid Redox Signal.* 2010;13(9):1341-58.
190. Youle RJ, van der Bliek AM. Mitochondrial fission, fusion, and stress. *Science.* 2012;337(6098):1062-5.
191. Tan DQ, Suda T. Reactive Oxygen Species and Mitochondrial Homeostasis as Regulators of Stem Cell Fate and Function. *Antioxid Redox Signal.* 2018;29(2):149-68.
192. de Almeida MJ, Luchsinger LL, Corrigan DJ, Williams LJ, Snoeck HW. Dye-Independent Methods Reveal Elevated Mitochondrial Mass in Hematopoietic Stem Cells. *Cell Stem Cell.* 2017;21(6):725-9 e4.
193. Yao CH, Wang R, Wang Y, Kung CP, Weber JD, Patti GJ. Mitochondrial fusion supports increased oxidative phosphorylation during cell proliferation. *Elife.* 2019;8.
194. Szweczyk A, Wojtczak L. Mitochondria as a pharmacological target. *Pharmacol Rev.* 2002;54(1):101-27.
195. Khan AUH, Allende-Vega N, Gitenay D, Garaude J, Vo DN, Belkhala S, et al. Mitochondrial Complex I activity signals antioxidant response through ERK5. *Sci Rep.* 2018;8(1):7420.
196. Redza-Dutordoir M, Averill-Bates DA. Activation of apoptosis signalling pathways by reactive oxygen species. *Biochim Biophys Acta.* 2016;1863(12):2977-92.
197. Zhang W, Hu X, Shen Q, Xing D. Mitochondria-specific drug release and reactive oxygen species burst induced by polyprodrug nanoreactors can enhance chemotherapy. *Nat Commun.* 2019;10(1):1704.
198. Yan C, Li X, Wei P, Zhang X, Wang H, Chen Z, et al. Targeted mitochondrial metabolism for anti-tumor therapy. *Mitochondrion.* 2025:102073.

199. Hua X, Sun Z, Wang C, Cui H, Shan D, Tao M, et al. Pyruvate Dehydrogenase Kinase 4 Underlies the Metabolic Disorder of Cardiomyocytes in Patients With Hypertrophic Cardiomyopathy From Hypertrophy to Heart Failure. *J Am Heart Assoc.* 2025:e041401.
200. Martinez-Reyes I, Chandel NS. Mitochondrial TCA cycle metabolites control physiology and disease. *Nat Commun.* 2020;11(1):102.
201. Mitchell P. Chemiosmotic coupling in oxidative and photosynthetic phosphorylation. *Biol Rev Camb Philos Soc.* 1966;41(3):445-502.
202. Wilson DF. Oxidative phosphorylation: regulation and role in cellular and tissue metabolism. *J Physiol.* 2017;595(23):7023-38.
203. Nolfi-Donagan D, Braganza A, Shiva S. Mitochondrial electron transport chain: Oxidative phosphorylation, oxidant production, and methods of measurement. *Redox Biol.* 2020;37:101674.
204. Berry BJ, Trewin AJ, Amitrano AM, Kim M, Wojtovich AP. Use the Protonmotive Force: Mitochondrial Uncoupling and Reactive Oxygen Species. *J Mol Biol.* 2018;430(21):3873-91.
205. Yin M, O'Neill LAJ. The role of the electron transport chain in immunity. *FASEB J.* 2021;35(12):e21974.
206. Cogliati S, Cabrera-Alarcon JL, Enriquez JA. Regulation and functional role of the electron transport chain supercomplexes. *Biochem Soc Trans.* 2021;49(6):2655-68.
207. Lai Y, Zhang Y, Zhou S, Xu J, Du Z, Feng Z, et al. Structure of the human ATP synthase. *Mol Cell.* 2023;83(12):2137-47 e4.
208. Yoshida M, Muneyuki E, Hisabori T. ATP synthase--a marvellous rotary engine of the cell. *Nat Rev Mol Cell Biol.* 2001;2(9):669-77.
209. Korla K, Mitra CK. Modelling the Krebs cycle and oxidative phosphorylation. *J Biomol Struct Dyn.* 2014;32(2):242-56.
210. Shimano H, Sato R. SREBP-regulated lipid metabolism: convergent physiology - divergent pathophysiology. *Nat Rev Endocrinol.* 2017;13(12):710-30.
211. Mashek DG. Hepatic lipid droplets: A balancing act between energy storage and metabolic dysfunction in NAFLD. *Mol Metab.* 2021;50:101115.
212. Guo W, Choi JK, Kirkland JL, Corkey BE, Hamilton JA. Esterification of free fatty acids in adipocytes: a comparison between octanoate and oleate. *Biochem J.* 2000;349(Pt 2):463-71.
213. Schlaepfer IR, Joshi M. CPT1A-mediated Fat Oxidation, Mechanisms, and Therapeutic Potential. *Endocrinology.* 2020;161(2).
214. Fletcher JA, Deja S, Satapati S, Fu X, Burgess SC, Browning JD. Impaired ketogenesis and increased acetyl-CoA oxidation promote hyperglycemia in human fatty liver. *JCI Insight.* 2019;5(11).
215. Gompertz D. Phospholipids and their metabolism. *J Clin Pathol Suppl (Assoc Clin Pathol).* 1973;5:11-6.
216. Marchan R, Lesjak MS, Stewart JD, Winter R, Seeliger J, Hengstler JG. Choline-releasing glycerophosphodiesterase EDI3 links the tumor metabolome to signaling network activities. *Cell Cycle.* 2012;11(24):4499-506.
217. Coleman RA, Mashek DG. Mammalian triacylglycerol metabolism: synthesis, lipolysis, and signaling. *Chem Rev.* 2011;111(10):6359-86.
218. Olsen L, Thum E, Rohner N. Lipid metabolism in adaptation to extreme nutritional challenges. *Dev Cell.* 2021;56(10):1417-29.

219. Jeukendrup AE, Saris WH, Wagenmakers AJ. Fat metabolism during exercise: a review. Part I: fatty acid mobilization and muscle metabolism. *Int J Sports Med.* 1998;19(4):231-44.
220. Running CA, Mattes RD. Different oral sensitivities to and sensations of short-, medium-, and long-chain fatty acids in humans. *Am J Physiol Gastrointest Liver Physiol.* 2014;307(3):G381-9.
221. Stahl A, Gimeno RE, Tartaglia LA, Lodish HF. Fatty acid transport proteins: a current view of a growing family. *Trends Endocrinol Metab.* 2001;12(6):266-73.
222. Shin S. Regulation of Adipose Tissue Biology by Long-Chain Fatty Acids: Metabolic Effects and Molecular Mechanisms. *J Obes Metab Syndr.* 2022;31(2):147-60.
223. Schonfeld P, Wojtczak L. Short- and medium-chain fatty acids in energy metabolism: the cellular perspective. *J Lipid Res.* 2016;57(6):943-54.
224. He J, Zhang P, Shen L, Niu L, Tan Y, Chen L, et al. Short-Chain Fatty Acids and Their Association with Signalling Pathways in Inflammation, Glucose and Lipid Metabolism. *Int J Mol Sci.* 2020;21(17).
225. May KS, den Hartigh LJ. Gut Microbial-Derived Short Chain Fatty Acids: Impact on Adipose Tissue Physiology. *Nutrients.* 2023;15(2).
226. Airhart S, Cade WT, Jiang H, Coggan AR, Racette SB, Korenblat K, et al. A Diet Rich in Medium-Chain Fatty Acids Improves Systolic Function and Alters the Lipidomic Profile in Patients With Type 2 Diabetes: A Pilot Study. *J Clin Endocrinol Metab.* 2016;101(2):504-12.
227. Shahidi F, Zhong Y. Lipid oxidation and improving the oxidative stability. *Chem Soc Rev.* 2010;39(11):4067-79.
228. van Meer G, Voelker DR, Feigenson GW. Membrane lipids: where they are and how they behave. *Nat Rev Mol Cell Biol.* 2008;9(2):112-24.
229. Ferrari A, Tontonoz P. Nonvesicular cholesterol transport in physiology. *J Clin Invest.* 2025;135(6).
230. Miller WL, Auchus RJ. The molecular biology, biochemistry, and physiology of human steroidogenesis and its disorders. *Endocr Rev.* 2011;32(1):81-151.
231. Guo J, Chen S, Zhang Y, Liu J, Jiang L, Hu L, et al. Cholesterol metabolism: physiological regulation and diseases. *MedComm (2020).* 2024;5(2):e476.
232. Dawson PA, Karpen SJ. Intestinal transport and metabolism of bile acids. *J Lipid Res.* 2015;56(6):1085-99.
233. Eehalt R, Fullekrug J, Pohl J, Ring A, Herrmann T, Stremmel W. Translocation of long chain fatty acids across the plasma membrane--lipid rafts and fatty acid transport proteins. *Mol Cell Biochem.* 2006;284(1-2):135-40.
234. Ginsberg HN, Packard CJ, Chapman MJ, Boren J, Aguilar-Salinas CA, Aversa M, et al. Triglyceride-rich lipoproteins and their remnants: metabolic insights, role in atherosclerotic cardiovascular disease, and emerging therapeutic strategies-a consensus statement from the European Atherosclerosis Society. *Eur Heart J.* 2021;42(47):4791-806.
235. Albitar O, D'Souza CM, Adeghate EA. Effects of Lipoproteins on Metabolic Health. *Nutrients.* 2024;16(13).
236. Tiwari S, Siddiqi SA. Intracellular trafficking and secretion of VLDL. *Arterioscler Thromb Vasc Biol.* 2012;32(5):1079-86.
237. Subczynski WK, Pasenkiewicz-Gierula M, Widomska J, Mainali L, Raguz M. High Cholesterol/Low Cholesterol: Effects in Biological Membranes: A Review. *Cell Biochem Biophys.* 2017;75(3-4):369-85.

238. Yuan Y, Li P, Li J, Zhao Q, Chang Y, He X. Protein lipidation in health and disease: molecular basis, physiological function and pathological implication. *Signal Transduct Target Ther.* 2024;9(1):60.
239. Jiang H, Zhang X, Chen X, Aramsangtienchai P, Tong Z, Lin H. Protein Lipidation: Occurrence, Mechanisms, Biological Functions, and Enabling Technologies. *Chem Rev.* 2018;118(3):919-88.
240. Chen B, Sun Y, Niu J, Jarugumilli GK, Wu X. Protein Lipidation in Cell Signaling and Diseases: Function, Regulation, and Therapeutic Opportunities. *Cell Chem Biol.* 2018;25(7):817-31.
241. Krishnarjuna B, Ramamoorthy A. Detergent-Free Isolation of Membrane Proteins and Strategies to Study Them in a Near-Native Membrane Environment. *Biomolecules.* 2022;12(8).
242. Piper SJ, Johnson RM, Wootten D, Sexton PM. Membranes under the Magnetic Lens: A Dive into the Diverse World of Membrane Protein Structures Using Cryo-EM. *Chem Rev.* 2022;122(17):13989-4017.
243. Pepino MY, Kuda O, Samovski D, Abumrad NA. Structure-function of CD36 and importance of fatty acid signal transduction in fat metabolism. *Annu Rev Nutr.* 2014;34:281-303.
244. Wang J, Hao JW, Wang X, Guo H, Sun HH, Lai XY, et al. DHHC4 and DHHC5 Facilitate Fatty Acid Uptake by Palmitoylating and Targeting CD36 to the Plasma Membrane. *Cell Rep.* 2019;26(1):209-21 e5.
245. Zhao L, Zhang C, Luo X, Wang P, Zhou W, Zhong S, et al. CD36 palmitoylation disrupts free fatty acid metabolism and promotes tissue inflammation in non-alcoholic steatohepatitis. *J Hepatol.* 2018;69(3):705-17.
246. Thorne RF, Ralston KJ, de Bock CE, Mhaidat NM, Zhang XD, Boyd AW, et al. Palmitoylation of CD36/FAT regulates the rate of its post-transcriptional processing in the endoplasmic reticulum. *Biochim Biophys Acta.* 2010;1803(11):1298-307.
247. Karunakaran U, Elumalai S, Moon JS, Won KC. CD36 Signal Transduction in Metabolic Diseases: Novel Insights and Therapeutic Targeting. *Cells.* 2021;10(7).
248. Pohl J, Ring A, Korkmaz U, Eehalt R, Stremmel W. FAT/CD36-mediated long-chain fatty acid uptake in adipocytes requires plasma membrane rafts. *Mol Biol Cell.* 2005;16(1):24-31.
249. Glatz JFC, Luiken J. Dynamic role of the transmembrane glycoprotein CD36 (SR-B2) in cellular fatty acid uptake and utilization. *J Lipid Res.* 2018;59(7):1084-93.
250. Cucchi D, Camacho-Munoz D, Certo M, Pucino V, Nicolaou A, Mauro C. Fatty acids - from energy substrates to key regulators of cell survival, proliferation and effector function. *Cell Stress.* 2019;4(1):9-23.
251. Hao JW, Wang J, Guo H, Zhao YY, Sun HH, Li YF, et al. CD36 facilitates fatty acid uptake by dynamic palmitoylation-regulated endocytosis. *Nat Commun.* 2020;11(1):4765.
252. Abumrad NA, el-Maghrabi MR, Amri EZ, Lopez E, Grimaldi PA. Cloning of a rat adipocyte membrane protein implicated in binding or transport of long-chain fatty acids that is induced during preadipocyte differentiation. Homology with human CD36. *J Biol Chem.* 1993;268(24):17665-8.
253. Anderson CM, Stahl A. SLC27 fatty acid transport proteins. *Mol Aspects Med.* 2013;34(2-3):516-28.
254. Furuhashi M, Hotamisligil GS. Fatty acid-binding proteins: role in metabolic diseases and potential as drug targets. *Nat Rev Drug Discov.* 2008;7(6):489-503.

255. Schwenk RW, Holloway GP, Luiken JJ, Bonen A, Glatz JF. Fatty acid transport across the cell membrane: regulation by fatty acid transporters. *Prostaglandins Leukot Essent Fatty Acids*. 2010;82(4-6):149-54.
256. Weimar JD, DiRusso CC, Delio R, Black PN. Functional role of fatty acyl-coenzyme A synthetase in the transmembrane movement and activation of exogenous long-chain fatty acids. Amino acid residues within the ATP/AMP signature motif of *Escherichia coli* FadD are required for enzyme activity and fatty acid transport. *J Biol Chem*. 2002;277(33):29369-76.
257. Liang K. Mitochondrial CPT1A: Insights into structure, function, and basis for drug development. *Front Pharmacol*. 2023;14:1160440.
258. Roche CM, Blanch HW, Clark DS, Glass NL. Physiological role of Acyl coenzyme A synthetase homologs in lipid metabolism in *Neurospora crassa*. *Eukaryot Cell*. 2013;12(9):1244-57.
259. Joshi PR, Zierz S. Muscle Carnitine Palmitoyltransferase II (CPT II) Deficiency: A Conceptual Approach. *Molecules*. 2020;25(8).
260. Adeva-Andany MM, Carneiro-Freire N, Seco-Filgueira M, Fernandez-Fernandez C, Mourino-Bayolo D. Mitochondrial beta-oxidation of saturated fatty acids in humans. *Mitochondrion*. 2019;46:73-90.
261. Hashimoto T, Fujita T, Usuda N, Cook W, Qi C, Peters JM, et al. Peroxisomal and mitochondrial fatty acid beta-oxidation in mice nullizygous for both peroxisome proliferator-activated receptor alpha and peroxisomal fatty acyl-CoA oxidase. Genotype correlation with fatty liver phenotype. *J Biol Chem*. 1999;274(27):19228-36.
262. Modre-Osprian R, Osprian I, Tilg B, Schreier G, Weinberger KM, Graber A. Dynamic simulations on the mitochondrial fatty acid beta-oxidation network. *BMC Syst Biol*. 2009;3:2.
263. Spriet LL. New insights into the interaction of carbohydrate and fat metabolism during exercise. *Sports Med*. 2014;44 Suppl 1(Suppl 1):S87-96.
264. Pratama AM, Sharma M, Naidu S, Bommel H, Prabhuswamimath SC, Madhusudhan T, et al. Peroxisomes and PPARs: Emerging role as master regulators of cancer metabolism. *Mol Metab*. 2024;90:102044.
265. Le LTM, Thompson JR, Dang PX, Bhandari J, Alam A. Structures of the human peroxisomal fatty acid transporter ABCD1 in a lipid environment. *Commun Biol*. 2022;5(1):7.
266. Wanders RJA, Vaz FM, Waterham HR, Ferdinandusse S. Fatty Acid Oxidation in Peroxisomes: Enzymology, Metabolic Crosstalk with Other Organelles and Peroxisomal Disorders. *Adv Exp Med Biol*. 2020;1299:55-70.
267. Tannoury M, Ayoub M, Dehgane L, Nemazanyy I, Dubois K, Isabelle C, et al. ACOX1-mediated peroxisomal fatty acid oxidation contributes to metabolic reprogramming and survival in chronic lymphocytic leukemia. *Leukemia*. 2024;38(2):302-17.
268. Puchalska P, Crawford PA. Multi-dimensional Roles of Ketone Bodies in Fuel Metabolism, Signaling, and Therapeutics. *Cell Metab*. 2017;25(2):262-84.
269. Kolb H, Kempf K, Rohling M, Lenzen-Schulte M, Schloot NC, Martin S. Ketone bodies: from enemy to friend and guardian angel. *BMC Med*. 2021;19(1):313.
270. Suresh VV, Sivaprakasam S, Bhutia YD, Prasad PD, Thangaraju M, Ganapathy V. Not Just an Alternative Energy Source: Diverse Biological Functions of Ketone Bodies and Relevance of HMGCS2 to Health and Disease. *Biomolecules*. 2025;15(4).

271. Wakazono A, Fukao T, Yamaguchi S, Hori T, Orii T, Lambert M, et al. Molecular, biochemical, and clinical characterization of mitochondrial acetoacetyl-coenzyme A thiolase deficiency in two further patients. *Hum Mutat.* 1995;5(1):34-42.
272. Hegardt FG. Mitochondrial 3-hydroxy-3-methylglutaryl-CoA synthase: a control enzyme in ketogenesis. *Biochem J.* 1999;338 ( Pt 3)(Pt 3):569-82.
273. Qi J, Gan L, Fang J, Zhang J, Yu X, Guo H, et al. Beta-Hydroxybutyrate: A Dual Function Molecular and Immunological Barrier Function Regulator. *Front Immunol.* 2022;13:805881.
274. Newman JC, Verdin E. Ketone bodies as signaling metabolites. *Trends Endocrinol Metab.* 2014;25(1):42-52.
275. Metallo CM, Vander Heiden MG. Understanding metabolic regulation and its influence on cell physiology. *Mol Cell.* 2013;49(3):388-98.
276. Zhang L, Wang X, Chen XW. The biogenesis and transport of triglyceride-rich lipoproteins. *Trends Endocrinol Metab.* 2024.
277. Hodson L, Gunn PJ. The regulation of hepatic fatty acid synthesis and partitioning: the effect of nutritional state. *Nat Rev Endocrinol.* 2019;15(12):689-700.
278. Fatehi-Hassanabad Z, Chan CB. Transcriptional regulation of lipid metabolism by fatty acids: a key determinant of pancreatic beta-cell function. *Nutr Metab (Lond).* 2005;2(1):1.
279. Tontonoz P, Mangelsdorf DJ. Liver X receptor signaling pathways in cardiovascular disease. *Mol Endocrinol.* 2003;17(6):985-93.
280. Montaigne D, Butruille L, Staels B. PPAR control of metabolism and cardiovascular functions. *Nat Rev Cardiol.* 2021;18(12):809-23.
281. Kleiner S, Nguyen-Tran V, Bare O, Huang X, Spiegelman B, Wu Z. PPARdelta agonism activates fatty acid oxidation via PGC-1alpha but does not increase mitochondrial gene expression and function. *J Biol Chem.* 2009;284(28):18624-33.
282. Poulsen L, Siersbaek M, Mandrup S. PPARs: fatty acid sensors controlling metabolism. *Semin Cell Dev Biol.* 2012;23(6):631-9.
283. Harmon GS, Lam MT, Glass CK. PPARs and lipid ligands in inflammation and metabolism. *Chem Rev.* 2011;111(10):6321-40.
284. Ahmadian M, Suh JM, Hah N, Liddle C, Atkins AR, Downes M, et al. PPARgamma signaling and metabolism: the good, the bad and the future. *Nat Med.* 2013;19(5):557-66.
285. Latruffe N, Cherkaoui Malki M, Nicolas-Frances V, Jannin B, Clemencet MC, Hansmannel F, et al. Peroxisome-proliferator-activated receptors as physiological sensors of fatty acid metabolism: molecular regulation in peroxisomes. *Biochem Soc Trans.* 2001;29(Pt 2):305-9.
286. Evans RM, Barish GD, Wang YX. PPARs and the complex journey to obesity. *Nat Med.* 2004;10(4):355-61.
287. Mandard S, Muller M, Kersten S. Peroxisome proliferator-activated receptor alpha target genes. *Cell Mol Life Sci.* 2004;61(4):393-416.
288. Chakravarthy MV, Zhu Y, Lopez M, Yin L, Wozniak DF, Coleman T, et al. Brain fatty acid synthase activates PPARalpha to maintain energy homeostasis. *J Clin Invest.* 2007;117(9):2539-52.
289. Lefebvre P, Chinetti G, Fruchart JC, Staels B. Sorting out the roles of PPAR alpha in energy metabolism and vascular homeostasis. *J Clin Invest.* 2006;116(3):571-80.

290. Grygiel-Gorniak B. Peroxisome proliferator-activated receptors and their ligands: nutritional and clinical implications--a review. *Nutr J.* 2014;13:17.
291. Nakagawa H. Lipogenesis and MASLD: re-thinking the role of SREBPs. *Arch Toxicol.* 2025;99(6):2299-312.
292. Barish GD, Narkar VA, Evans RM. PPAR delta: a dagger in the heart of the metabolic syndrome. *J Clin Invest.* 2006;116(3):590-7.
293. Barish GD, Atkins AR, Downes M, Olson P, Chong LW, Nelson M, et al. PPARdelta regulates multiple proinflammatory pathways to suppress atherosclerosis. *Proc Natl Acad Sci U S A.* 2008;105(11):4271-6.
294. Malodobra-Mazur M, Oldakowska M, Dobosz T. Exploring PPAR Gamma and PPAR Alpha's Regulation Role in Metabolism via Epigenetics Mechanism. *Biomolecules.* 2024;14(11).
295. Ikeda J, Ichiki T, Takahara Y, Kojima H, Sankoda C, Kitamoto S, et al. PPARgamma Agonists Attenuate Palmitate-Induced ER Stress through Up-Regulation of SCD-1 in Macrophages. *PLoS One.* 2015;10(6):e0128546.
296. Tontonoz P, Spiegelman BM. Fat and beyond: the diverse biology of PPARgamma. *Annu Rev Biochem.* 2008;77:289-312.
297. Ye J, DeBose-Boyd RA. Regulation of cholesterol and fatty acid synthesis. *Cold Spring Harb Perspect Biol.* 2011;3(7).
298. Horton JD, Goldstein JL, Brown MS. SREBPs: activators of the complete program of cholesterol and fatty acid synthesis in the liver. *J Clin Invest.* 2002;109(9):1125-31.
299. DeBose-Boyd RA, Ye J. SREBPs in Lipid Metabolism, Insulin Signaling, and Beyond. *Trends Biochem Sci.* 2018;43(5):358-68.
300. Li N, Li X, Ding Y, Liu X, Diggie K, Kisseleva T, et al. SREBP Regulation of Lipid Metabolism in Liver Disease, and Therapeutic Strategies. *Biomedicines.* 2023;11(12).
301. Kim HJ, Miyazaki M, Man WC, Ntambi JM. Sterol regulatory element-binding proteins (SREBPs) as regulators of lipid metabolism: polyunsaturated fatty acids oppose cholesterol-mediated induction of SREBP-1 maturation. *Ann N Y Acad Sci.* 2002;967:34-42.
302. Laurencikiene J, Ryden M. Liver X receptors and fat cell metabolism. *Int J Obes (Lond).* 2012;36(12):1494-502.
303. Bilotta MT, Petillo S, Santoni A, Cippitelli M. Liver X Receptors: Regulators of Cholesterol Metabolism, Inflammation, Autoimmunity, and Cancer. *Front Immunol.* 2020;11:584303.
304. Joseph SB, Laffitte BA, Patel PH, Watson MA, Matsukuma KE, Walczak R, et al. Direct and indirect mechanisms for regulation of fatty acid synthase gene expression by liver X receptors. *J Biol Chem.* 2002;277(13):11019-25.
305. Rong S, Cortes VA, Rashid S, Anderson NN, McDonald JG, Liang G, et al. Expression of SREBP-1c Requires SREBP-2-mediated Generation of a Sterol Ligand for LXR in Livers of Mice. *Elife.* 2017;6.
306. Peet DJ, Turley SD, Ma W, Janowski BA, Lobaccaro JM, Hammer RE, et al. Cholesterol and bile acid metabolism are impaired in mice lacking the nuclear oxysterol receptor LXR alpha. *Cell.* 1998;93(5):693-704.
307. Li B, Cai SY, Boyer JL. The role of the retinoid receptor, RAR/RXR heterodimer, in liver physiology. *Biochim Biophys Acta Mol Basis Dis.* 2021;1867(5):166085.
308. Li Y, Wong K, Walsh K, Gao B, Zang M. Retinoic acid receptor beta stimulates hepatic induction of fibroblast growth factor 21 to promote fatty acid oxidation and

- control whole-body energy homeostasis in mice. *J Biol Chem.* 2013;288(15):10490-504.
309. Szczepanska E, Gietka-Czernel M. FGF21: A Novel Regulator of Glucose and Lipid Metabolism and Whole-Body Energy Balance. *Horm Metab Res.* 2022;54(4):203-11.
310. Hormaechea-Agulla D, Le DT, King KY. Common Sources of Inflammation and Their Impact on Hematopoietic Stem Cell Biology. *Curr Stem Cell Rep.* 2020;6(3):96-107.
311. Forte E. A cell-intrinsic regulator of emergency hematopoiesis. *Nat Cardiovasc Res.* 2023;2(1):8.
312. Sohail I, Ghosh S, Mukundan S, Zelewski S, Khan MN. Role of Inflammatory Risk Factors in the Pathogenesis of *Streptococcus pneumoniae*. *Front Immunol.* 2018;9:2275.
313. Daigneault M, De Silva TI, Bewley MA, Preston JA, Marriott HM, Mitchell AM, et al. Monocytes regulate the mechanism of T-cell death by inducing Fas-mediated apoptosis during bacterial infection. *PLoS Pathog.* 2012;8(7):e1002814.
314. Fiorcari S, Strati P, Dondi E. Editorial: Tumor microenvironment and hematological malignancies: new evidences and new questions. *Front Immunol.* 2024;15:1407981.
315. Howell DA, Smith AG, Jack A, Patmore R, Macleod U, Mironska E, et al. Time-to-diagnosis and symptoms of myeloma, lymphomas and leukaemias: a report from the Haematological Malignancy Research Network. *BMC Hematol.* 2013;13(1):9.
316. Buettner R, Nguyen LXT, Morales C, Chen MH, Wu X, Chen LS, et al. Targeting the metabolic vulnerability of acute myeloid leukemia blasts with a combination of venetoclax and 8-chloro-adenosine. *J Hematol Oncol.* 2021;14(1):70.
317. Sriskanthadevan S, Jeyaraju DV, Chung TE, Prabha S, Xu W, Skrtic M, et al. AML cells have low spare reserve capacity in their respiratory chain that renders them susceptible to oxidative metabolic stress. *Blood.* 2015;125(13):2120-30.
318. Jones CL, Inguva A, Jordan CT. Targeting Energy Metabolism in Cancer Stem Cells: Progress and Challenges in Leukemia and Solid Tumors. *Cell Stem Cell.* 2021;28(3):378-93.
319. Kuntz EM, Baquero P, Michie AM, Dunn K, Tardito S, Holyoake TL, et al. Targeting mitochondrial oxidative phosphorylation eradicates therapy-resistant chronic myeloid leukemia stem cells. *Nat Med.* 2017;23(10):1234-40.
320. Herst PM, Howman RA, Neeson PJ, Berridge MV, Ritchie DS. The level of glycolytic metabolism in acute myeloid leukemia blasts at diagnosis is prognostic for clinical outcome. *J Leukoc Biol.* 2011;89(1):51-5.
321. Chen WL, Wang JH, Zhao AH, Xu X, Wang YH, Chen TL, et al. A distinct glucose metabolism signature of acute myeloid leukemia with prognostic value. *Blood.* 2014;124(10):1645-54.
322. Yang SY, Park SK, Kang HR, Kim HL, Lee EK, Kwon SH. Haematological cancer versus solid tumour end-of-life care: a longitudinal data analysis. *BMJ Support Palliat Care.* 2020.
323. Shao L, Wang Y, Chang J, Luo Y, Meng A, Zhou D. Hematopoietic stem cell senescence and cancer therapy-induced long-term bone marrow injury. *Transl Cancer Res.* 2013;2(5):397-411.

324. Testa NG, Hendry JH, Molineux G. Long-term bone marrow damage in experimental systems and in patients after radiation or chemotherapy. *Anticancer Res.* 1985;5(1):101-10.
325. Shao L, Luo Y, Zhou D. Hematopoietic stem cell injury induced by ionizing radiation. *Antioxid Redox Signal.* 2014;20(9):1447-62.
326. Zhang Y, Chen X, Wang X, Chen J, Du C, Wang J, et al. Insights into ionizing radiation-induced bone marrow hematopoietic stem cell injury. *Stem Cell Res Ther.* 2024;15(1):222.
327. Mohrin M, Bourke E, Alexander D, Warr MR, Barry-Holson K, Le Beau MM, et al. Hematopoietic stem cell quiescence promotes error-prone DNA repair and mutagenesis. *Cell Stem Cell.* 2010;7(2):174-85.
328. Qing Y, Wang Z, Bunting KD, Gerson SL. Bcl2 overexpression rescues the hematopoietic stem cell defects in Ku70-deficient mice by restoration of quiescence. *Blood.* 2014;123(7):1002-11.
329. Gencheva M, Hare I, Kurian S, Fortney J, Piktel D, Wysolmerski R, et al. Bone marrow osteoblast vulnerability to chemotherapy. *Eur J Haematol.* 2013;90(6):469-78.
330. Zhou BO, Yu H, Yue R, Zhao Z, Rios JJ, Naveiras O, et al. Bone marrow adipocytes promote the regeneration of stem cells and haematopoiesis by secreting SCF. *Nat Cell Biol.* 2017;19(8):891-903.
331. Batsivari A, Haltalli MLR, Passaro D, Pospori C, Lo Celso C, Bonnet D. Dynamic responses of the haematopoietic stem cell niche to diverse stresses. *Nat Cell Biol.* 2020;22(1):7-17.
332. Lucas D, Scheiermann C, Chow A, Kunisaki Y, Bruns I, Barrick C, et al. Chemotherapy-induced bone marrow nerve injury impairs hematopoietic regeneration. *Nat Med.* 2013;19(6):695-703.
333. Hawkes N. Cancer survival data emphasise importance of early diagnosis. *BMJ.* 2019;364:l408.
334. He S, Roberts PJ, Sorrentino JA, Bisi JE, Storrie-White H, Tiessen RG, et al. Transient CDK4/6 inhibition protects hematopoietic stem cells from chemotherapy-induced exhaustion. *Sci Transl Med.* 2017;9(387).
335. Zhao Y, Zhan Y, Burke KA, Anderson WF. Soluble factor(s) from bone marrow cells can rescue lethally irradiated mice by protecting endogenous hematopoietic stem cells. *Exp Hematol.* 2005;33(4):428-34.
336. Lee SH, Hsu TC, Lee MG, Chao CC, Lee WC, Lai CC, et al. Nationwide Trend of Sepsis: A Comparison Among Octogenarians, Elderly, and Young Adults. *Crit Care Med.* 2018;46(6):926-34.
337. Trevisan C, Noale M, Amidei CB, Ferroni E, Basso C, Fedeli U, et al. Frailty and the risk of infection-related hospitalizations in older age: Differences by sex. *Maturitas.* 2023;168:1-6.
338. Secondary Care Open Data and Publications NE. Hospital Admitted Patient Care Activity, 2022-23. Online: NHS Digital; 2023.
339. Filippi MD. The multifaceted role of mitochondria in HSC fate decisions: energy and beyond. *Exp Hematol.* 2023;128:19-29.
340. Mansell E, Sigurdsson V, Deltcheva E, Brown J, James C, Miharada K, et al. Mitochondrial Potentiation Ameliorates Age-Related Heterogeneity in Hematopoietic Stem Cell Function. *Cell Stem Cell.* 2021;28(2):241-56 e6.

341. Karimnia N, Harris J, Heazlewood SY, Cao B, Nilsson SK. Metabolic regulation of aged hematopoietic stem cells: key players and mechanisms. *Exp Hematol.* 2023;128:2-9.
342. Filippi MD, Ghaffari S. Mitochondria in the maintenance of hematopoietic stem cells: new perspectives and opportunities. *Blood.* 2019;133(18):1943-52.
343. Chambers SM, Shaw CA, Gatza C, Fisk CJ, Donehower LA, Goodell MA. Aging hematopoietic stem cells decline in function and exhibit epigenetic dysregulation. *PLoS Biol.* 2007;5(8):e201.
344. Dykstra B, Olthof S, Schreuder J, Ritsema M, de Haan G. Clonal analysis reveals multiple functional defects of aged murine hematopoietic stem cells. *J Exp Med.* 2011;208(13):2691-703.
345. Si-Tahar M, Touqui L, Chignard M. Innate immunity and inflammation--two facets of the same anti-infectious reaction. *Clin Exp Immunol.* 2009;156(2):194-8.
346. Chen R, Zou J, Chen J, Zhong X, Kang R, Tang D. Pattern recognition receptors: function, regulation and therapeutic potential. *Signal Transduct Target Ther.* 2025;10(1):216.
347. Cui J, Chen Y, Wang HY, Wang RF. Mechanisms and pathways of innate immune activation and regulation in health and cancer. *Hum Vaccin Immunother.* 2014;10(11):3270-85.
348. Herb M, Gluschko A, Schramm M. LC3-associated phagocytosis - The highway to hell for phagocytosed microbes. *Semin Cell Dev Biol.* 2020;101:68-76.
349. Freeman SA, Grinstein S. Phagocytosis: receptors, signal integration, and the cytoskeleton. *Immunol Rev.* 2014;262(1):193-215.
350. Levin R, Grinstein S, Canton J. The life cycle of phagosomes: formation, maturation, and resolution. *Immunol Rev.* 2016;273(1):156-79.
351. Canton J. Phagosome maturation in polarized macrophages. *J Leukoc Biol.* 2014;96(5):729-38.
352. Inomata M, Xu S, Chandra P, Meydani SN, Takemura G, Philips JA, et al. Macrophage LC3-associated phagocytosis is an immune defense against *Streptococcus pneumoniae* that diminishes with host aging. *Proc Natl Acad Sci U S A.* 2020;117(52):33561-9.
353. Shachar I, Karin N. The dual roles of inflammatory cytokines and chemokines in the regulation of autoimmune diseases and their clinical implications. *J Leukoc Biol.* 2013;93(1):51-61.
354. Clark R, Kupper T. Old meets new: the interaction between innate and adaptive immunity. *J Invest Dermatol.* 2005;125(4):629-37.
355. Mittal M, Siddiqui MR, Tran K, Reddy SP, Malik AB. Reactive oxygen species in inflammation and tissue injury. *Antioxid Redox Signal.* 2014;20(7):1126-67.
356. Lim JJ, Grinstein S, Roth Z. Diversity and Versatility of Phagocytosis: Roles in Innate Immunity, Tissue Remodeling, and Homeostasis. *Front Cell Infect Microbiol.* 2017;7:191.
357. Haltalli MLR, Watcham S, Wilson NK, Eilers K, Lipien A, Ang H, et al. Manipulating niche composition limits damage to haematopoietic stem cells during *Plasmodium* infection. *Nat Cell Biol.* 2020;22(12):1399-410.
358. Vainieri ML, Blagborough AM, MacLean AL, Haltalli ML, Ruivo N, Fletcher HA, et al. Systematic tracking of altered haematopoiesis during sporozoite-mediated malaria development reveals multiple response points. *Open Biol.* 2016;6(6).

359. Rashidi NM, Scott MK, Scherf N, Krinner A, Kalchschmidt JS, Gounaris K, et al. In vivo time-lapse imaging shows diverse niche engagement by quiescent and naturally activated hematopoietic stem cells. *Blood*. 2014;124(1):79-83.
360. Luo R, Yao Y, Chen Z, Sun X. An examination of the LPS-TLR4 immune response through the analysis of molecular structures and protein-protein interactions. *Cell Commun Signal*. 2025;23(1):142.
361. Boettcher S, Gerosa RC, Radpour R, Bauer J, Ampenberger F, Heikenwalder M, et al. Endothelial cells translate pathogen signals into G-CSF-driven emergency granulopoiesis. *Blood*. 2014;124(9):1393-403.
362. Andonegui G, Zhou H, Bullard D, Kelly MM, Mullaly SC, McDonald B, et al. Mice that exclusively express TLR4 on endothelial cells can efficiently clear a lethal systemic Gram-negative bacterial infection. *J Clin Invest*. 2009;119(7):1921-30.
363. Kolaczowska E, Kubes P. Neutrophil recruitment and function in health and inflammation. *Nat Rev Immunol*. 2013;13(3):159-75.
364. Paudel S, Ghimire L, Jin L, Jeansonne D, Jeyaseelan S. Regulation of emergency granulopoiesis during infection. *Front Immunol*. 2022;13:961601.
365. Westerterp M, Gourion-Arsiquaud S, Murphy AJ, Shih A, Cremers S, Levine RL, et al. Regulation of hematopoietic stem and progenitor cell mobilization by cholesterol efflux pathways. *Cell Stem Cell*. 2012;11(2):195-206.
366. Gregory CD, Devitt A. The macrophage and the apoptotic cell: an innate immune interaction viewed simplistically? *Immunology*. 2004;113(1):1-14.
367. Schuettpeitz LG, Borgerding JN, Christopher MJ, Gopalan PK, Romine MP, Herman AC, et al. G-CSF regulates hematopoietic stem cell activity, in part, through activation of Toll-like receptor signaling. *Leukemia*. 2014;28(9):1851-60.
368. Gonzalez-Fernandez C, Basauri A, Fallanza M, Bringas E, Oostenbrink C, Ortiz I. Fighting Against Bacterial Lipopolysaccharide-Caused Infections through Molecular Dynamics Simulations: A Review. *J Chem Inf Model*. 2021;61(10):4839-51.
369. Maldonado RF, Sa-Correia I, Valvano MA. Lipopolysaccharide modification in Gram-negative bacteria during chronic infection. *FEMS Microbiol Rev*. 2016;40(4):480-93.
370. Park BS, Lee JO. Recognition of lipopolysaccharide pattern by TLR4 complexes. *Exp Mol Med*. 2013;45(12):e66.
371. Tsukamoto H, Takeuchi S, Kubota K, Kobayashi Y, Kozakai S, Ukai I, et al. Lipopolysaccharide (LPS)-binding protein stimulates CD14-dependent Toll-like receptor 4 internalization and LPS-induced TBK1-IKK $\epsilon$ -IRF3 axis activation. *J Biol Chem*. 2018;293(26):10186-201.
372. Kawai T, Akira S. Signaling to NF-kappaB by Toll-like receptors. *Trends Mol Med*. 2007;13(11):460-9.
373. Kwak HJ, Liu P, Bajrami B, Xu Y, Park SY, Nombela-Arrieta C, et al. Myeloid cell-derived reactive oxygen species externally regulate the proliferation of myeloid progenitors in emergency granulopoiesis. *Immunity*. 2015;42(1):159-71.
374. Valdovinos-Flores C, Limon-Pacheco JH, Leon-Rodriguez R, Petrosyan P, Garza-Lombo C, Gonsebatt ME. Systemic L-Buthionine -S-R-Sulfoximine Treatment Increases Plasma NGF and Upregulates L-cys/L-cys2 Transporter and gamma-Glutamylcysteine Ligase mRNAs Through the NGF/TrkA/Akt/Nrf2 Pathway in the Striatum. *Front Cell Neurosci*. 2019;13:325.
375. Mistry JJ, Marlein CR, Moore JA, Hellmich C, Wojtowicz EE, Smith JGW, et al. ROS-mediated PI3K activation drives mitochondrial transfer from stromal cells to

- hematopoietic stem cells in response to infection. *Proc Natl Acad Sci U S A*. 2019;116(49):24610-9.
376. Wang M, Feng J, Zhou D, Wang J. Bacterial lipopolysaccharide-induced endothelial activation and dysfunction: a new predictive and therapeutic paradigm for sepsis. *Eur J Med Res*. 2023;28(1):339.
377. Salauddin M, Bhattacharyya D, Samanta I, Saha S, Xue M, Hossain MG, et al. Role of TLRs as signaling cascades to combat infectious diseases: a review. *Cell Mol Life Sci*. 2025;82(1):122.
378. Nazir J, Manzoor T, Saleem A, Gani U, Bhat SS, Khan S, et al. Combatting Salmonella: a focus on antimicrobial resistance and the need for effective vaccination. *BMC Infect Dis*. 2025;25(1):84.
379. Won G, Lee JH. Salmonella Typhimurium, the major causative agent of foodborne illness inactivated by a phage lysis system provides effective protection against lethal challenge by induction of robust cell-mediated immune responses and activation of dendritic cells. *Vet Res*. 2017;48(1):66.
380. Stecher B, Robbiani R, Walker AW, Westendorf AM, Barthel M, Kremer M, et al. Salmonella enterica serovar typhimurium exploits inflammation to compete with the intestinal microbiota. *PLoS Biol*. 2007;5(10):2177-89.
381. Winter SE, Thiennimitr P, Winter MG, Butler BP, Huseby DL, Crawford RW, et al. Gut inflammation provides a respiratory electron acceptor for Salmonella. *Nature*. 2010;467(7314):426-9.
382. Zeng MY, Inohara N, Nunez G. Mechanisms of inflammation-driven bacterial dysbiosis in the gut. *Mucosal Immunol*. 2017;10(1):18-26.
383. Dos Santos AMP, Ferrari RG, Conte-Junior CA. Type three secretion system in Salmonella Typhimurium: the key to infection. *Genes Genomics*. 2020;42(5):495-506.
384. Medzhitov R. Toll-like receptors and innate immunity. *Nat Rev Immunol*. 2001;1(2):135-45.
385. Broz P, Ohlson MB, Monack DM. Innate immune response to Salmonella typhimurium, a model enteric pathogen. *Gut Microbes*. 2012;3(2):62-70.
386. Galan JE. Salmonella Typhimurium and inflammation: a pathogen-centric affair. *Nat Rev Microbiol*. 2021;19(11):716-25.
387. Patel S, McCormick BA. Mucosal Inflammatory Response to Salmonella typhimurium Infection. *Front Immunol*. 2014;5:311.
388. Ahmad M, Aduru SV, Smith RP, Zhao Z, Lopatkin AJ. The role of bacterial metabolism in antimicrobial resistance. *Nat Rev Microbiol*. 2025.
389. Acierno C, Barletta F, Nevola R, Rinaldi L, Sasso FC, Adinolfi LE, et al. Metabolic Rewiring of Bacterial Pathogens in Response to Antibiotic Pressure-A Molecular Perspective. *Int J Mol Sci*. 2025;26(12).
390. Kohanski MA, Dwyer DJ, Collins JJ. How antibiotics kill bacteria: from targets to networks. *Nat Rev Microbiol*. 2010;8(6):423-35.
391. Chen L, Deng H, Cui H, Fang J, Zuo Z, Deng J, et al. Inflammatory responses and inflammation-associated diseases in organs. *Oncotarget*. 2018;9(6):7204-18.
392. Favier AL, Nikovics K. Molecular and Cellular Mechanisms of Inflammation and Tissue Regeneration. *Biomedicines*. 2023;11(5).
393. Antoniak S, Mackman N. Multiple roles of the coagulation protease cascade during virus infection. *Blood*. 2014;123(17):2605-13.
394. Weavers H, Martin P. The cell biology of inflammation: From common traits to remarkable immunological adaptations. *J Cell Biol*. 2020;219(7).

395. Arredouani MS, Yang Z, Imrich A, Ning Y, Qin G, Kobzik L. The macrophage scavenger receptor SR-AI/II and lung defense against pneumococci and particles. *Am J Respir Cell Mol Biol.* 2006;35(4):474-8.
396. Pietras EM. Inflammation: a key regulator of hematopoietic stem cell fate in health and disease. *Blood.* 2017;130(15):1693-8.
397. Caiado F, Pietras EM, Manz MG. Inflammation as a regulator of hematopoietic stem cell function in disease, aging, and clonal selection. *J Exp Med.* 2021;218(7).
398. Yamashita M, Passegue E. TNF-alpha Coordinates Hematopoietic Stem Cell Survival and Myeloid Regeneration. *Cell Stem Cell.* 2019;25(3):357-72 e7.
399. Hemmati S, Sinclair T, Tong M, Bartholdy B, Okabe RO, Ames K, et al. PI3 kinase alpha and delta promote hematopoietic stem cell activation. *JCI Insight.* 2019;5(13).
400. Qing H, Desrouleaux R, Israni-Winger K, Mineur YS, Fogelman N, Zhang C, et al. Origin and Function of Stress-Induced IL-6 in Murine Models. *Cell.* 2020;182(6):1660.
401. Park SD, Saunders AS, Reidy MA, Bender DE, Clifton S, Morris KT. A review of granulocyte colony-stimulating factor receptor signaling and regulation with implications for cancer. *Front Oncol.* 2022;12:932608.
402. Edmeads JG. Migraine--better understanding, better treatment? *Eur Neurol.* 1996;36 Suppl 2:1-3.
403. Hirche C, Frenz T, Haas SF, Doring M, Borst K, Tegtmeyer PK, et al. Systemic Virus Infections Differentially Modulate Cell Cycle State and Functionality of Long-Term Hematopoietic Stem Cells In Vivo. *Cell Rep.* 2017;19(11):2345-56.
404. Pietras EM, Lakshminarasimhan R, Techner JM, Fong S, Flach J, Binnewies M, et al. Re-entry into quiescence protects hematopoietic stem cells from the killing effect of chronic exposure to type I interferons. *J Exp Med.* 2014;211(2):245-62.
405. Dang EV, McDonald JG, Russell DW, Cyster JG. Oxysterol Restraint of Cholesterol Synthesis Prevents AIM2 Inflammasome Activation. *Cell.* 2017;171(5):1057-71 e11.
406. Rathinam VA, Fitzgerald KA. Inflammasome Complexes: Emerging Mechanisms and Effector Functions. *Cell.* 2016;165(4):792-800.
407. King KY, Goodell MA. Inflammatory modulation of HSCs: viewing the HSC as a foundation for the immune response. *Nat Rev Immunol.* 2011;11(10):685-92.
408. Liao W, Zai X, Zhang J, Xu J. Hematopoietic stem cell state and fate in trained immunity. *Cell Commun Signal.* 2025;23(1):182.
409. Chen Z, Guo Q, Song G, Hou Y. Molecular regulation of hematopoietic stem cell quiescence. *Cell Mol Life Sci.* 2022;79(4):218.
410. Piccoli C, Agriesti F, Scrima R, Falzetti F, Di Ianni M, Capitanio N. To breathe or not to breathe: the haematopoietic stem/progenitor cells dilemma. *Br J Pharmacol.* 2013;169(8):1652-71.
411. Maryanovich M, Zaltsman Y, Ruggiero A, Goldman A, Shachnai L, Zaidman SL, et al. An MTCH2 pathway repressing mitochondria metabolism regulates haematopoietic stem cell fate. *Nat Commun.* 2015;6:7901.
412. Umemoto T, Hashimoto M, Matsumura T, Nakamura-Ishizu A, Suda T. Ca(2+)-mitochondria axis drives cell division in hematopoietic stem cells. *J Exp Med.* 2018;215(8):2097-113.

413. Hinge A, He J, Bartram J, Javier J, Xu J, Fjellman E, et al. Asymmetrically Segregated Mitochondria Provide Cellular Memory of Hematopoietic Stem Cell Replicative History and Drive HSC Attrition. *Cell Stem Cell*. 2020;26(3):420-30 e6.
414. Spees JL, Olson SD, Whitney MJ, Prockop DJ. Mitochondrial transfer between cells can rescue aerobic respiration. *Proc Natl Acad Sci U S A*. 2006;103(5):1283-8.
415. Liu L, Li Y, Chen G, Chen Q. Crosstalk between mitochondrial biogenesis and mitophagy to maintain mitochondrial homeostasis. *J Biomed Sci*. 2023;30(1):86.
416. Liao Y, Octaviani S, Tian Z, Wang SR, Huang C, Huang J. Mitochondrial quality control in hematopoietic stem cells: mechanisms, implications, and therapeutic opportunities. *Stem Cell Res Ther*. 2025;16(1):180.
417. Lee HC, Yin PH, Lu CY, Chi CW, Wei YH. Increase of mitochondria and mitochondrial DNA in response to oxidative stress in human cells. *Biochem J*. 2000;348 Pt 2(Pt 2):425-32.
418. Kim JH, Choi TG, Park S, Yun HR, Nguyen NNY, Jo YH, et al. Mitochondrial ROS-derived PTEN oxidation activates PI3K pathway for mTOR-induced myogenic autophagy. *Cell Death Differ*. 2018;25(11):1921-37.
419. Zeng Y, Riquelme MA, Hua R, Zhang J, Acosta FM, Gu S, et al. Mechanosensitive piezo1 calcium channel activates connexin 43 hemichannels through PI3K signaling pathway in bone. *Cell Biosci*. 2022;12(1):191.
420. Meng Y, Pospiech M, Ali A, Chandwani R, Vergel M, Onyemaechi S, et al. Deletion of CD36 exhibits limited impact on normal hematopoiesis and the leukemia microenvironment. *Cell Mol Biol Lett*. 2023;28(1):45.
421. Mistry JJ, Hellmich C, Moore JA, Jibril A, Macaulay I, Moreno-Gonzalez M, et al. Free fatty-acid transport via CD36 drives beta-oxidation-mediated hematopoietic stem cell response to infection. *Nat Commun*. 2021;12(1):7130.
422. Glatz JF, Nabben M, Heather LC, Bonen A, Luiken JJ. Regulation of the subcellular trafficking of CD36, a major determinant of cardiac fatty acid utilization. *Biochim Biophys Acta*. 2016;1861(10):1461-71.
423. Marechal L, Laviolette M, Rodrigue-Way A, Sow B, Brochu M, Caron V, et al. The CD36-PPARgamma Pathway in Metabolic Disorders. *Int J Mol Sci*. 2018;19(5).
424. Paumelle R, Haas JT, Hennuyer N, Bauge E, Deleye Y, Mesotten D, et al. Hepatic PPARalpha is critical in the metabolic adaptation to sepsis. *J Hepatol*. 2019;70(5):963-73.
425. Motojima K, Passilly P, Peters JM, Gonzalez FJ, Latruffe N. Expression of putative fatty acid transporter genes are regulated by peroxisome proliferator-activated receptor alpha and gamma activators in a tissue- and inducer-specific manner. *J Biol Chem*. 1998;273(27):16710-4.
426. Lim HJ, Lee S, Lee KS, Park JH, Jang Y, Lee EJ, et al. PPARgamma activation induces CD36 expression and stimulates foam cell like changes in rVSMCs. *Prostaglandins Other Lipid Mediat*. 2006;80(3-4):165-74.
427. Li J, Bai J, Pham VT, Hashimoto M, Sezaki M, Shi Q, et al. Loss of Cpt1a results in elevated glucose-fueled mitochondrial oxidative phosphorylation and defective hematopoietic stem cells. *J Clin Invest*. 2025;135(5).
428. Hellmich C, Wojtowicz E, Moore JA, Mistry JJ, Jibril A, Johnson BB, et al. p16INK4A-dependent senescence in the bone marrow niche drives age-related metabolic changes of hematopoietic progenitors. *Blood Adv*. 2023;7(2):256-68.
429. Sun N, Youle RJ, Finkel T. The Mitochondrial Basis of Aging. *Mol Cell*. 2016;61(5):654-66.

430. Luo X, Li Y, Yang P, Chen Y, Wei L, Yu T, et al. Obesity induces preadipocyte CD36 expression promoting inflammation via the disruption of lysosomal calcium homeostasis and lysosome function. *EBioMedicine*. 2020;56:102797.
431. Cai L, Wang Z, Ji A, Meyer JM, van der Westhuyzen DR. Scavenger receptor CD36 expression contributes to adipose tissue inflammation and cell death in diet-induced obesity. *PLoS One*. 2012;7(5):e36785.
432. Lee JM, Govindarajah V, Goddard B, Hinge A, Muench DE, Filippi MD, et al. Obesity alters the long-term fitness of the hematopoietic stem cell compartment through modulation of Gfi1 expression. *J Exp Med*. 2018;215(2):627-44.
433. Borcherding N, Jia W, Giwa R, Field RL, Moley JR, Kopecky BJ, et al. Dietary lipids inhibit mitochondria transfer to macrophages to divert adipocyte-derived mitochondria into the blood. *Cell Metab*. 2022;34(10):1499-513 e8.
434. Maher M, Diesch J, Casquero R, Buschbeck M. Epigenetic-Transcriptional Regulation of Fatty Acid Metabolism and Its Alterations in Leukaemia. *Front Genet*. 2018;9:405.
435. Zhang J, Ruan K, Chu Z, Wang X, Gu Y, Jin H, et al. Reprogramming of fatty acid metabolism: a hidden force regulating the occurrence and progression of cholangiocarcinoma. *Cell Death Discov*. 2025;11(1):72.
436. Hodson L. Hepatic fatty acid synthesis and partitioning: the effect of metabolic and nutritional state. *Proc Nutr Soc*. 2019;78(1):126-34.
437. Petrus P, Arner P. The impact of dietary fatty acids on human adipose tissue. *Proc Nutr Soc*. 2020;79(1):42-6.
438. Marcelin G, Chua S, Jr. Contributions of adipocyte lipid metabolism to body fat content and implications for the treatment of obesity. *Curr Opin Pharmacol*. 2010;10(5):588-93.
439. Dowker-Key PD, Jadi PK, Gill NB, Hubbard KN, Elshaarawi A, Alfatlawy ND, et al. A Closer Look into White Adipose Tissue Biology and the Molecular Regulation of Stem Cell Commitment and Differentiation. *Genes (Basel)*. 2024;15(8).
440. Mallick R, Basak S, Das RK, Banerjee A, Paul S, Pathak S, et al. Fatty Acids and their Proteins in Adipose Tissue Inflammation. *Cell Biochem Biophys*. 2024;82(1):35-51.
441. Seale P, Kajimura S, Spiegelman BM. Transcriptional control of brown adipocyte development and physiological function--of mice and men. *Genes Dev*. 2009;23(7):788-97.
442. Saponaro C, Gaggini M, Carli F, Gastaldelli A. The Subtle Balance between Lipolysis and Lipogenesis: A Critical Point in Metabolic Homeostasis. *Nutrients*. 2015;7(11):9453-74.
443. Mann JP, Savage DB. What lipodystrophies teach us about the metabolic syndrome. *J Clin Invest*. 2019;129(10):4009-21.
444. Berland C, Small DM, Luquet S, Gangarossa G. Dietary lipids as regulators of reward processes: multimodal integration matters. *Trends Endocrinol Metab*. 2021;32(9):693-705.
445. Frayn K, Bernard S, Spalding K, Arner P. Adipocyte triglyceride turnover is independently associated with atherogenic dyslipidemia. *J Am Heart Assoc*. 2012;1(6):e003467.
446. Liu L. Lessons from cavin-1 deficiency. *Biochem Soc Trans*. 2020;48(1):147-54.
447. Fiorenza CG, Chou SH, Mantzoros CS. Lipodystrophy: pathophysiology and advances in treatment. *Nat Rev Endocrinol*. 2011;7(3):137-50.

448. Wang J, Guo H, Zheng LF, Li P, Zhao TJ. Context-specific fatty acid uptake is a finely-tuned multi-level effort. *Trends Endocrinol Metab.* 2024.
449. Frayn KN. Plasma non-esterified fatty acids: why are we not measuring them routinely? *Ann Clin Biochem.* 2005;42(Pt 6):413-4.
450. Chen W, Xu Z, You W, Zhou Y, Wang L, Huang Y, et al. Cold exposure alters lipid metabolism of skeletal muscle through HIF-1 $\alpha$ -induced mitophagy. *BMC Biol.* 2023;21(1):27.
451. Wang J, Li DL, Zheng LF, Ren S, Huang ZQ, Tao Y, et al. Dynamic palmitoylation of STX11 controls injury-induced fatty acid uptake to promote muscle regeneration. *Dev Cell.* 2024;59(3):384-99 e5.
452. Trefts E, Gannon M, Wasserman DH. The liver. *Curr Biol.* 2017;27(21):R1147-R51.
453. Bechmann LP, Hannivoort RA, Gerken G, Hotamisligil GS, Trauner M, Canbay A. The interaction of hepatic lipid and glucose metabolism in liver diseases. *J Hepatol.* 2012;56(4):952-64.
454. Alves-Bezerra M, Cohen DE. Triglyceride Metabolism in the Liver. *Compr Physiol.* 2017;8(1):1-8.
455. Ipsen DH, Lykkesfeldt J, Tveden-Nyborg P. Molecular mechanisms of hepatic lipid accumulation in non-alcoholic fatty liver disease. *Cell Mol Life Sci.* 2018;75(18):3313-27.
456. Pan CQ, Reau N. New perspectives in liver diseases with challenges. *Gastroenterol Rep (Oxf).* 2024;12:goae098.
457. Lorente S, Hautefeuille M, Sanchez-Cedillo A. The liver, a functionalized vascular structure. *Sci Rep.* 2020;10(1):16194.
458. Mathew RP, Venkatesh SK. Liver vascular anatomy: a refresher. *Abdom Radiol (NY).* 2018;43(8):1886-95.
459. Torres Rojas AM, Lorente S, Hautefeuille M, Sanchez-Cedillo A. Hierarchical Modeling of the Liver Vascular System. *Front Physiol.* 2021;12:733165.
460. Zhou Z, Xu MJ, Gao B. Hepatocytes: a key cell type for innate immunity. *Cell Mol Immunol.* 2016;13(3):301-15.
461. Gao B, Jeong WI, Tian Z. Liver: An organ with predominant innate immunity. *Hepatology.* 2008;47(2):729-36.
462. Qin X, Gao B. The complement system in liver diseases. *Cell Mol Immunol.* 2006;3(5):333-40.
463. Pepys MB, Hirschfield GM. C-reactive protein: a critical update. *J Clin Invest.* 2003;111(12):1805-12.
464. Bode JG, Albrecht U, Haussinger D, Heinrich PC, Schaper F. Hepatic acute phase proteins--regulation by IL-6- and IL-1-type cytokines involving STAT3 and its crosstalk with NF-kappaB-dependent signaling. *Eur J Cell Biol.* 2012;91(6-7):496-505.
465. Dixon LJ, Barnes M, Tang H, Pritchard MT, Nagy LE. Kupffer cells in the liver. *Compr Physiol.* 2013;3(2):785-97.
466. Ezhilarasan D. Advantages and challenges in nanomedicines for chronic liver diseases: A hepatologist's perspectives. *Eur J Pharmacol.* 2021;893:173832.
467. Wu X, Li Y, Peng K, Zhou H. HIV protease inhibitors in gut barrier dysfunction and liver injury. *Curr Opin Pharmacol.* 2014;19:61-6.
468. Xu GX, Wei S, Yu C, Zhao SQ, Yang WJ, Feng YH, et al. Activation of Kupffer cells in NAFLD and NASH: mechanisms and therapeutic interventions. *Front Cell Dev Biol.* 2023;11:1199519.

469. Diehl KL, Vorac J, Hofmann K, Meiser P, Unterweger I, Kuerschner L, et al. Kupffer Cells Sense Free Fatty Acids and Regulate Hepatic Lipid Metabolism in High-Fat Diet and Inflammation. *Cells*. 2020;9(10).
470. Jones H, Alpini G, Francis H. Bile acid signaling and biliary functions. *Acta Pharm Sin B*. 2015;5(2):123-8.
471. Maroni L, Haibo B, Ray D, Zhou T, Wan Y, Meng F, et al. Functional and structural features of cholangiocytes in health and disease. *Cell Mol Gastroenterol Hepatol*. 2015;1(4):368-80.
472. Munshi MK, Priester S, Gaudio E, Yang F, Alpini G, Mancinelli R, et al. Regulation of biliary proliferation by neuroendocrine factors: implications for the pathogenesis of cholestatic liver diseases. *Am J Pathol*. 2011;178(2):472-84.
473. Cheung AC, Lorenzo Pisarello MJ, LaRusso NF. Pathobiology of biliary epithelia. *Biochim Biophys Acta Mol Basis Dis*. 2018;1864(4 Pt B):1220-31.
474. Salas-Silva S, Simoni-Nieves A, Chavez-Rodriguez L, Gutierrez-Ruiz MC, Bucio L, Quiroz LEG. Mechanism of cholangiocellular damage and repair during cholestasis. *Ann Hepatol*. 2021;26:100530.
475. de Aguiar Vallim TQ, Tarling EJ, Edwards PA. Pleiotropic roles of bile acids in metabolism. *Cell Metab*. 2013;17(5):657-69.
476. Tabibian JH, Masyuk AI, Masyuk TV, O'Hara SP, LaRusso NF. Physiology of cholangiocytes. *Compr Physiol*. 2013;3(1):541-65.
477. Xia X, Francis H, Glaser S, Alpini G, LeSage G. Bile acid interactions with cholangiocytes. *World J Gastroenterol*. 2006;12(22):3553-63.
478. Fleishman JS, Kumar S. Bile acid metabolism and signaling in health and disease: molecular mechanisms and therapeutic targets. *Signal Transduct Target Ther*. 2024;9(1):97.
479. Xia X, Jung D, Webb P, Zhang A, Zhang B, Li L, et al. Liver X receptor beta and peroxisome proliferator-activated receptor delta regulate cholesterol transport in murine cholangiocytes. *Hepatology*. 2012;56(6):2288-96.
480. Garcon D, Berger JM, Cariou B, Le May C. Transintestinal cholesterol excretion in health and disease. *Curr Atheroscler Rep*. 2022;24(3):153-60.
481. Poisson J, Lemoine S, Boulanger C, Durand F, Moreau R, Valla D, et al. Liver sinusoidal endothelial cells: Physiology and role in liver diseases. *J Hepatol*. 2017;66(1):212-27.
482. Mo H, Yue P, Li Q, Tan Y, Yan X, Liu X, et al. The role of liver sinusoidal endothelial cells in metabolic dysfunction-associated steatotic liver diseases and liver cancer: mechanisms and potential therapies. *Angiogenesis*. 2025;28(2):14.
483. Maslak E, Gregorius A, Chlopicki S. Liver sinusoidal endothelial cells (LSECs) function and NAFLD; NO-based therapy targeted to the liver. *Pharmacol Rep*. 2015;67(4):689-94.
484. Hammoutene A, Rautou PE. Role of liver sinusoidal endothelial cells in non-alcoholic fatty liver disease. *J Hepatol*. 2019;70(6):1278-91.
485. Gramignoli R, Ranade AR, Venkataramanan R, Strom SC. Effects of Pro-Inflammatory Cytokines on Hepatic Metabolism in Primary Human Hepatocytes. *Int J Mol Sci*. 2022;23(23).
486. Sauvant P, Cansell M, Atgie C. Vitamin A and lipid metabolism: relationship between hepatic stellate cells (HSCs) and adipocytes. *J Physiol Biochem*. 2011;67(3):487-96.

487. Senoo H, Yoshikawa K, Morii M, Miura M, Imai K, Mezaki Y. Hepatic stellate cell (vitamin A-storing cell) and its relative--past, present and future. *Cell Biol Int*. 2010;34(12):1247-72.
488. Jing XY, Yang XF, Qing K, Ou-yang Y. Roles of the lipid metabolism in hepatic stellate cells activation big up tri, open. *Chin Med Sci J*. 2013;28(4):233-6.
489. Donnelly KL, Smith CI, Schwarzenberg SJ, Jessurun J, Boldt MD, Parks EJ. Sources of fatty acids stored in liver and secreted via lipoproteins in patients with nonalcoholic fatty liver disease. *J Clin Invest*. 2005;115(5):1343-51.
490. Qiu P, Wang H, Zhang M, Zhang M, Peng R, Zhao Q, et al. FATP2-targeted therapies - A role beyond fatty liver disease. *Pharmacol Res*. 2020;161:105228.
491. Perez VM, Gabell J, Behrens M, Wase N, DiRusso CC, Black PN. Deletion of fatty acid transport protein 2 (FATP2) in the mouse liver changes the metabolic landscape by increasing the expression of PPARalpha-regulated genes. *J Biol Chem*. 2020;295(17):5737-50.
492. Enooku K, Tsutsumi T, Kondo M, Fujiwara N, Sasako T, Shibahara J, et al. Hepatic FATP5 expression is associated with histological progression and loss of hepatic fat in NAFLD patients. *J Gastroenterol*. 2020;55(2):227-43.
493. Doege H, Baillie RA, Ortegon AM, Tsang B, Wu Q, Punreddy S, et al. Targeted deletion of FATP5 reveals multiple functions in liver metabolism: alterations in hepatic lipid homeostasis. *Gastroenterology*. 2006;130(4):1245-58.
494. Wilson CG, Tran JL, Erion DM, Vera NB, Febbraio M, Weiss EJ. Hepatocyte-Specific Disruption of CD36 Attenuates Fatty Liver and Improves Insulin Sensitivity in HFD-Fed Mice. *Endocrinology*. 2016;157(2):570-85.
495. Dennis K, Heather LC. Post-translational palmitoylation of metabolic proteins. *Front Physiol*. 2023;14:1122895.
496. Hertzog AV, Bernlohr DA. The mammalian fatty acid-binding protein multigene family: molecular and genetic insights into function. *Trends Endocrinol Metab*. 2000;11(5):175-80.
497. Digel M, Eehalt R, Stremmel W, Fullekrug J. Acyl-CoA synthetases: fatty acid uptake and metabolic channeling. *Mol Cell Biochem*. 2009;326(1-2):23-8.
498. Ma Y, Nenkov M, Chen Y, Press AT, Kaemmerer E, Gassler N. Fatty acid metabolism and acyl-CoA synthetases in the liver-gut axis. *World J Hepatol*. 2021;13(11):1512-33.
499. Schroeder F, McIntosh AL, Martin GG, Huang H, Landrock D, Chung S, et al. Fatty Acid Binding Protein-1 (FABP1) and the Human FABP1 T94A Variant: Roles in the Endocannabinoid System and Dyslipidemias. *Lipids*. 2016;51(6):655-76.
500. Demers A, Samami S, Lauzier B, Des Rosiers C, Ngo Sock ET, Ong H, et al. PCSK9 Induces CD36 Degradation and Affects Long-Chain Fatty Acid Uptake and Triglyceride Metabolism in Adipocytes and in Mouse Liver. *Arterioscler Thromb Vasc Biol*. 2015;35(12):2517-25.
501. Li Y, Yang P, Zhao L, Chen Y, Zhang X, Zeng S, et al. CD36 plays a negative role in the regulation of lipophagy in hepatocytes through an AMPK-dependent pathway. *J Lipid Res*. 2019;60(4):844-55.
502. Badmus OO, Hillhouse SA, Anderson CD, Hinds TD, Stec DE. Molecular mechanisms of metabolic associated fatty liver disease (MAFLD): functional analysis of lipid metabolism pathways. *Clin Sci (Lond)*. 2022;136(18):1347-66.
503. Tong L. Acetyl-coenzyme A carboxylase: crucial metabolic enzyme and attractive target for drug discovery. *Cell Mol Life Sci*. 2005;62(16):1784-803.

504. Stamatikos AD, Paton CM. Role of stearyl-CoA desaturase-1 in skeletal muscle function and metabolism. *Am J Physiol Endocrinol Metab.* 2013;305(7):E767-75.
505. Srivastava RAK. A Review of Progress on Targeting LDL Receptor-Dependent and -Independent Pathways for the Treatment of Hypercholesterolemia, a Major Risk Factor of ASCVD. *Cells.* 2023;12(12).
506. Sato R. Recent advances in regulating cholesterol and bile acid metabolism. *Biosci Biotechnol Biochem.* 2020;84(11):2185-92.
507. Rui L. Energy metabolism in the liver. *Compr Physiol.* 2014;4(1):177-97.
508. Lee SH, Veeriah V, Levine F. Liver fat storage is controlled by HNF4alpha through induction of lipophagy and is reversed by a potent HNF4alpha agonist. *Cell Death Dis.* 2021;12(6):603.
509. Roumans KHM, Basset Sagarminaga J, Peters HPF, Schrauwen P, Schrauwen-Hinderling VB. Liver fat storage pathways: methodologies and dietary effects. *Curr Opin Lipidol.* 2021;32(1):9-15.
510. Reid BN, Ables GP, Otlivanchik OA, Schoiswohl G, Zechner R, Blaner WS, et al. Hepatic overexpression of hormone-sensitive lipase and adipose triglyceride lipase promotes fatty acid oxidation, stimulates direct release of free fatty acids, and ameliorates steatosis. *J Biol Chem.* 2008;283(19):13087-99.
511. Maurotti S, Geirola N, Frosina M, Mirarchi A, Scionti F, Mare R, et al. Exploring the impact of lipid droplets on the evolution and progress of hepatocarcinoma. *Front Cell Dev Biol.* 2024;12:1404006.
512. Chen J, Fang Z, Luo Q, Wang X, Warda M, Das A, et al. Unlocking the mysteries of VLDL: exploring its production, intracellular trafficking, and metabolism as therapeutic targets. *Lipids Health Dis.* 2024;23(1):14.
513. Tran K, Thorne-Tjomslund G, DeLong CJ, Cui Z, Shan J, Burton L, et al. Intracellular assembly of very low density lipoproteins containing apolipoprotein B100 in rat hepatoma McA-RH7777 cells. *J Biol Chem.* 2002;277(34):31187-200.
514. Yoshikawa T, Ide T, Shimano H, Yahagi N, Amemiya-Kudo M, Matsuzaka T, et al. Cross-talk between peroxisome proliferator-activated receptor (PPAR) alpha and liver X receptor (LXR) in nutritional regulation of fatty acid metabolism. I. PPARs suppress sterol regulatory element binding protein-1c promoter through inhibition of LXR signaling. *Mol Endocrinol.* 2003;17(7):1240-54.
515. Zelcer N, Tontonoz P. Liver X receptors as integrators of metabolic and inflammatory signaling. *J Clin Invest.* 2006;116(3):607-14.
516. Knebel B, Haas J, Hartwig S, Jacob S, Kollmer C, Nitzgen U, et al. Liver-specific expression of transcriptionally active SREBP-1c is associated with fatty liver and increased visceral fat mass. *PLoS One.* 2012;7(2):e31812.
517. Sivri D, Akdevelioglu Y. Effect of Fatty Acids on Glucose Metabolism and Type 2 Diabetes. *Nutr Rev.* 2025;83(5):897-907.
518. Hodson L, Rosqvist F, Parry SA. The influence of dietary fatty acids on liver fat content and metabolism. *Proc Nutr Soc.* 2020;79(1):30-41.
519. Robinson MW, Harmon C, O'Farrelly C. Liver immunology and its role in inflammation and homeostasis. *Cell Mol Immunol.* 2016;13(3):267-76.
520. Kubes P, Mehal WZ. Sterile inflammation in the liver. *Gastroenterology.* 2012;143(5):1158-72.
521. Takeuchi O, Akira S. Pattern recognition receptors and inflammation. *Cell.* 2010;140(6):805-20.

522. Knolle P, Schlaak J, Uhrig A, Kempf P, Meyer zum Buschenfelde KH, Gerken G. Human Kupffer cells secrete IL-10 in response to lipopolysaccharide (LPS) challenge. *J Hepatol.* 1995;22(2):226-9.
523. Knolle PA, Uhrig A, Hegenbarth S, Loser E, Schmitt E, Gerken G, et al. IL-10 down-regulates T cell activation by antigen-presenting liver sinusoidal endothelial cells through decreased antigen uptake via the mannose receptor and lowered surface expression of accessory molecules. *Clin Exp Immunol.* 1998;114(3):427-33.
524. Hammerich L, Tacke F. Hepatic inflammatory responses in liver fibrosis. *Nat Rev Gastroenterol Hepatol.* 2023;20(10):633-46.
525. Gabay C, Kushner I. Acute-phase proteins and other systemic responses to inflammation. *N Engl J Med.* 1999;340(6):448-54.
526. Goldstein I, Paakinaho V, Baek S, Sung MH, Hager GL. Synergistic gene expression during the acute phase response is characterized by transcription factor assisted loading. *Nat Commun.* 2017;8(1):1849.
527. Inatsu A, Kinoshita M, Nakashima H, Shimizu J, Saitoh D, Tamai S, et al. Novel mechanism of C-reactive protein for enhancing mouse liver innate immunity. *Hepatology.* 2009;49(6):2044-54.
528. Pellicoro A, Ramachandran P, Iredale JP, Fallowfield JA. Liver fibrosis and repair: immune regulation of wound healing in a solid organ. *Nat Rev Immunol.* 2014;14(3):181-94.
529. Hellerbrand C, Stefanovic B, Giordano F, Burchardt ER, Brenner DA. The role of TGFbeta1 in initiating hepatic stellate cell activation in vivo. *J Hepatol.* 1999;30(1):77-87.
530. Michalopoulos GK. Liver regeneration. *J Cell Physiol.* 2007;213(2):286-300.
531. Cressman DE, Greenbaum LE, DeAngelis RA, Ciliberto G, Furth EE, Poli V, et al. Liver failure and defective hepatocyte regeneration in interleukin-6-deficient mice. *Science.* 1996;274(5291):1379-83.
532. Mansouri RM, Bauge E, Staels B, Gervois P. Systemic and distal repercussions of liver-specific peroxisome proliferator-activated receptor-alpha control of the acute-phase response. *Endocrinology.* 2008;149(6):3215-23.
533. Zu L, He J, Jiang H, Xu C, Pu S, Xu G. Bacterial endotoxin stimulates adipose lipolysis via toll-like receptor 4 and extracellular signal-regulated kinase pathway. *J Biol Chem.* 2009;284(9):5915-26.
534. Fong YM, Marano MA, Moldawer LL, Wei H, Calvano SE, Kenney JS, et al. The acute splanchnic and peripheral tissue metabolic response to endotoxin in humans. *J Clin Invest.* 1990;85(6):1896-904.
535. van Hall G, Steensberg A, Sacchetti M, Fischer C, Keller C, Schjerling P, et al. Interleukin-6 stimulates lipolysis and fat oxidation in humans. *J Clin Endocrinol Metab.* 2003;88(7):3005-10.
536. Han MS, White A, Perry RJ, Camporez JP, Hidalgo J, Shulman GI, et al. Regulation of adipose tissue inflammation by interleukin 6. *Proc Natl Acad Sci U S A.* 2020;117(6):2751-60.
537. Thomas T, Stefanoni D, Reisz JA, Nemkov T, Bertolone L, Francis RO, et al. COVID-19 infection alters kynurenine and fatty acid metabolism, correlating with IL-6 levels and renal status. *JCI Insight.* 2020;5(14).
538. Trinh B, Peletier M, Simonsen C, Plomgaard P, Karstoft K, Klarlund Pedersen B, et al. Blocking endogenous IL-6 impairs mobilization of free fatty acids during rest and exercise in lean and obese men. *Cell Rep Med.* 2021;2(9):100396.

539. Wolsk E, Mygind H, Grondahl TS, Pedersen BK, van Hall G. IL-6 selectively stimulates fat metabolism in human skeletal muscle. *Am J Physiol Endocrinol Metab.* 2010;299(5):E832-40.
540. Wueest S, Item F, Boyle CN, Jirkof P, Cesarovic N, Ellingsgaard H, et al. Interleukin-6 contributes to early fasting-induced free fatty acid mobilization in mice. *Am J Physiol Regul Integr Comp Physiol.* 2014;306(11):R861-7.
541. Schindelin J, Arganda-Carreras I, Frise E, Kaynig V, Longair M, Pietzsch T, et al. Fiji: an open-source platform for biological-image analysis. *Nat Methods.* 2012;9(7):676-82.
542. Pfaffl MW, Tichopad A, Prgomet C, Neuvians TP. Determination of stable housekeeping genes, differentially regulated target genes and sample integrity: BestKeeper--Excel-based tool using pair-wise correlations. *Biotechnol Lett.* 2004;26(6):509-15.
543. Bouman BJ, Demerdash Y, Sood S, Grunschlager F, Pilz F, Itani AR, et al. Single-cell time series analysis reveals the dynamics of HSPC response to inflammation. *Life Sci Alliance.* 2024;7(3).
544. Lu B, Lu Y, Moser AH, Shigenaga JK, Grunfeld C, Feingold KR. LPS and proinflammatory cytokines decrease lipin-1 in mouse adipose tissue and 3T3-L1 adipocytes. *Am J Physiol Endocrinol Metab.* 2008;295(6):E1502-9.
545. Palomurto S, Virtanen KA, Karja V, Schwab U, Kaminska D, Kakela P, et al. Metabolic dysfunction-associated steatotic liver disease alters fatty acid profiles in the liver and adipose tissue. *J Clin Endocrinol Metab.* 2025.
546. Merchant S, Paul A, Reyes A, Cassidy D, Leach A, Kim D, et al. Different effects of fatty acid oxidation on hematopoietic stem cells based on age and diet. *Cell Stem Cell.* 2025;32(2):263-75 e5.
547. Sachot C, Poole S, Luheshi GN. Circulating leptin mediates lipopolysaccharide-induced anorexia and fever in rats. *J Physiol.* 2004;561(Pt 1):263-72.
548. Kim KK, Jin SH, Lee BJ. Herpes virus entry mediator signaling in the brain is imperative in acute inflammation-induced anorexia and body weight loss. *Endocrinol Metab (Seoul).* 2013;28(3):214-20.
549. Yang Y, Zhong W, Zhang Y, Cheng Y, Lai H, Yu H, et al. Sustained Inflammation Induced by LPS Leads to Tolerable Anorexia and Fat Loss via Tlr4 in Mice. *J Inflamm Res.* 2022;15:5635-48.
550. Karczewska-Kupczewska M, Nikolajuk A, Majewski R, Filarski R, Stefanowicz M, Matulewicz N, et al. Changes in adipose tissue lipolysis gene expression and insulin sensitivity after weight loss. *Endocr Connect.* 2020;9(2):90-100.
551. Frayn KN, Arner P, Yki-Jarvinen H. Fatty acid metabolism in adipose tissue, muscle and liver in health and disease. *Essays Biochem.* 2006;42:89-103.
552. Spiteri AG, Wishart CL, Pamphlett R, Locatelli G, King NJC. Microglia and monocytes in inflammatory CNS disease: integrating phenotype and function. *Acta Neuropathol.* 2022;143(2):179-224.
553. Miyazaki H, Sawada T, Kiyohira M, Yu Z, Nakamura K, Yasumoto Y, et al. Fatty acid binding protein 7 regulates phagocytosis and cytokine production in Kupffer cells during liver injury. *Am J Pathol.* 2014;184(9):2505-15.
554. Moore SM, Holt VV, Malpass LR, Hines IN, Wheeler MD. Fatty acid-binding protein 5 limits the anti-inflammatory response in murine macrophages. *Mol Immunol.* 2015;67(2 Pt B):265-75.

555. Taranto D, Ramirez CFA, Vegna S, de Groot MHP, de Wit N, Van Baalen M, et al. Multiparametric Analyses of Hepatocellular Carcinoma Somatic Mouse Models and Their Associated Tumor Microenvironment. *Curr Protoc.* 2021;1(6):e147.
556. Oliveira BM, Pinto A, Correia A, Ferreira PG, Vilanova M, Teixeira L. Characterization of Myeloid Cellular Populations in Mesenteric and Subcutaneous Adipose Tissue of Holstein-Friesian Cows. *Sci Rep.* 2020;10(1):1771.
557. van Lookeren Campagne M, Verschoor A. Pathogen clearance and immune adherence "revisited": Immuno-regulatory roles for CRIg. *Semin Immunol.* 2018;37:4-11.
558. de Carvalho DC, Fonseca FAH, Izar MCO, Silveira A, Tuleta ID, do Amaral JB, et al. Monocytes presenting a pro-inflammatory profile persist in patients submitted to a long-term pharmacological treatment after acute myocardial infarction. *Front Physiol.* 2022;13:1056466.
559. Thomas G, Tacke R, Hedrick CC, Hanna RN. Nonclassical patrolling monocyte function in the vasculature. *Arterioscler Thromb Vasc Biol.* 2015;35(6):1306-16.
560. Ma APY, Yeung CLS, Tey SK, Mao X, Wong SWK, Ng TH, et al. Suppression of ACADM-Mediated Fatty Acid Oxidation Promotes Hepatocellular Carcinoma via Aberrant CAV1/SREBP1 Signaling. *Cancer Res.* 2021;81(13):3679-92.
561. Coleman RA. It takes a village: channeling fatty acid metabolism and triacylglycerol formation via protein interactomes. *J Lipid Res.* 2019;60(3):490-7.
562. Zhou Y, Gu T, Hu S, Luo Z, Huang L, Yu C, et al. Liver HMGCS2 is critical in the maintenance of liver lipid homeostasis during fasting. *Genes Dis.* 2023;10(3):694-7.
563. Sharpe LJ, Brown AJ. Controlling cholesterol synthesis beyond 3-hydroxy-3-methylglutaryl-CoA reductase (HMGCR). *J Biol Chem.* 2013;288(26):18707-15.
564. Soto-Catalan M, Opazo-Rios L, Quiceno H, Lazaro I, Moreno JA, Gomez-Guerrero C, et al. Semaglutide Improves Liver Steatosis and De Novo Lipogenesis Markers in Obese and Type-2-Diabetic Mice with Metabolic-Dysfunction-Associated Steatotic Liver Disease. *Int J Mol Sci.* 2024;25(5).
565. Jump DB, Tripathy S, Depner CM. Fatty acid-regulated transcription factors in the liver. *Annu Rev Nutr.* 2013;33:249-69.
566. Mashek DG. Hepatic fatty acid trafficking: multiple forks in the road. *Adv Nutr.* 2013;4(6):697-710.
567. Hagenfeldt L, Wahren J, Pernow B, Raf L. Uptake of individual free fatty acids by skeletal muscle and liver in man. *J Clin Invest.* 1972;51(9):2324-30.
568. Aydin A, Sokal JE. Uptake of Plasma Free Fatty Acids by the Isolated Rat Liver: Effect of Glucagon. *Am J Physiol.* 1963;205:667-70.
569. Shi J, Fan J, Su Q, Yang Z. Cytokines and Abnormal Glucose and Lipid Metabolism. *Front Endocrinol (Lausanne).* 2019;10:703.
570. Patel A, Kutuzov MA, Dustin ML, van der Merwe PA, Dushek O. Regulation of temporal cytokine production by co-stimulation receptors in TCR-T cells is lost in CAR-T cells. *Immunother Adv.* 2024;4(1):ltae004.
571. Sharma VM, Puri V. Mechanism of TNF-alpha-induced lipolysis in human adipocytes uncovered. *Obesity (Silver Spring).* 2016;24(5):990.
572. Barbier L, Ferhat M, Salame E, Robin A, Herbelin A, Gombert JM, et al. Interleukin-1 Family Cytokines: Keystones in Liver Inflammatory Diseases. *Front Immunol.* 2019;10:2014.
573. Vida M, Gavito AL, Pavon FJ, Bautista D, Serrano A, Suarez J, et al. Chronic administration of recombinant IL-6 upregulates lipogenic enzyme expression and

aggravates high-fat-diet-induced steatosis in IL-6-deficient mice. *Dis Model Mech*. 2015;8(7):721-31.

574. Kharitonov A, Shiyanova TL, Koester A, Ford AM, Micanovic R, Galbreath EJ, et al. FGF-21 as a novel metabolic regulator. *J Clin Invest*. 2005;115(6):1627-35.

575. Zhang X, Yeung DC, Karpisek M, Stejskal D, Zhou ZG, Liu F, et al. Serum FGF21 levels are increased in obesity and are independently associated with the metabolic syndrome in humans. *Diabetes*. 2008;57(5):1246-53.

576. Cesari M, Pahor M, Incalzi RA. Plasminogen activator inhibitor-1 (PAI-1): a key factor linking fibrinolysis and age-related subclinical and clinical conditions. *Cardiovasc Ther*. 2010;28(5):e72-91.

577. Lin H, Xu L, Yu S, Hong W, Huang M, Xu P. Therapeutics targeting the fibrinolytic system. *Exp Mol Med*. 2020;52(3):367-79.

578. Shaikh SB, Balaya RDA, Dagamajalu S, Bhandary YP, Unwalla H, Prasad TSK, et al. A signaling pathway map of plasminogen activator inhibitor-1 (PAI-1/SERPINE-1): a review of an innovative frontier in molecular aging and cellular senescence. *Cell Commun Signal*. 2024;22(1):544.

579. Alessi MC, Juhan-Vague I. PAI-1 and the metabolic syndrome: links, causes, and consequences. *Arterioscler Thromb Vasc Biol*. 2006;26(10):2200-7.

580. Lim JH, Woo CH, Li JD. Critical role of type 1 plasminogen activator inhibitor (PAI-1) in early host defense against nontypeable *Haemophilus influenzae* (NTHi) infection. *Biochem Biophys Res Commun*. 2011;414(1):67-72.

581. Kager LM, van der Windt GJ, Wieland CW, Florquin S, van 't Veer C, van der Poll T. Plasminogen activator inhibitor type I may contribute to transient, non-specific changes in immunity in the subacute phase of murine tuberculosis. *Microbes Infect*. 2012;14(9):748-55.

582. Baycan OF, Barman HA, Bolen F, Atici A, Erman H, Korkmaz R, et al. Plasminogen activator inhibitor-1 levels as an indicator of severity and mortality for COVID-19. *North Clin Istanb*. 2023;10(1):1-9.

583. Sillen M, Miyata T, Vaughan DE, Strelkov SV, Declerck PJ. Structural Insight into the Two-Step Mechanism of PAI-1 Inhibition by Small Molecule TM5484. *Int J Mol Sci*. 2021;22(3).

584. Gils A, Declerck PJ. Plasminogen activator inhibitor-1. *Curr Med Chem*. 2004;11(17):2323-34.

585. Zhou A, Huntington JA, Pannu NS, Carrell RW, Read RJ. How vitronectin binds PAI-1 to modulate fibrinolysis and cell migration. *Nat Struct Biol*. 2003;10(7):541-4.

586. Vaughan DE. PAI-1 antagonists: the promise and the peril. *Trans Am Clin Climatol Assoc*. 2011;122:312-25.

587. Krause MP, Moradi J, Nissar AA, Riddell MC, Hawke TJ. Inhibition of plasminogen activator inhibitor-1 restores skeletal muscle regeneration in untreated type 1 diabetic mice. *Diabetes*. 2011;60(7):1964-72.

588. Baxi S, Crandall DL, Meier TR, Wroblewski S, Hawley A, Farris D, et al. Dose-dependent thrombus resolution due to oral plasminogen activator inhibitor (PAI)-1 inhibition with tiplaxtinin in a rat stenosis model of venous thrombosis. *Thromb Haemost*. 2008;99(4):749-58.

589. Hennan JK, Morgan GA, Swillo RE, Antrilli TM, Mugford C, Vlasuk GP, et al. Effect of tiplaxtinin (PAI-039), an orally bioavailable PAI-1 antagonist, in a rat model of thrombosis. *J Thromb Haemost*. 2008;6(9):1558-64.

590. Gomes-Giacoia E, Miyake M, Goodison S, Rosser CJ. Targeting plasminogen activator inhibitor-1 inhibits angiogenesis and tumor growth in a human cancer xenograft model. *Mol Cancer Ther.* 2013;12(12):2697-708.
591. Luo L, Li T, Zeng Z, Li H, He X, Chen Y. CSE reduces OTUD4 triggering lung epithelial cell apoptosis via PAI-1 degradation. *Cell Death Dis.* 2023;14(9):614.
592. Simone TM, Higgins SP, Archambeault J, Higgins CE, Ginnan RG, Singer H, et al. A small molecule PAI-1 functional inhibitor attenuates neointimal hyperplasia and vascular smooth muscle cell survival by promoting PAI-1 cleavage. *Cell Signal.* 2015;27(5):923-33.
593. Levine JA, Oleaga C, Eren M, Amaral AP, Shang M, Lux E, et al. Role of PAI-1 in hepatic steatosis and dyslipidemia. *Sci Rep.* 2021;11(1):430.
594. Piao L, Jung I, Huh JY, Miyata T, Ha H. A novel plasminogen activator inhibitor-1 inhibitor, TM5441, protects against high-fat diet-induced obesity and adipocyte injury in mice. *Br J Pharmacol.* 2016;173(17):2622-32.
595. Jeong BY, Uddin MJ, Park JH, Lee JH, Lee HB, Miyata T, et al. Novel Plasminogen Activator Inhibitor-1 Inhibitors Prevent Diabetic Kidney Injury in a Mouse Model. *PLoS One.* 2016;11(6):e0157012.
596. Medipally A, Xiao M, Biederman L, Dasgupta A, Satoskar AA, Parikh S, et al. Role of plasminogen activated inhibitor-1 in the pathogenesis of anticoagulant related nephropathy. *Front Nephrol.* 2024;4:1406655.
597. Lang SQ, Lang WH, Yu HY, Wang L. Metabolic activation of TM5441 in vitro and in vivo: Formation of reactive metabolites and human enzymes involved. *Eur J Pharm Sci.* 2020;143:105195.
598. Sueyoshi K, Ledderose C, Shen Y, Lee AH, Shapiro NI, Junger WG. Lipopolysaccharide suppresses T cells by generating extracellular ATP that impairs their mitochondrial function via P2Y11 receptors. *J Biol Chem.* 2019;294(16):6283-93.
599. Huebner BR, Moore EE, Moore HB, Stettler GR, Nunns GR, Lawson P, et al. Thrombin Provokes Degranulation of Platelet alpha-Granules Leading to the Release of Active Plasminogen Activator Inhibitor-1 (PAI-1). *Shock.* 2018;50(6):671-6.
600. Brogren H, Karlsson L, Andersson M, Wang L, Erlinge D, Jern S. Platelets synthesize large amounts of active plasminogen activator inhibitor 1. *Blood.* 2004;104(13):3943-8.
601. Hill SA, Shaughnessy SG, Joshua P, Ribau J, Austin RC, Podor TJ. Differential mechanisms targeting type 1 plasminogen activator inhibitor and vitronectin into the storage granules of a human megakaryocytic cell line. *Blood.* 1996;87(12):5061-73.
602. Brogren H, Wallmark K, Deinum J, Karlsson L, Jern S. Platelets retain high levels of active plasminogen activator inhibitor 1. *PLoS One.* 2011;6(11):e26762.
603. Mossberg K, Olausson J, Fryk E, Jern S, Jansson PA, Brogren H. The role of the platelet pool of Plasminogen Activator Inhibitor-1 in well-controlled type 2 diabetes patients. *PLoS One.* 2022;17(8):e0267833.
604. Ciesielska A, Matyjek M, Kwiatkowska K. TLR4 and CD14 trafficking and its influence on LPS-induced pro-inflammatory signaling. *Cell Mol Life Sci.* 2021;78(4):1233-61.
605. Martyanov AA, Maiorov AS, Filkova AA, Ryabykh AA, Svidelskaya GS, Artemenko EO, et al. Effects of bacterial lipopolysaccharides on platelet function: inhibition of weak platelet activation. *Sci Rep.* 2020;10(1):12296.

606. Damien P, Cognasse F, Eyraud MA, Arthaud CA, Pozzetto B, Garraud O, et al. LPS stimulation of purified human platelets is partly dependent on plasma soluble CD14 to secrete their main secreted product, soluble-CD40-Ligand. *BMC Immunol.* 2015;16(1):3.
607. Bergmeier W, Rackebrandt K, Schroder W, Zirngibl H, Nieswandt B. Structural and functional characterization of the mouse von Willebrand factor receptor GPIb-IX with novel monoclonal antibodies. *Blood.* 2000;95(3):886-93.
608. Calvente CJ, Tameda M, Johnson CD, Del Pilar H, Lin YC, Adronikou N, et al. Neutrophils contribute to spontaneous resolution of liver inflammation and fibrosis via microRNA-223. *J Clin Invest.* 2019;129(10):4091-109.
609. Wick JY. Bone marrow: the workhorse organ. *Consult Pharm.* 2013;28(1):16-22.
610. Wang H, Shah CA, Hu L, Huang W, Plataniias LC, Eklund EA. An aberrantly sustained emergency granulopoiesis response accelerates postchemotherapy relapse in MLL1-rearranged acute myeloid leukemia in mice. *J Biol Chem.* 2020;295(28):9663-75.
611. Abidin BM, Hammami A, Stager S, Heinonen KM. Infection-adapted emergency hematopoiesis promotes visceral leishmaniasis. *PLoS Pathog.* 2017;13(8):e1006422.
612. Nedeva C. Inflammation and Cell Death of the Innate and Adaptive Immune System during Sepsis. *Biomolecules.* 2021;11(7).
613. Snoeck HW. Mitochondrial regulation of hematopoietic stem cells. *Curr Opin Cell Biol.* 2017;49:91-8.
614. Mistry JJ, Bowles K, Rushworth SA. HSC-derived fatty acid oxidation in steady-state and stressed hematopoiesis. *Exp Hematol.* 2023;117:1-8.
615. Sun X, Song L, Feng S, Li L, Yu H, Wang Q, et al. Fatty Acid Metabolism is Associated With Disease Severity After H7N9 Infection. *EBioMedicine.* 2018;33:218-29.
616. Stromberg S, Baxter BA, Dooley G, LaVergne SM, Gallichotte E, Dutt T, et al. Relationships between plasma fatty acids in adults with mild, moderate, or severe COVID-19 and the development of post-acute sequelae. *Front Nutr.* 2022;9:960409.
617. Cusi K, Abdelmalek MF, Apovian CM, Balapattabi K, Bannuru RR, Barb D, et al. Metabolic Dysfunction-Associated Steatotic Liver Disease (MASLD) in People With Diabetes: The Need for Screening and Early Intervention. A Consensus Report of the American Diabetes Association. *Diabetes Care.* 2025;48(7):1057-82.
618. Li Y, Yang P, Ye J, Xu Q, Wu J, Wang Y. Updated mechanisms of MASLD pathogenesis. *Lipids Health Dis.* 2024;23(1):117.
619. Feingold KR, Wang Y, Moser A, Shigenaga JK, Grunfeld C. LPS decreases fatty acid oxidation and nuclear hormone receptors in the kidney. *J Lipid Res.* 2008;49(10):2179-87.
620. Feingold KR, Moser A, Patzek SM, Shigenaga JK, Grunfeld C. Infection decreases fatty acid oxidation and nuclear hormone receptors in the diaphragm. *J Lipid Res.* 2009;50(10):2055-63.
621. Zeerleder S, Schroeder V, Hack CE, Kohler HP, Wuillemin WA. TAFI and PAI-1 levels in human sepsis. *Thromb Res.* 2006;118(2):205-12.
622. Corgosinho FC, de Piano A, Sanches PL, Campos RM, Silva PL, Carnier J, et al. The role of PAI-1 and adiponectin on the inflammatory state and energy balance in obese adolescents with metabolic syndrome. *Inflammation.* 2012;35(3):944-51.

623. Fang X, Lan X, Zhu M, He M, Sun M, Cao Y, et al. Puerarin Induces Macrophage M2 Polarization to Exert Antinonalcoholic Steatohepatitis Pharmacological Activity via the Activation of Autophagy. *J Agric Food Chem.* 2024;72(13):7187-202.
624. Wang L, Zhang Z, Lin M, Qi L, Liu L, Chen Z, et al. Mechanistic insights into the PAI-1 inhibitor PAItrap3: enhancing lipid metabolism in adipose tissue of diabetic db/db mice. *Front Pharmacol.* 2025;16:1596655.
625. Xu Z, Huang Y. Blood PAI-1 and cardiovascular and metabolic risk factors among the middle-aged women from SWAN study. *Sci Rep.* 2024;14(1):21207.
626. Khoukaz HB, Ji Y, Braet DJ, Vadali M, Abdelhamid AA, Emal CD, et al. Drug Targeting of Plasminogen Activator Inhibitor-1 Inhibits Metabolic Dysfunction and Atherosclerosis in a Murine Model of Metabolic Syndrome. *Arterioscler Thromb Vasc Biol.* 2020;40(6):1479-90.
627. Choi GH, Cho SH, An HJ, Park HS, Lee JY, Ko EJ, et al. Association between PAI-1 Polymorphisms and Ischemic Stroke in a South Korean Case-Control Cohort. *Int J Mol Sci.* 2023;24(9).
628. Chen R, Yan J, Liu P, Wang Z, Wang C. Plasminogen activator inhibitor links obesity and thrombotic cerebrovascular diseases: The roles of PAI-1 and obesity on stroke. *Metab Brain Dis.* 2017;32(3):667-73.
629. Casqueiro J, Casqueiro J, Alves C. Infections in patients with diabetes mellitus: A review of pathogenesis. *Indian J Endocrinol Metab.* 2012;16 Suppl 1(Suppl1):S27-36.
630. Shi K, Wood K, Shi FD, Wang X, Liu Q. Stroke-induced immunosuppression and poststroke infection. *Stroke Vasc Neurol.* 2018;3(1):34-41.
631. Bekkering S, Burgner D. Viruses and cardiovascular disease: from bad to worse. *Nat Cardiovasc Res.* 2022;1(7):601-2.
632. Duffy MJ, McGowan PM, Harbeck N, Thomssen C, Schmitt M. uPA and PAI-1 as biomarkers in breast cancer: validated for clinical use in level-of-evidence-1 studies. *Breast Cancer Res.* 2014;16(4):428.
633. Nekarda H, Schmitt M, Ulm K, Wenninger A, Vogelsang H, Becker K, et al. Prognostic impact of urokinase-type plasminogen activator and its inhibitor PAI-1 in completely resected gastric cancer. *Cancer Res.* 1994;54(11):2900-7.
634. Koundouros N, Poulogiannis G. Reprogramming of fatty acid metabolism in cancer. *Br J Cancer.* 2020;122(1):4-22.
635. Humphries BA, Buschhaus JM, Chen YC, Haley HR, Qyli T, Chiang B, et al. Plasminogen Activator Inhibitor 1 (PAI1) Promotes Actin Cytoskeleton Reorganization and Glycolytic Metabolism in Triple-Negative Breast Cancer. *Mol Cancer Res.* 2019;17(5):1142-54.
636. Misiewicz M, Robak M, Chojnowski K, Trelinski J. [Correlations between ROTEM fibrinolytic activity and t-PA, PAI-1 levels in patients with newly diagnosed multiple myeloma]. *Pol Merkuri Lekarski.* 2014;36(215):316-9.
637. Zhang H, Wu G, Feng J, Lu X, Liu P. Expression of STOML2 promotes proliferation and glycolysis of multiple myeloma cells via upregulating PAI-1. *J Orthop Surg Res.* 2021;16(1):667.
638. Alessi MC, Bastelica D, Mavri A, Morange P, Berthet B, Grino M, et al. Plasma PAI-1 levels are more strongly related to liver steatosis than to adipose tissue accumulation. *Arterioscler Thromb Vasc Biol.* 2003;23(7):1262-8.
639. Henkel AS, Khan SS, Olivares S, Miyata T, Vaughan DE. Inhibition of Plasminogen Activator Inhibitor 1 Attenuates Hepatic Steatosis but Does Not

- Prevent Progressive Nonalcoholic Steatohepatitis in Mice. *Hepatol Commun.* 2018;2(12):1479-92.
640. Safa, Norton CE. Plasminogen Activation Inhibitor-1 Promotes Resilience to Acute Oxidative Stress in Cerebral Arteries from Females. *Pharmaceuticals (Basel)*. 2024;17(9).
641. Rehill AM, Leon G, McCluskey S, Schoen I, Hernandez-Santana Y, Annett S, et al. Glycolytic reprogramming fuels myeloid cell-driven hypercoagulability. *J Thromb Haemost.* 2024;22(2):394-409.
642. Passaro S, Corso G, Wohlwend J, Reveiz M, Thaler S, Somnath VR, et al. Boltz-2: Towards Accurate and Efficient Binding Affinity Prediction. *bioRxiv*. 2025.
643. Chu Y, Bucci JC, Peterson CB. Identification of a PAI-1-binding site within an intrinsically disordered region of vitronectin. *Protein Sci.* 2020;29(2):494-508.
644. Lee SM, Dorotea D, Jung I, Nakabayashi T, Miyata T, Ha H. TM5441, a plasminogen activator inhibitor-1 inhibitor, protects against high fat diet-induced non-alcoholic fatty liver disease. *Oncotarget.* 2017;8(52):89746-60.
645. Hosaka S, Yamada T, Takahashi K, Dan T, Kaneko K, Kodama S, et al. Inhibition of Plasminogen Activator Inhibitor-1 Activation Suppresses High Fat Diet-Induced Weight Gain via Alleviation of Hypothalamic Leptin Resistance. *Front Pharmacol.* 2020;11:943.
646. Kobayashi H, Morikawa T, Okinaga A, Hamano F, Hashidate-Yoshida T, Watanuki S, et al. Environmental Optimization Enables Maintenance of Quiescent Hematopoietic Stem Cells Ex Vivo. *Cell Rep.* 2019;28(1):145-58 e9.
647. Ling B, Xu Y, Qian S, Xiang Z, Xuan S, Wu J. Regulation of hematopoietic stem cells differentiation, self-renewal, and quiescence through the mTOR signaling pathway. *Front Cell Dev Biol.* 2023;11:1186850.
648. Takizawa H, Boettcher S, Manz MG. Demand-adapted regulation of early hematopoiesis in infection and inflammation. *Blood.* 2012;119(13):2991-3002.
649. Zanoni I, Ostuni R, Marek LR, Barresi S, Barbalat R, Barton GM, et al. CD14 controls the LPS-induced endocytosis of Toll-like receptor 4. *Cell.* 2011;147(4):868-80.
650. Galgano L, Guidetti GF, Torti M, Canobbio I. The Controversial Role of LPS in Platelet Activation In Vitro. *Int J Mol Sci.* 2022;23(18).
651. Zhang G, Han J, Welch EJ, Ye RD, Voyno-Yasenetskaya TA, Malik AB, et al. Lipopolysaccharide stimulates platelet secretion and potentiates platelet aggregation via TLR4/MyD88 and the cGMP-dependent protein kinase pathway. *J Immunol.* 2009;182(12):7997-8004.
652. Shashkin PN, Brown GT, Ghosh A, Marathe GK, McIntyre TM. Lipopolysaccharide is a direct agonist for platelet RNA splicing. *J Immunol.* 2008;181(5):3495-502.
653. Chaurasia SN, Kushwaha G, Kulkarni PP, Mallick RL, Latheef NA, Mishra JK, et al. Platelet HIF-2alpha promotes thrombogenicity through PAI-1 synthesis and extracellular vesicle release. *Haematologica.* 2019;104(12):2482-92.
654. Katta S, Karnewar S, Panuganti D, Jerald MK, Sastry BKS, Kotamraju S. Mitochondria-targeted esculetin inhibits PAI-1 levels by modulating STAT3 activation and miR-19b via SIRT3: Role in acute coronary artery syndrome. *J Cell Physiol.* 2018;233(1):214-25.
655. Nilsson L, Banfi C, Diczfalusy U, Tremoli E, Hamsten A, Eriksson P. Unsaturated fatty acids increase plasminogen activator inhibitor-1 expression in endothelial cells. *Arterioscler Thromb Vasc Biol.* 1998;18(11):1679-85.

656. John S, Bhowmick K, Park A, Huang H, Yang X, Mishra L. Recent advances in targeting obesity, with a focus on TGF-beta signaling and vagus nerve innervation. *Bioelectron Med.* 2025;11(1):10.
657. Lundgren CH, Brown SL, Nordt TK, Sobel BE, Fujii S. Elaboration of type-1 plasminogen activator inhibitor from adipocytes. A potential pathogenetic link between obesity and cardiovascular disease. *Circulation.* 1996;93(1):106-10.
658. Kaji H. Adipose Tissue-Derived Plasminogen Activator Inhibitor-1 Function and Regulation. *Compr Physiol.* 2016;6(4):1873-96.
659. Ekstrand C, Linder M, Cherif H, Kieler H, Bahmanyar S. Increased susceptibility to infections before the diagnosis of immune thrombocytopenia. *J Thromb Haemost.* 2016;14(4):807-14.
660. Sandvad M, Pedersen EA, Frederiksen H, Mannering N. Risk of infection in adult patients with primary immune thrombocytopenia (ITP): a systematic review. *Expert Rev Hematol.* 2021;14(10):961-74.
661. Sheeba MS, Elwafa M, Abdelfatah RG. Plasminogen Activator Inhibitor 1 in Patients with Primary Immune Thrombocytopenia: A Case Control Study. *Indian J Hematol Blood Transfus.* 2025;41(3):599-604.
662. Han S, Lu H, Yu Y, Liu X, Jing F, Wang L, et al. Hyperlipidemia in immune thrombocytopenia: a retrospective study. *Thromb J.* 2023;21(1):102.
663. Xu P, Han S, Hou M, Zhao Y, Xu M. The serum lipid profiles in immune thrombocytopenia: Mendelian randomization analysis and a retrospective study. *Thromb J.* 2023;21(1):107.
664. Karpe F, Dickmann JR, Frayn KN. Fatty acids, obesity, and insulin resistance: time for a reevaluation. *Diabetes.* 2011;60(10):2441-9.
665. Carlsson M, Wessman Y, Almgren P, Groop L. High levels of nonesterified fatty acids are associated with increased familial risk of cardiovascular disease. *Arterioscler Thromb Vasc Biol.* 2000;20(6):1588-94.
666. Herd OJ, Rani GF, Hewitson JP, Hogg K, Stone AP, Cooper N, et al. Bone marrow remodeling supports hematopoiesis in response to immune thrombocytopenia progression in mice. *Blood Adv.* 2021;5(23):4877-89.
667. Zmijewski JW, Bae HB, Deshane JS, Peterson CB, Chaplin DD, Abraham E. Inhibition of neutrophil apoptosis by PAI-1. *Am J Physiol Lung Cell Mol Physiol.* 2011;301(2):L247-54.
668. Praetner M, Zuchriegel G, Holzer M, Uhl B, Schaubacher J, Mittmann L, et al. Plasminogen Activator Inhibitor-1 Promotes Neutrophil Infiltration and Tissue Injury on Ischemia-Reperfusion. *Arterioscler Thromb Vasc Biol.* 2018;38(4):829-42.
669. Wang X, Guo L, Huang J, Jiang S, Li N, Mu HH, et al. Plasminogen Activator Inhibitor-1 Potentiates Neutrophil Infiltration and Tissue Injury in Colitis. *Int J Biol Sci.* 2023;19(7):2132-49.
670. Oishi K, Yasui H, Inoue Y, Hozumi H, Suzuki Y, Karayama M, et al. PAI-1 Inhibitor TM5441 Attenuates Emphysema and Airway Inflammation in a Murine Model of Chronic Obstructive Pulmonary Disease. *International Journal of Molecular Sciences.* 2025;26(15):7086.
671. Lisman T. Platelet-neutrophil interactions as drivers of inflammatory and thrombotic disease. *Cell Tissue Res.* 2018;371(3):567-76.
672. Rosales C, Demaurex N, Lowell CA, Uribe-Querol E. Neutrophils: Their Role in Innate and Adaptive Immunity. *J Immunol Res.* 2016;2016:1469780.

673. Page C, Pitchford S. Neutrophil and platelet complexes and their relevance to neutrophil recruitment and activation. *Int Immunopharmacol.* 2013;17(4):1176-84.
674. Ibrahim AA, Yahata T, Muguruma Y, Miyata T, Ando K. Blockade of plasminogen activator inhibitor-1 empties bone marrow niche sufficient for donor hematopoietic stem cell engraftment without myeloablative conditioning. *Biochem Biophys Res Commun.* 2019;516(2):500-5.

## 9 Appendix

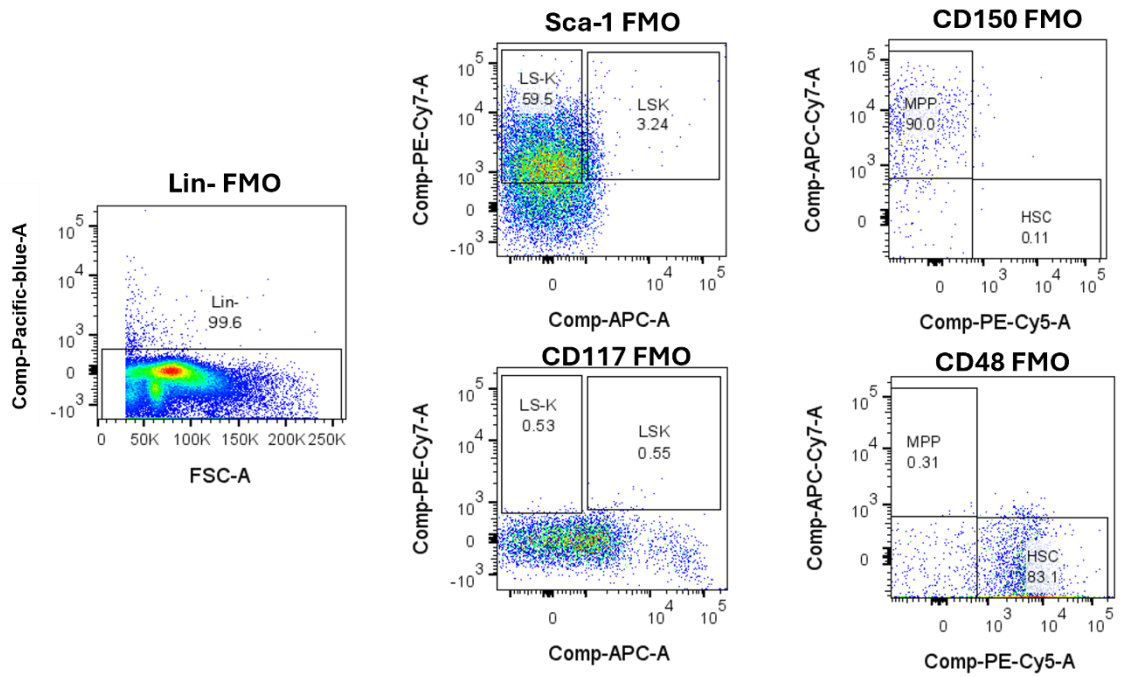


**Figure 9.1, FMOs for HSC panel.**

FMOs for HSC flow panel to demonstrate the gating strategy. This links to Figure 3.1.

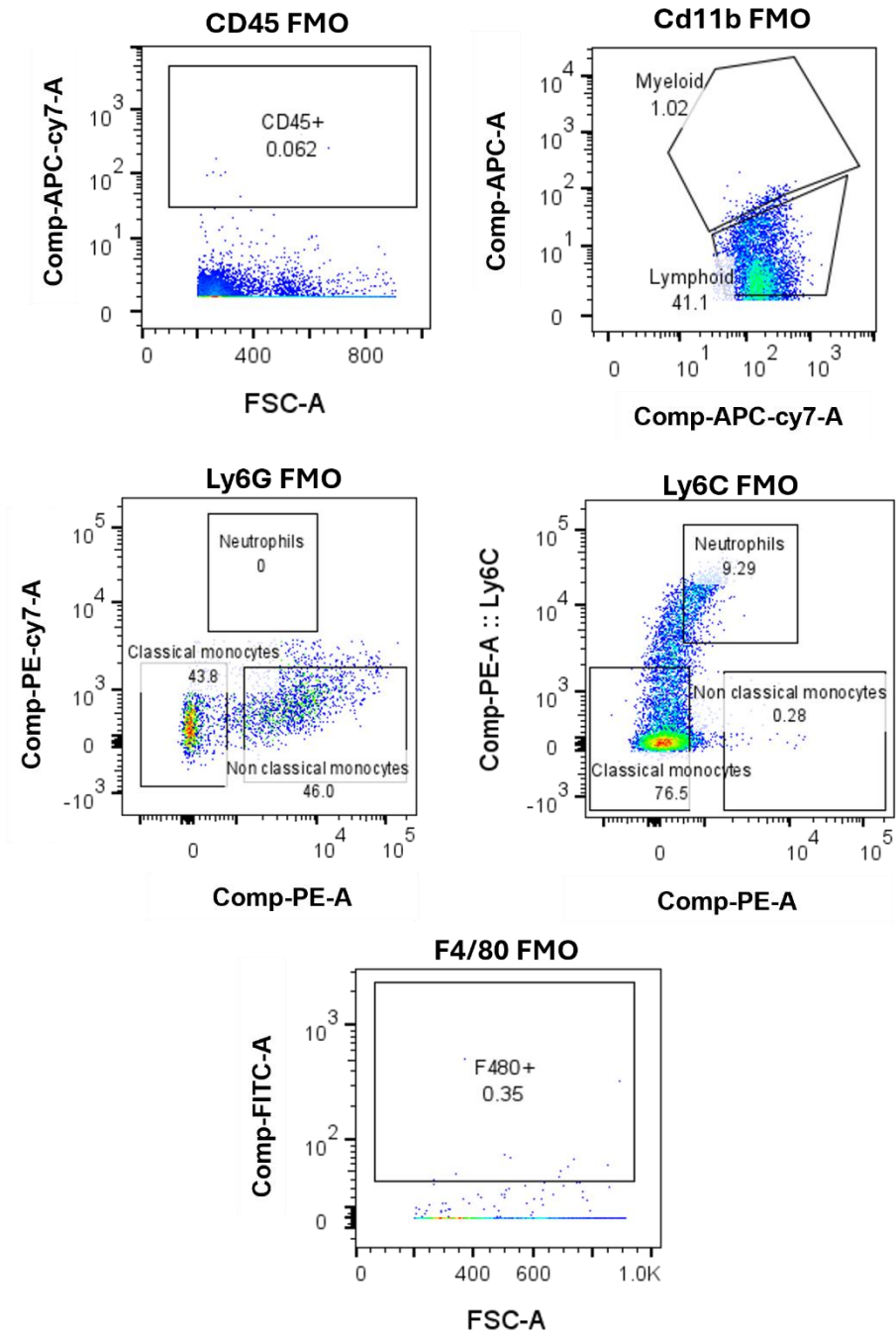


**Figure 9.2, FMOs for liver immune cell panel.**  
FMOs for the liver immune cell panel. This links to Figure 3.15.

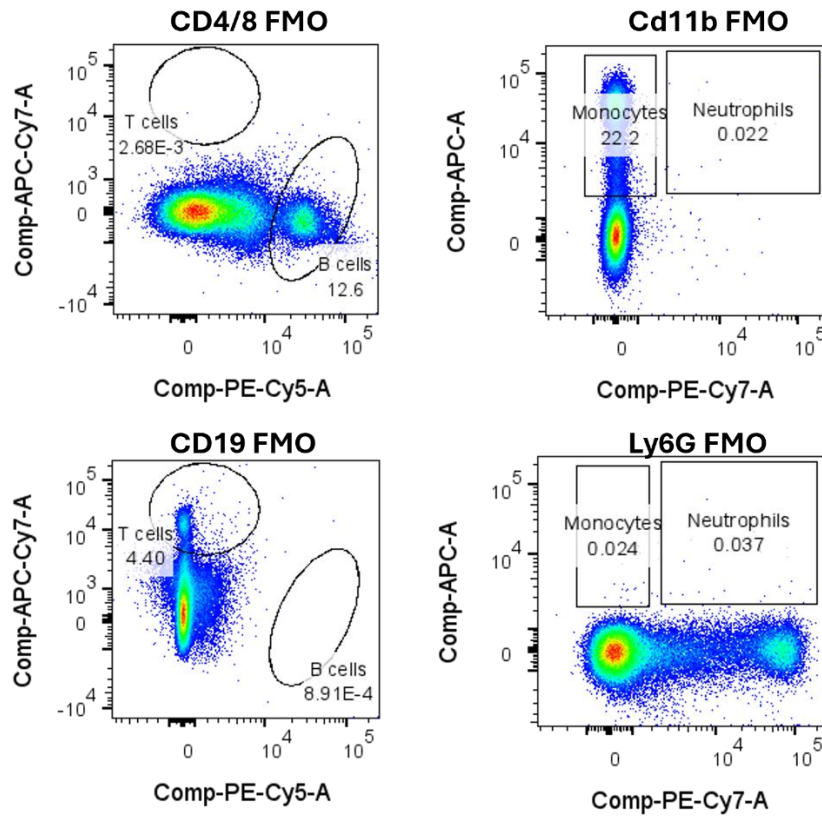


**Figure 9.3, FMOs for peripheral blood and mature bone marrow cell panels.**  
 FMOs for peripheral blood and mature bone marrow cell panel. This links to Figure 5.39.